OGOUN, E. 2024. *Experimental analysis of natural gas transport: using nanoporous ceramic cores as mimetic model for low permeability reservoirs*. Robert Gordon University, PhD thesis. Hosted on OpenAIR [online]. Available from: https://doi.org/10.48526/rgu-wt-2795722

Experimental analysis of natural gas transport: using nanoporous ceramic cores as mimetic model for low permeability reservoirs.

OGOUN, E.

2024

EXPERIMENTAL ANALYSIS OF NATURAL GAS TRANSPORT: USING NANOPOROUS CERAMIC CORES AS MIMETIC MODEL FOR LOW PERMEABILITY RESERVOIRS.

EVANS OGOUN

PhD 2024

EXPERIMENTAL ANALYSIS OF NATURAL GAS TRANSPORT: USING NANOPOROUS CERAMIC CORES AS MIMETIC MODEL FOR LOW PERMEABILITY RESERVOIRS.

EVANS OGOUN

A thesis submitted in partial fulfilment of the requirements of Robert Gordon University for the degree of Doctor of Philosophy

This research programme was carried out in collaboration with the Centre for Process Integration and Membrane Technology

September 2024

Abstract

This research investigates the use of nanoporous ceramic cores as mimetic models for studying natural gas transport in low permeability reservoirs. Low permeability reservoirs, such as tight sands, coalbed methane, and shale gas formations, present significant challenges for natural gas extraction due to their complex pore structures and limited flow characteristics.

Traditional methods for studying these reservoirs, like sand pack simulations and direct core analyses, have limitations including difficulty in replicating the heterogeneity of natural rocks and high costs. Synthetic nanoporous ceramic cores may offer opportunities, but literature on their use for reservoir studies is yet scarce. This study aim to bridge this knowledge gap by adopting Flux, Permeability, Mobility, and Reservoir Quality Index as objective functions to evaluate the use of nanoporous ceramic cores in describing the micro-geological characteristics of low permeability reservoirs.

The research involved rigorous data mining and experimental methodologies, comprising the analysis of extensive experimental data points from numerous CH_4 and CO_2 permeation tests, enhancing the reliability and validity of the findings. Additionally, wide-ranging field data from reservoirs that have implemented CH_4, and CO_2 gas dynamics were analysed. Five distinct nanoporous ceramic core samples with varied petrophysical properties were utilised in the experimental setup. Statistical tools, including clustering, mean, and coefficient of variation (CV), were employed to analyse, couple, and compare the datasets from the gas experiments and field data.

Machine learning techniques were used to enhance the analysis, utilising algorithms to analyse permeability, mobility, Darcy flux and reservoir quality index based on the experimental and field data. The use of machine learning models, such as linear regression, allowed for the identification of complex patterns and relationships between the variables, providing deeper insights into the gas transport mechanisms within the nanoporous ceramic cores.

The correlation analysis revealed significant relationships between temperature, pressure, and viscosity with permeability, mobility, Darcy flux and reservoir quality index. These relationship findings were further integrated with established theoretical and empirical research from the domains of petroleum engineering,

geomechanics, and hydrogeology, thus significantly bolstering the study's scientific rigour and validity.

The results indicated that the nanoporous ceramic cores significantly mimic the behaviour of reservoirs, displaying analogous patterns in permeability, mobility, reservoir quality index, and Darcy flux. Specifically, statistical means and cluster geometry demonstrated that CH_4 exhibited higher permeability ($4.62e^{-04}$ mD) and mobility (0.03 mD/cp) compared to CO_2 ($4.21e^{-04}$ mD and 0.02 mD/cp, respectively) in the experimental settings. These results align with the data mining analysis of field data, where mean permeability for CH_4 ($6.87e^{2}$ mD) is higher than that for CO_2 ($1.00e^{2}$ mD). Furthermore, the graphical rendering and coupling of the two datasets indicate an opportunity for the geometric transformation of the experiment to reservoir realities. Suggesting that nanoporous ceramic cores can serve as analogues for low permeability reservoir cores in natural gas transport studies, offering a cost-effective and environmentally friendly alternative to traditional coring methods, which are often expensive and environmentally intrusive.

The study highlights how factors such as pressure, temperature, and fluid viscosity impact gas transport in nanoporous ceramic cores and how these impacts are mirrored in the field. This aids in optimising gas injection strategies and improving overall reservoir management practices.

In conclusion, this study gives credence to the use of nanoporous ceramic cores as mimetic models for low-permeability reservoirs, opening new avenues for research and technological advancements in the field. The successful application of these cores can lead to better modelling of reservoir conditions, improved extraction techniques, and enhanced reservoir management practices, resulting in cost savings, technical advantages, and reduced environmental impacts associated with traditional coring methods.

Keywords: Nanoporous ceramic cores, low permeability, natural gas transport, permeability, mobility, Darcy’s equation adaptation, temperature effect, pressure effect, Darcy’s flux, reservoir quality index.

Dedication

I dedicate this research work to the grace of God Almighty, who, in His boundless mercies, guided me through every stage of this journey. Additionally, I express my heartfelt gratitude to my wonderful and loving wife, Edel-quin, whose unwavering emotional and moral support enabled me to successfully complete this program.

Declaration

I confirm that all the content within this report is entirely my own creation. In situations where I have referred to external sources, I have duly acknowledged and credited the relevant materials.

Acknowledgment

I wish to commence by expressing my profound gratitude to the Divine Creator for bestowing upon me the abundant grace and fortitude required to successfully conclude this program. I extend my heartfelt thanks to my cherished spouse, Mrs. Edel-quin Evans Ogoun, for her unwavering support and constant motivation throughout this remarkable journey.

To my principal supervisor, the late Professor Edward Gobina, words fall short in conveying my appreciation for his unwavering support and the wealth of wisdom and expertise he imparted to me. I also wish to extend my gratitude to Professor Nadimul Faisal for stepping into the primary supervisory role after the unfortunate passing of Professor Edward Gobina. Your willingness to provide guidance and assistance during this challenging period holds immense significance for me. I also want to express my deep gratitude to Professor Mamdud Hossain for his remarkable co-supervision throughout this research.

I am also thankful to my exceptional colleagues at the Centre for Process Integration and Membrane Technology, including Dr. Ofasa Abunumah, Priscilla Ogunlude, Florence Aisueni, Idris Hashim, Woyintonye Igbagara, Muktar Ramalan, and Abdulrahman Helal, for their camaraderie and unwavering support.

I owe a profound debt of gratitude to my sponsors, the Niger Delta Development Commission (NDDC), for recognising my potential and granting me a scholarship for this program.

Special appreciation goes to my wonderful daughters, Lifted Ogoun, Davina Ogoun, and Catherine Ogoun, for the precious quality time they shared with me after my work commitments.

Also, I would like to convey my sincere thanks to the School of Engineering at Robert Gordon University for affording me the invaluable learning opportunity and steadfast technical support during my program.

Table of content

List of figures

List of tables

Contribution to publications and conference proceedings

1. **OGOUN, E.,** ABUNUMAH, O., AISUENI, F., HOSSAIN, M., GIWA, A. and GOBINA, E. 2022. Using nanoporous core-samples to mimic the effect of petrophysical parameters on natural gas flowrate in an unconventional gas reservoir. In Techconnect briefs 2022: papers from 2022 TechConnect world innovation conference and expo, 13-15 June 2022, Washington, USA. Danville: TechConnect [online], pages 67-70. Available from: https://briefs.techconnect.org/wp-content/volumes/TCB2022/pdf/352.pdf

2. **OGOUN, E.,** OGUNLUDE, P., ABUNOMAH, O. and GOBINA, E. 2022. Nanoporous gas transport in shale gas reservoirs. International journal on engineering, science and technology [online], 4(1), pages 73-84. Available from: https://doi.org/10.46328/ijonest.70

3. **OGOUN, E.,** AISUENI, F., OGUNLUDE, P. and GOBINA, E. 2021. Gas flow mechanisms in fractured low permeability reservoirs. Presented at 2021 International congress of Scientific Advances (ICONSAD'21), 22-25 December 2021, [virtual conference]. Available from: https://rgu-repository.worktribe.com/output/1563482

4. **OGOUN, E**., AISUENI, F., RAMALAN, M., ABUNUMAH, O., OGUNLUDE, P., ORAKWE, I., GIWA, A., SHEHU, H. and GOBINA, E. 2022. Gas diffusion, transport characteristics and modelling in porous membrane systems with application for polymer electrolyte membrane fuel cells. In Proceedings of the 2nd International congress on scientific advances 2022 (ICONSAD'22), 21-24 December 2022, [virtual conference]. Turkey: ICONSAD [online], pages 144-157. Available from: https://en.iconsad.org/_files/ugd/1dd905_c45aeddf416d497e93113f00f465739b.pdf

5. HASHIM, I.A., AISUENI, F., OGUNLUDE, P., RAMALAN, M., **OGOUN, E.,** HUSSAINI, M. and GOBINA, E. 2022. Using contact angle measurements

for determination of the surface free energy of the ceramic membranes. In Techconnect briefs 2022: papers from 2022 TechConnect world innovation conference and expo, 13-15 June 2022, Washington, USA. Danville: TechConnect [online], pages 5-8. Available from: https://briefs.techconnect.org/wp-content/volumes/TCB2022/pdf/177.pdf

6. IGBAGARA, W., HASHM, I.A., AISUENI, F., OGUNLUDE, P., RAMALAN, M., **OGOUN, E.,** ASIM, T. and GOBINA, E. 2022. Characteristics of gas transport through inorganic ceramic membranes as porous media using air and nitrogen. In Proceedings of the 2nd International congress on scientific advances 2022 (ICONSAD'22), 21-24 December 2022, [virtual conference]. Turkey: ICONSAD [online], pages 417-425. Available from: https://en.iconsad.org/_files/ugd/1dd905_c45aeddf416d497e93113f00f465739b.pdf

7. OGUNLUDE, P., HASHIM, I., RAMALAN, M., **OGOUN, E.,** MUHAMMAD-SUKKI, F., GIWA, A. and GOBINA, E. 2022. An experimental study on the effect of methane potent biogas mixture on gas permeation mechanism. In Techconnect briefs 2022: papers from 2022 TechConnect world innovation conference and expo, 13-15 June 2022, Washington, USA. Danville: TechConnect [online], pages 43-46. Available from: https://briefs.techconnect.org/wp-content/volumes/TCB2022/pdf/188.pdf

8. SHEHU, H., ORAKWE, I., ABUNOMAH, O., OGUNLUDE, P., **OGOUN, E.,** RAMALAN, M., AISUENI, F., OKO, E., IBHADON, A., GAD-BRIGGS, A., GIANNOPOULOS, I., GIWA, A. and GOBINA, E. 2022. Development of dense membranes for high-density hydrogen production from ammonia catalytic decomposition (cracking) for PEM fuel cells power in long-haul passenger aircraft transportation. Techconnect briefs 2022: papers from 2022 TechConnect world innovation conference and expo, 13-15 June 2022, Washington, USA. Danville: TechConnect [online], pages 134-137. Available from: https://briefs.techconnect.org/wp-content/volumes/TCB2022/pdf/310.pdf

9. AISUENI, F., ABUNUMAH, O., HASHIM, I., RAMALAN, M., **OGOUN, E.,** PRABHU, R., GIWA, A. and GOBINA, E. 2022. Effect of pore size and porosity on contact angle of ceramic membrane for oil-in-water emulsion separation. In Techconnect briefs 2022: papers from 2022 TechConnect world innovation conference and expo, 13-15 June 2022, Washington, USA. Danville: TechConnect [online], pages 59-62. Available from: https://briefs.techconnect.org/wp-content/volumes/TCB2022/pdf/174.pdf

10. HASHIM, I.A., AISUENI, F., ABUNOMAH, O., OGUNLUDE, P., RAMALAN, M., **OGOUN, E.** and GOBINA, E. 2022. Characterization of membranes for advanced direct air carbon capture. In Techconnect briefs 2022: papers from 2022 TechConnect world innovation conference and expo, 13-15 June 2022, Washington, USA. Danville: TechConnect [online], pages 148-151. Available from: https://briefs.techconnect.org/wp-content/volumes/TCB2022/pdf/386.pdf

11. AISUENI, F., GOBINA, E., HASHIM, I. and **OGOUN, E.** 2022. Characterization and hydrodynamic evaluation of the relationship between permeability and microstructure parameters ceramic membranes for the separation of oil-in-water emulsion. International journal of engineering, science and technology [online], 4(1), pages 14-20. Available from: https://doi.org/10.46328/ijonest.69

12. ABUNUMAH, O., OGUNLUDE, P., **OGOUN, E.,** RAMALAN, M., ANTWI, S., AISUENI, F., HASHIM, I. and GOBINA, E. 2022. Effect of reservoir structural rhythm on carbon capture and sequestration (CCS) performance. International journal on engineering, science and technology [online], 4(1), pages 41-53. Available from: https://doi.org/10.46328/ijonest.72

13. OGUNLUDE, P., ABUNOMAH, O., HASHIM, I., AISUENI, F., **OGOUN, E.,** ANTWI, S., RAMALAN, M., WILLIAMWEST, T., SUKKI, F.M. and GOBINA, E. 2022. Mass transfer characteristics through alumina membranes with different pores sizes and porosity. International journal of engineering, science and technology [online], 4(1), pages 99-123. Available from: https://doi.org/10.46328/ijonest.71

14. AISUENI, F.A., **OGUON, E.,** HASHIM, I. and GOBINA, E. 2021. Characterization and evaluation of nanoparticles ceramic membrane for the separation of oil-in-water emulsion. In Proceedings of the ICANM 2021: 8th International conference and exhibition on advanced and nanomaterials 2021 (ICANM 2021), 9-11 August 2021, [virtual conference]. Ontario: ICANM, pages 17-26.

15. AISUENI, F., HASHIM, I., **OGOUN, E.** and GOBINA, E. 2021. Comparattive [sic] evaluation of oil-in-water emulsion separation with aluminium oxide and zinc oxide nanoparticles ceramic membrane. Presented to 2021 TUBA (Turkish Academy of Science) World conference on energy science and technology (TUBA WCEST-2021), 8-12 August 2021, [virtual conference].

Nomenclature

Symbol	Description	Units
A	Core area	cm^2
dp	Pressure drops	atm
h	Core height	cm
J	Flux	$cm^3 . cm^{-2} . s^{-1}$
Kb	Boltzmann constant	J/K
k	Permeability	mD
L	Core length	cm
M_g	Gas mobility	$mD.cp^{-1}$
P_1	Inlet pressure	atm
P_2	Outlet pressure	atm
Q	Flow rate	$cm^3 . s^{-1}$
r_1	Core external radius	cm
r_2	Core internal radius	cm
R	Universal gas constant	$J\ kg^{-1}\ mol^{-1}$
t	Core thickness	cm
T	Temperature	K
v	Velocity	cm/sec
Greek Letters		
ϕ	Porosity	%
ρ	Density	g/cm^2
τ	Tortuosity	
μ	Viscosity	cp
λ	Mean free path	cm
σ	Surface tension	$dynes.cm^{-1}$

Abbreviations

atm	Atmosphere
B	Big
CH_4	Methane
CO_2	Carbon dioxide
COSHH	Control of substances hazardous to health
EDAX	Energy Dispersive X-Ray Analysis
EIA	Environmental Impact Assessment
EOR	Enhanced Oil Recovery
LPM	Liters per minute
M_w	Molecular weight
mol	Mole
nm	Nanometer
RA	Risk assessment
S	Small
SEM	Scanning electron microscopy
TDS	Total dissolved solid
TOC	Total organic carbon
W_d	Dry weight
W_w	Wet weight

CHAPTER 1
INTRODUCTION

This chapter offers a succinct overview of the research background, detailing the statement of the research problem and the rationale behind the study. It outlines the research aim and objectives, briefly touches on its contributions to the existing body of knowledge and provides an outline of the research layout.

1.1 Research background.

Understanding the transport of natural gas within reservoirs characterised by low permeability is pivotal for advancing the oil and gas industry's capabilities in tapping unconventional energy resources. This phenomenon is marked by significant challenges as detailed by Li et al. (2022) and Zou et al. (2018), which are intensified by the surge in global demand for energy that drives exploration in complex geological structures like tight sands, coalbed methane, and shale gas formations. The development of such challenging reservoirs relies heavily on state-of-the-art technologies, including horizontal well drilling, enhanced oil recovery techniques, and intricate fracturing processes, as documented by Zeinabady et al. (2022), Yu et al. (2021), and Asadi et al. (2020).

The intrinsic properties of these reservoirs, specifically their low porosity and permeability, demand novel and sometimes aggressive extraction methods to realise economically viable yields of natural gas. Large-scale fracturing, for example, is one such technique integral to the recovery process in these settings, as indicated by Hao et al. (2023). The divergent flow patterns and transport mechanisms observed in these low-permeability environments stand in contrast to traditional models, thus necessitating a deep analytical understanding for effective reservoir evaluation and production optimisation, as explained by Marsden et al. (2022), Heider (2021), Xu et al. (2019) and Bunger and Lecampion (2017).

Despite the strategic importance of unconventional gas resources, there is an acknowledged gap in the understanding of gas flow mechanics within low-permeability reservoirs, particularly at the nano-pore scale where gas molecules and rock formations interact intimately (Wang et al. 2024). This calls for comprehensive and continuous experimental investigations and mathematical analyses to delineate the various factors that influence complex seepage phenomena, a necessity highlighted by Liu et al. (2015), Zhao et al. (2014), King (2010) and Bybee (2008). Continual advancements in knowledge and methodological approaches are thus necessary to guide the development and optimisation of low-permeability reservoirs, contributing to the energy sector's growth and stability (Ren et al. 2021, Lin et al. 2020 and Burrows et al. 2020).

Researchers have endeavoured to study these reservoirs' transport characteristics, storage mechanisms, and flow dynamics using an array of laboratory methodologies. Si et al. (2023), Wang et al. (2022), Chang Liu (2022), Freeman et al. (2011), Meissner et al. (2009), Shen et al. (2018) and El-Amin et al. (2018), and others have utilised sand packs as analogues for reservoir studies and conducted direct core sample analyses, among other experimental and modelling techniques. While these methods strive to enhance our understanding of the fundamental properties and behaviours within such reservoirs, they are not without limitations.

Sand packs, for example, can replicate reservoir properties to an extent but cannot capture the complexity and nano-scale geometries present in actual low-permeability formations, as discussed by Wang et al. (2022) and Chang Liu (2022). The uniformity of sand grains in a sand pack often does not reflect the true diversity in pore shapes, sizes, and connectivity found in low permeability reservoirs, which significantly influence gas flow. The direct core analysis remains a preferred method for evaluating these formations, providing insights into physical and petrophysical properties. However, as Lee et al. (2024), Mitchell et al. (2013), Wang et al. (2015), and Meissner et al. (2009) highlighted, this method faces practical challenges such as high costs and feasibility issues, particularly in remote or deeper reservoir locations, as well as the potential for core properties to alter during extraction.

In light of these challenges, this research aim to investigate the application of nanoporous ceramic cores as a cutting-edge alternative in the experimental analysis of gas transport within low-permeability reservoirs. These nano-engineered cores offer a unique mimicry of micro-geological characteristics, including distinctive pore formation and gas seepage behaviours, aligning with the heterogeneous distribution patterns found in low-permeability environments. This research involves a series of carefully controlled laboratory experiments, complemented by detailed data analysis and machine learning regression analysis, to deepen the understanding of gas flow phenomena in low-permeability contexts and coupling the findings with field data sourced from global low permeability reservoirs.

Through a systematic and in-depth research approach, the study aim to provide a substantiated assessment of nanoporous ceramic cores' efficacy as mimetic models. It seeks to bridge existing knowledge gaps, particularly in applying nanotechnology to gas transport studies, and contribute to the development of more efficient gas recovery methods tailored for the complexities of low-permeability reservoirs within the oil and gas industry. This research not only targets academic advancement but also practical implications, aiming to underpin technological and strategic development in natural gas extraction practices.

1.2 Problem statement

The research problem presented in this thesis is centred on the significant challenges posed by the extraction of natural gas from low permeability reservoirs, as substantiated by Li et al. (2022). The present research body has yet to fully capture contemporary insights into gas transport behaviour within low permeability reservoirs, especially at the nano-pore scale—where pivotal interactions between gas molecules and rock formations take place, emphasising the critical need for a continuous and in-depth understanding of gas transport mechanisms in such reservoirs to improve recovery techniques and maximise resource extraction. Established experimental methods, including sand pack simulations, are acknowledged to possess limitations in simulating the true complexity of these challenging environments, consequently stifling the development of effective recovery strategies. Alternative methods, such as direct core analysis, though insightful, are beset with practical limitations, including high costs and feasibility issues, particularly for deeper or more remote reservoirs, as noted by Chang Liu (2022), Wang et al. (2022), McPhee et al. (2015), Mitchell et al. (2013), and Meissner et al. (2009).

Considering these challenges, there is an unequivocal need for innovative methodologies to experimentally analyse gas transport phenomena within low permeability reservoirs. The advent and utilisation of nanoporous ceramic core samples as mimetic models stand as a promising pathway for simulating low permeability reservoir conditions and examining gas transport dynamics in a regulated laboratory environment (He et al. 2016 and Guo et al. 2015). Nevertheless, a notable knowledge gap persists concerning the extent to which nanoporous ceramic cores can represent the intricacies of low permeability reservoirs and furnish actionable insights for reservoir engineers.

This thesis is committed to rigorously investigating the use of nanoporous ceramic cores as mimetic models for studying natural gas transport in low permeability formations. This research will endeavour to bridge the current knowledge gap on the applicability of nanotechnology in gas transport studies, with the goal of advancing more gas recovery methodologies for low permeability reservoirs within the oil and gas industry. The success of this research holds the potential to significantly enhance the sector's operational efficiency and economic viability, contributing to a sustainable energy future.

1.3 Rationale

The rationale behind this research lies in addressing the critical challenges of natural gas extraction from low permeability reservoirs, which has been underscored by numerous scholars. Li et al. (2022), Zeinabady et al. (2022), Yu et al. (2021), Asadi et al. (2020), and Zou et al. (2018) have pointed out the complexities due to the intricate pore structures and limited flow within these formations, which conventional recovery methods fail to efficiently address, leading to suboptimal outcomes and economic losses. Hao et al. (2023) and others have further highlighted the need for a deeper and continuous understanding of gas transport mechanisms to improve recovery techniques and resource extraction.

Given that current research has not fully captured the nuanced behaviours of gas transport at the nano-pore scale, where critical interactions between gas molecules and rock formations take place, there is a need for more innovative experimental methodologies. Traditional methods, such as sand pack simulations, fall short of replicating the actual reservoir conditions, and direct core analysis is often prohibitively expensive and logistically challenging, as emphasised by researchers like Chang Liu (2022) and Wang et al. (2022).

Therefore, this research seeks to explore the potential of nanoporous ceramic core samples as mimetic models that could bridge this gap. These core samples, known for their durability, cost-effectiveness, low energy usage, and tuneable properties, present an innovative pathway to simulate reservoir conditions and enable the study of gas transport dynamics in a controlled laboratory environment. Yet, there are unresolved questions about how well these nanoporous ceramic cores can replicate the complexities of low permeability reservoirs and provide actionable insights for reservoir engineers.

This research aim to systematically assess the efficacy of nanoporous ceramic cores as reliable models for studying natural gas transport in low permeability formations. By conducting a series of meticulous experimental analyses with regression models, and developing a comparative model with field data, the study intends to advance the application of nanotechnology in gas transport studies. Thereby contributing to the development of more efficient gas recovery methods tailored for the challenges unique to low permeability reservoirs in the oil and gas industry.

1.4 Aim and objectives

The study aim to investigate the applicability of nanoporous ceramic cores as a mimetic model to study the transport of natural gas in low permeability reservoirs. To accomplish the designated aim, the following objectives were achieved:

1. To characterise the nanoporous ceramic core structures to estimate their analogue petrophysical properties through experimental observations and measurements.

2. To develop experimental setups to quantify gas permeability, and other pivotal reservoir parameters across the nanoporous ceramic cores under varying operating conditions, including temperatures and pressure gradients.

3. Develop a regression model to examine the interdependencies among reservoir parameters and operating conditions, aiming to ascertain their effects on gas transport. This model will not only quantify the influence of these variables but also integrate findings with established theoretical and empirical research to enhance understanding of gas dynamics within the reservoir.

4. Coupling reservoir parameters obtained from experimental data with field data to support the reliability and applicability of using nanoporous ceramic cores as a model for studying gas transport in low permeability reservoirs.

1.5 Contribution to knowledge

This thesis significantly advances the field of petroleum engineering and reservoir management through the advanced application of nanoporous ceramic cores to replicate gas transport behaviours in low-permeability reservoir. By combining experimental methodologies with comprehensive data mining and advanced machine learning techniques, this research provides innovative perceptions and practical improvements for understanding and optimising fluid transport mechanisms within these challenging reservoir formations.

One of the primary contributions of this study is the support of nanoporous ceramic cores as analogues for natural reservoirs. This research demonstrates that these ceramic cores can mimic the permeability, mobility, and overall fluid transport characteristics of low-permeability reservoirs. This confirmation offers a cost-effective and environmentally friendly alternative to traditional coring methods, significantly reducing the need for extensive field sampling and its associated costs and environmental impacts.

The thesis provides a comprehensive analysis of gas transport properties by examining key parameters such as temperature, pressure, and viscosity. It offers a detailed understanding of how these factors influence gas permeability, mobility, and flux within nanoporous ceramic cores. The findings align with those of established researchers like Berg (2019), Tiab and Donaldson (2014), and Ahmed (2006), thereby enhancing the credibility of the experimental approach and solidifying the validity of the results.

A particularly novel aspect of this research is the application of machine learning techniques to analyse permeability, mobility, Darcy flux and reservoir quality index based on experimental and field data. By employing linear regression, the study identifies complex patterns and relationships between variables, providing deeper awareness into gas transport mechanisms and enabling better predictions. This integration of machine learning represents a significant advancement in reservoir engineering, showcasing the potential for data-driven approaches to enhance traditional analytical methods.

The study's extensive dataset, comprising over 10,000 experimental data points and 2,000 field data points, enabled rigorous correlation and data mining analyses. This comprehensive analysis identified significant relationships between reservoir parameters, offering valuable information for optimising gas injection strategies and improving overall reservoir management practices. The robustness of the dataset and the analytical techniques applied contribute to the reliability and applicability of the findings. Furthermore, the research emphasises the importance of understanding reservoir flux for enhanced oil recovery (EOR) techniques. It highlights how modifying fluid flow dynamics can maximise hydrocarbon recovery, particularly in low-permeability reservoirs where traditional methods may be less effective. These insights provide practical guidance for developing more efficient EOR strategies, directly impacting field operations and economic outcomes.

The environmental and economic implications of this study are also noteworthy. By supporting the use of nanoporous ceramic cores as reservoir analogues, the research promotes more sustainable and cost-effective reservoir management practices. This aligns with global efforts to minimise the environmental footprint of the oil and gas industry, contributing to the development of practices that are both economically viable and environmentally responsible.

1.6 Outline of the thesis

The research is structured into five distinct chapters, excluding references and appendices. Each chapter's summary is provided below.

Chapter 1: This chapter provides a concise introduction to the context of the research, emphasising the statement of the research problem and its rationale. It presents the aim and objectives of the study, its contributions to existing knowledge, and an overview of the study’s layout.

Chapter 2: This chapter presents a comprehensive review of relevant literature. It offers detailed theoretical insights and an overview of the study background. The literature review covers topics such as low-permeability reservoirs, an overview of transport through nanoporous cores, the concept of hydraulic fracturing, the reservoir's petrophysical parameters under review, and the natural gas transport mechanism in porous media.

Chapter 3: This chapter details the research design methodology and experimental procedures, including data collection techniques and tools for manipulation and visualisation. It elaborates on how porosity and permeability were determined and provides calculations for other relevant parameters.

Chapter 4: This chapter focuses on presenting the research results and initiating the discussion. It includes data manipulation, visualisation techniques, and interpretations to facilitate a comprehensive understanding.

Chapter 5: In this chapter, the research concludes by summarising the findings and their implications for industries. Recommendations for further studies are also provided to extend the knowledge in this area.

CHAPTER 2
LITERATURE REVIEW

The preceding chapter provided a concise overview of the study. In this chapter, a comprehensive review of the literature related to low-permeability reservoirs were studied, including shale gas, tight sand, and coalbed methane. The chapter also explores hydrocarbon production from these reservoirs, investigating horizontal drilling, hydraulic fracturing, and enhanced oil/gas recovery techniques. Additionally, nanotechnology and its applications are introduced, and gas transport through nanoporous ceramic cores is examined. Critical parameters influencing gas transport in low-permeability reservoirs are also identified and discussed. The chapter concludes with a summary.

2.1 Description of low permeability reservoirs

The significant shift in the energy sector's focus from conventional to unconventional reservoirs, notably low permeability reservoirs, is a crucial aspect in understanding the evolving landscape of the oil and gas industry. These reservoirs, which include shale gas, tight sands, and coalbed methane, have gained prominence due to their potential to meet growing energy demands. However, their unique geological characteristics pose distinct challenges to extraction processes. Melikoglu (2014) and Bocora (2012) highlight the intricacies of these reservoirs, characterised by their complex pore structures and limited flow capabilities. Khan and Al-Nakhli (2012) further explain the challenges posed by the low porosity and permeability of these formations, underscoring the need for innovative extraction techniques. Arthur and Cole (2014), along with Aguilera and Radetzki (2014), discuss the decline in conventional oil and gas fields and the consequential shift towards exploiting these unconventional resources. They emphasise that the transition is not only a response to diminishing traditional resources but also a reflection of technological advancements facilitating the extraction of hydrocarbons from these complex formations. Soeder (2018) contributes to this narrative by examining how these advancements have reshaped the energy sector.

Low permeability reservoirs harbour substantial reserves of natural gas, a resource that can be harnessed to address the ever-growing global energy demand.

Hongjun et al. (2016) detail the global distribution of recoverable low permeability gas resources, pinpointing 37 countries as key players, with a major concentration in the top ten. The United States tops the list with 39 trillion cubic meters, representing 17.4% of the global total, primarily in shale gas. China, with its substantial reserves of 31 trillion cubic meters (13.9%), mainly comprises shale gas, coalbed methane, and tight gas. Russia and its 29 trillion cubic meters reserve (12.6%) focus mainly on shale gas and coalbed methane. Canada and Australia, each with 16 trillion cubic meters, contribute 7% and 6.4% respectively to the global total, concentrating on coalbed methane and shale gas.

These top four nations collectively account for 57.2% of global unconventional gas resources, with shale gas being the predominant type at 71.1%, followed by coalbed methane (21.7%) and tight gas (7%). This distribution emphasises the leading role of these countries in the realm of unconventional gas, especially shale gas as shown in **Figure 1**

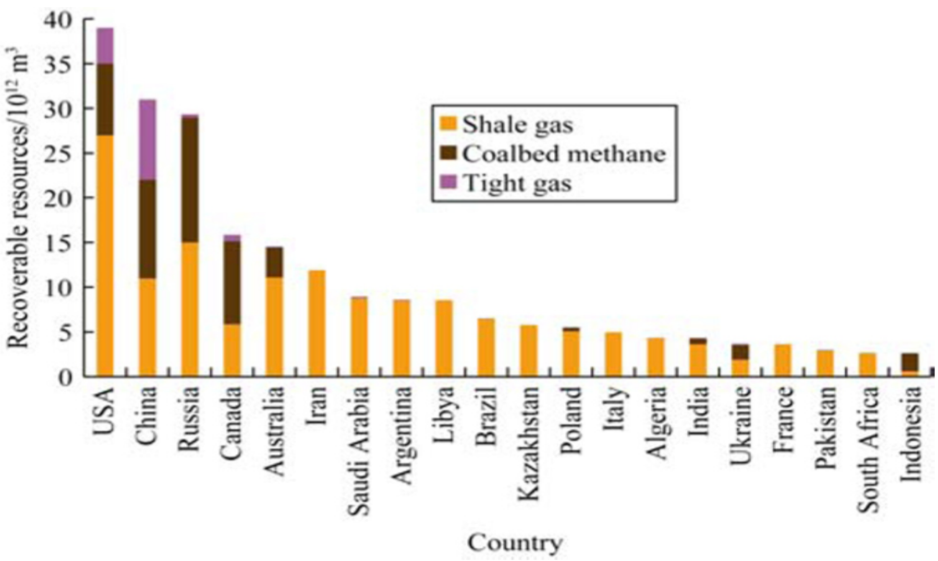

Figure 1 Potential for Recoverable Unconventional Gas Resources in the Top 20 Countries.

The environmental and economic implications of exploiting these low permeability reservoirs are not to be overlooked. Wenrui et al. (2018) discuss the challenges faced in both experimental and commercial contexts due to the low permeabilities of these resources. Zhang et al. (2016) further investigate the complexity of the specific characteristics of these reservoirs, including their porosity and matrix permeability. Liu et al. (2021), Wu et al. (2018), and Yu et al. (2020) underscore various key aspects of these reservoirs, including the geological intricacies and the challenges in fluid extraction and hydrocarbon distribution prediction.

In addressing the complexities of developing these reservoirs effectively, Gao et al. (2019) point out the necessity of specialised techniques, such as hydraulic fracturing, horizontal drilling and enhance oil/gas recovery techniques to liberate hydrocarbons from these reservoirs.

2.1.1 Shale gas reservoir

Bustin (2006) presents a nuanced description of shale gas reservoirs, identifying them as organic-rich, fine-grained unconventional resources. He notes, however, that not all shale formations function as reservoir rocks; some may act as seals or caps for other reservoirs. His analysis focuses on four critical characteristics for defining shale gas plays: the maturity level of organic matter, the nature of the gas (biogenic or thermogenic), the total organic carbon (TOC) in the strata, and the reservoir's permeability index.

Traditionally viewed as potential sources or caps for conventional hydrocarbons, shale formations have recently been redefined as unconventional hydrocarbon reservoirs. Their low permeability and high organic content set them apart from conventional reservoirs, as discussed by Cramer (2008). Shale gas reservoirs exhibit dual modes of gas presence: adsorption in organic matter (similar to coal bed methane) and free gas in the shale matrix pores (akin to conventional reservoirs), necessitating unique exploration and production approaches due to their low permeability.

Han et al. (2020) and Huang et al. (2013) elaborates on the diverse geological and geochemical attributes within organic-rich shale formations, suggesting the need for tailored techniques in drilling, completion, and resource assessment. Shale gas generation can occur via thermogenic or biogenic processes, or a combination of both. Martin et al. (2004) explains that thermogenic gas forms from organic matter cracking or oil secondary cracking, while biogenic gas is produced by microbes in areas with freshwater recharge.

Further detailing shale's geological composition, de Oliveira et al. (2022), Blatt and Tracy (2000) describe it as a fissile terrigenous sedimentary rock, primarily made up of silt and clay particles. The term "fissile" refers to shale's ability to split into thin layers, and "terrigenous" indicates the sediment's origin. Shale reservoirs contain small clay-sized minerals like illites, kaolinites, and smectites, in addition to quartz, cherts, and feldspars. They also feature various other constituents such as organic particles, carbonates, iron oxides, sulfides, and heavy minerals. Speight (2013) further discusses the formation of shale as a result of fine sediment accumulation in calm environments like ancient seas and lakes, underscoring its dual role in petroleum geology as both a source and seal for hydrocarbons.

2.1.2 Coal bed methane

The perception of coalbed methane has undergone a significant shift, as noted by Goraya et al. (2019), Sharon (2014), and Yanda (2014). Previously viewed as a problematic by-product during coal mining operations, its potential as a valuable energy resource has gained recognition in recent years. This re-evaluation emphasises the need for a deeper understanding of coalbed methane's characteristics and the conditions under which it forms.

Ling (2014) and Moore (2012) stress the importance of understanding the genesis of coalbed methane within sedimentary basins. This understanding is instrumental in developing cost-effective methods for exploration and extraction, focusing on factors such as geological settings and the properties of the coal seams. Characterising coalbed methane reservoirs as a type of unconventional gas reservoir, Gao and Schimmelmann (2020), Jack (2014), and Yanjun et al. (2014) discuss their relative simplicity in terms of gas storage and production. These reservoirs function similar to microporous polymers, with a significant portion of gas stored in an adsorbed state on the pore surfaces. This characterisation helps in conceptualising the gas extraction process from these reservoirs. Caineng (2013) expands on this by defining coalbed methane reservoirs as coal-rich formations sharing similar geological attributes and having relatively independent fluid systems. He delineates five distinct boundaries influencing coalbed methane: hydrodynamic, aero-oxidation zone, fault, physical, and lithology boundaries, each playing a role in the distribution and accessibility of coalbed methane.

The dynamics within the hydrodynamic boundary are particularly crucial, as explored by Li et al. (2023) and Wang et al. (2021). The interaction between coalbed methane and the underground water table, including processes like recharge, migration, and drainage, significantly influences methane accumulation.

Gensterblum et al. (2014) highlight the role of fault boundaries in describing the reservoirs, which is determined by the interplay of displacement pressure and reservoir pressure. Yanbin (2019) raises concerns about the limitations of conventional methods used to investigate the petrophysical properties of coal. He advocates for low-field nuclear magnetic resonance (NMR) techniques, which could offer improved accuracy and insights. This innovation is part of a broader trend in the field, where advanced technologies like ceramic nanotechnology are being employed to enhance the accuracy and reliability of data related to coalbed methane exploration and extraction.

2.1.3 Tight sand gas

Aleriza (2014) describes tight sand reservoirs as unconventional hydrocarbon sources, mainly characterised by their significantly low permeability. These reservoirs, often composed of densely packed sandstone or similar rock materials, have minimal pore spaces, hindering fluid movement. Such structural features set tight sand reservoirs apart from their more porous conventional counterparts. According to Sander et al. (2017), tight sand gas reservoirs generally possess porosity below 10% and matrix permeability under 0.1 milli Darcy (mD), requiring advanced methods like hydraulic fracturing and horizontal drilling to extract viable oil and gas from these formations. Zuo et al. (2012) notes that tight gas reservoirs, in the absence of hydraulic fracturing, tend to show low flow rates due to radial flow conditions. However, fracturing treatments can shift the flow mechanism to linear, with the success of this transition depending heavily on the extent of the hydraulic fracture and the quantity of propping agents used.

David (2017) and Hongjun et al. (2016) assert that gas fundamentally differs from oil, and strategies effective in oilfield operations may not apply to tight gas fields. Particularly in tight gas reservoirs, conventional compression techniques might not significantly enhance production due to their low permeability, resulting in a temporary production boost followed by a plateau. Furthermore, Holditch (2006) and Stephen (2006) noted that tight sand primarily yield dry natural gas and emphasise the need for assembling expert teams of engineers and geoscientists to optimise drilling and completion strategies, underlining the importance of well planning and execution for successful development of these reservoirs.

2.2 Hydrocarbon production from low permeability reservoirs

The hydrocarbon exploration and exploitation lifecycle, as described by Ahmed and Meehan (2016), encompasses several phases. Initially, the decision to explore a specific region is made, considering an array of factors such as technical feasibility and economic viability. This is followed by the seismic survey phase and the drilling of exploratory wells. The insights obtained from these activities inform the development strategy, leading to the eventual extraction of commercially viable hydrocarbons. The culmination of this lifecycle is marked by the decommissioning phase, which occurs when a field's economic output declines permanently. This entire process, thoroughly examined by experts like Waples (2013) and Lumpkin and Dess (2001), underlines the complex and multi-faceted nature of hydrocarbon exploration and development as illustrated in **Figure 2.**

The process of discovering hydrocarbons starts with a geological analysis, where geologists study the Earth's composition to identify possible hydrocarbon formations. They use seismic surveys, conducted both onshore and offshore, to gather essential data on the geological characteristics of reservoirs. This thorough exploration is crucial for locating sites worthy of further investigation. Didi et al. (2024) and Sunday et al. (2015) have emphasised the significance of these preliminary efforts in targeting potential hydrocarbon reserves.

Following the initial exploration, exploratory wells are drilled based on the promising indicators from seismic surveys. These wells serve a critical role in ascertaining the viability of the reserves. Through rigorous testing, valuable data is gathered regarding both the quantity and quality of the hydrocarbon contained within these reservoirs. Studies by Liu et al. (2022) and Kuuskraa and Haas (1988) have underlined the importance of these assessments in determining the feasibility of proceeding with extraction efforts. If the findings from these exploratory wells suggest economically viable reserves, further steps are undertaken to tap into these resources.

Yuncong et al. (2014), Qinghai et al. (2013), and Wenbin et al. (2009) highlight how horizontal drilling and hydraulic fracturing have revolutionised the energy industry. These techniques have been instrumental in making the extraction of natural gas from previously unviable reservoirs possible. Furthermore, the development of Enhanced Oil/Gas Recovery (EOR/EGR) methods is an ongoing process that aims to improve the efficiency and minimise the environmental impact of extracting natural gas from low permeability formations. These advancements continue to drive innovation in the field, ensuring more sustainable and effective extraction methods.

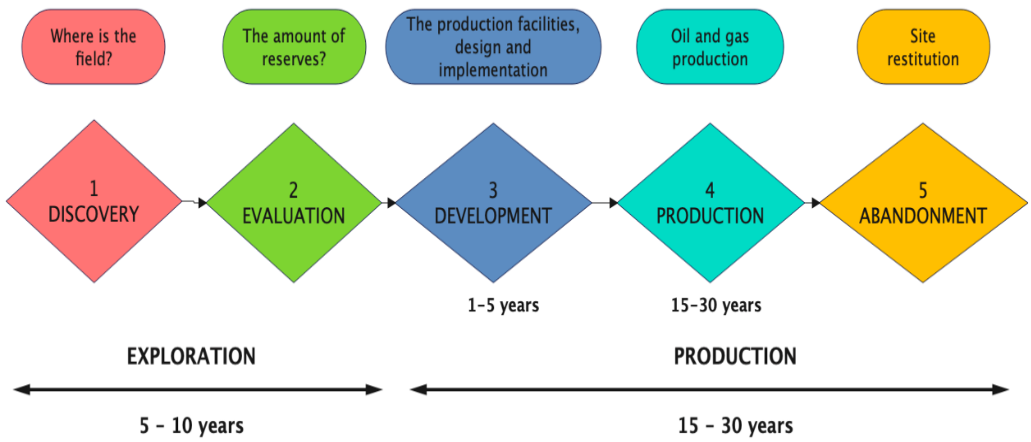

Figure 2 Hydrocarbon exploration and production field life cycle.

2.2.1 Horizontal drilling

The evolution of horizontal drilling in low permeability reservoirs marks a significant turning point in the oil and gas industry, particularly in extracting hydrocarbons from geologically challenging areas. This advanced technique, championed by authors like Kang et al. (2022), Shiyi and Oiang (2018), and Wenrui et al. (2018), differs from traditional vertical drilling by turning the drill bit horizontally after reaching a certain depth as illustrated in **Figure 3**. This approach increases the wellbore's exposure to the reservoir, leading to more efficient extraction.

As highlighted by Qun et al. (2022) and Ma et al. (2016) low permeability reservoirs such as shale formations, tight sands, and coalbed methane are characterised by their dense rock matrices, which limit the natural flow of fluids. The strategic application of horizontal drilling in these settings, as demonstrated in the research by Guo et al. (2019), addresses this challenge by maximising the contact area between the wellbore and the hydrocarbon-bearing formation. This maximised exposure is crucial in formations with restricted fluid flow, allowing for a more efficient extraction process.

The integration of horizontal drilling with hydraulic fracturing has revolutionised the extraction process in these tough geological environments. Hydraulic fracturing, which involves injecting fluids at high pressure to create fractures in the rock, complements horizontal drilling by further enhancing hydrocarbon recovery. Wang et al. (2017) note that this combination not only extends the well's reach but also increases the area contributing to the flow, leading to significantly higher recovery rates.

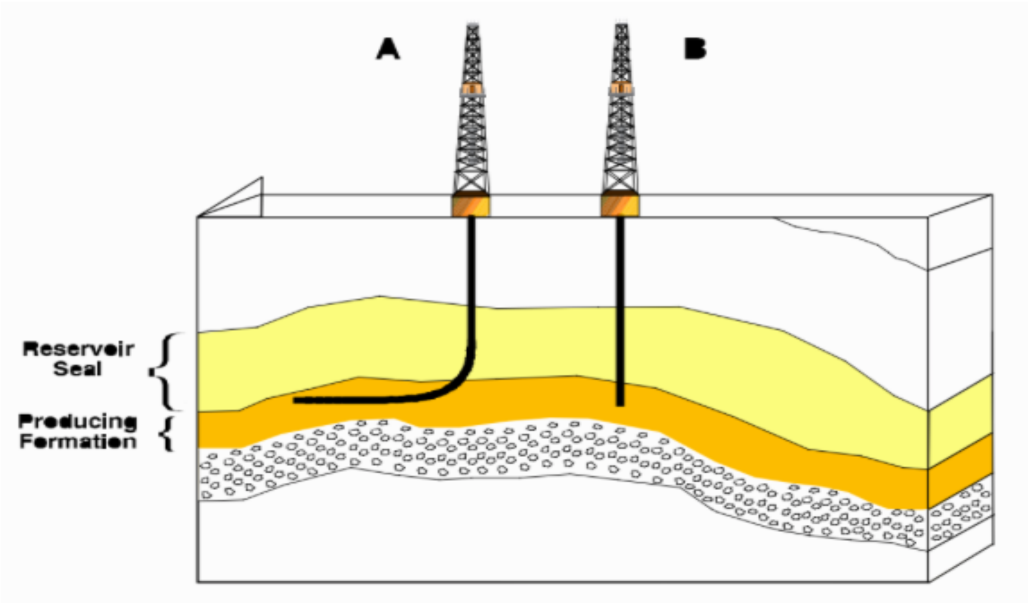

Figure 3 (A) Horizontal drilling (B) Vertical drilling (Vestavik et al. 2010)

2.2.2 Hydraulic fracturing

Hydraulic fracturing, commonly known as fracking, has emerged as a vital technological advancement in the extraction of hydrocarbons from low permeability reservoirs, revolutionising the oil and gas industry. Its development, as explored by researchers such as Qinghai et al. (2013) and Wenbin et al. (2009), has been integral in making the extraction of resources from shale formations, tight sands, and coalbed methane both viable and economically feasible.

Lucas and Ulrik (2013) detail the process of fracking, which involves injecting a high-pressure mixture of water, sand and chemicals into rock formations to create fractures as illustrated in **Figure 4**. These fractures improve the permeability of the rock, thereby enabling more efficient oil or gas flow. Fracking's significance in low permeability reservoirs, particularly evident in the U.S. shale gas boom, was initially recognised in the late 1940s and has been highlighted in the work of Qun et al. (2009). The combination of fracking with horizontal drilling, as discussed by Shen et al. (2021) and Al-Muntasheri (2014), has been transformative, allowing for increased exposure of the wellbore to the reservoir and thus higher production rates. Kaiser (2012) notes the importance of selecting suitable fracking fluids and proppants. These proppants are essential in keeping the fractures open once the injection pressure is released, allowing for sustained hydrocarbon flow.

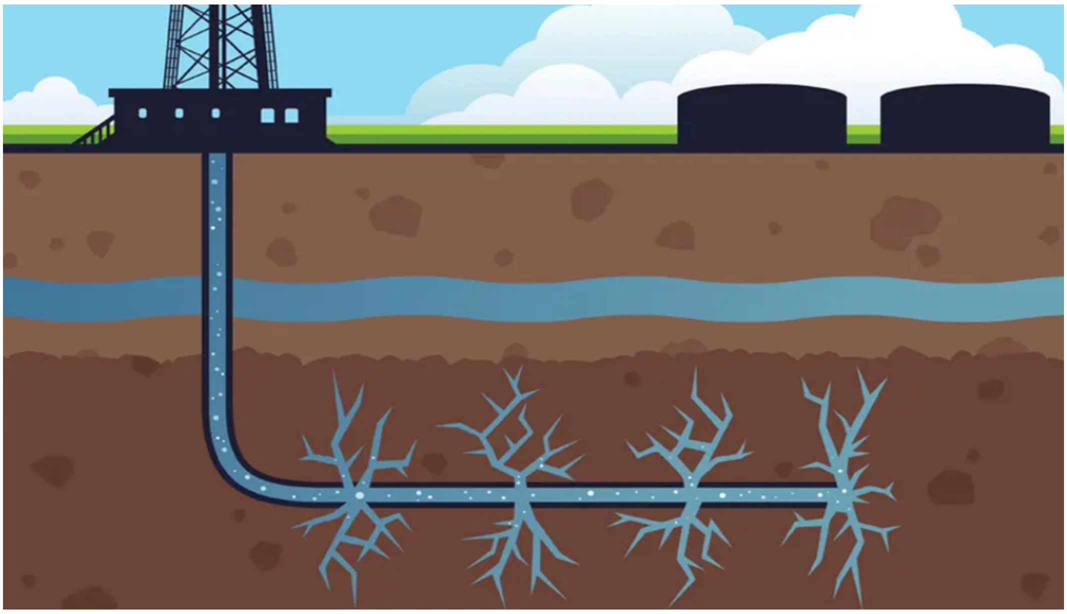

Figure 4 Hydraulic fracturing (Texas Tribune 2011).

2.2.3 Enhance oil/gas recovery

The increasing focus on low permeability oil and gas resources on a global scale signifies a pivotal shift in the energy sector's exploration and production strategies. These resources, once overlooked due to their challenging extraction conditions, are now at the forefront of energy discussions. Despite the use of conventional primary and secondary recovery methods, there remains a substantial quantity of untapped oil in these reservoirs, highlighting the need for more efficient recovery techniques (Kalantari-Dahaghi, 2011).

The response to this challenge has been the advancement of Enhanced Oil Recovery (EOR) and Enhanced Gas Recovery (EGR) techniques. These methods are specifically designed for low permeability reservoirs and aim to significantly boost crude oil and natural gas production. Kang et al. (2022) emphasise that these advancements are key in addressing the hurdles faced in accessing unrecovered oil and gas in these complex reservoirs, suggesting that the future of EOR/EGR lies in continual technological advancement.

2.3 Study of low permeability reservoirs

Research on low permeability reservoirs in laboratory settings is essential for advancing petroleum engineering, focusing on enhancing fluid flow dynamics and improving hydrocarbon recovery from geologically challenging formations (Yakimchuk et al. 2019). Such reservoirs, including tight sandstones and shale formations, are characterised by limited pore connectivity and low porosity, which complicates the extraction of oil and gas, making it both technically challenging and economically strenuous. Laboratory studies frequently utilise physical models and advanced simulation techniques to replicate and analyse the behaviour of fluids within these reservoirs under controlled conditions (Li et al. 2021).

A typical approach in these laboratory studies involves using sand packs and core samples to simulate the porous media of low permeability reservoirs (Wang et al. 2022, Chang Liu, 2022, Ahad et al. 2020). Sand packs are especially valuable for conducting permeability tests, enabling researchers to observe how fluids traverse through these densely packed materials and to identify key factors influencing fluid flow. These experiments range from straightforward water flooding tests to more complex ones incorporating various Enhanced Oil Recovery (EOR) techniques like chemical injection or gas flooding. Insights from these studies are crucial for developing more effective extraction techniques and for predicting the performance of reservoirs under varying operational conditions (Hodge 2002).

For example, Wang et al. (2022) conducted a detailed analysis using sand packs to study the formation and evolution of different micro-facies in the fan delta of the Gaoshangpu oilfield in the Nanpu sag, China. Wang et al. (2022) study sheds light on the genetic mechanisms of low-permeability reservoirs, identifying dominant facies belts and favourable diagenetic sequences critical for the efficient development and evaluation of similar geological settings. Similarly, Chang Liu (2022) explored the ultra-low permeability tight sandstone reservoir properties of the Chang 6 Member in the Huaqing area of the Ordos Basin, focusing on sedimentary-structural characteristics. These insights are pivotal for predicting hydrocarbon enrichment and high-yield areas in such challenging reservoir environments.

In laboratory environments, researchers employ a mix of synthetic and natural samples to mimic the geological conditions of low permeability reservoirs. Core samples extracted directly from the field are especially valuable as they provide the most realistic representation of the reservoir conditions (Shafer 2013). These samples undergo various tests, including stress and strain measurements, porosity and permeability assessments, and fluid injection experiments under different pressure and temperature conditions. Such comprehensive evaluations elucidate how various rock properties, such as grain size, cementation, and clay content, impact fluid flow. Understanding these relationships is essential for predicting how reservoirs will respond to enhanced recovery processes and for designing interventions that maximise oil and gas production while minimising environmental impact (Anovitz and Cole, 2015).

These investigations underscore the complex nature of low-permeability reservoirs and highlight the need for precise and comprehensive modelling to correctly predict their behaviour. The contributions of researchers in this field are fundamental to advancing extraction techniques for challenging reservoir environments, emphasising the importance of both experimental and simulation approaches in the development of effective extraction strategies.

However, these approaches also acknowledge significant limitations. For example, sand packs used in simulations do not fully replicate the complex heterogeneity and structural nuances of actual rock formations. Natural rocks exhibit a wide variety of pore shapes, sizes, and connectivity—factors that significantly impact fluid dynamics but are difficult to significantly model in laboratory settings. Furthermore, the high costs and logistical challenges associated with direct core sample drilling, particularly in deep-water or remote locations, can limit the number of cores obtained, reducing the scope of geological data available for analysis. The time-intensive nature of preparing, testing, and analysing core samples can also delay operational decision-making in dynamic drilling environments. To address these issues, this research explores the application of nanotechnology to overcome some of the constraints faced in reservoir engineering, potentially revolutionising the field by enhancing the application of nanoporous ceramic cores as an alternative for the direct reservoir core sample in studying gas transport behaviour.

2.4 Nanotechnology

Nanotechnology encompasses a broad range of materials and methods used in the development of ceramic cores, covering everything from material selection and core fabrication to characterisation and the design of core modules. It also involves studying the transport phenomena within these cores and optimising their performance, particularly focusing on the mechanical separation processes for both gas and liquid streams (Tawfik and Vinoid, 2016).

As Kanyo et al. (2020) and Tasselli (2015) note, a critical aspect of this field is selecting suitable materials that are tailored for specific applications. The choice of material significantly influences how the core interacts with permeants, impacting the core's transport mechanisms, stability, and overall performance. These cores are constructed from a variety of materials, including organics like polymers and inorganics such as carbons, alumina, zeolites, etc., known for their high thermal stability, robust mechanical strength, chemical resistance, and durable operational properties.

According to Ho and Bum (2017), the effectiveness of porous ceramic materials hinges on three key factors: pore size, overall porosity and permeability. Typically, these materials are composite structures comprising multiple layers, each serving a distinct purpose. The core's architecture usually includes a microporous support layer that provides mechanical strength, an intermediate layer with significantly smaller mesoporous pores that act as a bridge, and a microporous top layer where the primary functions of the core occur (Shehu et al 2019). Materials used in these structures, such as alumina (Al_2O_3), silica (SiO_2), zirconia (ZrO_2), titania (TiO_2), and various metal oxides, are selected to optimise functionality and performance.

Beil and Beyrich (2013) describe ceramic cores as functioning selective barriers between two phases—be it gas, liquid, or vapor. These cores may be either passive or active interfaces that regulate the transport processes between phases. Designed with fine mesh, small pores, and layered materials, these cores are adept at allowing selective passage of molecules and particles, enabling them to retain specific components while permitting others to pass through. This ability to selectively differentiate between components, known as selectivity, is central to the core’s utility in various applications (Ho and Bum, 2017).

These ceramic cores, therefore, play a crucial role in a wide range of industrial and scientific applications, thanks to their ability to control the flow and separation of different substances effectively. The nanoporous ceramic cores are utilised in this research to focus on enhancing these cores' efficiency and adaptability, ensuring they meet the specific demands of emerging technologies and complex industrial processes.

2.5 Advantages of nanoporous ceramic core in Reservoir studies

In this study, synthetic nanoporous ceramic cores are utilised, representing a significant departure from traditional reservoir evaluation methods. These ceramic cores are increasingly being recognised within the scientific community for their distinctive properties and the unique benefits they offer in reservoir evaluation.

Nanoporous ceramic cores have been extensively studied and employed by various researchers such as Liu et al. (2022), Abunumah et al. (2021), Ehdaie et al. (2017), and Teklu et al. (2016), who have documented their advantageous attributes. These include high tensile strength and exceptional durability, which make them resistant to the physical and chemical stresses often encountered in sub-surface environments. Additionally, their cost-effectiveness and energy efficiency make them an attractive option for sustained use in multiple experimental setups and real-world applications.

Furthermore, nanoporous ceramic cores allow for precise control over pore size distribution, a vital factor in the study of fluid transport in porous media. This control helps in significantly simulating the porous structures of natural reservoirs, thereby providing deeper insights into the flow dynamics and transport mechanisms of hydrocarbons.

The ability of nano ceramic cores to withstand mechanical and thermal stresses adds another layer of utility, making them suitable for high-pressure and high-temperature experiments that are typical in studies of natural gas transport. This resilience enables researchers to explore a wider range of conditions and scenarios, thus expanding the boundaries of current understanding and contributing to more effective reservoir studies.

2.6 Gas transport through nanoporous ceramic cores

Pioneering researchers like Dybbs and Edwards (1984) have outlined that fluid transport through porous media is fundamentally governed by principles rooted in continuum mechanics. These principles are crucial for adapting fluid transport processes to meet the challenges of specific and often difficult conditions. Adler (2013) further emphasised that the main theories describing fluid dynamics—applicable to both liquids and gases—through porous media are based on constitutive equations and established engineering principles. These theories are supported by fundamental thermodynamic and conservation laws, including Boyle’s and Charles's laws, and conservation laws such as those of momentum and mass-energy. Other critical theoretical frameworks that inform these theories include Darcy's Law, Material Balance, Hagen–Poiseuille Law, Buckley–Leverett theory, Welge's method, and Fick’s laws, making them especially applicable for studying gas transport in porous media.

Pandey and Chauhan (2001) described gas transport through nanoporous ceramic cores as a multifaceted process influenced by adsorption, diffusion, and capillary condensation. These cores are integral in applications such as gas separation and filtration, featuring a matrix of nano-sized pores that govern molecular-level gas movement. Constructed from materials like alumina, silica, or zirconia, nanoporous ceramic cores offer exceptional thermal and chemical stability. The specific arrangement and size distribution of the pores are crucial, determining the core's selectivity and permeability for different gases (Marchetti and Livingston, 2015).

The efficiency of gas transport through nanoporous ceramic cores is influenced by several factors. The size and uniformity of the pores directly impact the selectivity and flow rate of gases. Higher temperatures tend to increase diffusion and adsorption rates, while pressure differences across the core drive the flow, pushing more gas molecules through the pores. Additionally, the chemical properties of the gas, such as viscosity, and affinity for the core material, significantly affect how it interacts with the pores (Baker, 2023).

2.7 Critical parameters influencing gas transport in low-permeability reservoirs

As postulated by Refe (2000) several factors influenced the transport of gas from low permeability reservoirs. Which include reservoir porosity and permeability, pore pressure and reservoir stress, rock composition and texture, temperature and thermal effect, fracture network and connectivity, fluid properties, reservoir depth and geothermal gradient, technological and operational factors. This research has considered six critical parameters that governs the transport of gas in these challenging reservoirs. These parameters include permeability, mobility porosity, fluid viscosity, operating temperature and pressure conditions.

2.7.1 Permeability

Permeability is the ability of a reservoir rock to transmit fluids through its structure, as stated in the Schlumberger Oilfield Glossary (2021). **Figure 5** offers a visual representation of this concept. Permeability is quantified in Darcies or milliDarcies, a measure established by Henry Darcy (1856), who drew parallels between heat transfer and fluid flow in porous media.

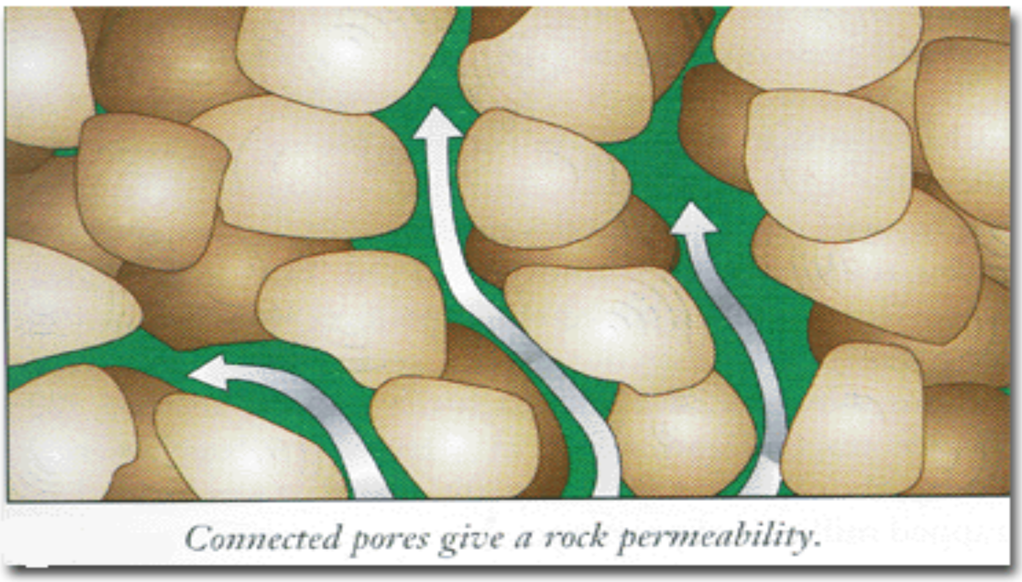

Figure 5 Reservoir permeability schematic (MPG 2003).

Permeability is particularly critical in sandstone formations, which typically feature large, well-connected pores that facilitate the flow of fluids. Conversely, shales and tight sands, with their finer grains and less interconnected pores, are regarded as less permeable. Understanding these properties is essential for the successful extraction of natural gas from such challenging environments (Pan and Connell, 2015). Studies like those by Gensterblum et al. (2015) emphasise the importance of choosing the right experimental techniques to measure permeability in ultra-low permeability rocks, which can be time intensive.

Advanced techniques for measuring permeability, like the steady-state and unsteady-state methods reviewed by Regina et al. (2017), play a critical role in this context. Although unsteady-state techniques, which include various pressure decay methods, are favoured for their speed and accuracy, the complexity increases as permeability decreases. Field tests often provide the most reliable permeability measurements, accounting for the natural conditions of the reservoir (Wasaki and Akkutlu, 2015). Such comprehensive assessments are essential to understand the flow dynamics in low permeability reservoirs and to devise appropriate strategies for their development.

This study identifies permeability as a key reservoir parameter, adopts Darcy's equation for its determination and correlates it with other factors such as porosity, viscosity, temperature, and pressure-drop to assess their impact and align with existing literature. Consequently, the research investigates permeability in the nanoporous ceramic cores and compares it with the permeability observed in oil fields that have undergone gas (CH_4 and CO_2) injection. The aim is to determine the extent to which ceramic porous media can serve as an analogue for permeability studies in hydrocarbon reservoirs.

2.7.1.1 Darcy's law

Numerous equations are utilised in the industry for PVT analysis and the evaluation of reservoir flow regimes. These equations have been thoroughly examined, and a thorough selection process was employed to determine the appropriate equations for application at various stages of the research. The most frequently used are categorised into three primary groups: those based on experimental results, such as Darcy's (1856) and Poiseuille's (1940) equations; those derived from analytical or semi-analytical models, like the Martin-Hou (MH) and the Buckley-Leverett fractional flow model for fluid dynamics, as well as Welge's equation; and those formulated from numerical models. Additionally, others like Fick's, Navier-Stokes, Euler's, Bernoulli's, and Poiseuille's equations are also employed in various studies. Lukaszewicz and Kalita (2016) have documented their use of the Navier-Stokes equation in fluid flow studies. Similarly, Titze et al. (2015) utilised Fick's equation in research focused on hydrocarbon recovery and utilisation technologies. Certain equations, such as the Martin-Hou (MH), necessitate that researchers estimate or approximate specific constants and parameters, as noted by Bai-Gang et al. (2012).

This study predominantly relied on the Darcy's law, originally formulated by Henry Darcy in 1856, due to its clear methodology and the straightforwardness of directly measuring its variables in laboratory settings. Darcy's original experiments, which led to the formulation of the Darcy equation, were conducted by observing the flow of water through beds of sand, leading to insights that have profoundly influenced hydrodynamics. The equation he derived, often visualised in educational materials as the linear Darcy Flow model, shows the direct relationship between the volumetric flow rate and variables such as viscosity, permeability, and pressure gradient as shown in **Figure 6**.

This quantitative model, expressed mathematically in **Equation 1**, serves as a foundational principle in the study of fluid dynamics within porous materials. It highlights the predictable nature of fluid flow in engineered and natural systems, facilitating the design and optimisation of systems for water management, oil recovery, and in the environmental engineering sectors where fluid migration through substrates is relevant.

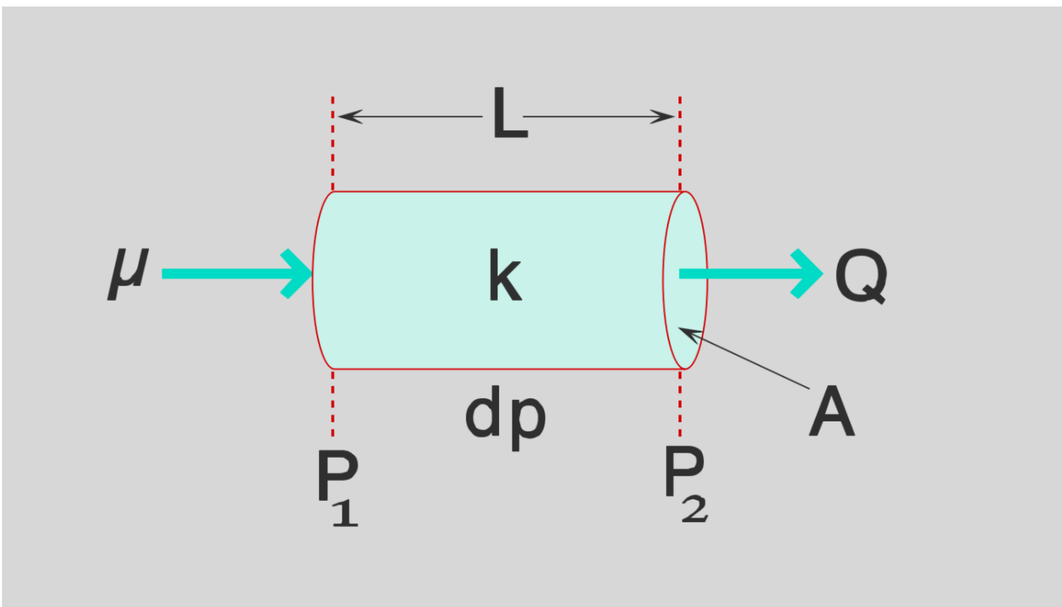

Figure 6 Diagram of linear Darcy flow through a porous media.

$$Q = -\frac{k.A}{\mu}\frac{dp}{dl} \quad (1)$$

Where:

Q is the volumetric flow rate in $cm^3.sec^{-1}$.
k is the permeability in mD.
A is the cross-sectional area of the porous media in cm^2.
μ is the fluid viscosity in cp.
$\frac{dp}{dl}$ is the pressure gradient across the porous medium in $atm.cm^{-1}$.

2.7.1.2 Adaptation of Darcy equation

Numerous early researchers, including Swartzendruber (1962), Yu-shu and Karsten (1996), and Wada et al. (1985), have proposed and implemented several adaptations of the original Darcy (1856) equation, which describes single-phase linear flow, to analytically address various reservoir challenges. Buckley and Leverett (1942) expanded upon Darcy's framework by incorporating a capillary pressure term in conjunction with material conservation principles to better characterise fluid dynamics in complex reservoirs. Alternatively, Welge (1952) removed the capillary terms from the Buckley-Leverett formulation and introduced a graphical method to estimate oil production based on fluid saturation levels.

Yu-shu and Karsten (1996) further refined the equation to include additional parameters such as permeability and viscosity, extending its applicability to two-phase flow conditions under a single-phase framework. Additionally, the Darcy equation has been adapted to facilitate the development of numerical simulators; for example, Pruess (1991) utilised an extension of Darcy's law to create a simulator capable of describing multiphase fluid dynamics.

In this study, the Darcy equation was specifically modified to determine the permeability of the nanoporous ceramic cores, taking into account the radial flow observed in the experimental setup and the use of compressible fluids (gas).

2.7.1.3 Modification of Darcy's equation for radial flow

Equation 1 describes flow through linearly configured porous media. In this study, however, a tubular core was utilised where the flow follows a radial path. Consequently, **Equation 1** requires modification to suit radial flow dynamics. This modification addresses the flow through media characterised by internal and external radii r_2 and r_1, respectively, and height h respectively, as depicted in **Figure 7**. The adapted form of the Darcy equation will accommodate the geometrical configuration of the radial pathway.

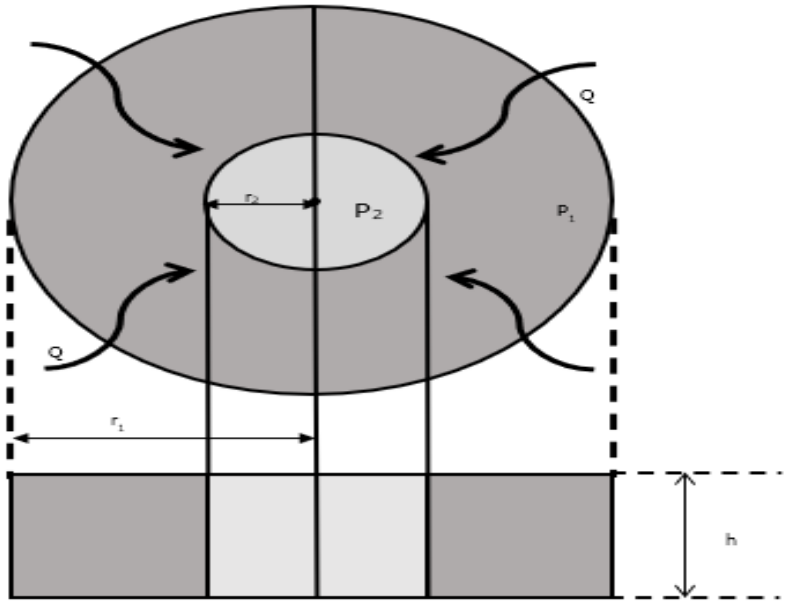

Figure 7 Schematic depicting radial flow directed towards the core.

Note that the area, A, in the radial configuration is represented as $2\pi rh$, transforming **Equation 1** into **Equation 2**. However, **Equation 4** assumes the fluid is incompressible, whereas this study involves gases, which are compressible. Therefore, it is necessary to derive a version of the Darcy equation that accommodates compressible fluids.

$$Q = -\frac{k.2\pi rh}{\mu}\frac{dp}{dr} \quad (2)$$

2.7.1.4 Adaptation of Darcy equation for compressible fluid

Liu et al. (2018), Li and Horne (2001b) have developed a modified version of the Darcy equation specifically tailored for the flow of compressible fluids such as gases as presented in **Equation 3.**

$$Q_g = -\frac{K_g A dP}{\mu_g L}\frac{P_m}{P_{atm}} \tag{3}$$

Where:

Q_g is the flow rate of the gas in $cm^3.sec^{-1}$;

K_g is the gas phase permeability in mD;

μ_g is the gas phase viscosity in cp;

P_m is the mean pressure in atm;

P_{atm} is the atmospheric pressure in atm;

dP is the pressure differential across the core in atm;

A is the cross-sectional area of the core in cm^2;

L is the length of the core in cm.

Equation 3 incorporates P_m and P_{atm} into the traditional Darcy equation (**Equation 1**), suggesting that gas mobility is inversely related to the average pressure. Notably, many formulations of the Darcy equation omit temperature considerations, which is a critical factor given the temperature sensitivity of gas behaviour. Kuuskraa (1982) incorporated a temperature component in his research on gas flow, although the derivation details were not disclosed. This modification is grounded in the principles of the ideal and combined gas laws, encompassing both Boyle's and Charles's laws as outlined by Slider (1983).

$$PV = znRT \tag{4}$$

Where:

P is the pressure in atm

V is the gas volume in cm^3

z is the compressibility factor of gas and is dimensionless n is the number of moles in mol

R is gas constant in $J.mol^{-1}K^{-1}$

T is temperature in K

Rearranging **Equation 6** results in the following expression:

$$\frac{PV}{zT} = nR = Constant \tag{5}$$

It can be deduced that for any two conditions involving variations in pressure, temperature, and volume, the product 'nR' remains constant. Given that gas properties might be assessed under various non-standard conditions relevant to engineering applications, it is essential to normalise these measurements to standard operating conditions. Examples of these include laboratory settings and actual reservoir conditions. Based on **Equation 5**, we can establish the following correlation:

$$(\frac{PV}{zT})_{res} = (\frac{PV}{T})_{std} = Constant \tag{6}$$

The subscripts 'res' and 'std' refer to reservoir and standard conditions, respectively.

Considering the volumetric rate, **Equation 6** is expressed as follows:

$$\frac{PQ}{zT} = \frac{P_{std}Q_{std}}{T_{std}} \tag{7}$$

For simplicity, the subscript 'res' has been omitted from the expression on the left side of **Equation 7**

Rearranging the formula to solve for Q, the reported volumetric flow rate, the expression becomes:

$$Q = \frac{zP_{std}Q_{std}}{T_{std}} \frac{T}{P} \tag{8}$$

Inserting the value for Q into **Equation 2** results in:

$$\frac{zP_{std}Q_{std}}{T_{std}}\frac{T}{P} = \frac{k.2\pi rh}{\mu}\frac{dp}{dr} \tag{9}$$

Solving for the volumetric flow rate at the standard condition the expression becomes:

$$Q_{std} = \frac{k.2\pi hT_{std}}{z\mu TP_{std}}\frac{Pdp}{dr} \tag{10}$$

Equation 10 can be rearranged to give:

$$Q_{std}\frac{dr}{r} = \frac{k.2\pi hT_{std}P}{z\mu TP_{std}}dp \tag{11}$$

Integrating both sides of **Equation 11**:

$$Q_{std}\int_{r_2}^{r_1}\frac{dr}{r} = \frac{k.2\pi hT_{std}}{z\mu TP_{std}}\int_{P_2}^{P_1}Pdp \tag{12}$$

Considering the boundary conditions:

r_1 and r_2 represent the external and internal radii of the flow path, respectively, aligned with the direction of increasing pressure. Consequently, leading to the omitting of the negative sign in the original Darcy equation.

P_1 and P_2 denote the pressures at the injection and exit points, respectively. Furthermore, the integration of P will result in a factor of 2 in the denominator, cancelling out the 2 in the numerator

$$Q_{std}\,In\,\frac{r_1}{r_2} = \frac{k\pi hT_{std}(P_1^2 - P_2^2)}{z\mu TP_{std}} \tag{13}$$

In many laboratory settings, including those of this experiment, zμ can be regarded as constant across a range of pressure conditions, as suggested by published works from Zhuang (2020). Ahmed and Meehan (2012) along with John (2007) have documented experimental results showing that zμ remains constant at pressures below 2000 psi (136 atm). Given that this study was conducted under

3atm pressure and was designed as a comparative analysis, **Equation 13** can be further simplified.

$$Q_{std} = \frac{k}{\mu} \frac{\pi h T_{std}}{T P_{std}} \frac{(P_1^2 - P_2^2)}{In \frac{r_1}{r_2}} \tag{14}$$

Equation 14 reflects the formula presented by Kuuskraa in 1982. The volumetric flow meter utilised in this research is calibrated to standard conditions of pressure (P_{std}) and temperature (T_{std}) at 1 atm and 273 K, respectively, as specified by the manufacturer. Given that the experimental procedure maintains isothermal conditions, ensuring uniform temperature throughout the system, substituting these standard values into Equation 16 results in the following expression:

$$Q_{std} = \frac{k\pi h}{\mu} \frac{(P_1^2 - P_2^2)}{In \frac{r_1}{r_2}} \tag{15}$$

Further solving for k will give:

$$k = \frac{Q_{std}\,\mu}{\pi h} \frac{In \frac{r_1}{r_2}}{(P_1^2 - P_2^2)} \tag{16}$$

Where:

Q_{std} is the volumetric flow rate in $cm^3.sec^{-1}$.

k is the permeability in mD.

μ is the fluid viscosity in cp.

h is the height of the core in cm.

r_1 and r_2 are the external and internal radii respectively.

P_1 and P_2 denote the pressures at the inlet and outlet respectively.

2.7.2 Mobility

Mobility, as defined by Heidari (2019), is a key parameter in the study of fluid dynamics within porous media, quantifying the ease with which a fluid traverses a porous material. It is calculated as the ratio of permeability to fluid viscosity, typically expressed in units of Darcy per centipoise (D/cp) or milliDarcy per centipoise (mD/cp). This parameter is critically important across various fields including petroleum engineering, hydrogeology, and environmental engineering, significantly impacting the efficiency of processes such as oil recovery, groundwater management, and contaminant transport.

Mobility is a combinatorial reservoir quantity in that it is determined by both the intrinsic properties of the fluid, such as viscosity, and the characteristics of the porous medium, such as permeability (Zhou and Thakur 2020). The relationship between these factors is straightforward: higher permeability coupled with lower viscosity leads to greater mobility, facilitating fluid movement. This interaction is fundamental for designing effective extraction strategies, managing reservoirs efficiently, and implementing environmental remediation at contaminated sites (Tran and Nguyen 2019). The theoretical basis of mobility is anchored in Darcy's Law, which describes how fluids flow through porous substrates.

In practical applications, particularly in enhanced oil recovery (EOR) scenarios, understanding and manipulating mobility is essential for selecting the most effective recovery methods. For example, a higher mobility ratio of oil to water can enhance displacement efficiency, leading to increased oil recovery rates. Conversely, scenarios characterised by low mobility may require interventions such as hydraulic fracturing to improve the reservoir's flow characteristics (Dullien, 1992). However, implementing mobility-focused strategies can be complex. As Satter and Iqbal (2015) note, several factors can complicate the straightforward application of mobility concepts. The complexity of pore structures, the interaction between fluids and the rock matrix, and varying operational conditions like temperature and pressure all significantly influence mobility. Temperature variations, for example, typically decrease oil viscosity, potentially enhancing mobility, whereas increased pressure can compress the pore structure, reducing both permeability and mobility, as discussed by Lake and Fanchi (2006).

In the study, mobility was adopted as an objective function because of its combinatorial qualities, enabling the research to essentially couple field and experimental data. Based on extant literature, fluids with relatively lower viscosity are expected to engender comparatively higher mobility in both field and experimental data. Consequently, in this study, we investigated the mobility of field data and experimental data of common gases (CH_4 and CO_2) in reservoir hydrocarbon recovery. The extent of the coupling determines how significant nanoporous ceramic core samples can be used to mimic reservoir core samples.

2.7.3 Darcy flux (Darcy velocity)

Reservoir flux also known as the Darcy velocity (Woessner and Peter, 2020), is a critical concept in reservoir engineering and geosciences. It refers to the flow of fluids per unit area—such as oil, gas, and water—through the porous media. This flow is driven by various forces and influenced by multiple factors, which together determine the efficiency and behaviour of fluid extraction from subsurface reservoirs (Agosti et al. 2015). Understanding reservoir flux is essential for optimising hydrocarbon recovery, managing reservoir pressure, and ensuring the long-term sustainability of the reservoir (Ahmed, 2018).

According to Dake (2001), fluid properties, including type, viscosity, density, and compressibility, significantly impact reservoir flux. Different fluids exhibit distinct flow behaviours through porous rocks, influencing overall reservoir performance. Similarly, the properties of the reservoir rock, such as permeability and porosity, are fundamental in determining the ease with which fluids can flow. High-permeability rocks allow for more straightforward fluid flow, while high-porosity rocks can store larger volumes of fluids (Lake and Fanchi, 2006). The pressure gradient is another primary driver of fluid flow in reservoirs; higher pressure differences between two points result in a higher flow rate of fluids. This gradient is influenced by natural reservoir pressure and any artificial pressure applied through injection wells (Craft et al. 2014). Temperature also plays a crucial role in reservoir flux by affecting fluid viscosity and, consequently, flow rates. Higher temperatures typically reduce oil viscosity, enhancing fluid mobility (Holstein, 2007).

Measurement and analysis of reservoir flux involve various techniques. Core sample analysis in laboratories provides detailed information about permeability, porosity, and fluid flow characteristics (Liu et al. 2022). Well testing, including drawdown and buildup tests, estimates reservoir properties and fluid flow dynamics in the field (Zhuang et al. 2020). Advanced reservoir simulation models integrate geological, petrophysical, and fluid properties to predict fluid flow behaviour under various production scenarios (Craft et al. 2014). Continuous reservoir surveillance, including production data monitoring and 4D seismic surveys, helps manage reservoir flux in real time (Jahns, 2001).

This study adopts flux as a key reservoir parameter and relates how various factors influences its behaviour. Alfarge et al. (2020) pointed out that understanding reservoir flux is crucial for enhanced oil recovery (EOR) techniques, which aim to maximise hydrocarbon recovery by modifying fluid flow dynamics. Effective reservoir management relies on knowledge of reservoir flux to extend reservoir life and optimise economic returns (Lake and Fanchi, 2006). Monitoring and controlling reservoir flux is also essential for minimising environmental risks, such as subsurface contamination and unintended migration of injected fluids (Bachu, 2008). In unconventional resources like shale gas and tight oil, reservoir flux analysis is vital due to the complex nature of the porous media and the need for advanced stimulation techniques to enhance fluid flow.

2.7.4 Quality index

The Quality Index (RQI) is a crucial parameter in reservoir studies, employed to evaluate and quantify the quality of a reservoir rock. This index integrates various geological and petrophysical properties to provide a comprehensive measure of the reservoir's capacity to store and transmit fluids such as oil, gas, and water. (Abouzar and Behzad, 2022).

As documented by Kausik et al. (2015), several factors influence the RQI, including porosity and permeability, grain size and sorting, cementation and compaction, mineral composition, and pore throat size and distribution. The types of minerals present in the reservoir rock influence its mechanical properties and fluid interactions, with rocks composed of minerals like quartz typically having higher porosity and permeability compared to those with significant clay content (Chevalier et al. 2013).

The RQI is vital in various aspects of reservoir characterisation and management. It helps identify high-quality reservoir zones likely to yield higher hydrocarbon recovery and assists in mapping the spatial distribution of reservoir properties, aiding in developing more accurate geological models (Craft et al. 2014). In enhanced oil recovery (EOR) techniques, the RQI helps determine the most effective methods for improving oil extraction from reservoirs. High RQI values are more likely to respond positively to EOR methods such as water flooding, gas injection, or chemical EOR. The RQI is used as an input parameter in reservoir simulation models to predict fluid flow behaviour and recovery potential under different production scenarios, improving the reliability of simulation results (Mirzaei-Paiaman and Ghanbarian, 2022.).

Moreover, the RQI informs decisions regarding well placement and drilling strategies. Wells are strategically located in areas with higher RQI to maximise production efficiency and economic returns. By providing insights into reservoir quality, the RQI aids in the economic evaluation of exploration and production projects, helping estimate recoverable reserves and assess the feasibility of development plans (Zhou and Kamal 2019).

The research takes into account the importance of RQI in reservoir management and has investigated parameters that could impact on the RQI using experimental data coupled with field data.

2.7.5 Porosity

Ezekwe (2011) describes porosity as the ability of a reservoir rock to store fluids, including water, gas, or oil, expressed as a percentage ratio of the pore volume to the total volume of the rock. It is a geometric property of the rock, which depends on factors such as grain size, shape, and the arrangement and distribution of these grains as illustrated in **Figure 8**. These aspects are critical for assessing a reservoir's capability.

Mathematically,

$$Porosity\ (\emptyset) = \frac{Reservoir\ pore\ volume\ (Vp)}{Reservoir\ bulk\ volume\ (Vb)} \tag{17}$$

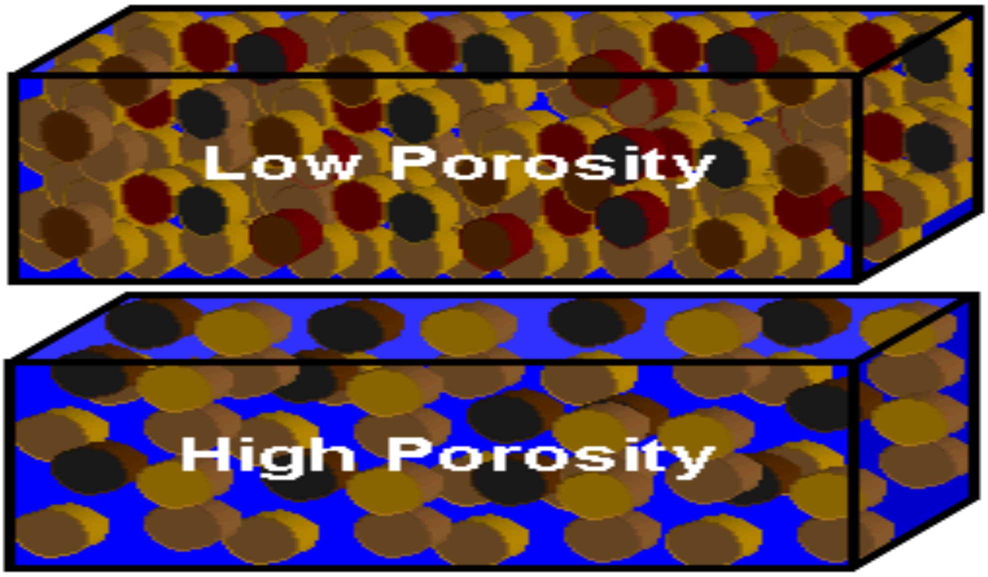

Figure 8 Diagram of porosity showing grain effect (Alberta 2013).

Porosity stands as a crucial characteristic that significantly impacts the physical properties of materials, encompassing attributes like density, thermal conductivity, and strength. Given the intricate and diverse nature of porous materials, a plethora of experimental techniques have been developed to effectively characterise them. Previous research endeavours have dedicated substantial efforts to create and enhance various porosity assessment methods. For instance, Sulistyo and Rizky (2018) explored porosity control in ceramic materials during manufacturing by employing pore formers. They assessed the ceramic products' porosity using the Archimedes method and scanning electron microscopy. Möri et al. (2021) quantified the porosity of crystalline rocks through in situ and laboratory injection methods. Maurya et al. (2019) harnessed genetic algorithms to characterise reservoirs solely from seismic data, demonstrating the effectiveness and applicability of genetic algorithms in reservoir characterisation.

Consequently, a spectrum of approaches has emerged and evolved, each with its unique advantages and limitations based on distinct physical principles. For instance, image analysis evaluates both open and closed porosity but lacks the capacity to distinguish between the two. Archimedean porosimetry offers a cost-effective means of measuring open porosity but does not provide detailed information regarding pore size, shape, or distribution. Conversely, mercury porosimetry furnishes precise results concerning open porosity but is relatively harsh on samples, making it commonly employed for comparison and correlation (Andre, 2000).

In this research, the method employed for porosity determination relies on the concept of Archimedes' buoyancy, widely regarded as the most used technique for this purpose. The procedure entails fully submerging the porous sample in a beaker of fluid mostly water over an extended duration to ensure complete filling of the interconnected porous network by the fluid. A specialised beam balance kit, facilitating the weighing of samples in both air and fluid without altering the balance's configuration, is employed. Knowledge of the fluid's density is noted to facilitate the calculation. The change in weight of the sample before and after immersion is measured to determine the pore volume, obtained by dividing this change by the density of the fluid.

2.7.5.1 Engineering basis for porosity

Several researchers have established theoretical and empirical relationships between porosity and how it influences permeability and mobility. For instance, Mohammed et al. (2019) and Zhao et al. (2018), highlighted that higher porosity indicates a greater capacity of the reservoir to retain fluids and thus a higher flow rate, whereas lower porosity suggests limited storage capacity. Tiab and Donaldson (2024) offer an extensive review of petrophysical properties of a porous media, explaining how porosity may not directly correlate with permeability due to factors like pore connectivity and rock fabric. Zoback (2010) further discusses how geological stress factors and rock mechanics can complexly influence permeability, often disconnecting it from porosity in environments under stress. Similarly, the research conducted by Anovitz and Cole (2015) examines the behaviour of porosity and permeability under varying stress conditions, illustrating instances where increased porosity does not necessarily lead to higher permeability due to alterations in pore structure and alignment.

Research by Hommel et al. (2018) introduces a perspective based on fluid dynamics, noting that variables such as fluid properties and interfacial phenomena can separate porosity from permeability in specific situations. Alabi (2011) provide insights into fluid flow in heterogeneous porous media, showing that local variations in porosity do not consistently impact overall permeability owing to structural complexities. Additionally, the foundational principles established by

Darcy (1856) continue to influence contemporary models of fluid flow, underscoring the intricate interactions between porosity and permeability.

Blunt (2017) offers an extensive review of fluid dynamics within porous media, addressing everything from basic properties like porosity to the complex interactions that influence fluid mobility. His work supports the notion that higher porosity alone does not necessarily lead to increased mobility, highlighting how porosity interplays with other physical characteristics of the media to affect fluid movement. Civan (2016) investigates the intricate dynamics between porosity, permeability, and mobility in porous formations. His comprehensive discussion on formation damage adds depth to the understanding that mobility does not always linearly correlate with porosity, offering practical insights and empirical data that align with a trend in which porosity has a negligible influence on mobility.

On the other hand, Westkämper (2018) presents scenarios where increased porosity significantly boosts fluid mobility, suggesting that under specific conditions, the relationship between porosity and mobility might be more pronounced. Heidari (2019) explores how porosity changes under stress conditions can directly and substantially affect fluid mobility, challenging the notion of a minimal relationship between these factors. Furthermore, Zhou and Thakur (2020) examine how porosity alterations due to temperature and pressure variations can critically impact fluid mobility, providing a contrasting viewpoint.

This study uses porosity as a key parameter and investigates its correlation and influence on permeability and mobility, aiming to align the findings with these established studies.

2.7.6 Viscosity

Fluid viscosity is a measure of a fluid's resistance to flow, defined as its internal friction when subjected to shear stress (Beggs 1987). To understand viscosity, imagine a fluid confined between two plates—one stationary and the other moving at a constant velocity V. Viscous fluids resist changes in velocity by generating friction between their molecules. This characteristic is vital for determining the effort required to manipulate fluids in applications such as lubrication, pipeline transport, and in processes like spraying, injection moulding, and surface coating (Sanjari et al. 2011). Generally, fluids display a direct proportionality between shear strain rate and the shearing stress causing flow. This ratio, known as dynamic or absolute viscosity, typifies Newtonian fluids, named after Sir Isaac Newton, who formulated this concept.

Historical and recent research, including studies by Kadoya et al. (1985) and Jarrahian and Heidayan (2014), have noted that gases increase in viscosity with temperature due to more frequent molecular collisions as kinetic energy rises. Conversely, the viscosity of liquids decreases with temperature, facilitating easier flow. For instance, water's viscosity at 27°C (81°F) and 77°C (171°F) measures 0.85×10^{-3} and 0.36×10^{-3} pascal-second, respectively, whereas air's viscosity at these temperatures is 1.85×10^{-5} and $2.08 \times 10^{-}$ pascal-second.

Mamudu et al. (2015) found that oil recovery improves as the viscosity ratio between water and oil decreases during displacement processes. Azad and Ehsan (2014) extensively studied natural gas viscosity in relation to temperature, pressure, and composition, finding that gas viscosity generally increases with temperature at low to moderate pressures. Precise determination of gas viscosity is essential for efficient gas management, as it impacts various engineering calculations.

Heidaryan et al. (2011) pointed out that experimental techniques like vibrating cables, capillary tubes, rolling ball, or falling ball viscometers offer reliable measurements of natural gas viscosity. Although using density-based methods for calculating viscosity is highly accurate, it requires data on the compressibility factor under various pressure and temperature conditions, which can affect measurement accuracy.

Furthermore, Azad and Ehsan (2014) developed an innovative model for estimating the viscosity of light hydrocarbon gases mixed with heavy and non-hydrocarbon components. This model, based on the principle of corresponding states, can significantly predict viscosity across a broad spectrum of pressures, temperatures, and compositions. The fluid viscosity values for this study were obtained from already established literatures.

2.7.6.1 Engineering basis for viscosity

A range of authoritative sources from fluid dynamics and petroleum engineering have been drawn to provide both theoretical and empirical frameworks for the relation between viscosity, permeability and mobility. Notable research like that of Bear (2013) suggests that increased fluid viscosity does not necessarily impede the permeability of porous filtration media, such as the core samples used in this research. This implies potential adaptations in water treatment processes to handle more viscous fluids without sacrificing efficiency. Dullien (2012) delivers a detailed examination of fluid transport in porous media, highlighting how the interaction between fluid viscosity and material microstructure can occasionally boost permeability, defying conventional expectations. This insight is invaluable for chemical engineers tasked with designing reactors and separators.

Bird et al. (2002) discuss how fluid viscosity can enhance flow through porous media under specific geometric or pressure conditions, postulating a positive correlation between viscosity and permeability. Conversely, Mills et al. (2013) supports the traditional notion that higher viscosity generally restricts flow, suggesting that positive correlation may be unique to the specific properties of the media tested or may involve additional influencing factors not usually considered. Meanwhile, Lake (1989) explores various enhanced oil recovery methods where manipulating fluid properties, including viscosity, proves beneficial, lending support to the notion that higher viscosity can enhance permeability in reservoir rocks.

Muskat's (2020), built upon earlier foundational works, investigates into modern applications and experimental validations of theories concerning fluid flow through porous media. It specifically addresses how increases in fluid viscosity impact mobility. He finds that mobility reduces as the viscosity increases. Civan (2016) comprehensive guide on formation damage thoroughly discusses how fluid properties, including viscosity, influence permeability and mobility within reservoir engineering, offering both empirical data and theoretical models. This is complemented by Li and Horne's (2018) work, which provides in-depth analyses of the viscosity-mobility relationship under conditions typical of enhanced oil recovery, closely mirroring the trend where mobility increases as the viscosity deceases. Furthermore, Green and Willhite (2018) and Alfarge et al. (2020) affirm that an uptick in fluid viscosity generally leads to decreased mobility, a trend consistent with other authors. However, the studies by Tran et al. (2019) and Zhou et al. (2021) introduce a different perspective, suggesting that in certain scenarios, such as within fractured reservoirs or at a micro-scale, increased viscosity might not necessarily hinder and can sometimes enhance fluid mobility.

These observations underscore the complexities of fluid behaviour in porous media.
This research is designed to investigate the viscosity influence on permeability, mobility and aligning the findings to these established empirical and theoretical bases.

2.7.7 Operating condition (temperature and pressure condition)

The optimal temperature and pressure conditions for gas migration in a low permeability reservoir will vary depending on the specific characteristics of the reservoir and the gas being extracted. However, in general, higher temperatures and pressures tend to facilitate faster and more efficient gas migration through the reservoir (Hirofumi et al 2023). At higher temperatures, gas molecules possess greater kinetic energy, making them more likely to move through the rock, enabling easier flow through the reservoir. Similarly, high pressure causes gas molecules to be tightly packed together, creating a stronger driving force for gas migration. High pressure can also increase the permeability of the rock, allowing gas to migrate more readily (Bishnupriya and Modak 2023).

It's important to note that in hydraulic fracturing, the injected pressure is often much higher than the pressure at which gas is produced. Therefore, the pressure at which the gas is produced is not the sole factor affecting migration. It is crucial to carefully balance temperature and pressure conditions to achieve optimal gas migration while preserving the reservoir's integrity, as high temperature and pressure can make the rock more brittle and increase the risk of fractures and damage (Gajda et al. 2023).

In the industry, High Pressure, High Temperature (HPHT) wells refer to wells requiring pressure control equipment with a rated working pressure exceeding 69 MPa and having a bottom hole temperature above 150°C (300°F). Some wells even operate at Ultra HPHT conditions (205°C, 138MPa) or Extreme HPHT conditions (260°C, 241MPa) due to advancements in exploration, extraction, and production, as shown in **Figure 9** (Fluorocarbon 2017). In this study, we deliberately selected a temperature range that encompasses the typical spectrum of reservoir temperatures. The pressure range was chosen to include both low and high-pressure laboratory conditions, which can be interpolated to real reservoir conditions. This approach mitigates the environmental risks associated with operating at true reservoir pressures in laboratory settings.

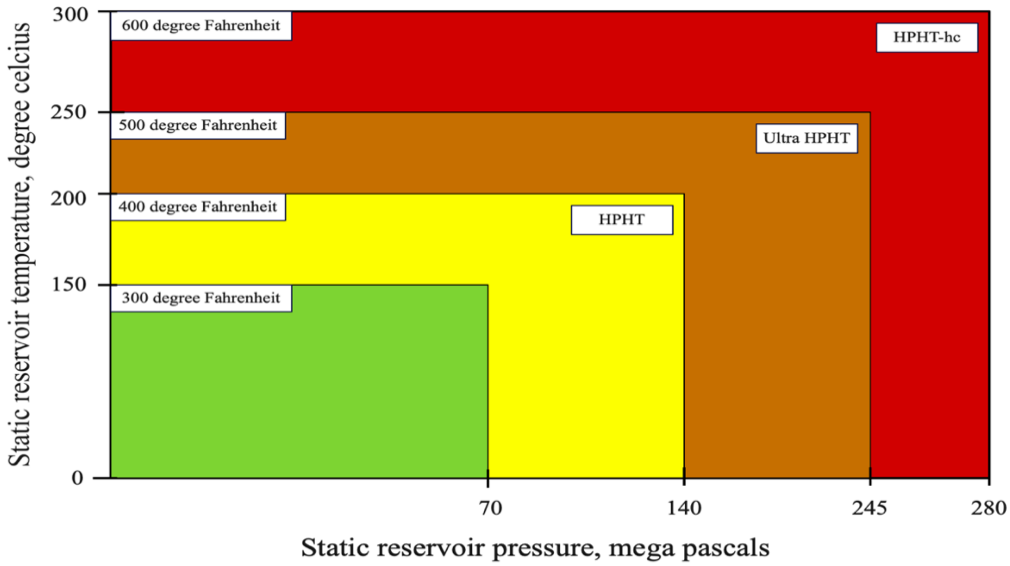

Figure 9 Illustration showing reservoir high temperature and high-pressure conditions (Adapted from Fluorocarbon 2017).

2.7.7.1 Engineering basis for operating conditions

Previous research underlines the significant influence of temperature on the permeability and mobility of porous materials. Ahmed (2018) and Zhou et al. (2020) observed that increases in temperature tend to improve the permeability of rock formations due to thermal expansion and decreased oil viscosity. These findings are corroborated by the empirical data from Li and Horne (2018), who recorded similar temperature-dependent permeability increases in their experiments. Moreover, Tian and Babadagli (2022) further support this trend in their examination of enhanced oil recovery (EOR) processes, linking higher temperature values directly to permeability enhancements.

Furthermore, Griffiths et al. (2018) have pointed out scenarios where temperature increases might reduce permeability due to the thermal contraction of certain rock components, challenging the typical expansion narrative. Marriott and Regenauer-Lieb (2020) also contribute to this discourse by demonstrating how thermal cycling in granitic formations might induce micro-fracture closures at higher temperatures, potentially reducing permeability.

Wang (2000) and Zoback (2010) explain how the mechanical properties of porous rocks, particularly permeability, are profoundly impacted by pressure changes due to the poroelastic nature of these materials. Empirical evidence from Nelson (2009) demonstrates that pressure variations can significantly alter the pore structure of reservoirs, leading to a reduction in their permeability. Additionally, Fjaer et al. (2008) detailed examination of rock mechanics within the context of petroleum engineering highlights the pivotal role of pressure in influencing rock permeability, particularly relevant to reservoir management practices.

Bear's (1972) seminal work on fluid dynamics within porous media, illustrates that temperature has a minimal effect on fluid mobility, reinforcing the idea that other variables might be more influential in determining these characteristics. This observation is echoed by Lake and Fanchi (2006), who noted a similarly limited impact of temperature on mobility in specific engineering contexts. This suggests that the influence of temperature on mobility may be less significant than traditionally understood across various industry applications. However, while McAllister et al. (2017) emphasises the profound effects of temperature on fluid mobility, the findings indicate that these impacts might be subdued under certain conditions, which calls for a deeper exploration into what factors reduce the role of temperature in fluid dynamics.

Contrasting with these authors, Tran and Nguyen (2019) found that temperature significantly affects waterflooding efficiency in low-permeability reservoirs, pointing to a possible variability in temperature's impact depending on geological and operational settings. This discrepancy underscores the complexity of fluid mobility dynamics and suggests that temperature effects may not be universally applicable across different contexts. Building on this, Zhou et al. (2021) advocate for the development of more sophisticated models that address both the direct and indirect influences of temperature on fluid mobility, particularly to enhance oil recovery strategies in complex reservoir environments.

Wilson et al. (2014) provides insights that explain how increased flow resistance due to increasing pressure could account for a negative correlation between mobility and pressure gradient. His discussions on the interplay between pressure gradients and fluid mobility directly relate to negative trends. Additionally, Darcy's seminal work (Darcy, 1856) supports Wilson et al. (2014) findings by demonstrating how fluid flow through porous media decreases as resistance from an increasing pressure gradient. Darcy's Law, a cornerstone in understanding fluid dynamics in porous media, offers empirical relationships that interpret why a higher-pressure drop might reduce mobility, indicating that flow resistance intensifies with pressure, thereby hindering fluid movement.

Lake and Walsh (2008) explore into advanced topics in oil recovery, providing detailed analyses on how pressure impacts oil mobility within reservoirs, further validating the negative correlation observed by other authors. Sharma et al. (2016) research on permeability and fluid flow also adds valuable context by showing how varying pressures can influence the mobility of different phases within a reservoir, enhancing our understanding of pressure-mobility dynamics.

Contrary to these findings, McAllister et al. (2017) presents scenarios where a pressure drop does not consistently reduce mobility, especially in media with complex pore structures or anisotropic properties. Sharma et al. (2016) also notes cases in petroleum engineering where increased pressure might paradoxically improve mobility, suggesting a more complex relationship than a straightforward negative correlation. Echoing the principles articulated by Bear (1972).

This research has critically investigated the role of operating temperature and pressure conditions in influencing the permeability and mobility of the porous media, which are key parameters in defining gas transport in reservoirs. The observed findings are then aligned to the empirical and theoretical bases established by other notable authors.

2.8 Parameter coupling – comparing experimental data with field data

Jones et al. (2022) highlight that comparing laboratory experimental data with field data from reservoirs offers valuable insights into fluid behaviours at the microscopic level and how these translate to the macroscopic realities of real-world reservoirs. The aim is to determine how properties measured in controlled settings using nanoporous ceramic cores correspond with real reservoir conditions. Statistical techniques are used to assess the laboratory and field data, pinpointing both similarities and differences that could suggest scale-dependent behaviours (White and Zhao, 2021). While scaling differences between laboratory and field observations present certain challenges in direct application, they are instrumental in identifying consistent patterns and trends between controlled experiments and actual field data, as noted by Smith (2020).

Building on this understanding, this study undertakes a coupling analysis to both qualitatively and quantitatively explore how well nanoporous ceramic cores serve as analogues for actual reservoir cores. The analysis concentrates on four crucial reservoir parameters: permeability, mobility, the reservoir quality index (a measure of a reservoir's ability to store and transmit fluids), and flux (the flow per unit area). The objective is to support that the experimental data derived from nano-ceramic cores can replicate the behaviours seen in field reservoirs. A successful validation would affirm the utility of nano-ceramic cores as effective models for examining fluid dynamics in low-permeability reservoirs.

2.9 Chapter summary

The literature review comprehensively examines low permeability reservoirs, particularly focusing on shale gas, tight sand, and coalbed methane. These reservoirs are becoming increasingly critical for meeting global energy demands as conventional resources dwindle. However, their extraction presents significant challenges due to their complex geological characteristics, such as intricate pore structures and low flow capabilities. This shift from conventional to unconventional reservoirs is necessitated by both the diminishing availability of traditional resources and the advancements in technology that now make extraction from these challenging formations feasible.

The global distribution of low permeability gas reserves shows a significant concentration in the United States, China, Russia, Canada, and Australia. These countries collectively hold the majority of the world's unconventional gas resources. Specifically, the United States leads with substantial shale gas reserves, while China, Russia, Canada, and Australia also contribute significantly, focusing on shale gas, coalbed methane, and tight gas. This distribution highlights the pivotal role these nations play in the unconventional gas sector.

To extract hydrocarbons efficiently from these low permeability reservoirs, advanced techniques such as horizontal drilling and hydraulic fracturing are essential. Horizontal drilling increases the wellbore's exposure to the reservoir, enhancing the efficiency of hydrocarbon extraction. Hydraulic fracturing further aids this process by creating fractures in the rock, which improves its permeability and allows for a more efficient flow of oil and gas. Additionally, Enhanced Oil/Gas Recovery (EOR/EGR) methods are continually being developed and refined to improve the recovery rates from these challenging formations while minimising environmental impacts.

Nanotechnology is highlighted for its significant role in improving the understanding and simulation of gas transport within low permeability reservoirs. The use of nanoporous ceramic cores is particularly noteworthy. These cores significantly mimic the conditions of actual reservoirs, providing a valuable tool for studying gas transport mechanisms and the impact of various parameters. The review identifies several critical factors that influence gas transport, including permeability, mobility, porosity, fluid viscosity, and operating conditions such as temperature and pressure. These parameters are crucial for understanding the behaviour of fluids within these complex geological formations and for developing effective extraction strategies.

The review also investigate the specific characteristics and extraction challenges of different types of low permeability reservoirs. Shale gas reservoirs are noted for their low permeability and high organic content, requiring unique exploration and production approaches. Coalbed methane, once considered a problematic by-product of coal mining, is now recognised as a valuable energy resource, with extraction processes focusing on the adsorbed state of gas within coal seams. Tight sand gas reservoirs, characterised by their densely packed sandstone with minimal pore spaces, also require advanced extraction techniques due to their low permeability.

In the methodology section, the study outlines its experimental design to investigate the impact of temperature and pressure on permeability and mobility in nanoporous ceramic cores. The study conducted over 1,000 permeation tests and collected more than 10,000 data points to ensure robust and reliable findings. The chosen temperature range covers typical reservoir conditions, while the pressure range includes both low and high-pressure laboratory settings. This approach allows the interpolation of laboratory results to real reservoir conditions, mitigating the environmental risks associated with high-pressure operations in laboratory settings.

The research introduces a modified Darcy's equation specifically tailored for nanoporous ceramic cores. This adaptation addresses the unique challenges posed by nanoporous materials, enhancing the accuracy of permeability and other reservoir parameter determinations. The modified equation and comprehensive experimental design aim to bridge the gap between theoretical models and practical applications, providing valuable insights for engineers and researchers in the field of petroleum engineering. By integrating these methodologies, the study aim to improve the understanding of gas transport in low permeability reservoirs, facilitating the development of more effective and efficient extraction techniques

CHAPTER 3
METHODOLOGY

This chapter provides a comprehensive overview of the methods and approaches employed to achieve the study's aim and objectives. It includes a detailed examination of the methodology, materials and equipment used, research technology, experimental setup and procedures, modification of Darcy's law, and data generation of key reservoir parameters for analysis. The chapter concludes with a discussion on precautions, potential errors and accuracy, and finally analysis and machine learning.

3.1 Overview

The experimental design of this research aim to investigate the use of nanoporous ceramic cores as mimetic models for low-permeability reservoir in studying gas transport. The design integrates several key principles and concepts to ensure the reliability and applicability of the results. By employing a comprehensive and methodical approach, the study provides robust insights into the dynamics of gas transport in environments such as tight sands, coalbed methane, and shale gas formations.

The research methodology adopted for this study is designed to integrate insights from key areas of engineering analysis, following the categorisation described by Kittner and Awiszus (2010), who delineate four primary investigative approaches: empirical, analytical, numerical simulation, and experimental. Dewals et al. (2008) elaborate on the distinct characteristics and benefits of each method, assessing their suitability for various engineering challenges.

In this study, two specific methods were employed after a thorough review of methodologies utilised in prior research concerning reservoir studies. The chosen approaches include laboratory experiments and the analysis of empirical field data from reservoirs. Laboratory experiments were conducted to assess the physical and thermodynamic properties of gases under simulated reservoir core conditions using nanoporous ceramic cores, offering direct insights into gas behaviour under varying pressures and temperatures that closely emulate real reservoir conditions. Concurrently, empirical field data was utilised to model fluid flow behaviour, providing an avenue to explore theoretical and practical scenarios that may be challenging to replicate in the lab due to constraints such as time, cost, or scale.

The field data selected were particularly reflective of the complexities associated with gas transport in porous structures, thus enriching the empirical insights derived from laboratory experiments.

The research unfolded in three distinct phases: The initial phase focused on the thorough selection and characterisation of nanoporous ceramic cores through direct measurement techniques and detailed experimental analyses. This foundational phase was essential for understanding the core properties and their impact on gas transport dynamics. Scanning electron microscopy (SEM) analysis and energy dispersive X-ray analysis (EDXA) were performed on the core samples to examine their surface morphology and chemical compositions as recommended by Worden and Utley (2022).

The second phase leveraged the initial experimental data to develop comprehensive regression models that correlated various parameters, providing a virtual platform to support and enrich the experimental observations with theoretical and empirical literature.

The third phase involved an integrative analysis that combined and scrutinised experimental results and field data. Various reservoir parameters, including permeability, mobility, Darcy flux, and reservoir quality index from the experimental data, were correlated with similar parameters from the field data. This was crucial in demonstrating the usefulness of nanoporous ceramic cores as mimetic models for representing reservoirs. The primary goal of this phase was to bridge the gap between small-scale laboratory findings and larger-scale reservoir behaviours, extrapolating insights to a broader reservoir context and addressing the main aim of this research.

3.2 Materials

The experimental research in this study involved the use of various materials and equipment.

3.2.1 Nanoporous ceramic core samples

The study involved the use of five cylindrical nanoporous ceramic core samples denoted by S15, B15, S200, S6000, and B6000 (S represents small and B represents Big) each with distinct pore throat sizes and dimensions summarised in **Table 1**. These cores are primarily composed of about 77% alumina and 23% titanium dioxide (TiO_2). While the material composition remains consistent across all samples, they exhibit variations in geometric and structural properties such as mean pore size, thickness, and surface area. To ensure uniformity in the evaluation of fluid flow behaviour and to preserve the material integrity, all core samples were obtained from the same supplier, Ceramiques Techniques et Industrielles (CTI SA) in France. It is posited that the distribution of pore sizes within each core is homogeneous, which simplifies the comparison of fluid transport properties across different samples. These cores were chosen as they closely mirror low permeability reservoir conditions, and the use of five cores was to enhance the robustness of the study. **Figure 10, 11 and 12** depicts the aerial and cross-sectional views of B6000, B15 and S15 respectively. While **Figure 13** represents the comparison view of the five core samples.

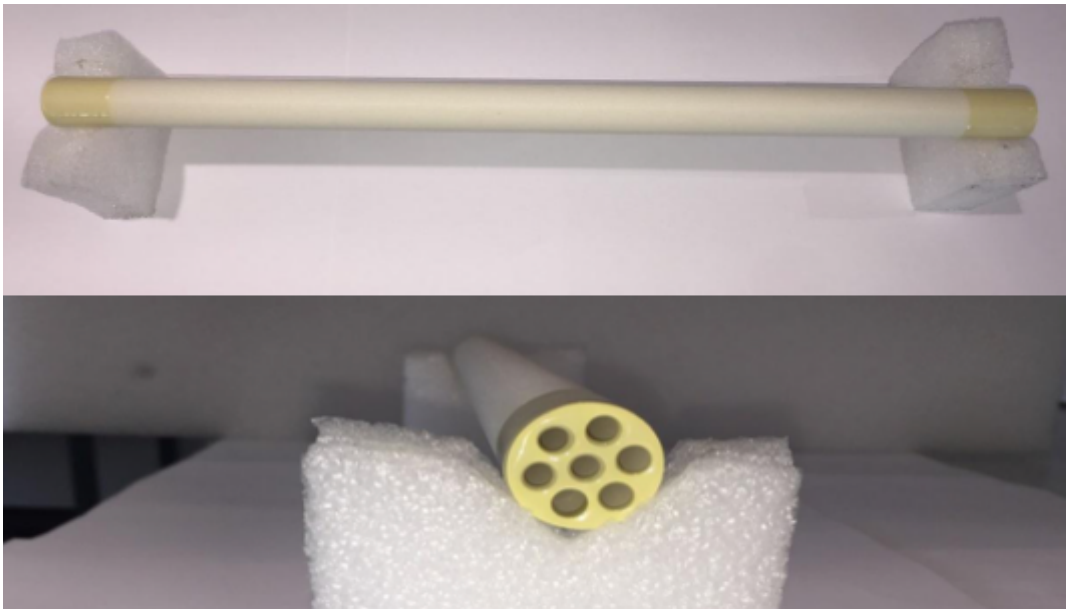

Figure 10 Aerial and cross-sectional view of B6000nm core.

Figure 11 Aerial and cross-sectional view of B15nm core.

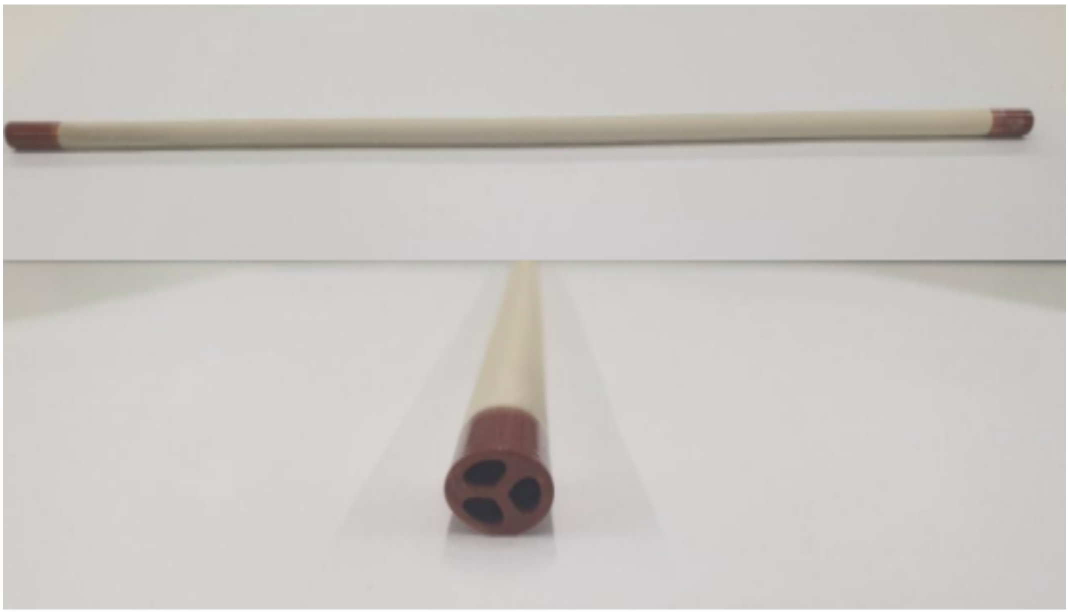

Figure 12 Aerial and cross-sectional view of S15nm core.

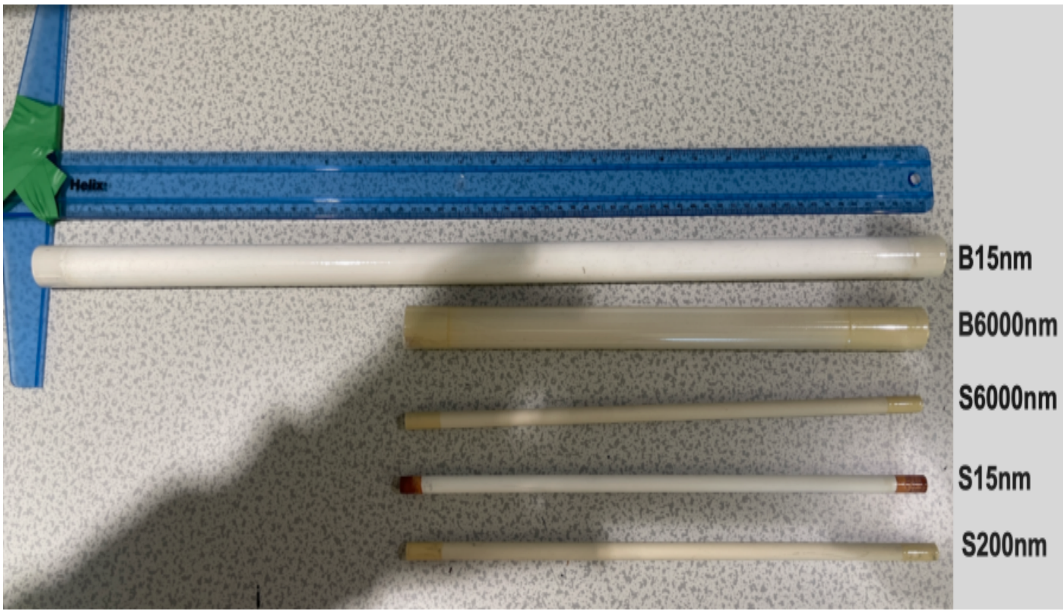

Figure 13 Comparing aerial view of the five core samples

Table 1 Physical dimensions of the five core samples

Core (nm)	Outer diameter (cm)	Inner diameter (cm)	Radius (cm)	Core length (cm)	Thickness (cm)	Core surface area (cm^2)
S15	1.01	0.71	0.51	34.7	0.30	111.3
B15	2.62	1.96	1.31	61	0.66	501.8
S200	1.05	0.78	0.53	33.8	0.27	112.2
S6000	1.04	0.77	0.52	32.8	0.27	107.1
B6000	2.59	2.07	1.30	32.8	0.52	267.8

3.2.2 Core holder

Three distinct core holders were utilised for the experimental set-up of this study. These core holders are constructed using stainless steel and come in various lengths and widths to accommodate the appropriate core samples. The core holders are designed as shell and tube modules, resembling a circular pipe with two flat ends. The void space at these flat ends allows for the insertion of the core, aligning it axially with the shell. These core holders are typically welded, pressure tested up to 40 bar, and leak tested by government-approved company named Hydrasun. **Figure 14** shows a more detailed view of the core holders.

The core holders are divided into three primary sections: feed, retentate, and permeate. The feed section is where the gas or gas mixture is introduced into the ceramic core system, while the retentate section collects the portion of the feed that does not pass through the core sample. This fraction contains the larger particles or molecules that are retained on the surface or within the pores of the ceramic core and is mostly useful for separation processes and the permeate section is where the filtered components of the feed, which have passed through the ceramic core, are collected.

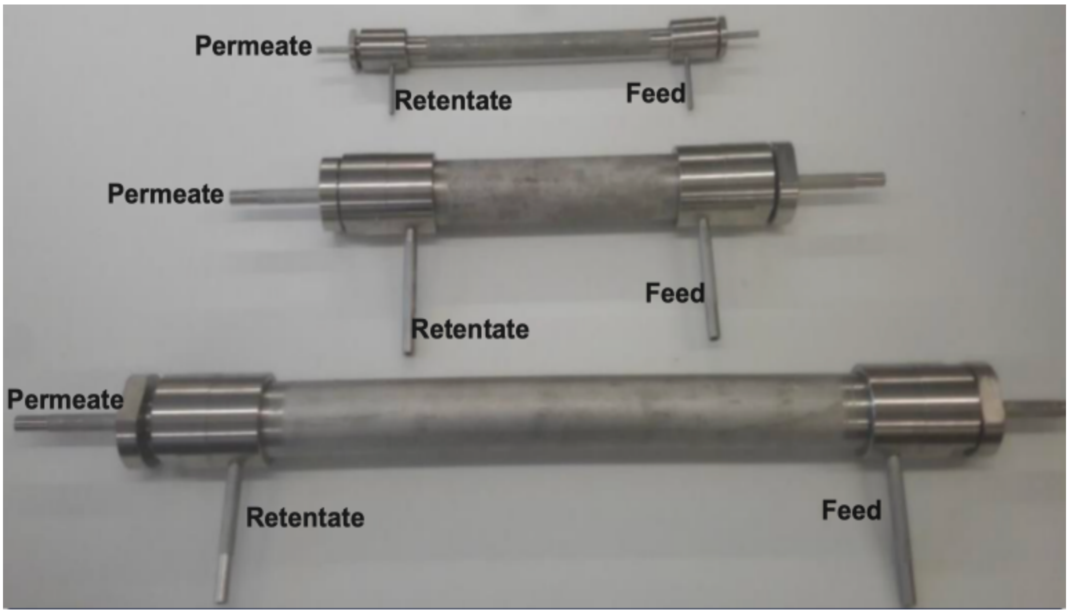

Figure 14 Aerial view of the stainless-steel core holders.

3.2.3 Gas

The experiment utilised methane (CH_4), carbon dioxide (CO_2), and a mixture of the two gases (60%CH_4/40%CO_2) as the test gases. Methane, being the principal component of natural gas (Dantas et al. 2014), was chosen for its relevance to most natural gas reservoirs. Carbon dioxide was included as a secondary component to provide a comparative baseline with methane, given its smaller presence in natural gas compositions but significant role in enhanced oil recovery and hydraulic fracturing techniques (Balcombe et al. 2017). Additionally, the gas mixture was used to mimic natural gas containing impurities, enabling an analysis of flow behaviours in both pure and mixed gas scenarios.

3.2.4 Equipment used

These equipment pieces played essential roles in conducting the experiments and gathering data for the study.

a) Beam balance scale: Utilised for measuring the weights of the samples.
b) Graphite seals: Employed to seal both ends of the core holder to prevent leaks.
c) Snoop solution: Used for leak detection.

d) Oxygen gas detectors: Ensured safety during gas handling.
e) Heat regulator: Controlled and adjusted the heating process.
f) Heat jackets: Used to maintain controlled temperatures.
g) Temperature transducer: Monitored and recorded temperature data.
h) Vernier calliper and meter rule: Tools for precise measurements.
i) Pressure gauge: Measured pressure conditions.
j) Flow meter: Recorded flow rates.
k) Gas cylinders: Contained various gases used in the experiments.
l) Thermometer: Measured temperature.
m) Conventional oven: Employed for specific heating processes.
n) Fume cupboard: Ensured safe handling of chemicals and gases.

3.3 Flow experiment and procedure

Five nanoporous core samples, each with different pore throat sizes and dimensions, were utilised in the experiments. Additionally, three unique core holders were employed to accommodate the various core sizes. These core holders are capable of being heated up to a temperature of 400°C without significantly compromising the structural integrity of the shell material. To achieve this, heating tape is wrapped around the outer shell, and three to four strategically placed thermocouples are used to monitor the temperature inside the core holder at the top, middle, and bottom positions across the core as illustrated in **Figure 15**. These thermocouples are connected to a thermocouple selector switch, which, in turn, is linked to a temperature controller managing the heating tape. A digital thermometer is also connected to the thermocouple selector switch, allowing researchers to monitor and control the desired temperature. This setup not only ensures the safety of the researchers from high temperatures but also maintains a constant temperature within the reactor system.

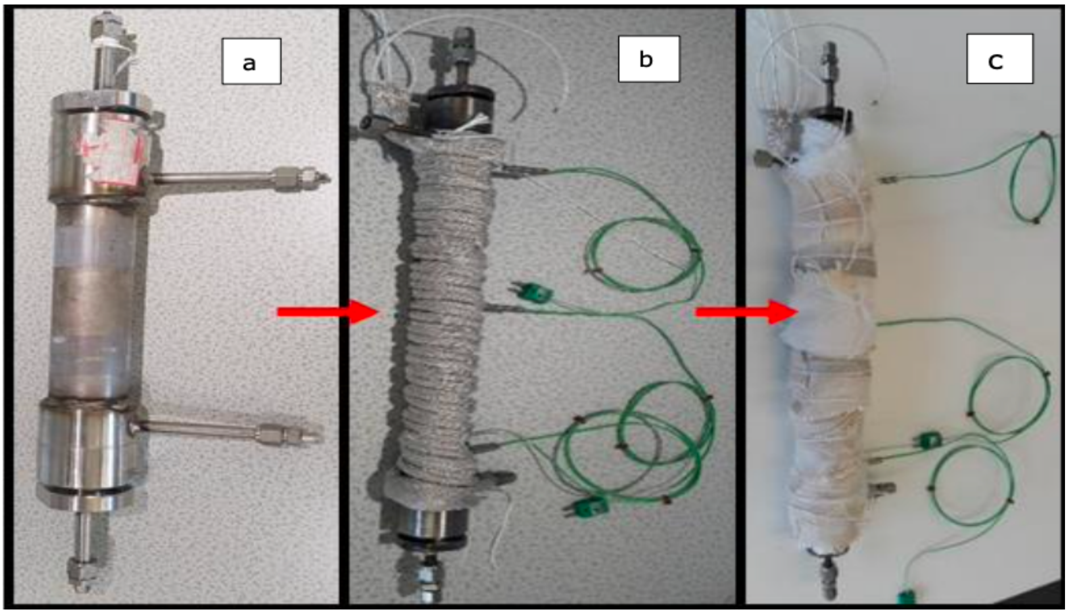

Figure 15 (a) Plain core holder (b) Core holder wrapped with heating tape and equipped with thermocouples, (c) Heating tapes enclosed with a fibre material.

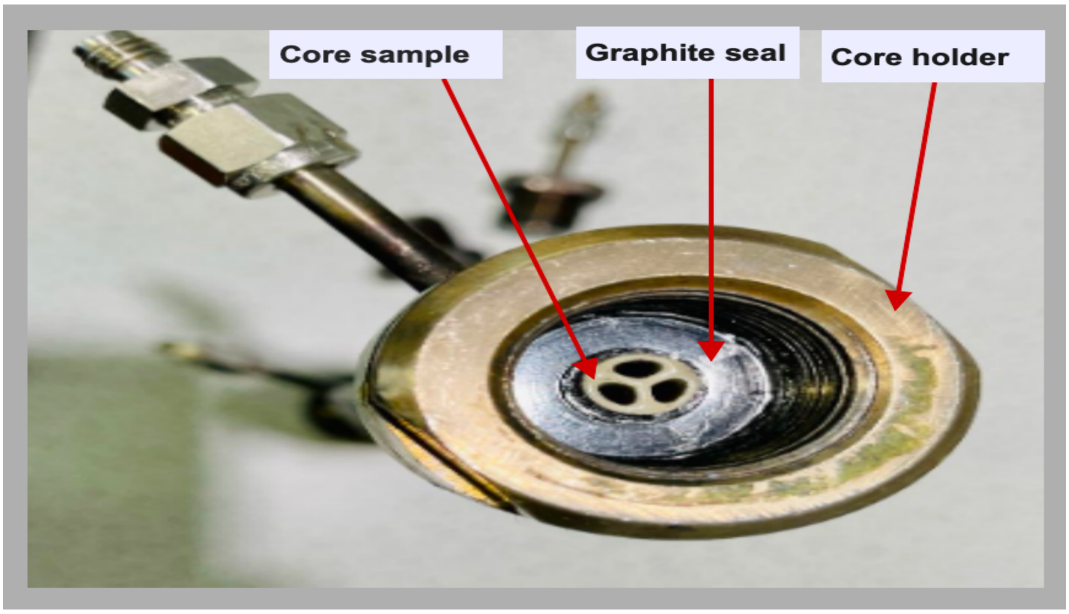

Figure 16 Image of the core sample securely sealed within the core holder using graphite rings.

A rig was meticulously assembled, consisting of the cylindrical nanoporous ceramic core placed within the annular space of a shell and tube mechanism (core holder), with both ends securely sealed with graphite to prevent gas leakage (**Figure 16**). Before each experiment, a leak test was conducted using a snoop solution, where the feed gas was released at double the required pressure to detect any pressure drops along the lines. The outer shell was insulated with fire-resistant glass fibre material, and thermocouples were strategically placed to maintain the system's temperature stability.

Once the system reached the desired temperature and thermal stability, gas from the cylinder was released through the gas regulator and introduced into the nanoporous core sample via the pressure valve. The gas flowed through the porous core and exited through an outlet line connected to the flow meter, where it was safely discharged. The flow meter readings were recorded after the system achieved a stable flow rate.

The experimental procedure was conducted for the five nano-core samples. The experiments were systematically carried out at predefined pressure intervals, ranging from 0.4 bar to 2.5 bar, with 0.3 bar increments, aligning with the methodology established by Yildirim and Hughes (2003). This approach allowed for comprehensive coverage of low and high-pressure conditions in laboratory settings. Additionally, the experiments were meticulously conducted under assumed reservoir conditions, with thermal stability maintained at 293K, 323K, 373K, and 473K for each core sample. These temperature settings spanned the spectrum from low to high reservoir temperature conditions, as documented by Fluorocarbon (2017). The feed gases employed in these experiments included methane (CH_4), carbon dioxide (CO_2) and a mixture (60%CH_4/40%CO_2). The experimental set up is illustrated in **Figure 17 and 18.**

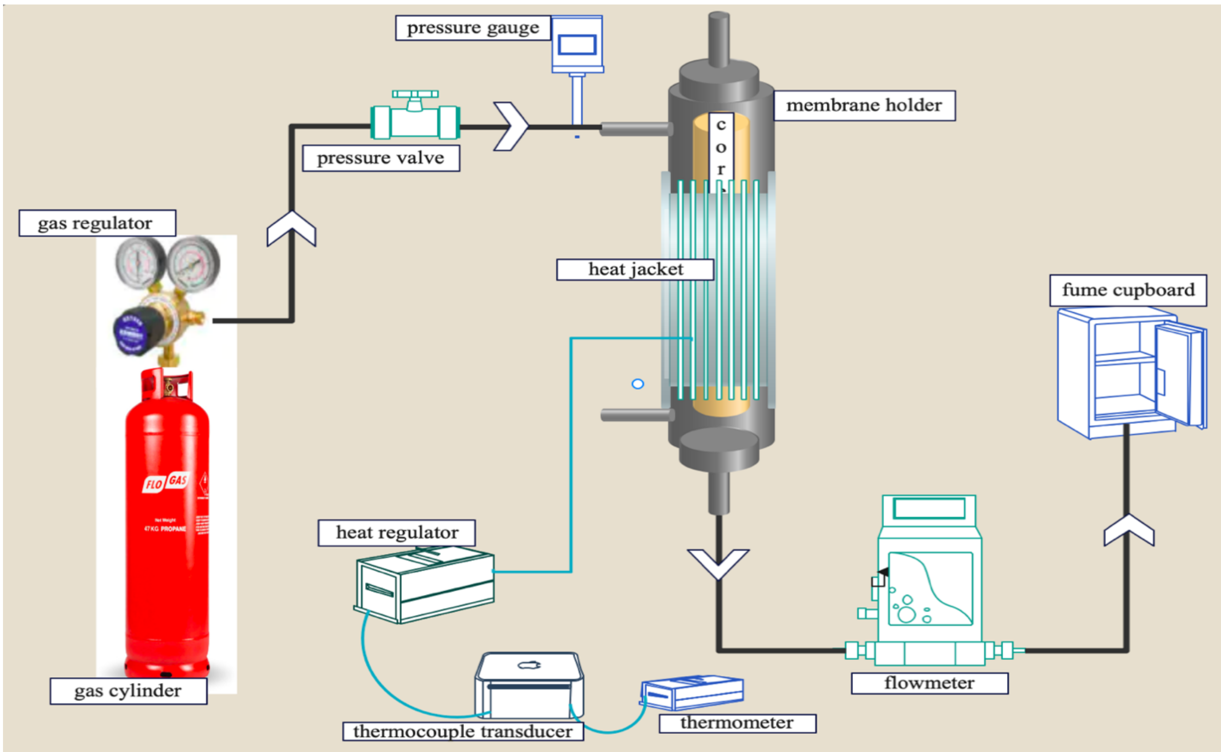

Figure 17 Schematic of the experimental set-up.

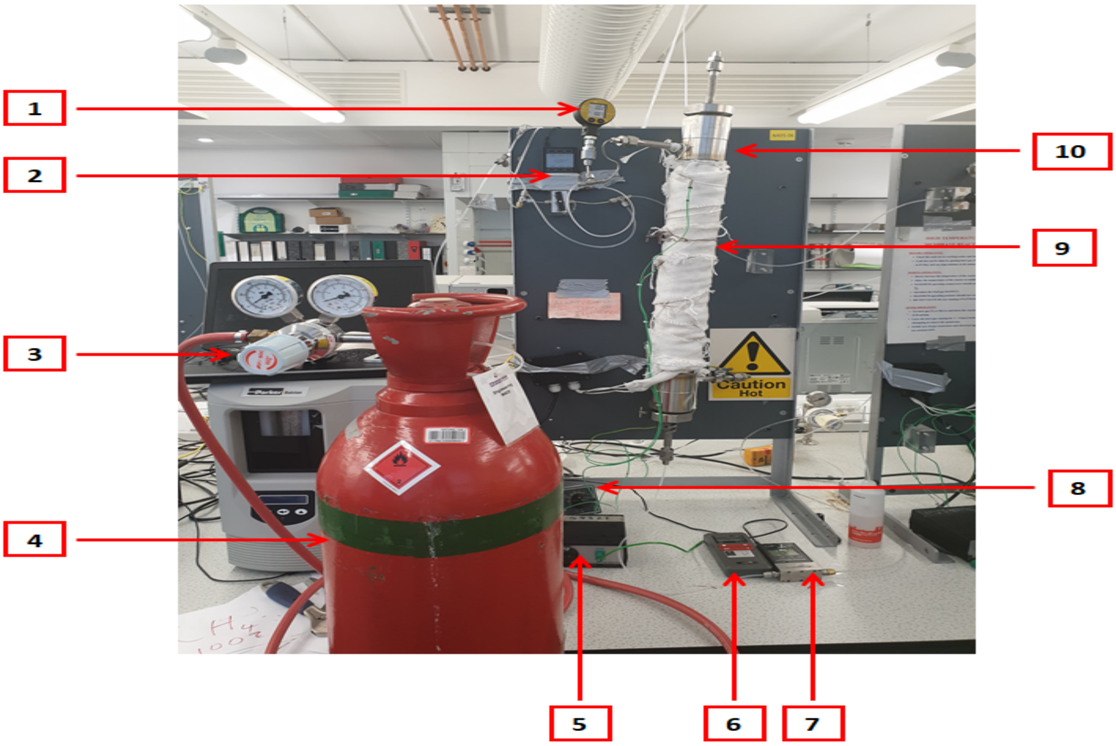

Figure 18 Laboratory view of experimental set-up: (1) pressure gauge, (2) pressure valve, (3) gas regulator, (4) gas cylinder, (5) thermocouple transducer, (6) thermometer, (7) flow meter, (8) heat regulator, (9) heat jacket, and (10) core holder.

3.4 Porosity determination

In this study, the porosity of the ceramic core samples was determined through the direct measurement of the core samples using Archimedes buoyancy principle. The porosity determination procedure is as follows: The core sample is initially fully submerged in water to thoroughly saturate it **(Figure 19).** The saturated core's weight is measured using a specialised beam balance after removing it from the water and wiping the outer surface with tissue paper **(Figure 20).** This weight is the wet weight (W_W). The core sample is then placed in an oven at about 100^oC for 12 hours to remove any moisture **(Figure 21)**. The oven-dried core is weighed to obtain the dry weight (W_D). By subtracting the dry weight (W_D) from the wet weight (W_W) and dividing by the density of water, the pore volume (V_P) of the core sample is determined. Next, the core is immersed in water again for complete saturation. The saturated core is then fully submerged in a beaker of water with a known volume, and the displaced water volume is measured. From Archimedes' principle ('which states that a body submerged in a fluid experience an upward force equivalent to the weight of the fluid displaced'), this displaced water volume is the bulk volume (V_B) of the core sample. The porosity, represented by the ratio of the pore volume (V_P) to the bulk volume (V_B), as shown in **Equation 17**, is estimated for each sample. The experiment was conducted three times for each core sample, and the summarised average results are presented in **Table 2.**

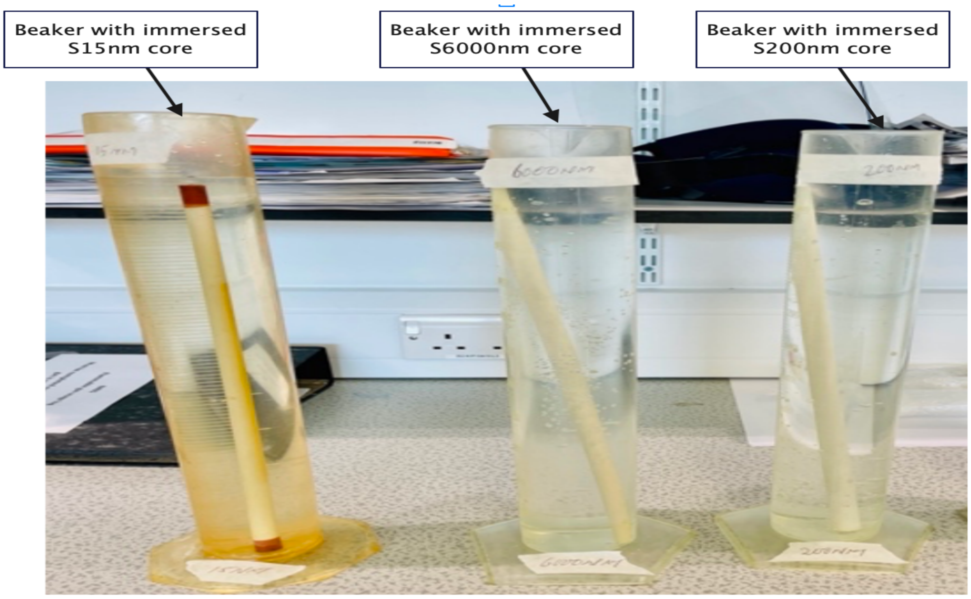

Figure 19 Illustrations of core samples completely immersed in water

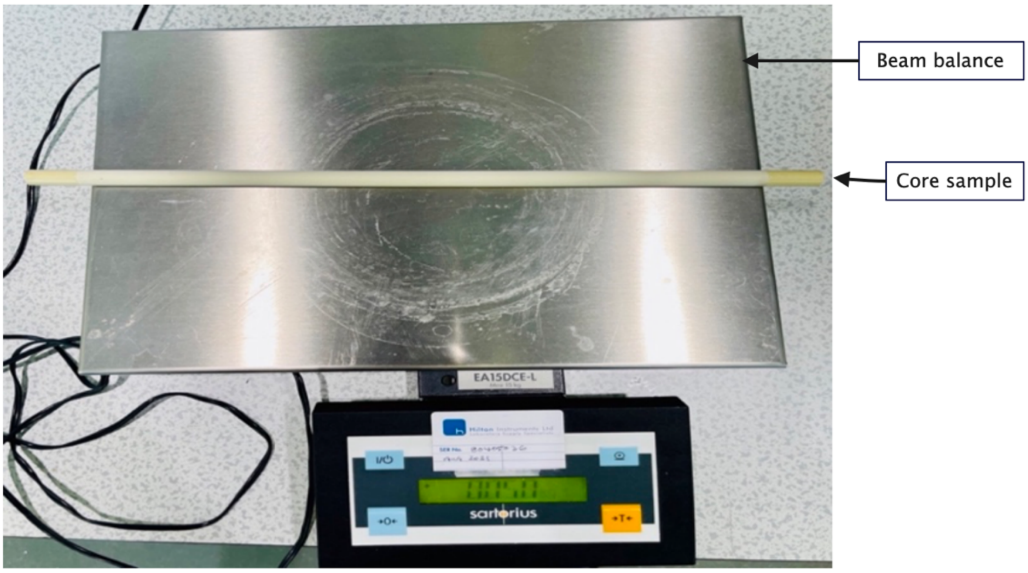

Figure 20 Picture showing beam balance scale measuring the weight of the core sample

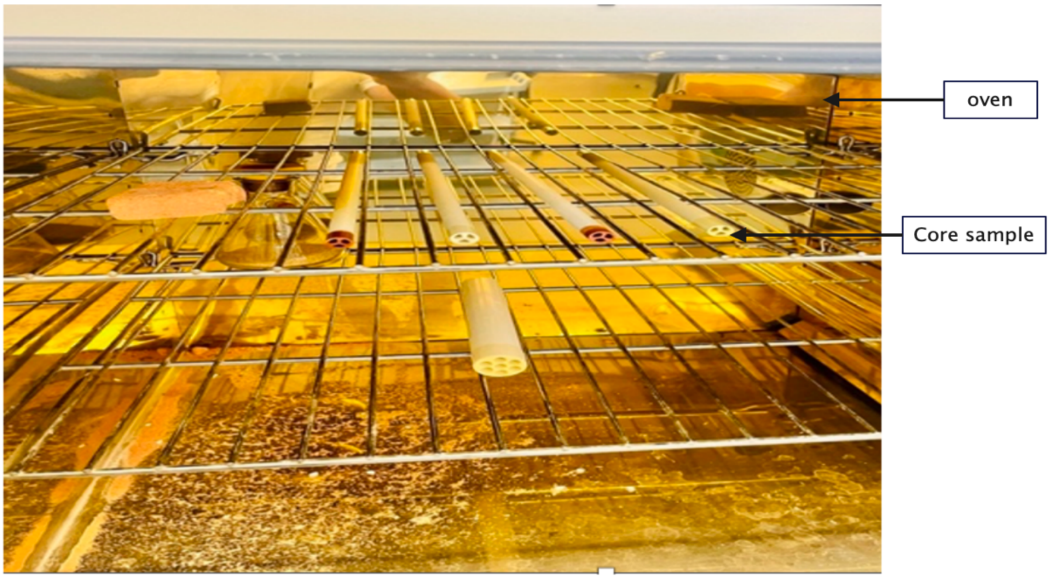

Figure 21 Picture showing the oven drying of the core samples.

Table 2 Core sample porosity summary

Core (nm)	Dry weight (g)	Wet weight (g)	Pore volume (cm^3)	Bulk volume (cm^3)	Porosity (%)
S15	50.64	56.75	6.11	20	0.306
B15	488.4	553.8	65.5	200	0.327
S200	52.35	59.53	7.18	20	0.359
S6000	48.93	56.03	7.1	20	0.355
B6000	277.2	317.9	40.7	140	0.29

3.5 Permeability

Permeability is a crucial factor to consider when studying a reservoir properly, as areas with high permeability are favourable for production. Accurate permeability estimation is essential for depicting many physical processes. However, creating theoretical models for permeability can be challenging due to the complex geometry of interconnected pore spaces and porous media complexities (Costa 2006).

Numerous techniques are available to assess permeability, such as well testing assessments and core laboratory investigations, yet these methods often entail substantial costs and time investments (Pouria et al. 2017). In this study, laboratory-based measurements were employed to estimate the permeability of the core samples. The flow experiments, as detailed earlier, were performed on the five core samples. The volumetric flow rates obtained from these experiments, and other measured parameters were incorporated into the modified version of Darcy's equation, denoted as **Equation 16,** the results of these experiments have been compiled in an Excel spreadsheet (**Appendix B**) for detailed analysis.

3.6 Mobility

Li and Horne (2018) emphasise the importance of understanding fluid mobility within porous media to effectively determine how substances like oil, water, and gas traverse reservoirs. Fluid mobility, quantified as the ease with which a fluid passes through a porous structure, is calculated using the ratio of permeability to fluid viscosity.

$$Mobility = \frac{k}{\mu} \tag{18}$$

Where k represents the permeability in millidarcies (mD), and μ denotes the fluid viscosity in centipoise (cp). This equation, referred to as **Equation 18,** was utilised to determine the mobility values, and the results were systematically organised in an Excel spreadsheet for subsequent analysis.

3.7 Darcy flux (Darcy velocity)

The Darcy flux (J) which is the flow by unit area measured in cm^3/cm^2sec, is calculated using Darcy's law, which states that the flow rate (Q) through a porous medium is proportional to the pressure gradient (ΔP) and the permeability (k) of the medium, and inversely proportional to the viscosity (μ) of the fluid and the length (L) of the flow path, expressed in **Equation 19.**

$$Flux\ (J)\ = \frac{Q}{A} = \frac{k.\Delta\mathrm{P}}{\mu.\mathrm{L}} \tag{19}$$

Where:

J is the Darcy flux (cm^3/cm^2sec)'

Q is the volumetric flow rate in ($cm^3.sec^{-1}$),

A is the cross-sectional area of the core sample (cm^2),

K is permeability (mD),

ΔP is the pressure drop across the core samples (atm),

μ is the fluid viscosity (cp),

L is the length of the core sample (cm).

In this study, the volumetric flow rates were measured directly from the experiments, and the cross-sectional area of each core sample were estimated using the formula $2\pi rh$ (as described in **Section 2.7.1.3**), the Darcy flux was computed for different conditions, providing insights into the flow characteristics of the nanoporous ceramic cores. These values were subsequently organised in an Excel spreadsheet for further analysis.

3.8 Quality index

According to Abouzar and Behzad (2022), the ratio of permeability to porosity is used as a quality indicator in scaling capillary pressure data in reservoir engineering. This ratio is referred to as the Reservoir Quality Index (RQI), measured in micrometers (μm).

In this study, the RQI for the nanoporous ceramic cores was calculated using the measured permeability and porosity values. These values were obtained from laboratory experiments conducted under controlled conditions, mimicking reservoir environments. The calculated RQI values provide insights into how well these ceramic cores can replicate the fluid flow characteristics of reservoirs.

The study adopts **Equation 20** documented by Abouzar and Behzad (2022) to estimate the values of the reservoir quality index for both the experimental and field data.

$$Reservoir\ Quality\ Index\ =\ 0.0314\ x\ k\emptyset \qquad (20)$$

Where:

k is the permeability in millidarcy (mD),

$\emptyset$ is the porosity in %.

3.9 Viscosity

Viscosity values were sourced from established literature (Engineering ToolBox, 2004) corresponding to the temperatures used in this research and were measured at atmospheric pressure. For the gas mixture, the viscosity was calculated mathematically based on the respective component percentages at each temperature (60% x CH_4 viscosity + 40% x CO_2 viscosity). These values are summarised in **Table 3**.

Table 3 Summary of viscosity at gases at different temperatures and atmospheric pressure (Engineering ToolBox, 2004).

Gas	Viscosity (cp) at 293K	Viscosity (cp) at 323K	Viscosity (cp) at 373K	Viscosity (cp) at 473K
CH_4	0.011	0.0119	0.0135	0.0163
CO_2	0.0147	0.0161	0.0185	0.0230
60%CH_4 /40%CO_2	0.0125	0.0136	0.0155	0.0190

3.10 Temperature

To align the experiment closely with real-world reservoir conditions, the temperature range selected was based on documented global reservoir temperatures. According to a survey by the Oil and Gas Journal (2014), typical reservoir temperatures range from 290K to 573K, as further supported by data from Fluorocarbon (2017). Consequently, the experiment was conducted at four specific temperatures: 293K, 323K, 373K, and 473K. This selection covers both the lower and upper bounds of typical reservoir temperatures, thereby ensuring that the experimental conditions span from 293K to 573K.

3.11 Pressure

Conducting laboratory experiments at pressures equivalent to those found in reservoirs poses challenges. Nonetheless, establishing a well-defined laboratory pressure range that mirrors those in actual reservoirs allows researchers to extend their findings to real-world scenarios (Ding et al. 2017, Chevalier et al. 2013).

This methodology enhances understanding of reservoir behaviours and supports the development of effective management and optimisation strategies (Lin et al. 2019).

In this study, eight pressure points were selected: 0.4, 0.7, 1.0, 1.3, 1.6, 1.9, 2.2, and 2.5 bar, set at intervals of 0.3 bar as suggested by Yildirim and Hughes (2003). This range was designed to capture a variety of gas flow behaviours under both Darcy and non-Darcy flow conditions—where Darcy flow adheres to Darcy's law of flow rate being proportional to the pressure gradient, and non-Darcy flow occurs when the relationship between flow rate and pressure gradient is nonlinear, often observed at higher flow velocities or in highly permeable media (Dejam et al. 2017, Al-Otaibi and Wu, 2010).

3.12 Experimental and field data acquisition

Reservoir data from CH_4 and CO_2 projects were collected from various sources, including the Oil and Gas Journal's Global EOR Survey, various Canadian journals, and EOR surveys conducted in regions such as the North Sea, China, and Brazil (George et al. 2021, Liu et al. 2020, Guo et al. 2018 and Awan et al. 2006).

Some data were initially reported in different units and formats. These were standardised by applying the appropriate conversion factors. In cases where parameters, were reported as ranges, the simple arithmetic average of the range was computed (Saleh et al. 2014). The field fluid dynamics data were precisely processed to ensure accuracy and consistency, resulting in a robust field dataset for analysis. Concurrently, experimental data were gathered from tests conducted on nano-ceramic core samples. These experiments simulated the use of CH_4 and CO_2 under conditions closely replicating those of the reservoir, including matching temperature ranges.

Both qualitative and quantitative assessments were conducted on the datasets. The qualitative analysis utilised scatter plots and clustering techniques to visually examine relationships between parameters in both datasets, identifying patterns and similarities in fluid dynamic responses. Clustering techniques further classified data points based on their characteristics, highlighting analogous behaviours between the two sets. Quantitative analysis employed statistical tools such as mean and coefficient of variation to measure central tendency and dispersion within each parameter, facilitating detailed comparison. The parameters considered for comparison included permeability, mobility, reservoir quality index, and flux, which were determined for both the experimental and field data.

The coupling employed data normalisation, which is a critical preprocessing step in data analysis involving scaling features to a common range, such as 0 to 1. This process enhances model performance by ensuring that all features contribute equally, preventing bias towards features with larger values (Kotsiantis et al. 2006, Han et al. 2011, Singh and Chauhan, 2019). In this study, the field data scales were significantly larger than the laboratory experimental data. Hence, the permeability, mobility, Darcy flux and quality index were normalised to facilitate fair comparison, accurate distance calculations, and better visual interpretation of data while also mitigating the impact of outliers. Additionally, a log scale was applied to the features axis (y-axis) in the respective graphs to accommodate the wide range of values in the dataset. The features were plotted against temperature on the x-axis. The temperature variable was chosen because the experimental temperatures and the field temperatures fall within the same range, allowing for a more meaningful comparison.

3.13 Precautions and experimental conditions

During the material preparation for this research, several precautions were meticulously observed to handle the core samples with care. Specifically, only the laminated ends of the cores were held to prevent any contamination of the nanopores within the samples, ensuring that the surfaces through which permeation occurred remained untouched. Furthermore, the core samples were delicately secured within the stainless-steel core holder, with precautions taken to avoid contact with the inner walls, thus preventing any damage to the samples. To ensure the accuracy of the results, as advised by Morton-Thompson and Woods

(1993), all experiments were conducted under steady-state conditions. It was assumed that no chemical reactions occurred during the experimental procedures in both the PVT conditions and with the gases employed. Any potential system irregularities were expected to affect the performance of the various gases uniformly.

The gases were introduced at pressure intervals of 0.3 bar, commencing from an initial gauge pressure of 0.4 bar and ascending to 2.5 bar, following the guidelines proposed by Yildirim and Hughes (2003). These intervals were thoughtfully chosen to encompass multiple data points within both the Darcy and non-Darcy flow regions. The experiments were executed at standard temperatures of 293K, 323K, 373K, and 473K. This temperature range was selected to represent reservoir conditions spanning from low - high in-situ reservoir scenarios, aligning with the discussions presented in the literature review. Throughout the experimental process and parameter assessment, consistent unit conversions were applied for uniformity. For instance, the experiment was conducted in degree Celsius and later converted to Kelvin for analysis. The feed gas used in the experiments was methane (CH_4), the primary component of natural gas. Additionally, carbon dioxide (CO_2) gas, another component of natural gas but in smaller quantities, was employed as a reference gas to facilitate comparisons with methane. Furthermore, mixtures of CH_4 and CO_2 at a ratio of 60%/40% were used to simulate natural gas with impurities, allowing for the investigation of flow patterns under such conditions.

3.14 Errors and accuracy

The experiments were carefully conducted with a regulated variation in temperature and pressure. Temperature readings were taken with an accuracy of ±5°C, which accounted for less than 10% error. Similarly, the readings on the pressure gauge were collected with an accuracy of ±0.01bar, also within 10% error. Careful measures were taken while using the vernier calliper to ensure accurate core diameter readings, considering potential parallax inaccuracies.

To reduce potential errors, a calibrated digital weight balance was employed to measure sample weights, and electronic devices were frequently tared before taking new measurements. The aim was to maintain consistency and minimise any interference caused by changing operating conditions on experimental results. To maintain the integrity of the experiment, gas runs were attempted to be completed on the same day and time whenever possible. Previous test runs indicated that pausing and starting a series of tests for the same gas had only a negligible impact on the results.

For the experiment, a single set of apparatus was used to prevent calibration issues that might arise if different equipment were added to the setup. Before each new run, the core was flushed with fresh gas to ensure any remnants of the prior gas were removed, and it was qualitatively expected that the pressure differential would be enough to displace the older gas with the fresh gas. These precautions were taken to ensure the accuracy and reliability of the experimental results.

3.15 Analysis and machine learning

To generate the results for discussion, a systematic machine learning methodology which has been used by other authors like Ali et al. (2023), Rashid et al. (2022) and Otchere et al. (2021), was employed, encompassing several stages of data collection, preparation, analysis, and visualisation. The process began with the careful gathering and organisation of the experimental data into a structured format (CSV file) suitable for analysis. The data include key parameters such as permeability (with values ranging $7.9e^{-5}$mD to $1.74e^{-3}$mD), mobility (0.0054mD/cp to 0.11mD/cp), flux (0.049cm^3/cm^2sec to 0.619cm^3/cm^2sec), quality Index ($7.23e^{-7}$μm to $1.94e^{-5}$μm), temperature (293K to 473K), pressure (0.4atm to 2.5atm) and viscosity (0.011cp to 0.023cp).

Following data collection, the preparation phase involved importing essential python libraries necessary for data manipulation, analysis and visualisation in visual studio code (an integrated development environment software). These included pandas for data handling, seaborn for visualisation, matplotlib for plotting and sklearn for regression analysis. The data was then loaded into a panda DataFrame, enabling straightforward manipulation and access. It was crucial to ensure that the data was clean, which involved handling any missing values, duplicates, or outliers that could potentially skew the analysis. This step ensured that the data was ready for precise computation and visualisation.

The next step involved calculating the correlation matrix, which is a statistical tool used to measure the strength and direction of the linear relationship between two variables. The pandas library provides a straightforward method that computes pairwise correlation of columns, excluding null values. The correlation matrix was then stored in a new DataFrame for ease of visualisation. This matrix was essential as it provided the basis for the heatmap, representing the relationships between the different experimental parameters.

Following the computation of the correlation matrix, the visualisation phase was initiated. This involved setting up the plotting parameters using matplotlib and seaborn. The seaborn library's heatmap function was employed to create the heatmap, a graphical representation of data where individual values are represented as colours, highlighting areas of strong positive or negative correlation.

The next step involved conducting a linear regression analysis to explore the relationship between the parameters. Linear regression is the most straightforward regression approach, made up of a dependent variable that depends linearly on the independent variable, this regression analysis established a mathematical model that best fits the observed data. The independent variables, temperature, pressure, porosity and viscosity, the dependent variable, permeability, mobility, flux and quality index were used to fit a linear regression model. The analysis provided the slope and intercept of the best-fit line, as well as the coefficient of determination (R^2), which indicates the goodness of fit. These calculations were performed using the sklearn library in Python, which offers robust tools for statistical analysis.

The final stage involved visualising the relationship between the parameters. This was achieved using Matplotlib, a comprehensive library for creating static, animated, and interactive visualisations in Python. A linear regression line was overlaid to illustrate the best-fit model. Annotations were added to the plot to include the equation of the regression line and the R^2 value, providing a clear and informative representation of the data and the derived relationships.

In conclusion, this methodology ensures a rigorous and systematic approach to exploring the relationship between the dependent variables and the independent variables. By employing robust data collection, meticulous data preparation, comprehensive analysis, and clear visualisation, the study demonstrates the impact of temperature, pressure drop, porosity and viscosity on permeability, mobility, flux and reservoir quality index providing valuable insights for further research and practical applications in reservoir engineering.

CHAPTER 4
RESULTS AND DISCUSSION

This chapter begins by detailing the SEM/EDXA results for the core samples. It then proceeds to experimental data analysis, incorporating correlation and regression analysis, and provides a heatmap that illustrates the relationships between various parameters. The chapter further compares experimental data with field data for permeability, mobility, flux, and reservoir quality index.

4.1 Scanning electron microscopy (SEM) and energy dispersive x-ray analysis (EDXA) analysis of nanoporous ceramic cores.

The SEM and corresponding EDXA images are presented in **Figures 22** through **Figure 26. Figure 22** illustrates the SEM/EDXA images showing the outer surface of the S15nm core sample. Similarly, **Figure 23** displays SEM/EDXA images of the outer surface of the B15nm core sample. **Figure 24** showcases SEM/EDXA images of the outer surface of the S200nm core sample. **Figure 25** highlights SEM/EDXA visuals providing insight into the outer surface of the S6000nm core sample. Finally, **Figure 26** features SEM/EDXA imagery shedding light on the outer surface of the B6000nm core sample.

4.1.1 Scanning electron microscopy (SEM)

The Scanning Electron Microscope (SEM) images provide a detailed view of the core samples at a high magnification of 1.00 K X, using an accelerating voltage of 20.00 kV and a working distance of 7.5 mm. Captured with a backscattered electron (BSD) detector under a chamber pressure of 100 Pa, the images highlight the cores' grains and heterogeneous structures.

The grains vary significantly in size and shape across the five core samples, indicating a diverse particle size distribution. Dark areas in the images represent pores or void spaces, which are crucial for determining the material's permeability and fluid transport properties. The bright spots, indicative of areas with higher atomic numbers, suggest the presence of minerals or compounds with higher atomic masses, such as metal oxides or other heavy minerals commonly found in porous media (Chevalier et al. 2013).

The surface topography, characterised by sharp edges and irregular shapes, contributes to the material's rough texture. The observed microstructure implies significant porosity and potential permeability, essential factors for fluid extraction in reservoir studies. The varying brightness across the image's points to a composition of different elemental phases, affecting the material's mechanical strength and chemical reactivity (Ding et al. 2017).

These properties suggest that the materials are suitable for applications requiring specific porosity and permeability characteristics, such as enhanced oil recovery (EOR) processes collaborating with (Al-Otaibi and Wu, 2010). These SEM images offer significant insights into the material's suitability for various industrial applications, highlighting its potential for effective fluid transport and storage, supporting their suitability for describing low permeability reservoirs.

4.1.2 Energy dispersive x-ray analysis (EDXA)

The Energy Dispersive X-ray Spectroscopy (EDS) spectrum for each of the core samples provides a detailed analysis of their elemental composition. This technique identifies the elements present by detecting the characteristic X-ray energies emitted when the sample is bombarded with high-energy electrons. The spectrum reveals the presence and proportions of carbon (C), oxygen (O), aluminum (Al), and titanium (Ti), which are essential components of the material. The samples contain between 4.9% to 9.36% carbon by weight, which corresponds to 7.99% to 15.93% in atomic percentage. The presence of carbon suggests the possibility of organic materials or carbonates within the samples. Such quantities of carbon may affect the material's reactivity and structural properties, potentially indicating residual organic substances or specific carbon-based additives used during sample preparation (Dejam et al. 2017).

Oxygen is the most abundant element across the five core samples, with weight percentages ranging from 37.67% to 50.54% and atomic percentages from 58.52% to 61.61%. The high oxygen content indicates that the material is predominantly composed of oxides, a common characteristic in ceramics. The presence of oxides such as alumina (Al_2O_3) and titania (TiO_2) is suggested due to their prevalence in the spectrum and their known uses in creating stable, high-performance materials. These oxides contribute significantly to the thermal stability and mechanical robustness of the sample (Lin et al. 2019).

Aluminum and titanium are also present in substantial amounts. The combination of aluminum and oxygen suggests the presence of aluminum oxides (such as alumina), known for their hardness and thermal resistance. Similarly, the titanium content, likely in the form of titanium dioxide, is noted for its photocatalytic properties and high refractive index. The significant percentages of these elements suggest that the material is a composite, such as alumina-titania ceramics, widely used for their enhanced mechanical properties and stability (Chevalier et al. 2013).

The findings indicate that the material is predominantly an oxide-based composite, with significant amounts of alumina and titania aligning with the detailed manufacturer's specifications. The high oxygen content supports this, while the carbon detected may be due to minor organic contamination or specific preparation additives. The mechanical strength and stability provided by alumina and titania make the material suitable for various industrial applications.

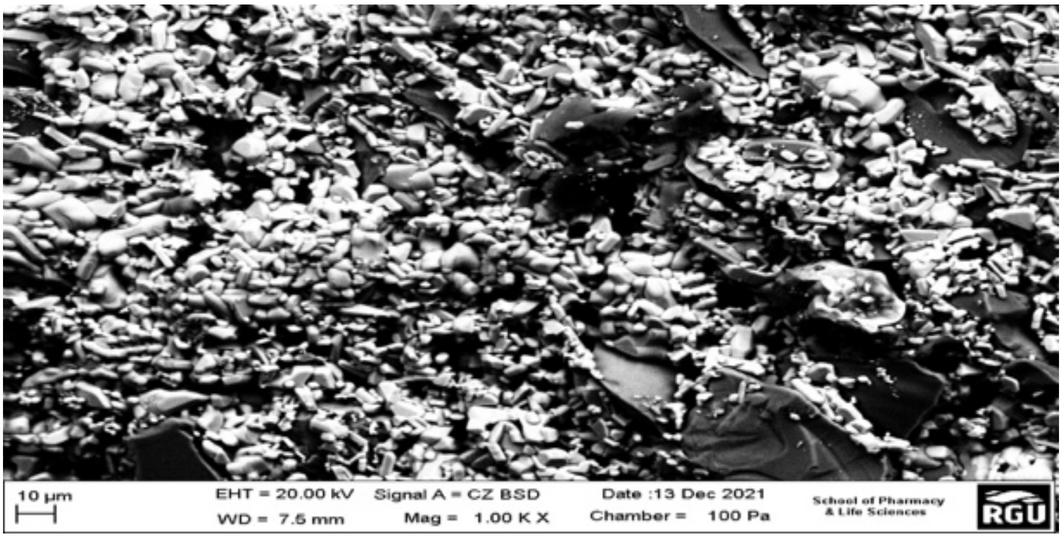

SEM

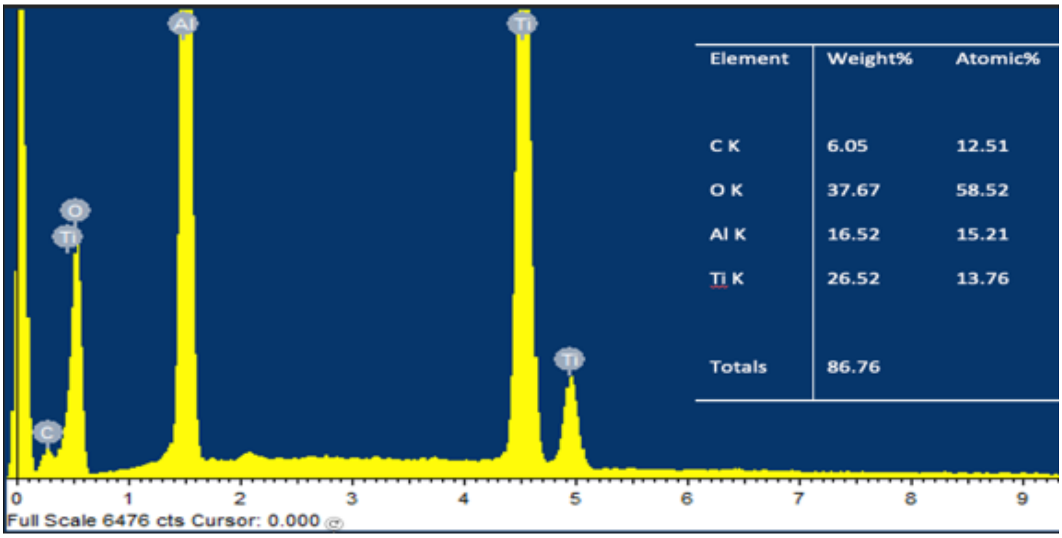

EDAX

Figure 22 SEM/EDAX images of the outer surface of the S15nm core sample

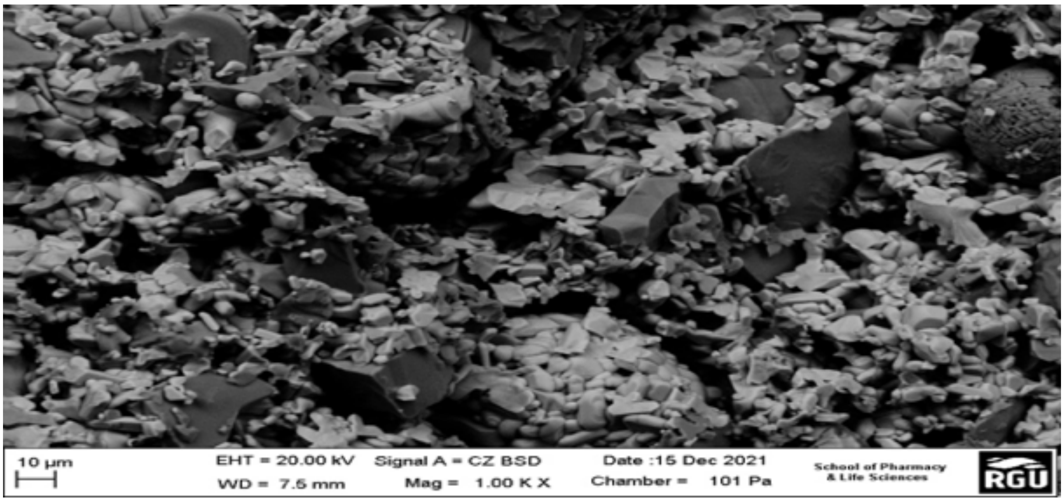

SEM

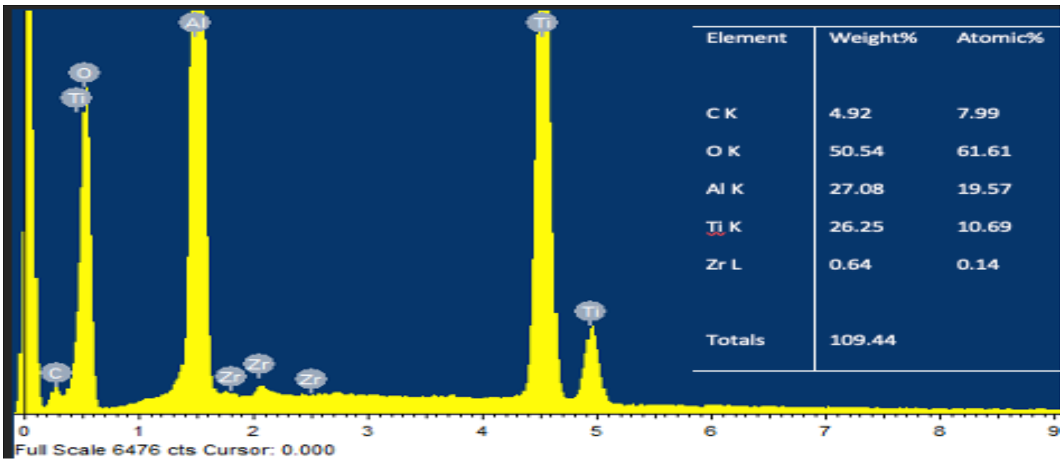

EDAX

Figure 23 SEM/EDAX images of the outer surface of the B15nm core sample.

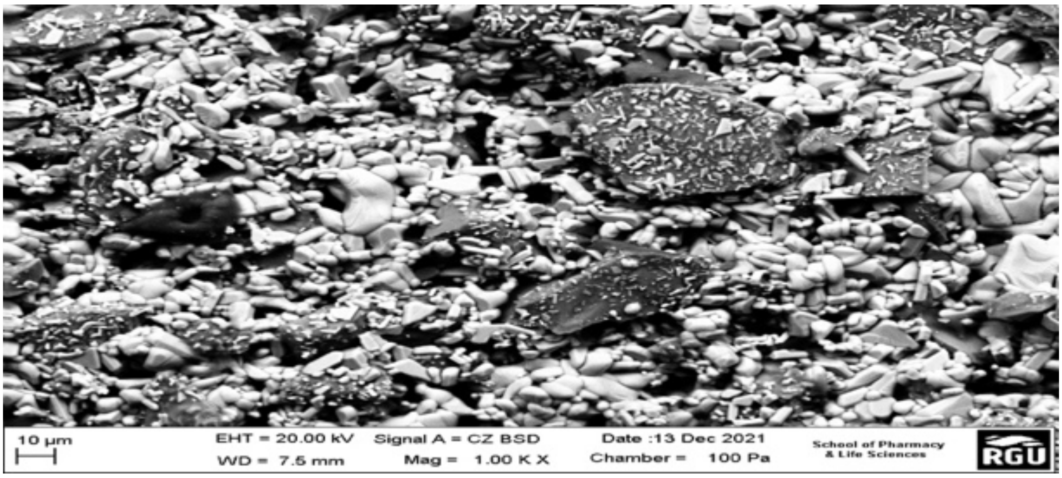

SEM

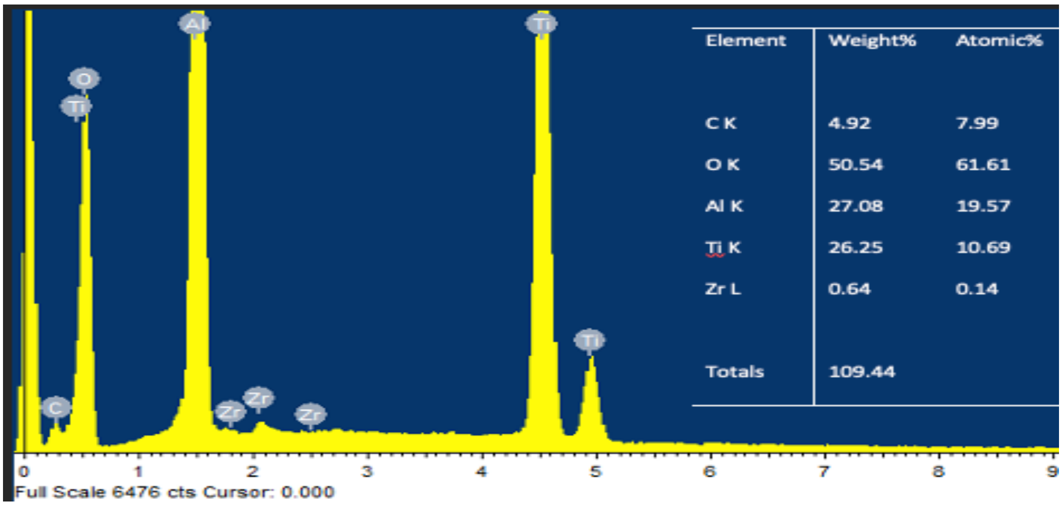

Element	Weight%	Atomic%
C K	4.92	7.99
O K	50.54	61.61
Al K	27.08	19.57
Ti K	26.25	10.69
Zr L	0.64	0.14
Totals	109.44	

EDAX

Figure 24 SEM/EDAX images of the outer surface of the S200nm core sample.

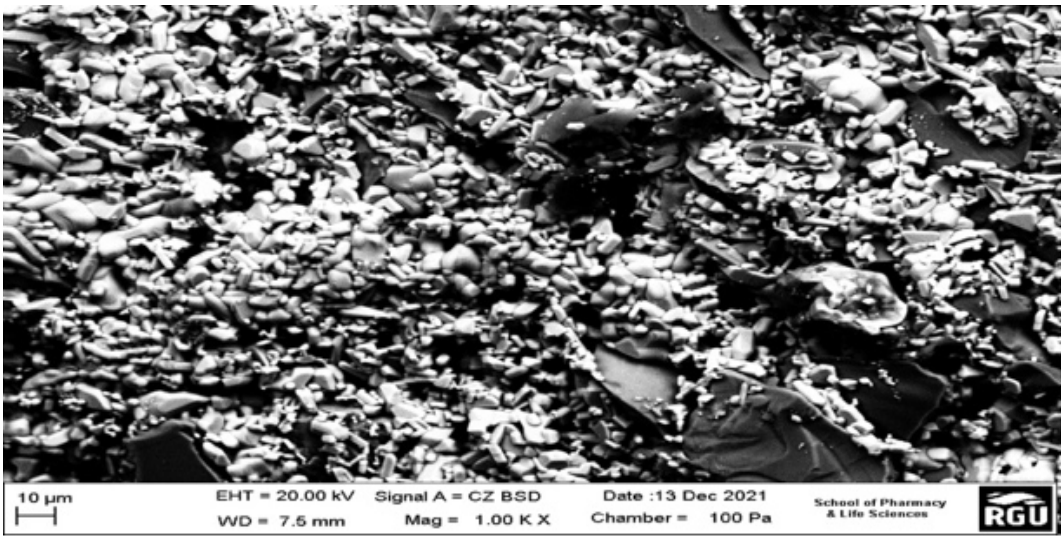

SEM

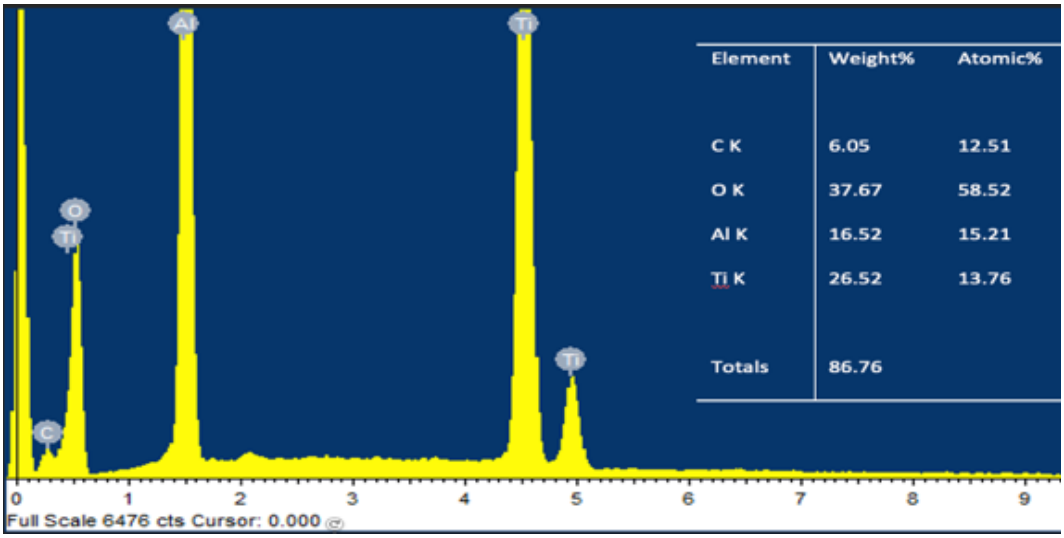

EDAX

Figure 25 SEM/EDAX images of the outer surface of the S6000nm core sample.

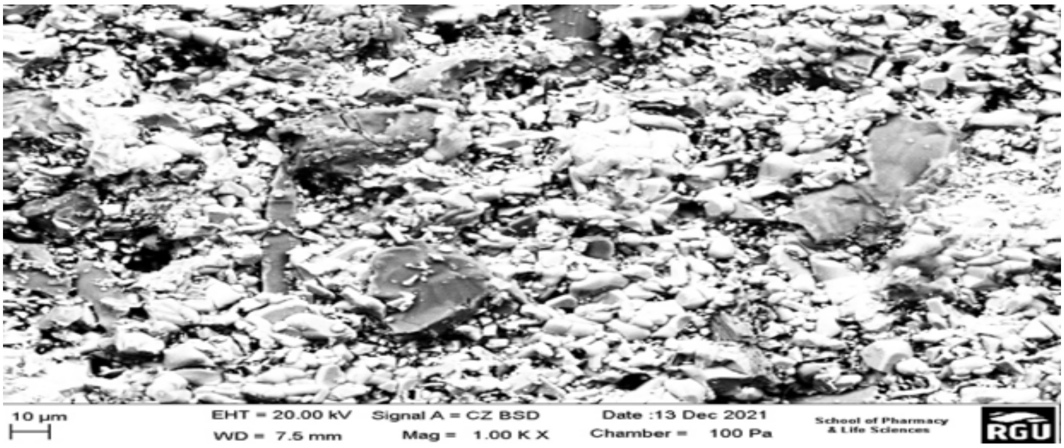

SEM

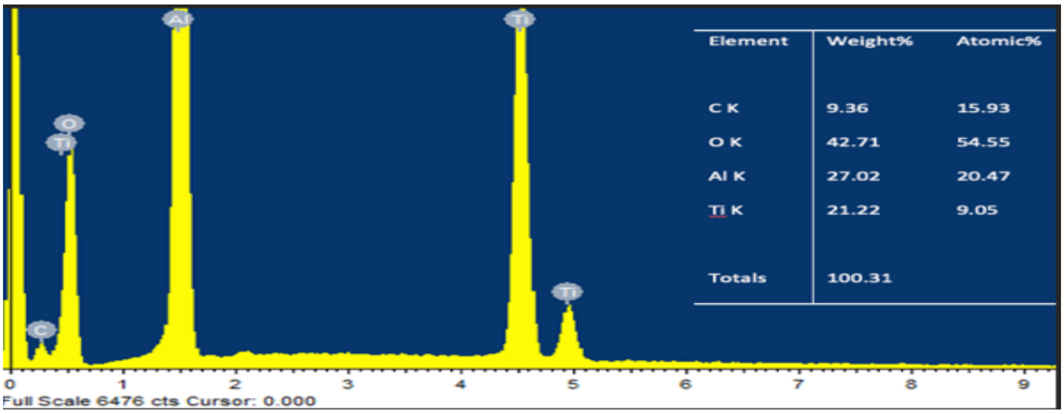

EDAX

Figure 26 SEM/EDAX images of the outer surface of the B6000nm core sample.

4.2 Overview of the experimental results and analysis

In this study, permeability serves as the fundamental parameter and was used in deriving additional engineering parameters, such as mobility, Darcy flux and reservoir quality index. These metrics are crucial for evaluating the transport properties of gases within nanoporous ceramic cores, which are utilised as analogues for low permeability reservoir cores. Kantzas et al. (2012) suggested that to achieve reliable experimental measurements of permeability, a minimum of 12 flow tests should be conducted, encompassing four distinct flow rates across three isobaric conditions.

The scope of experimental work in this research significantly expanded on these guidelines, with over 1,000 permeation tests conducted and more than 10,000 data points collected for analysis. This extensive dataset exceeds the recommendations of Kantzas et al. (2012) by more than a hundredfold, thereby enhancing the robustness and reliability of the findings. Such a comprehensive experimental approach not only solidifies the validity of the permeability measurements but also instils a high degree of confidence in the sophisticated analyses presented within this research.

Engineering interpretations and assumptions have been systematically formulated to explain the phenomena observed throughout the experimental investigations. The extensive dataset, encompassing numerous permeation test runs, facilitates the direct computation of the dependent parameters such as permeability, mobility, Darcy flux and reservoir quality index. This dataset integrates diverse experimental conditions across the five distinctive core samples, the three types of gases (including a mixture), eight isobaric conditions, and four isothermal conditions, recording variables such as flow rate, operating temperature, and pressure conditions.

For methodical analysis, the experimental data were systematically organised in an Excel spreadsheet, alongside additional parameters like the geometric dimensions and physical and petrophysical properties of the nanoporous core samples, as well as the viscosity of the gases involved. To enhance analytical robustness, this spreadsheet was subsequently imported into Python—a high-level, interpreted programming language celebrated for its readability, simplicity, and wide applicability in data analysis. Python was selected for data analysis due to its comprehensive standard library and a vast ecosystem of third-party packages, which significantly augment its analytical capabilities.

An extensive analysis of the dataset was performed, yielding summary statistics for each numerical attribute, such as mean, median, standard deviation, maximum, and minimum values, as outlined in **Table 4.** A correlation matrix was also developed to reveal the interdependencies among variables, which was subsequently visualised using a heatmap plot, as depicted in **Figure 27**. This visual representation proved instrumental in uncovering significant relationships among variables. Further investigations concentrated on the selection of pertinent variables, including temperature, pressure and viscosity, chosen for their pronounced effects on critical reservoir parameters such as permeability, mobility etc. Building upon these foundational analyses, a machine learning model employing a regression algorithm was developed. This model captures the intricate relationships between the identified key features and the target variables. The analysis was further substantiated by integrating findings with established theoretical and empirical research from the domains of petroleum engineering, geomechanics, and hydrogeology, thus significantly bolstering the study's scientific rigor and validity.

Finally, the analysis concludes with a comparison of experimental data and field data for permeability, mobility, Darcy flux, and reservoir quality index, to ascertain the applicability of nanoporous ceramic cores as mimetic models for low permeability reservoirs.

Table 4 Statistical summary of feature and target variables

Variables	Mean	Median	Standard Deviation	Min	Max
Temperature (K)	365.5	348	68.4	293	473
Pressure Drop (atm)	1.43	1.43	0.68	0.4	2.47
Viscosity (cp)	0.0155	0.0151	0.0033	0.011	0.023
Permeability (mD)	4.29×10^{-4}	3.17×10^{-4}	3.21×10^{-4}	7.9×10^{-5}	1.74×10^{-3}
Mobility (mD/cp)	0.028	0.021	0.021	0.0054	0.11
Flux (cm3/cm2*sec)	0.270	0.280	0.158	0.049	0.619
Reservoir Quality Index (mD)	4.45×10^{-6}	3.28×10^{-6}	3.41×10^{-6}	7.23×10^{-7}	1.94×10^{-5}

4.3 Experimental data correlation matrix of the nanoporous ceramic cores.

The correlation heatmap depicted in **Figure 27** provides a quantitative evaluation of the interrelationships among the key reservoir parameters pertinent to the conducted experimental investigations. Each cell within the heatmap represents the correlation coefficient between pairs of these variables, with values spanning from -1.0 to 1.0. These values reflect a spectrum from perfect negative correlation to perfect positive correlation, respectively, thereby quantifying the degree to which one variable may predictably vary in relation to another within the experimental context.

Temperature exhibits a strong positive correlation with viscosity (0.78), suggesting that as temperature increases, viscosity of the gas also tends to increase. Additionally, temperature exhibits a mild positive correlation with permeability (+0.23), suggesting that increase in temperature may slightly enhance permeability. These findings are backed by existing literatures such as Cramer (2012), Ling et al. (2009). Temperature also shows a weak or negligible correlations with other variables, meaning it has little to no direct effect on pressure, mobility, reservoir quality index, and Darcy flux.

Pressure shows strong negative correlations with permeability (-0.79), mobility (-0.79), and reservoir quality index (-0.77). These negative correlations suggest that higher pressure is associated with lower values of these variables, which could be because higher pressure indicates greater resistance within the medium, reducing these properties as documented by Lake and Fanchi (2006) and Naaktgeboren et al. (2012). There is also a moderate positive correlation with flux (0.30), implying that higher pressure is somewhat associated with increased Darcy flux, possibly due to the increased driving force overcoming resistance to fluid flow. Pressure has negligible correlations with temperature, indicating that it does not significantly influence these variables.

Viscosity demonstrates a strong positive correlation with temperature (0.78), reinforcing the idea that as temperature increases, the viscosity of gas increases because the gas molecules gain kinetic energy, leading to more frequent collisions (Palmer and Wright, 2003). A slight positive correlation (+0.14) was observed between viscosity and permeability, supporting the modified Darcy's equation that indicates a direct relationship between these two parameters. Conversely, a negative correlation (-0.14) was observed between viscosity and mobility. This aligns with the understanding that increased viscosity reduces mobility when permeability is constant, highlighting the significant impact of fluid properties on reservoir dynamics (Chen and Zhao, 2020, Li and Horne, 2018, Al-Busafi and Jones, 2021). Viscosity shows negligible correlations with other variables, indicating little to no direct impact on pressure, reservoir quality index and Darcy flux.

Permeability has strong negative correlations with pressure (-0.79) and strong positive correlations with mobility (0.94) and reservoir quality index (0.99). These correlations indicate that higher permeability is associated with lower pressure drops and higher mobility and reservoir quality index. This relationship highlights the interconnected nature of these properties in facilitating fluid flow. Permeability has a negligible correlation with flux (0.02), indicating almost no direct effect on flux.

Mobility shows strong negative correlations with pressure (-0.79) and strong positive correlations with permeability (0.94) and reservoir quality index (0.93). These strong relationships suggest that higher mobility is associated with lower pressure and higher permeability and reservoir quality. This indicates the interconnectedness of these variables in enhancing fluid flow properties. Mobility shows negligible correlations with other variables, indicating little to no direct impact on temperature, viscosity, and Darcy flux.

Reservoir quality index demonstrates strong negative correlations with pressure (-0.77) and strong positive correlations with permeability (0.99) and Mobility (0.93). These correlations indicate that a higher reservoir quality index is associated with lower pressure and higher permeability and mobility. The reservoir quality index has a negligible correlation with the Darcy flux (0.06), indicating almost no direct effect on flux.

Lastly, the Darcy flux has a weak positive correlation with pressure (0.30), indicating that higher Darcy flux can be associated with higher pressure, likely due to the increased driving force overcoming resistance to fluid flow. Flux shows negligible correlations with other variables, indicating little to no direct impact on temperature, viscosity, permeability, mobility, and reservoir quality.

In summary, the heatmap reveals that the strongest correlations are between temperature and viscosity, pressure and permeability/mobility/reservoir quality, and permeability/mobility/reservoir quality. These relationships are vital for optimising reservoir performance and fluid flow characteristics in experimental settings, providing valuable insights into how changes in one variable can affect others.

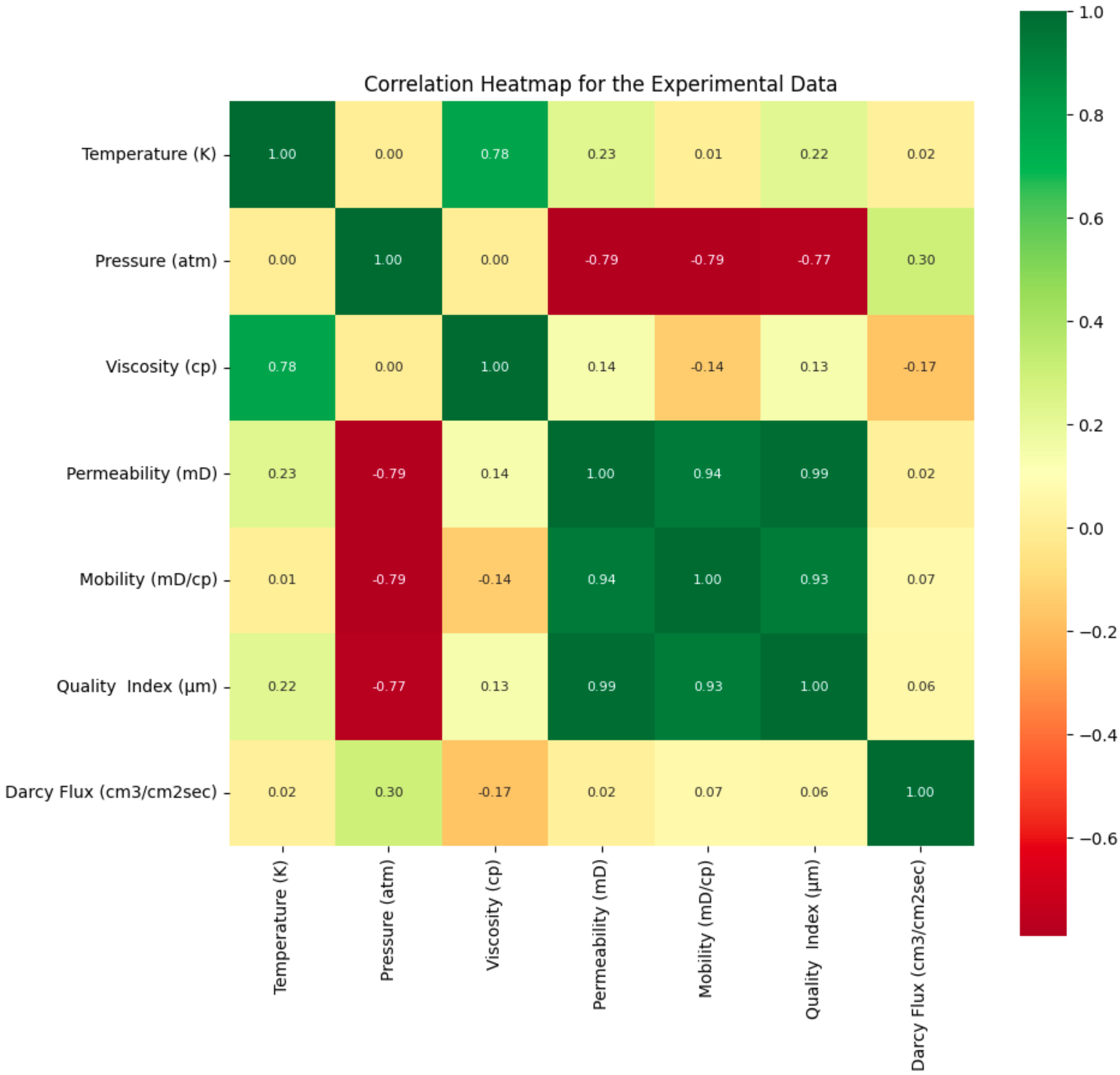

Figure 27 Correlation matrix.

4.4 Permeability analysis of the nanoporous ceramic cores

Permeability analysis is a fundamental aspect of evaluating the performance and suitability of nanoporous ceramic cores in simulating reservoirs. The research rigorously examines key parameters—temperature, pressure, and viscosity—and their effects on permeability, which has been extensively studied and documented by notable authors (Zhou et al. 2020, Ahmed, 2018, Johnson, 2018, Zoback, 2010, Holstein, 2007, Nelson, 2009 and Wang, 2000). The well-established permeability analysis serves as a model to enhance the application of nanoporous ceramic core samples in simulating reservoir core samples. This implies that if the permeability estimated in this study, when plotted against the independent pressure variables, corroborates widely discussed findings in the literature, the experimental data using the nanoporous ceramic cores can significantly be used to study other reservoir parameters. The study evaluates the correlations between these independent factors (temperature, pressure, and viscosity) and permeability, mobility, Darcy flux, and reservoir quality index. It also investigates the performance of the selected gases (CH_4, CO_2, and 60%CH_4/40%CO_2) across the five nanoporous ceramic cores. This approach aligns with the perspectives of Berg (2019), Tiab and Donaldson (2014), and Ahmed (2006), who emphasised that the geometry and connectivity of pore spaces are crucial in determining reservoir parameters, that fluid properties such as viscosity significantly affect the ease of flow through porous media, and that changes in temperature and pressure can alter both fluid and rock properties, thereby influencing permeability, mobility, Darcy flux, and reservoir quality index characteristics.

4.4.1 Permeability response to pressure in the nanoporous ceramic cores.

The graph provided in **Figure 28** illustrates the relationship between permeability (in milliDarcies, mD) and pressure (in atmospheres, atm) at various temperatures (293K, 323K, 373K, and 473K). Each temperature is represented by a different coloured line, showing how permeability changes as the pressure increases. Additionally, the graph includes a linear regression equation, and R-squared value, providing a statistical overview of the trend observed in the data.

One key observation is the negative correlation between pressure and permeability. As the pressure increases, permeability decreases consistently across all temperature conditions. This inverse relationship suggests that higher pressure result in lower permeability aligning with Darcy equation and reservoir studies from several notable literatures (such as Wang, 2000, Nelson, 2009 and Zoback, 2010). The alignment of these authoritative works with this current study’s findings enriches the analysis and lends substantial credibility to the application of the nanoporous ceramic core model.

Temperature also plays a significant role in influencing permeability. The graph shows that at higher temperatures (473K), the permeability values are generally higher across the entire pressure range compared to lower temperatures (293K). This indicates that higher temperatures enhance permeability, making it easier for fluids to pass through the porous medium. Consistent with this study's findings, both Ahmed (2018) and Zhou et al. (2020) observed that increases in temperature tend to slightly enhance the permeability of rock formations. These observations are further corroborated by empirical data from Li and Horne (2018) and Tian and Babadagli (2022). Collectively, these studies provide a robust scholarly foundation, supporting the validity of the study and deepening our understanding of the nuanced ways in which temperature influences permeability across various geological contexts.

The linear regression analysis further quantifies this relationship. The regression equation $y = -3.74 \times 10^{-4}x + 9.64 \times 10^{-4}$ and an R-squared (R^2) value of 0.62 are annotated on the graph

The negative slope of the regression equation, $-3.74 \times 10^{-4}x$ confirms the inverse relationship between pressure and permeability, while the R-squared value indicates that approximately 62% of the variability in permeability can be explained by changes in pressure. This moderate level of correlation suggests that other factors, in addition to pressure, may also influence permeability.

The shaded regions around each line represent confidence intervals, indicating the variability of the data. These intervals provide a visual representation of the degree of confidence in the measured permeability values at each pressure drop. The width of the confidence intervals varies, reflecting the precision of the measurements and the inherent variability in the data.

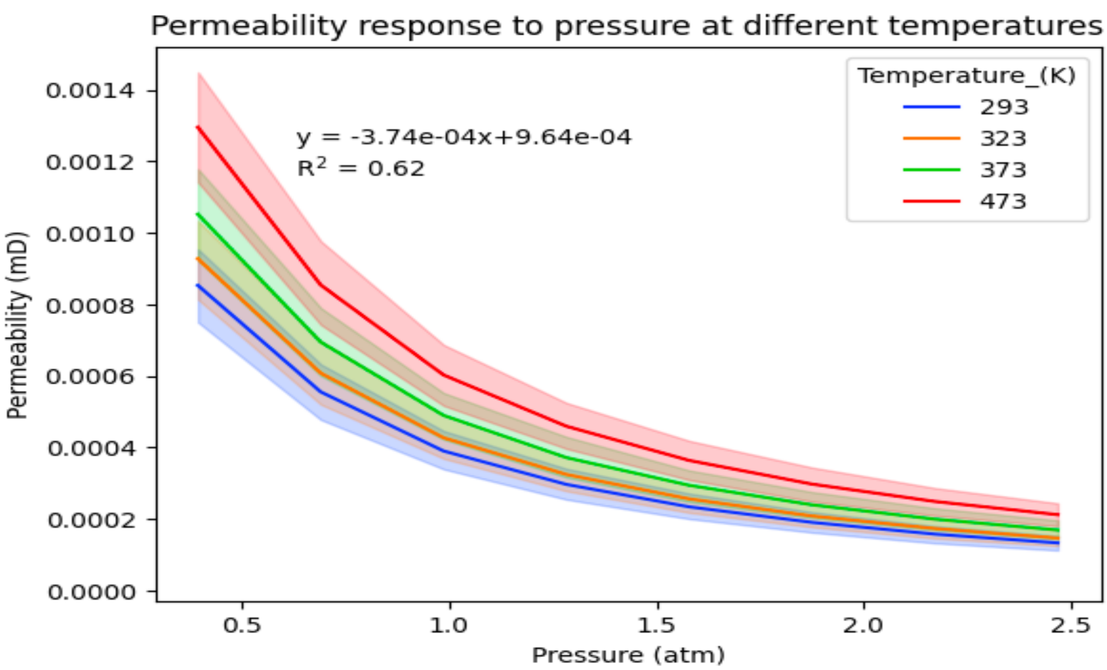

Figure 28 Permeability response to pressure at different temperatures across the entire experimental dataset.

4.4.1.1 Industrial and engineering implications

The findings from the analysis of permeability response to pressure at different temperatures have significant industrial and engineering implications, particularly in the fields of reservoir engineering, enhanced oil recovery (EOR), and fluid transport within porous media.

Firstly, the observed relationship between temperature and permeability highlights the potential benefits of thermal EOR techniques. As the study indicates that higher temperatures enhance permeability, EOR methods such as steam injection or in-situ combustion could be optimised to improve oil recovery rates. By increasing the temperature within the reservoir, the viscosity of the oil is reduced, facilitating its flow through the porous rock as emphasised by Johnson, (2018) and Holstein, (2007). This knowledge helps in designing more effective thermal EOR strategies, potentially leading to increased hydrocarbon recovery and prolonged reservoir life.

Secondly, understanding how pressure and temperature affect permeability is vital for reservoir simulation and management. The inverse relationship between pressure and permeability implies that managing reservoir pressure is fundamental to maintaining optimal fluid flow. Reservoir engineers can use this information to develop more meaningful models that predict fluid behaviour under varying pressure and temperature conditions (Dake, 2001). These models are essential for planning production schedules, designing well placements, and implementing pressure maintenance strategies to maximise extraction efficiency.

Thirdly, the findings also have implications for hydraulic fracturing and other well stimulation techniques. Knowing that higher temperatures can improve permeability suggests that pre-heating the reservoir rock before fracturing could enhance the effectiveness of the fractures (Alfarge et al. 2020). This approach could create more efficient pathways for oil and gas to flow to the wellbore, improving the overall productivity of the well. Additionally, understanding the pressure-permeability relationship helps in optimising the fracturing process to avoid excessive pressure drops that could hinder fluid flow.

4.4.2 Permeability response to viscosity in the nanoporous ceramic cores.

Figure 29 presents a plot that illustrates the relationship between viscosity, measured in centipoise (cp), and permeability, measured in millidarcies (mD for three different gases: methane (CH_4), a 60% methane and 40% carbon dioxide mixture (60%CH_4/40%CO_2), and carbon dioxide (CO_2). Each gas is represented by a different coloured line with shaded areas indicating confidence intervals, which enhances the visual representation of data variability and trend reliability.

The key observations from the plot include the linear fit equation $y = 1.35 \times 10^{-2} x + 2.21 \times 10^{-4}$ with an R^2 value of 0.02. This low R^2 value suggests that viscosity accounts for only a small fraction of the variability in permeability across the different gases. This indicates that other factors may significantly influence permeability, overshadowing the effect of viscosity.

For methane (CH_4), represented by the blue line, there is a slightly increasing trend in permeability as viscosity increases. The confidence interval for methane is relatively narrow, indicating consistent data with less variability. This suggests that methane's flow behaviour through the porous medium is more predictable compared to the other gases.

The 60% methane and 40% carbon dioxide mixture (60%CH_4/40%CO_2), represented by the orange line, also shows a slightly increasing trend in permeability with increasing viscosity. However, the confidence interval for the mixture is wider than that for methane, suggesting greater variability in the data. This could be due to the complex interactions between methane and carbon dioxide molecules within the pores.

Carbon dioxide (CO_2), represented by the green line, displays the highest permeability stretch among the three gases as viscosity increases. However, the confidence interval for carbon dioxide is the widest, indicating significant variability in the data. This could be due to CO_2's distinct physical properties, such as higher density and different molecular interactions with the porous medium, leading to more erratic flow behaviour.

The positive slopes for all three gases indicate that as viscosity increases, permeability also increases, albeit weakly aligning with the Darcy’s equation (Bear, 2013, Dullien, 2012, Bird et al. 2002).

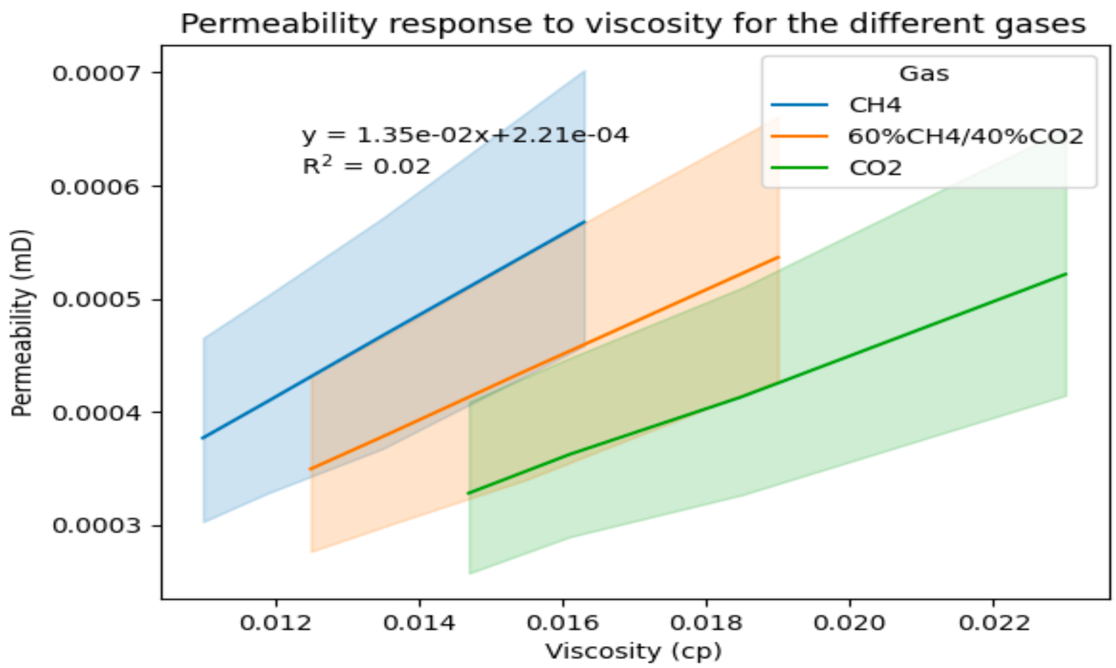

Figure 29 Permeability response to viscosity for the different gases across the entire dataset.

4.4.2.2 Industrial and engineering implications

The observed trend that permeability slightly increases with viscosity, suggests that other factors significantly influence fluid flow through the nanoporous ceramic cores. This insight can help engineers better predict and manage fluid behaviour in reservoirs. For instance, in EOR techniques, in-depth understanding of gas permeability can lead to more effective injection strategies. Methane (CH_4) shows a consistent relationship between permeability and viscosity, indicating it could be a reliable choice for gas injection projects aimed at improving oil recovery.

The significant variability observed with carbon dioxide (CO_2) permeability highlights the importance of considering gas-specific properties when designing and implementing CO_2 injection strategies for EOR or carbon sequestration. The wide confidence intervals indicate that CO_2's behaviour in the reservoir can be unpredictable, which necessitates careful monitoring and adaptive management techniques. This finding underscores the need for robust reservoir simulation models that incorporate the unique characteristics of CO_2 to ensure effective and safe operations.

The mixture of 60% methane and 40% carbon dioxide (60%CH4/40%CO2) showing intermediate permeability values suggests that blending gases could be a viable strategy for optimising gas injection processes. This blend might balance the predictable behaviour of methane with the effective displacement properties of CO_2, potentially leading to improved overall reservoir performance. This approach could be particularly useful in reservoirs where single gas injection has proven less effective

From an engineering perspective, the results highlight the importance of tailoring gas injection and fluid management strategies to the specific conditions of each reservoir. Engineers must consider not only the general properties of the injected gases but also how these properties interact with the unique geological and petrophysical characteristics of the reservoir. The findings advocate for a more nuanced approach to reservoir engineering.

4.5 Mobility analysis of the nanoporous ceramic cores

As delineated by Dake (2001), mobility stands as a critical parameter in influencing hydrocarbon recovery and production efficiency. Its role is essential within the oil and gas industry, primarily because it significantly impacts displacement efficiency during reservoir exploitation. A higher mobility ratio typically results in more efficient displacement and enhances sweep efficiency, both of which are vital for refining production strategies. In the context of enhanced oil recovery (EOR) operations, particularly those employing chemical and thermal methods, the manipulation of mobility is pivotal, as highlighted by Alfarge et al. (2020)

For analytical consistency, this research has identified three principal parameters (temperature, pressure and viscosity) that could affect mobility and explored their correlation with mobility.

As underlined by Berg (2019) and Selley (2000), higher viscosity tends to decrease mobility, impacting hydrocarbon recovery rates and the efficacy of displacement processes. Conversely, higher temperatures typically reduce oil viscosity, which may enhance mobility. Additionally, variations in pressure can modify fluid densities and viscosities, thereby influencing mobility.

4.5.1 Mobility response to pressure in the nanoporous ceramic cores.

The provided graph in **Figure 30** illustrates the relationship between mobility (mD/cp) and pressure (atm) for different temperatures (293K, 323K, 373K, and 473K). The graph presents a clear downward trend in mobility with increasing pressure across all temperature levels, which is indicated by the linear regression equation $y = -2.47\times10^{-2}x + 6.37 \times 10^{-2}$ and an R^2 value of 0.63.

The shaded regions around the lines represent the confidence intervals, showing the variability in the data. The steepness of the slope, which is negative, implies a significant decrease in mobility as pressure increases. This trend is consistent across all the temperatures tested, indicating a robust inverse relationship between pressure and mobility.

At lower pressures, mobility values are relatively higher, suggesting that fluids move more easily through the porous media under these conditions. As the pressure increases, the mobility decreases, likely due to the increased resistance to fluid flow within the pore spaces of the material. The near overlap of the mobility curves for different temperatures suggests that changes in temperature have virtually no effect on mobility within the studied dataset, and that pressure plays a more dominant role in this relationship. This observation aligned with Bear's (1972) seminal work on fluid dynamics within porous media, supporting the observed notion that temperature has a minimal effect on fluid mobility, reinforcing the idea that other variables might be more influential. This observation is also echoed by McAllister et al. (2017) and Lake and Fanchi (2006).

The R^2 value of 0.63 suggests a moderate fit of the linear model to the observed data, indicating that the linear relationship between pressure and mobility is reasonably moderate. This implies that the model can predict the mobility response based on pressure changes within the tested temperature range.

To bolsters the observed negative correlation between pressure and mobility, this study incorporates theoretical foundations and empirical evidence, enhancing the credibility of the analysis. Bear (1972), a seminal figure in hydrogeology and petroleum engineering, provides insights explaining how increased flow resistance due to increasing pressure could account for this correlation. His discussions on the interplay between pressure gradients and fluid mobility directly relate to the trends identified in this research. Additionally, Darcy's work (Darcy, 1856) supports these findings by demonstrating how fluid flow through porous media decreases as resistance from increasing pressure gradients intensifies. This empirical relationship elucidates why higher pressure might reduce mobility, indicating that flow resistance grows with pressure, hindering fluid movement.

Lake and Walsh (2008) research into advanced topics in oil recovery, providing detailed analyses on how pressure impacts oil mobility within reservoirs, further validating the negative correlation observed in this study. Hommel et al. (2018) research on permeability and fluid flow also adds valuable context, showing how varying pressures can influence the mobility of different phases within a reservoir, enhancing our understanding of pressure-mobility dynamics.

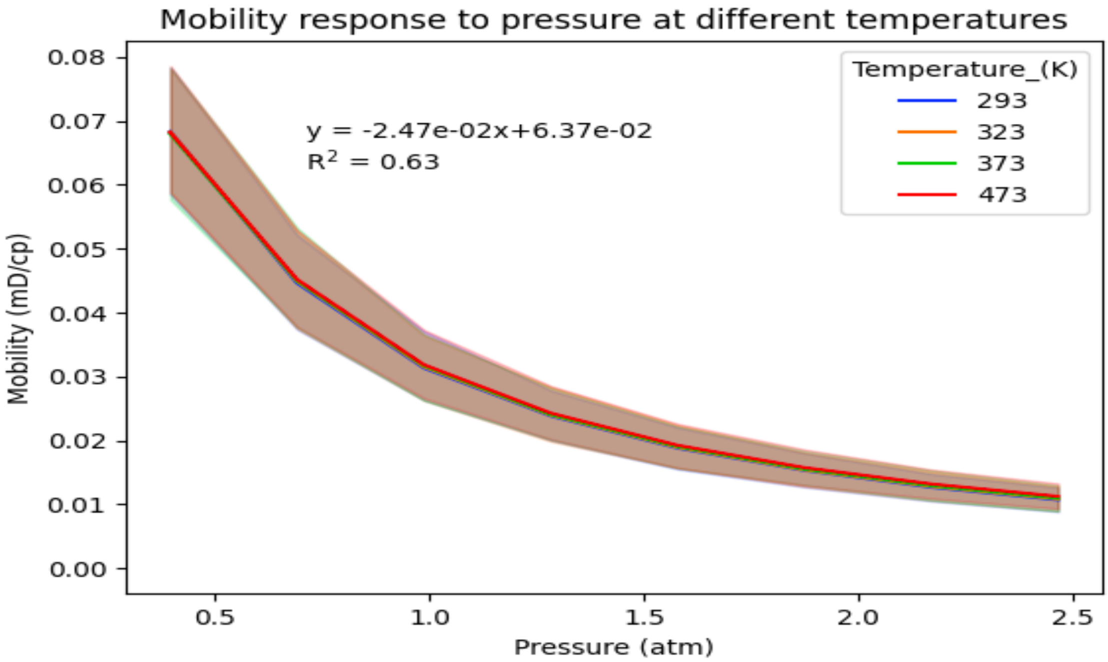

Figure 30 Mobility response to pressure at different temperatures across the entire experimental dataset.

4.5.1.1 Industrial and engineering implications

In enhanced oil recovery (EOR) operations, understanding how pressure influences mobility is essential for designing effective recovery strategies. The data suggests that maintaining lower pressures can enhance fluid mobility, thereby improving the efficiency of oil and gas extraction from reservoirs. This is particularly important in the context of unconventional reservoirs, such as shale gas and tight oil formations, where fluid flow is inherently more challenging due to low permeability. By strategically managing pressure, operators can maximise hydrocarbon recovery while minimising operational costs (Ahmed, 2018).

Furthermore, the findings indicate that temperature variations, while having some impact, are less significant than pressure changes in influencing mobility. This insight can guide the design of thermal EOR techniques, such as steam injection or in-situ combustion. These methods can be optimised by focusing more on pressure modulation rather than solely on temperature increases, potentially reducing the energy input required for heating and thereby lowering operational expenses (Green and Willhite, 2018).

In terms of reservoir management, the ability to predict mobility based on pressure conditions allows for more precise modelling and simulation of reservoir behaviour. Advanced reservoir simulation models that incorporate these findings can provide more meaninful forecasts of production rates and reservoir performance over time. This can aid in the planning and execution of drilling programs, well placement, and the design of artificial lift systems. It also helps in identifying the optimal operational settings to sustain reservoir pressure and enhance long-term production (Lake and Fanchi, 2006).

Additionally, the findings are relevant to the design and implementation of hydraulic fracturing operations. Understanding how pressure impacts mobility can inform the selection of fracturing fluids and proppant materials, ensuring that the induced fractures remain open and effective at enhancing fluid flow. This can lead to more efficient fracturing treatments, improving the overall productivity of wells (Tiab and Donaldson, 2014).

4.5.2 Mobility response to viscosity in the nanoporous ceramic cores.

Figure 31 presents a graph showing the relationship between mobility and viscosity for three different gases: methane (CH_4), a mixture of 60% methane and 40% carbon dioxide (60%CH4/40%CO_2), and pure carbon dioxide (CO_2). The mobility is measured in millidarcy per centipoise (mD/cp), and the viscosity is measured in centipoise (cp). The plot shows individual data points and the fitted regression lines for each gas, along with the shaded regions representing confidence intervals. The regression equation $y = -8.80 \times 10^{-1}x + 4.20 \times 10^{-2}$, and R-squared value $R^2 = 0.02$ for the overall fit are also displayed on the graph, indicating the strength and nature of the relationship between viscosity and mobility.

For methane (CH_4), represented by the blue data points and line, the regression line shows a slight downward trend, suggesting a minor decrease in mobility with increasing viscosity evident from the negative slop, -8.80×10^{-1}. However, the R-squared value is very low ($R^2 = 0.02$), indicating that viscosity has a minimal effect on the mobility of methane within the observed range. The confidence interval is relatively wide, reflecting significant variability in the data. This variability suggests that other factors may influence the mobility of methane more than viscosity alone.

The orange data points, and line correspond to the 60%CH_4/40%CO_2 gas mixture. The regression line for this mixture appears relatively flat, indicating little to no change in mobility with varying viscosity. The low R-squared value ($R^2 = 0.02$) further supports that viscosity does not significantly impact the mobility of this gas mixture within the observed range. Similar to methane, the confidence interval for the mixture is also wide, suggesting considerable variability in the data. This flat trend implies that the combination of methane and carbon dioxide in this ratio does not significantly alter the mobility as viscosity changes.

For carbon dioxide (CO_2), denoted by the green data points and line, the regression line is almost horizontal, indicating no significant relationship between viscosity and mobility. The R-squared value is again low, reinforcing that viscosity does not substantially affect the mobility of CO_2 within the observed range. Notably, the confidence interval for CO_2 is the narrowest among the three gases, indicating less variability in the data compared to methane and the gas mixture. This stability suggests that CO_2's mobility is less influenced by viscosity changes, possibly due to its consistent physical properties in the given range.

Overall, the regression analysis shows that for all three gases, there is no strong correlation between viscosity and mobility within the given viscosity range. The flat slopes of the regression lines and low R-squared values indicate that changes in viscosity do not significantly influence mobility for CH_4, CO_2, or their mixture. Methane and the gas mixture exhibit more variability in their mobility data compared to carbon dioxide, as indicated by the wider confidence intervals. These findings suggest that other factors, such as pressure, temperature, or the intrinsic properties of the porous medium, might play a more crucial role in determining mobility than viscosity alone.

The interpretation aligns with findings from studies by Ahmed (2018) and Lake and Fanchi (2006), which emphasise the complex interplay of various reservoir parameters on fluid flow. Alfarge et al. (2020) also highlight that while viscosity is a crucial factor in fluid dynamics, its impact on mobility must be considered alongside other parameters. Additionally, Bachu (2008) discusses the importance of understanding gas properties in the context of reservoir management and environmental implications.

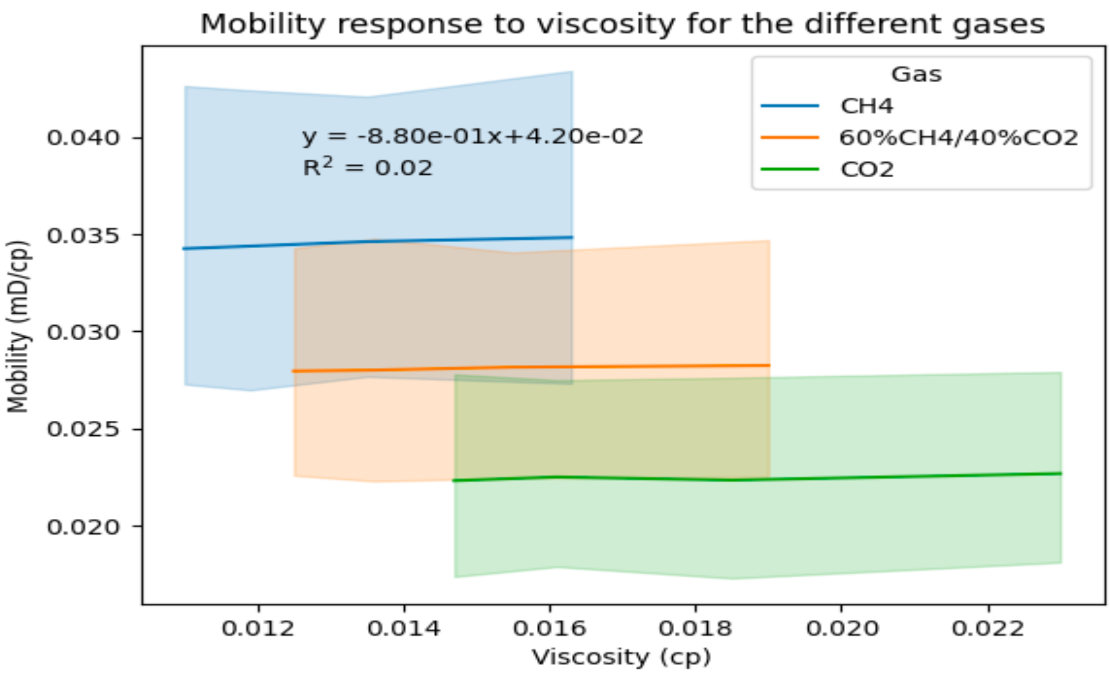

Figure 31 Mobility response to viscosity for the different gases across the entire dataset.

4.5.4.1 Industrial and engineering implications

The negative correlation between viscosity and mobility plays a crucial role across various industrial and engineering fields, especially in areas involving fluid dynamics such as chemical processing, oil and gas production, and hydraulic engineering.

In enhanced oil recovery (EOR) techniques, fluids with lower viscosity are preferred as they enhance mobility, facilitating more efficient oil extraction. This negative correlation implies that decreasing the viscosity of injected fluids improves their transport through the reservoir, thereby enhancing their ability to displace oil and boost recovery rates. Understanding this relationship is key for effectively managing fluid transport within reservoirs. For instance, heavier, more viscous oils may require heating or dilution with lighter hydrocarbons to enhance mobility and recovery efficiency. Terry et al. (2015), provide valuable insights into reservoir engineering techniques that explore how fluid properties like viscosity affect oil recovery.

The minimal impact of viscosity on mobility, as indicated by the low R-squared values in the regression analyses, suggests that viscosity alone may not be a primary factor influencing fluid movement through porous media. Enhanced oil recovery (EOR) techniques, which often rely on modifying fluid properties to improve extraction efficiency. The results imply that while viscosity adjustments can be beneficial, they should be considered alongside other factors such as pressure and temperature to achieve the desired mobility enhancements (Lake and Fanchi, 2006).

4.6 Darcy flux analysis of the nanoporous ceramic cores

Darcy flux, also known as Darcy velocity, is a fundamental concept in reservoir engineering that quantifies the flow rate of a fluid through a porous medium as described by Zijl (2004). In the context of the nanoporous ceramic cores analysed in this study, Darcy flux analysis involves calculating the volumetric flow rate per unit area of the core samples. This analysis helps to understand how much the cores can transmit fluids, which is crucial for applications in enhanced oil recovery and other reservoir engineering processes. This analysis is essential for evaluating the performance of the ceramic cores in mirroring natural reservoirs. By understanding the flux behaviour under various pressures, temperatures, and fluid viscosities, researchers can assess the suitability of these materials for reservoir applications and develop strategies to optimise fluid extraction processes.

4.6.1 Darcy flux response to pressure in the nanoporous ceramic cores.

The graph in **Figure 32** illustrates the Darcy flux response to pressure at different temperatures, providing insight into how pressure influences fluid flow through the nanoporous ceramic cores at various temperature levels. Darcy flux is plotted against the pressure applied across the core samples for four different temperatures: 293K, 323K, 373K, and 473K.

The linear regression equation displayed on the graph, $y = 6.93\times10^{-2}x + 1.71 \times 10^{-1}$, along with an R^2 value of 0.1, suggests a positive relationship between pressure and Darcy flux. However, the relatively low R^2 value indicates that the linear model explains only 10% of the variability in Darcy flux, implying that other factors may also significantly influence the flux.

At all temperature levels, an increase in pressure results in a higher Darcy flux. This trend is expected, as higher pressure generally enhances the driving force for fluid flow through the porous media. Notably, the flux increases more sharply at lower pressures, particularly between 0.5atm and 1.0atm, indicating a nonlinear relationship in this range.

The graph also reveals that temperature has a modest effect on Darcy flux. Higher temperatures (323K, 373K, and 473K) show a slightly higher flux compared to the lowest temperature (293K). However, the temperature effect appears less pronounced than the pressure effect, as the flux values at different temperatures converge closely.

The shaded regions around the lines represent the confidence intervals, highlighting the variability in the data. The overlapping shaded regions suggest that the differences in flux due to temperature changes are within a similar range of variability.

These findings are largely supported by the research works of notable authors such as Rosti et al. (2020), Srinivasan (2016), and Jiang and Tsuji (2014), who have extensively studied the interplay between pressure, temperature, and fluid flow in porous media. They examined the dynamics of fluid movement through nanoporous materials, highlighting how increased pressure enhances fluid flow by reducing resistance within the porous structure. This study corroborates the observation that higher pressures lead to a significant increase in Darcy flux, emphasising the critical role of pressure in optimising fluid extraction processes in various industrial applications.

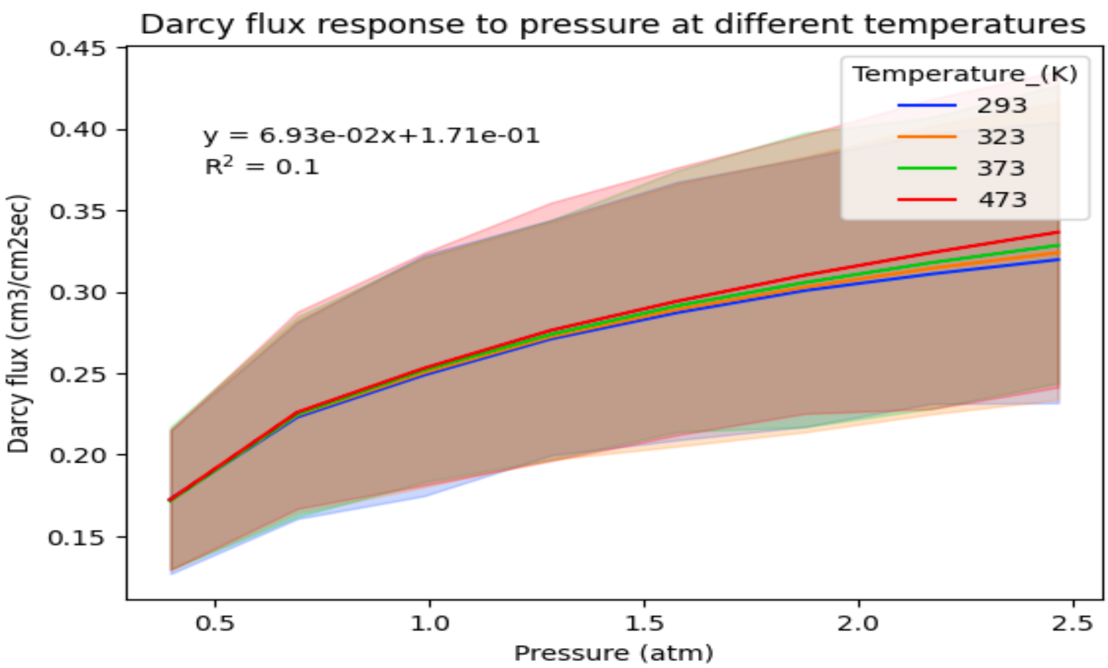

Figure 32 Darcy flux response to pressure at different temperatures across the entire experimental dataset.

4.6.1.1 Industrial and engineering implications

By comprehending how pressure influences fluid flow through porous media, engineers can better design and manage reservoir operations to maximise hydrocarbon recovery. For instance, knowing that higher pressures significantly increase Darcy flux suggests that applying higher injection pressures in EOR techniques can enhance the extraction efficiency, especially at the initial stages of fluid injection. The findings indicate that the combined effects of pressure and temperature should be carefully considered in reservoir management. For example, in geothermal energy extraction, where both high pressures and temperatures are encountered, understanding how these factors interact can help optimise the design of geothermal wells to enhance fluid circulation and heat extraction efficiency. It’s similar to optimising both the pressure and temperature settings on a coffee machine to brew the perfect cup of coffee.

Additionally, the data suggests that while temperature influences fluid flow, the primary driver remains pressure. This knowledge can inform the development of more efficient pumping systems and the selection of appropriate materials for wellbore construction that can withstand high pressures without significant loss of permeability.

4.6.2 Darcy flux response to viscosity in the nanoporous ceramic cores.

The graph in **Figure 33** presents an analysis of how the Darcy flux varies with changes in viscosity for three different gases: methane (CH_4), a 60% methane and 40% carbon dioxide mixture (60% CH_4/40% CO_2), and carbon dioxide (CO_2). Each gas is represented by a distinct line on the graph, and the shaded regions around each line denote the confidence intervals, reflecting the variability in the data.

For methane (CH_4), depicted by the blue line, the regression equation $y = -8.30 \times 10^{-4}x + 3.98 \times 10^{-1}$ suggests a slight negative slope, indicating that an increase in methane's viscosity slightly decreases its Darcy flux. The R^2 value of 0.030, however, signifies that only 3% of the variability in Darcy flux can be attributed to changes in viscosity. This low R^2 value implies that factors other than viscosity play a more significant role in determining the Darcy flux for methane. The broad confidence interval also indicates considerable variability in the measured data for methane.

The 60% methane and 40% carbon dioxide mixture, represented by the orange line, shows a relatively flat slope, suggesting minimal impact of viscosity on Darcy flux for this gas mixture. The flat slope implies that the flow through the porous medium remains relatively stable despite changes in viscosity. The confidence interval for this gas mixture is narrower compared to methane, indicating a higher degree of certainty in the measured values and reinforcing the observation that viscosity changes have a negligible effect on the flux.

For carbon dioxide (CO_2), shown by the green line, the graph similarly displays a flat relationship between viscosity and Darcy flux. This indicates that CO_2's Darcy flux is not significantly influenced by changes in viscosity within the observed range. The confidence interval around the CO_2 line, while broader than that of the gas mixture, still suggests a reasonable level of certainty, reinforcing the minimal impact of viscosity on the flux for CO_2.

Overall, the trends depicted in the graph reveal that changes in viscosity do not substantially alter the Darcy flux values for all three gases. This finding suggests that, within the range of viscosities tested, the flux remains relatively stable regardless of the gas type. The minimal impact of viscosity on Darcy flux implies that other parameters, such as pressure and temperature, likely play a more crucial role in determining fluid flow through the nanoporous ceramic cores. The low R^2 values across all gases underscore that viscosity alone does not sufficiently explain the variability in Darcy flux, highlighting the necessity of considering multiple factors in reservoir engineering analyses.

These findings are consistent with previous research by Xaba et al. (2020), Jiang and Tsuji (2014) and Karan et al. (2012) which have indicated that while viscosity can influence fluid flow, its effect may be overshadowed by other dominant factors in certain contexts. Understanding the interplay between these variables is essential for optimising fluid extraction processes in industrial applications, ensuring efficient and effective resource management.

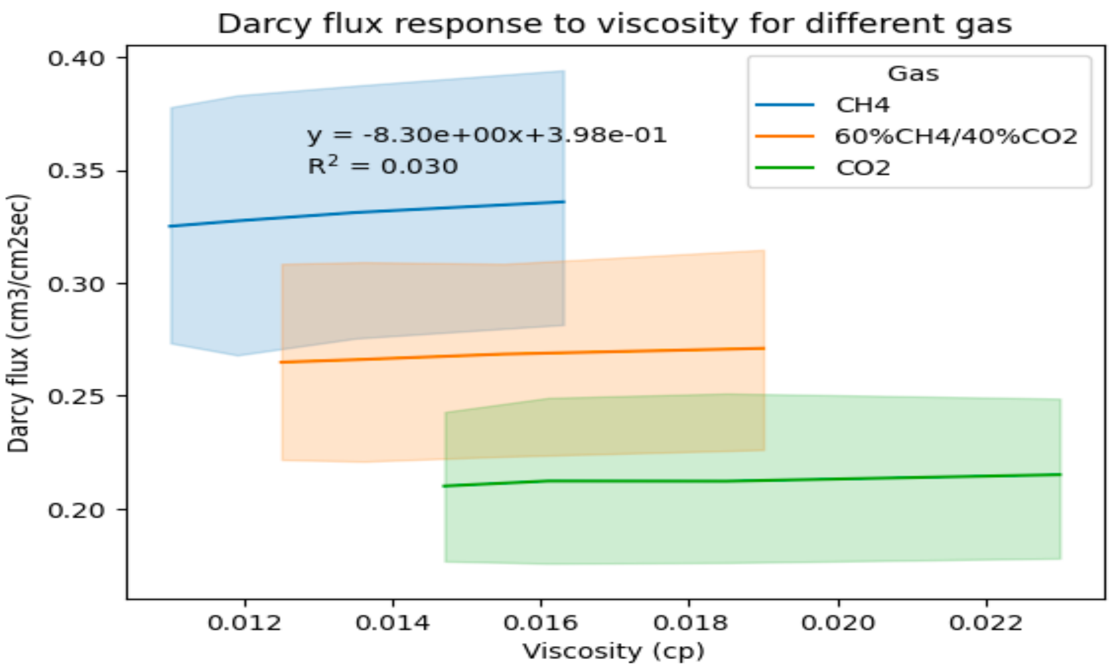

Figure 33 Darcy flux response to viscosity for the different gases across the entire dataset.

4.6.2.1 Industrial and engineering implications

the observed minimal impact of viscosity on Darcy flux for methane (CH_4), CO_2, and their mixture suggests that within the tested viscosity range, other parameters such as pressure and temperature might have a more pronounced influence on fluid flow. This insight can guide engineers to focus on optimising these other factors to enhance fluid extraction efficiency. For instance, in EOR operations, engineers might prioritise pressure management and temperature control over viscosity adjustments to improve hydrocarbon recovery rates. This approach aligns with the findings of Rosti et al. (2020), who emphasised the importance of considering multiple factors in fluid dynamics. In the context of natural gas extraction, the stability of Darcy flux across varying viscosities indicates that gas production can remain consistent even with fluctuations in gas composition. This is particularly relevant for unconventional reservoirs where the gas composition can vary significantly. The ability to maintain stable flux regardless of viscosity changes can simplify operational processes and reduce the need for complex adjustments, thereby lowering operational costs and enhancing productivity. Xaba et al. (2020), highlighted the relevance of such stability in ensuring efficient gas flow in porous media.

For CO_2 sequestration and enhanced oil recovery, the findings imply that injecting CO_2 into reservoirs can be done successfully without major concerns about changes in its viscosity significantly affecting the flux. This can streamline CO_2 injection processes and enhance the predictability of CO_2 behaviour in subsurface formations, contributing to more reliable and effective EOR strategies. Jiang and Tsuji (2014) noted the importance of understanding fluid dynamics in CO_2 sequestration to improve the effectiveness of these environmental and industrial initiatives.

4.7 Quality index analysis of the nanoporous ceramic cores

As pointed out in the literature, the reservoir quality index (RQI) is a crucial parameter in reservoir engineering used to evaluate the potential productivity of reservoir rocks. It combines permeability and porosity to provide a comprehensive assessment of the reservoir's ability to transmit and store fluids. In the analysis of nanoporous ceramic cores, the RQI is used to gauge the effectiveness of these synthetic cores in replicating the properties of low permeability reservoirs. By analysing the RQI, researchers can assess the suitability of the nanoporous ceramic cores for various industrial applications, such as enhanced oil recovery (EOR) and other reservoir management techniques. A higher RQI indicates better reservoir quality, suggesting that the core can transmit and store fluids, making it ideal for use in experimental and field studies.

4.7.1 Quality index response to pressure in the nanoporous ceramic cores.

The graph in **Figure 34** provides a comprehensive view of how the quality index, measured in micrometers (μm), responds to varying pressure levels at four distinct temperatures: 293K, 323K, 373K, and 473K.

The general trend observed in the graph is a consistent decrease in the quality index as pressure increases across all temperature conditions. This suggests that higher pressure levels tend to reduce the reservoir quality index, indicating a potential decrease in permeability or flow efficiency within the core samples. Such a trend underscores the inverse relationship between pressure and the quality of fluid flow through the porous medium.

Temperature has a notable impact on the quality index. At lower pressures, particularly between 0.5atm and 1.0atm, there is significant variability in the quality index values across different temperatures. However, as the pressure increases beyond 1.5atm, the quality index values for different temperatures tend to converge, showing less variability. For instance, at 293 K (blue line), the quality index starts higher but decreases more sharply compared to the other temperatures. This indicates that at lower temperatures, the quality index is more sensitive to pressure changes. Conversely, at higher temperatures, the initial quality index values are lower, but the rate of decrease with pressure is more gradual. For example, at 473 K (red line), the quality index starts lower and shows a less steep decline, implying that higher temperatures might mitigate the adverse impact of pressure on the quality index to some extent.

The regression analysis, represented by the equation $y = -3.88e^{-6} x + 1.00e^{-5}$ with an R^2 value of 0.6, indicates a moderate fit for the linear model. The negative slope ($-3.88e^{-6}$) confirms the downward trend of the quality index with increasing pressure. An R^2 value of 0.6 suggests that 60% of the variability in the quality index can be explained by changes in pressure, indicating a reasonably strong relationship. However, it also implies that other factors, possibly related to the inherent properties of the porous media or additional environmental conditions, contribute to the remaining 40% of the variability.

The shaded regions around each temperature line represent confidence intervals, highlighting the degree of uncertainty or variability in the measurements. The wider intervals at lower pressures suggest greater variability or uncertainty in the quality index values under these conditions. The narrowing of the shaded regions at higher pressures indicates more consistent quality index values, suggesting that the effects of pressure on the quality index stabilise as pressure increases.

These findings are strongly supported by the research of Nabawy et al. (2020), Zhuang et al. (2020), Al-Rbeawi and Kadhim (2017). These studies collectively underscore the significant impact of pressure and temperature on reservoir quality and fluid dynamics. Nabawy et al. (2020) provide comprehensive insights into the intricate relationship between reservoir properties and fluid behaviour under varying conditions. Al-Rbeawi and Kadhim (2017) highlight the importance of maintaining optimal reservoir conditions to maximise extraction efficiency and ensure reservoir longevity. Similarly, Zhuang et al. (2020) offer foundational knowledge on pressure and fluid flow in reservoirs, further validating the critical parameters identified in this study. These corroborations emphasise the robustness and applicability of the current research findings within the broader context of reservoir engineering and management.

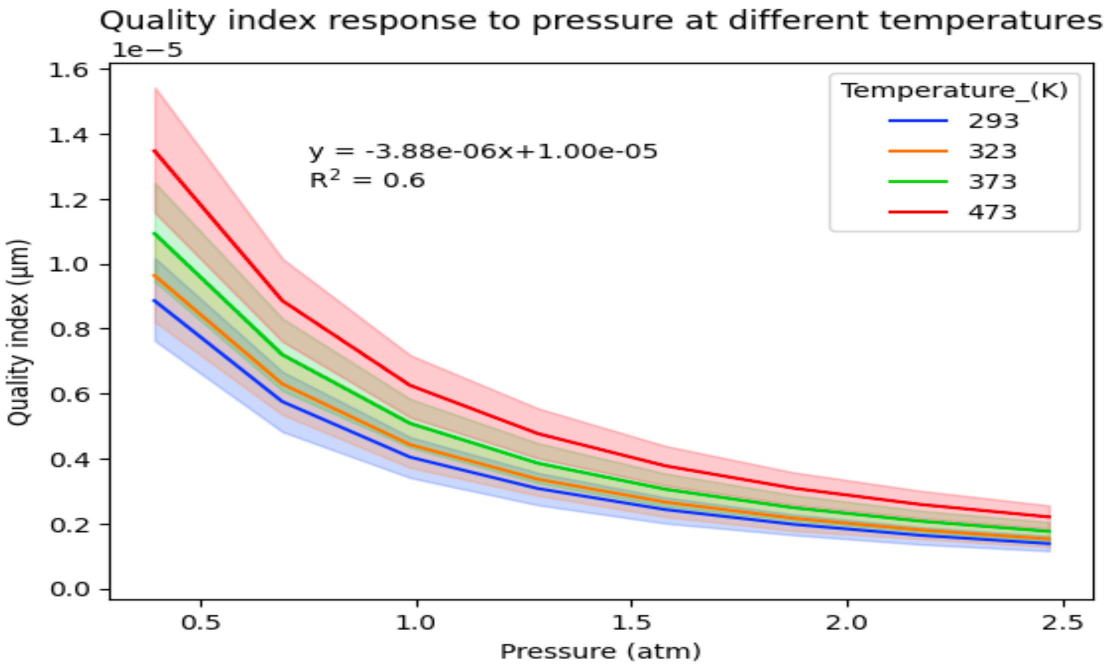

Figure 34 Quality index response to pressure at different temperatures across the entire experimental dataset.

4.7.1.1 Industrial and engineering implications

In the realm of enhanced oil recovery (EOR), the study reveals that maintaining higher temperatures can mitigate the adverse effects of pressure on the quality index. This suggests that thermal EOR techniques, such as steam injection, could be more effective in enhancing oil recovery. By managing the temperature within reservoirs, operators can sustain higher permeability and fluid flow efficiency, leading to increased hydrocarbon recovery rates. This insight aligns with the broader understanding in the industry that temperature management is critical for optimising extraction processes, as highlighted by previous research from Bear (1972) and Holstein (2007).

Effective reservoir management is another key area where these findings have substantial implications. Understanding the interaction between pressure and temperature on the quality index allows reservoir engineers to develop more effective pressure management strategies. Maintaining optimal pressure levels is crucial for preserving the quality index, especially at lower temperatures where the impact of pressure changes is more pronounced. This knowledge helps in designing reservoir management practices that maximise production efficiency and prolong the reservoir's productive life. Such practices are essential for ensuring the economic viability and sustainability of reservoir operations, as noted by Dake (2001) and Craft et al. (2014).

In terms of production strategies, the study's results can inform the optimisation of production parameters, such as pressure and temperature, to achieve the best possible outcomes in terms of hydrocarbon recovery and reservoir performance. Operators can use this information to adjust production strategies in real-time, ensuring that the conditions within the reservoir remain optimal for fluid extraction. This dynamic approach to reservoir management is crucial for maximising production efficiency and adapting to changing reservoir conditions, a practice supported by Zhuang et al. (2020).

4.7.2 Quality index response to viscosity in the nanoporous ceramic cores.

The graph in **Figure 35** depicts the quality index response to viscosity for different gases (CH_4, 60%CH_4/40%CO_2 mixture, and CO_2). The quality index (measured in micrometers, μm) is plotted on the y-axis, while viscosity (measured in centipoise, cp) is plotted on the x-axis. The data points for each gas are fitted with linear regression lines, each accompanied by a shaded area representing the confidence interval.

The linear regression equation for CH_4 is given by $y = 1.40e^{-4}x + 2.29e^{-6}$ with an R^2 value of 0.02, indicating a very weak positive correlation between viscosity and quality index for methane. The confidence interval for CH_4 is relatively wide, suggesting variability in the data points.

For the 60%CH_4/40%CO_2 mixture, the trend is similar, with a slightly weaker correlation, as indicated by the lower slope and the narrower confidence interval compared to CH_4. This suggests that the mixture behaves more consistently in terms of quality index response to viscosity.

The CO_2 data also shows a weak positive correlation between viscosity and quality index, with an R^2 value of 0.02, similar to CH_4. The confidence interval is wider than that of the mixture but narrower than that of CH_4, indicating moderate variability in the data points.

Overall, the findings indicate that the quality index slightly increases with increasing viscosity for all gases, but the correlations are weak. The variability in the confidence intervals suggests that other factors may be influencing the quality index beyond viscosity alone. This weak correlation and variability highlight the complexity of fluid dynamics within nanoporous ceramic cores and the need for further investigation to understand the underlying mechanisms fully.

These findings are supported by various studies such as Nabawy et al. (2020), Al-Rbeawi and Kadhim (2017), who investigated the effect of fluid viscosity on permeability and reservoir quality index in tight gas sandstones. Their study demonstrated that while viscosity influences permeability and the quality index, the correlation is often weak due to the complex interactions within the pore spaces.

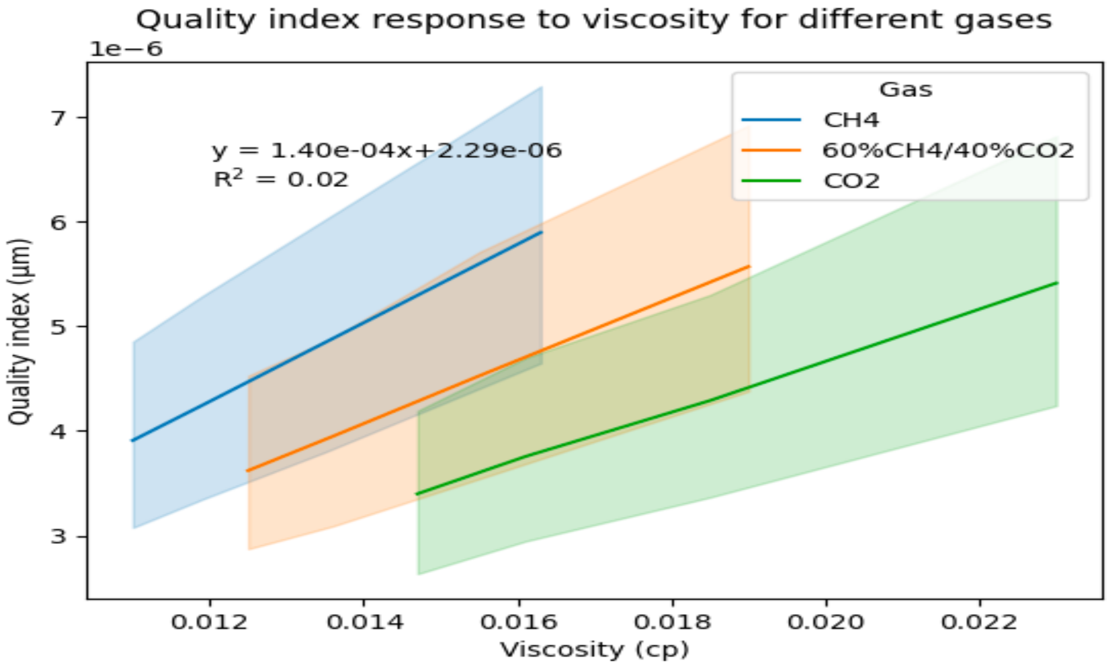

Figure 35 Quality index response to viscosity for the different gases across the entire dataset.

4.7.2.1 Industrial and engineering implications

The weak correlation between viscosity and the quality index suggests that while viscosity is an essential factor, other parameters such as pore structure and pressure conditions play a more significant role in determining the quality of the reservoir. This finding implies that reservoir engineers should consider a holistic approach, integrating multiple factors, when assessing reservoir quality and planning extraction strategies. Advanced characterisation techniques and modelling tools that account for the complex interactions between these factors can lead to more significant predictions and better reservoir management.

4.8 Parameters coupling: experimental data with field data

Experimental data were qualitatively and quantitatively compared with field data for four reservoir parameters—permeability, mobility, reservoir quality index, and Darcy flux—to identify patterns that could determine the suitability of nanoporous ceramic cores as mimetic models for low-permeability reservoirs.

4.6.1 Permeability coupling of experimental data with field data

Figure 36a and **Figure 36b** present the coupling of experimental permeability data and reservoir field data on a semi-log graph plotted against temperature. The geometry of the plots in both figures indicates a coupling correlation with similar patterns, qualitatively suggesting that the two datasets mirror each other extensively in terms of data point distribution. Both the field and experimental data show that methane (CH_4) permeability values exhibit a notable range. Despite differences in magnitude, both datasets display a significant spread in permeability values, with methane generally exhibiting higher permeability compared to carbon dioxide (CO_2). In the experimental data, CH_4 permeability values are concentrated around lower ranges, which is consistent with the trends observed in the field data.

Additionally, CO_2 clusters in both the field and experimental datasets are more dispersed, as indicated by their relatively higher coefficients of variation (CVs) of 3.22 and 0.97, respectively, compared to those of methane, which are 1.32 and 0.92, respectively. Despite differences in the range of permeability values and the magnitude of variability, both the field and experimental data for methane (CH_4) and carbon dioxide (CO_2) reveal significant similarities. The temperature influence on permeability is not the dominant factor in either dataset.

The observed trends and variability in permeability for both gases across the two datasets suggest that experimental conditions, while controlled, reasonably capture the fundamental behaviour observed in field conditions. This reinforces the validity of using experimental data to model and predict reservoir behaviour, acknowledging that natural variability in field conditions introduces a broader range of outcomes. These findings support the reliability of these experimental studies in providing insights into reservoir characteristics, which can be applied to improve the understanding and management of natural reservoirs.

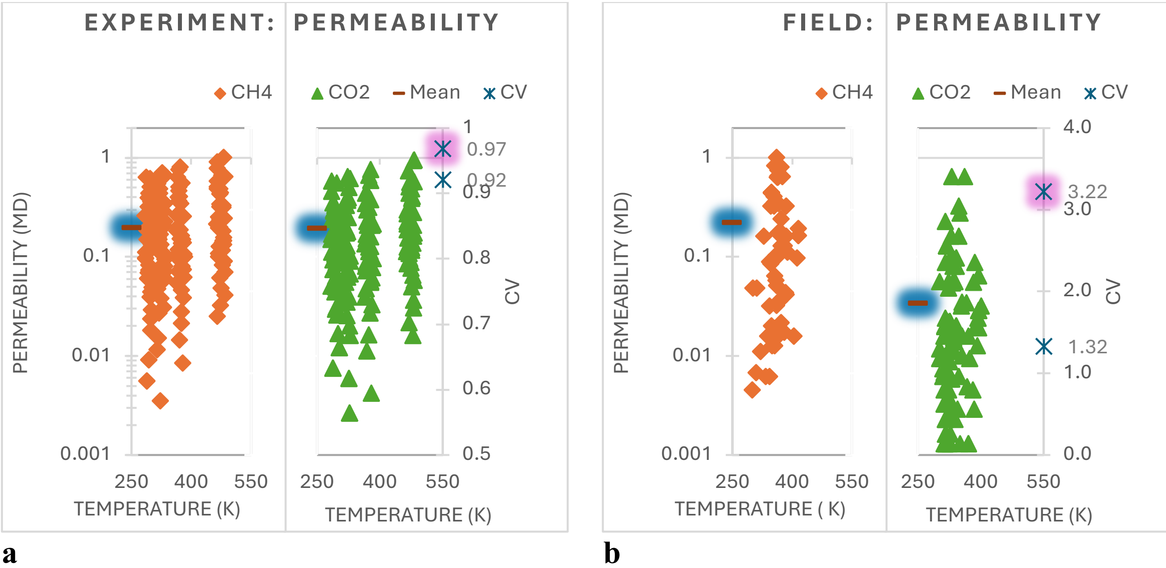

Figure 36 Permeability coupling of CH_4 and CO_2 dynamics (a) Experiment and (b) Field.

4.6.2 Mobility coupling of experimental data with field data

Figure 37a and **Figure 37b** display the mobility data from experimental and field measurements, respectively, plotted on a semi-log graph against temperature.

In both figures, the data distribution patterns for methane and carbon dioxide show notable similarities. Methane (CH_4) mobility values in the experimental data (**Figure 37a**) exhibit a range of values that are concentrated, indicating consistent mobility across different temperatures. This trend is mirrored in the field data (**Figure 37b**), where methane also shows a clustered distribution of mobility values, although with a broader range compared to the experimental data.

For carbon dioxide (CO_2), both the experimental and field data demonstrate a wider dispersion of mobility values. In the experimental data, CO_2 mobility values are spread out more than those of methane, with a CV of 0.75, indicating moderate variability. The field data show an even broader spread for CO_2 mobility values, with a higher CV of 2.62, indicating significant variability. Despite these differences, the overall trend of higher variability in CO_2 mobility compared to methane is consistent across both datasets.

Additionally, both **Figure 37a** and **37b** shows that temperature does not have a strong influence on the mobility of either gas. The mobility values for methane and carbon dioxide remain relatively stable across the temperature range examined.

This similarities between the experimental and field data, especially in terms of the general trends and variability patterns, reinforce the reliability of the experimental setup in replicating real-world conditions. This consistency supports the use of experimental data from the nanoporous ceramic cores to model and predict field behaviour, providing valuable insights into gas mobility in reservoir studies.

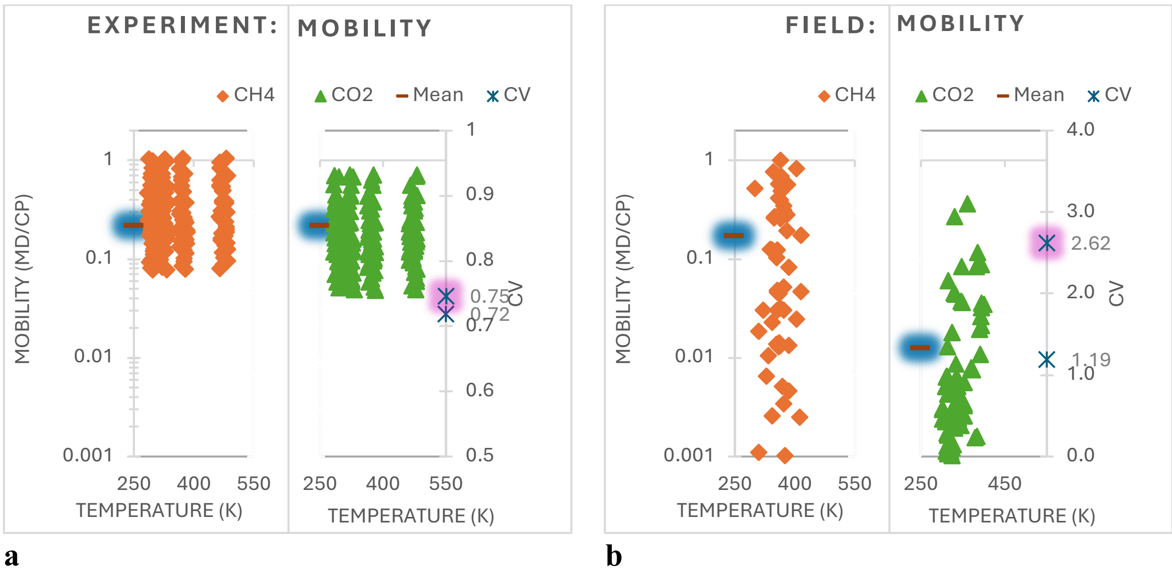

Figure 37 Mobility coupling of CH_4 and CO_2 dynamics (a) Experiment and (b) Field.

4.6.3 Darcy flux coupling of experimental data with field data

Figures 38a and **38b** illustrate the Darcy flux data from experimental and field measurements, respectively, plotted on a semi-log graph against temperature. The graphs display the Darcy flux (cm^3/s) for methane (CH_4) and carbon dioxide (CO_2), along with their coefficients of variation (CV) to highlight the variability in the data.

Methane (CH_4) shows a consistent pattern of Darcy flux values across the temperature range in both figures. In the experimental data, CH_4 values are tightly clustered, indicating a narrow range of variability, with a low CV of approximately 0.6. This consistency suggests a stable flow rate for methane under the controlled conditions of the experiment. In the field data, CH_4 also displays a relatively tight clustering, though with slightly more variation than the experimental data, as indicated by a CV of around 1.26. Despite this, the overall trend of stable methane flux is observed in both datasets.

The experimental data for CO_2 on the other hand shows a wider range of Darcy flux values compared to methane, with a CV of about 0.9, indicating moderate variability. This suggests that CO_2 flow rates are more variable under experimental conditions. While in the field data, CO_2 displays even greater variability, with a higher CV of approximately 3.36. This indicates significant variability in CO_2 flow rates in the field, reflecting the more complex and less controlled environmental conditions.

Both graphs reveal that temperature does not have a pronounced effect on the Darcy flux for either gas. The flux values for methane and carbon dioxide remain relatively stable across the temperature range examined, indicating that other factors, such as the intrinsic properties of the gases and the interaction with the porous media, have a more significant impact on flow rates than temperature alone.

The observed similarities between the experimental and field data, particularly in their general trends and variability patterns, underscore the reliability of the experimental setup. This consistency affirms the validity of the synthetic cores in modelling and predict field behaviour, offering valuable insights into gas flux dynamics in reservoir studies.

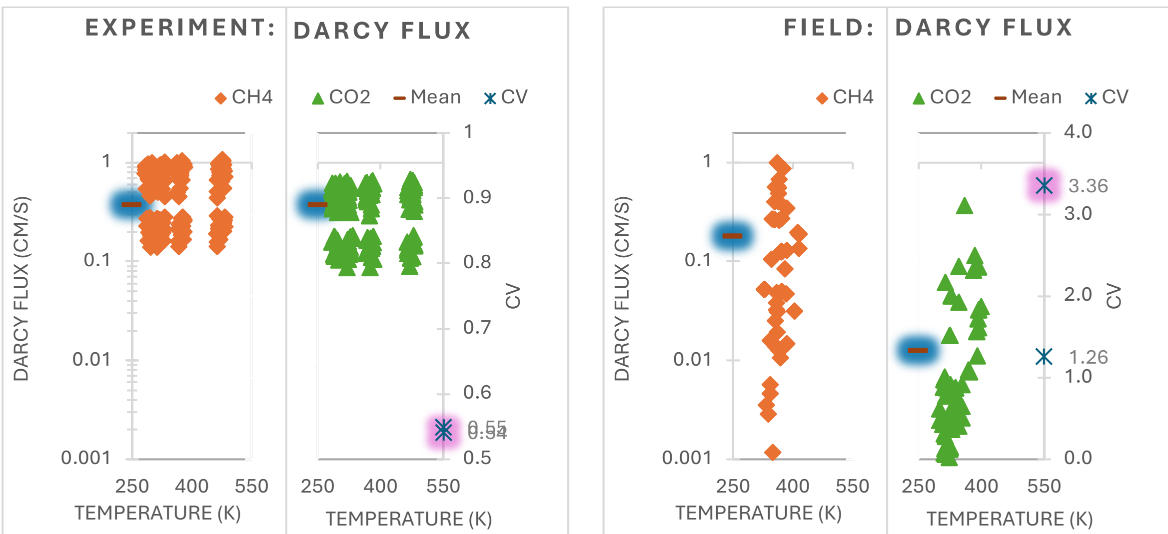

a b

Figure 38 Darcy flux coupling of CH_4 and CO_2 dynamics (a) Experiment and (b) Field.

4.6.4 Quality index coupling of experimental data with field data

Figures 39a and **39b** present the quality index data from experimental and field measurements, respectively, plotted on a semi-log graph against temperature. The graphs show the quality index for methane (CH_4) and carbon dioxide (CO_2), along with their coefficients of variation (CV) to highlight the variability in the data.

In both figures, methane (CH_4) shows a consistent pattern across the temperature range, with relatively lower variability as indicated by the lower CV values (0.68 for experimental data and 0.79 for field data). This suggests that methane maintains a more stable quality index across varying temperatures in both experimental and field conditions.

Carbon dioxide (CO_2) demonstrates a higher degree of variability, as seen in the higher CV values (0.97 for experimental data and 1.39 for field data). This indicates that CO_2's reservoir quality index is more sensitive to temperature changes, leading to greater fluctuations.

The similarity in the patterns and CV values between the experimental and field data reinforces the reliability of the experimental setup. It suggests that the experimental data can significantly replicate real-world conditions and provide valuable insights into the behaviour of methane and carbon dioxide in reservoir studies. The consistency in methane's stability and CO_2's variability across both datasets validates the experimental approach and supports its use for modelling and predicting reservoir behaviour.

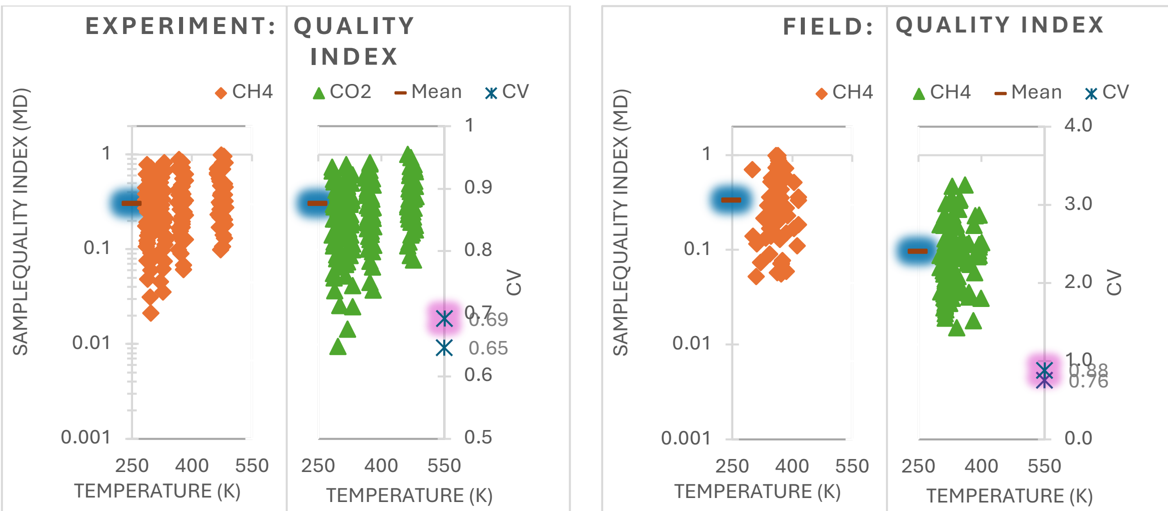

a b

Figure 39 Quality index coupling of CH_4 and CO_2 dynamics
(a) Experiment and (b) Field.

4.6.5 Coupling summary

The coupling analysis of the data sets and gases has extensively demonstrated that the four quantities examined have an analogous potential that can be qualitatively and quantitatively transformed. Consequently, the nano-ceramic core can be significantly used as a mimicking material for reservoirs in studying gas dynamics. This research presents a noteworthy opportunity to enhance reservoir studies by reducing costs, technical challenges, and environmental impacts associated with coring.

This comparison provided valuable insights into how various parameters influence fluid flow and reservoir performance, aiding in the optimisation of gas injection strategies and overall reservoir management practices. Additionally, the findings highlighted areas for further research to refine the use of ceramic cores as analogues, including exploring different types of ceramic materials, varying experimental conditions, and incorporating additional reservoir parameters and upscaling experimental data.

By integrating qualitative and quantitative analyses, this study offers a comprehensive assessment of the applicability of nano-ceramic cores in representing reservoir core characteristics, ultimately contributing to advancements in reservoir engineering and management.

CHAPTER 5
CONCLUSION AND RECOMMENDATION

5.1 Conclusion

This research has significantly advanced the understanding of gas transport in low-permeability reservoirs by employing nanoporous ceramic cores as mimetic models. Through an extensive experimental design involving over 1,000 permeation tests and the collection of more than 10,000 data points, the study has provided robust and reliable findings. The data from these experiments were meticulously compared with field data from over 100 reservoirs that have undergone CH_4 and CO_2 dynamics, demonstrating that nanoporous ceramic cores can describe the behaviour of low permeability reservoirs.

5.1.1 Key findings

Enhanced permeability and mobility with CH_4

The study's findings reveal that CH_4 exhibits higher permeability and mobility than CO_2 in both field and experimental settings. This suggests that CH_4 is more effective in enhancing reservoir performance under the tested conditions. This insight is crucial for optimising gas injection strategies, as it indicates that the choice of gas can significantly impact the efficiency of the reservoir management process.

Validation of nanoporous ceramic cores

The results indicates that nanoporous ceramic cores can serve as analogues in studying gas transport in low permeability reservoirs, offering a cost-effective and environmentally friendly alternative to traditional coring methods. This is based on the observed analogous potential between key reservoir parameters—permeability, mobility, Darcy flux and reservoir quality index—in experimental and field data.

Modified Darcy's equation

The introduction of a modified Darcy's equation tailored for nanoporous ceramic cores represents a significant advancement in determining permeability and other reservoir parameters. This modified equation accounts for the unique challenges posed by nanoporous materials, such as their distinct pore structures and the radial flow patterns observed in the experimental setup. This adaptation ensures that the experimental results are robust and applicable to real-world conditions.

5.1.2 Implications for reservoir management

Cost savings

Using nanoporous ceramic cores can significantly reduce the costs associated with traditional coring methods. Traditional coring processes are expensive and labour-intensive, requiring specialised equipment and personnel. By substituting real core samples with nano-ceramic cores, research and operational expenses can be substantially lowered without compromising the accuracy and reliability of the data.

Technical advantages

Nanoporous ceramic cores provide a controlled and consistent medium for experimentation. Unlike natural reservoir cores, which can exhibit significant variability due to heterogeneous geological formations, ceramic cores can be manufactured with precise specifications. This consistency enhances the reliability of experimental results and facilitates more reasonable comparisons between different studies.

Environmental impact

Traditional coring can be environmentally intrusive, often involving drilling and extraction processes that disturb the subsurface environment. Using nanoporous ceramic cores minimises the need for such invasive techniques, reducing the environmental footprint of reservoir studies. This aligns with the industry's goals of sustainability and reduced ecological disruption.

5.1.3 Advancements in reservoir engineering

The successful application of nanoporous ceramic cores can lead to significant advancements in reservoir engineering. It enables more precise modeling of reservoir conditions, which can improve the design and implementation of extraction techniques. Additionally, it supports the development of new technologies and methods for reservoir management. The insights gained from this research contribute to more effective reservoir management practices. By understanding the nuanced behaviors of different gases and the impact of various parameters, engineers can make informed decisions that enhance the sustainability and productivity of reservoir operations.

5.1.4 Practical implications

This study supports both academic research and practical applications in the field. For industry professionals, the findings offer valuable guidelines for optimising gas recovery and managing reservoirs. The ability to simulate reservoir conditions significantly using nanoporous ceramic cores can lead to better planning and execution of extraction strategies, ultimately improving the efficiency and profitability of reservoir operations.

5.1.5 Summary

In conclusion, this research not only support the use of nanoporous ceramic cores as mimetic models for low permeability reservoirs but also opens new avenues for research and technological advancements in the field. The findings contribute significantly to understanding and developing more efficient gas recovery methods tailored for the complexities of these reservoirs. The comprehensive approach adopted in this study ensures that the findings are robust and applicable, ultimately advancing the field of reservoir engineering and management. By integrating qualitative and quantitative analyses, this study provides a holistic assessment of the applicability of nano-ceramic cores in representing reservoir core characteristics, paving the way for future innovations and improvements in reservoir engineering practices.

5.2 Further recommendations

based on the findings and conclusions drawn from the experimental analysis presented in this study, the following recommendations are made to further advance research in this area and enhance the efficiency of natural gas extraction from these challenging geological formations:

1. **Exploration of different ceramic materials**

   Future research should explore a variety of ceramic materials to better replicate the properties of different low permeability reservoirs. This could involve experimenting with different compositions and manufacturing processes to optimise the physical and chemical properties of the ceramic cores. By tailoring the porosity, permeability, and mechanical strength of the ceramic cores, researchers can create more significant analogues for a wider range of reservoir conditions.

2. **Expanded range of experimental conditions**

   It is recommended to conduct experiments under a broader range of conditions to understand how various factors such as temperature, pressure, and fluid composition affect fluid dynamics in ceramic cores. This could involve simulating extreme reservoir conditions to test the robustness and reliability of the ceramic cores in different scenarios. By expanding the experimental conditions, researchers can gather more comprehensive data to support the applicability of ceramic cores in diverse reservoir environments.

3. **Incorporation of additional reservoir parameters**

   Future studies should incorporate a wider array of reservoir parameters, including but not limited to tortuosity, fluid density, thermal conductivity, and rock-fluid interaction properties. By including these parameters, researchers can develop a more holistic understanding of reservoir behaviour and improve the accuracy of the ceramic core models. This comprehensive approach will enhance the predictive capabilities of the models, making them more useful for practical applications in reservoir engineering.

4. **Long-term field studies**

   Conducting long-term field studies to validate the findings from laboratory experiments is essential. These studies should compare the performance of nano porous ceramic cores with actual reservoirs over extended periods and under varying operational conditions. By monitoring the long-term behaviour and performance of the ceramic cores in real-world settings, researchers can further confirm their reliability and effectiveness as analogues for reservoir studies.

5. **Integration with advanced simulation techniques**

   Future research should explore the integration of nano porous ceramic core experiments with advanced simulation techniques such as computational fluid dynamics (CFD) and machine learning models for upscaling experimental data. By combining experimental data with simulation results, researchers can develop more precise and predictive models of reservoir behaviour. This integrative approach will enhance the ability to optimise reservoir management strategies and improve the efficiency of gas recovery processes.

Implementing these recommendations will further enhance the understanding and application of nano porous ceramic cores in reservoir engineering. By exploring new materials, expanding experimental conditions, incorporating additional parameters, and validating findings through long-term studies, researchers can refine and improve the accuracy of ceramic core models. Collaboration with industry partners and the development of standardised protocols and training programs will ensure the successful integration of this technology into practical reservoir management practices.

REFERENCE

Abouzar Mirzaei-Paiaman and Behzad Ghanbarian, 2022, A new method for characterizing dynamic reservoir quality: Implications for quality maps in reservoir simulation and rock type classification, Journal of Petroleum Science and Engineering, Volume 218, 111049,

Adler, P., 2013. *Porous media: geometry and transports*. Elsevier.

Agosti, A., Formaggia, L. and Scotti, A., 2015. Analysis of a model for precipitation and dissolution coupled with a Darcy flux. *Journal of mathematical analysis and applications*, *431*(2), pp.752-781.

Aguilera, R.F., Harding, T. and Krause, F., 2008, June. Natural gas production from tight gas formations: a global perspective. In *World Petroleum Congress* (pp. WPC-19). WPC.

Aguilera, R.F. and Radetzki, M., 2014. The shale revolution: Global gas and oil markets under transformation. *Mineral Economics*, *26*, pp.75-84.

Ahad, N.A., Jami, M. and Tyson, S., 2020. A review of experimental studies on sand screen selection for unconsolidated sandstone reservoirs. *Journal of petroleum exploration and production technology*, *10*(4), pp.1675-1688.

Hodge, R.M., Burton, R.C., Constien, V. and Skidmore, V., 2002, February. An evaluation method for screen-only and gravel-pack completions. In *SPE International Conference and Exhibition on Formation Damage Control* (pp. SPE-73772). SPE.

Ahmed, T., 2018. Reservoir engineering handbook. Gulf professional publishing.

Ahmed, T. And Meehan, D.N., 2012. Chapter 6 - Introduction To Enhanced Oil Recovery. In: T. Ahmed and D.N. Meehan, Eds, Advanced Reservoir Management and Engineering (Second Edition). Boston: Gulf Professional Publishing, Pp. 541-585.

Ahmed, U. and Meehan, D.N. eds., 2016. Unconventional oil and gas resources: exploitation and development. CRC Press.

Al-Busafi, B., & Jones, T.J. 2021. "Advanced Reservoir Engineering and Petrophysics." Springer.

Al-Muntasheri, G.A., 2014. A critical review of hydraulic-fracturing fluids for moderate-to ultralow-permeability formations over the last decade. *SPE Production & Operations*, *29*(04), pp.243-260.

Al-Otaibi, A., & Wu, Y. S. 2010. *Enhanced Oil Recovery Techniques in Low-Permeability Reservoirs*. Petroleum Science and Technology.

Al-Rbeawi, S. and Kadhim, F., 2017. The impact of hydraulic flow unit & reservoir quality index on pressure profile and productivity index in multi-segments reservoirs. *Petroleum*, *3*(4), pp.414-430.

Alabi, O.O., 2011. Fluid flow in homogeneous and heterogeneous porous media. *Electronic Journal of Geotechnical Engineering*, *16*, pp.61-70.

Alfarge, D., Wei, M. and Bai, B., 2020. *Fundamentals of enhanced oil recovery methods for unconventional oil reservoirs*. Elsevier.

Ali, N., Chen, J., Fu, X., Hussain, W., Ali, M., Iqbal, S.M., Anees, A., Hussain, M., Rashid, M. and Thanh, H.V., 2023. Classification of reservoir quality using unsupervised machine learning and cluster analysis: Example from Kadanwari gas field, SE Pakistan. *Geosystems and Geoenvironment*, *2*(1), p.100123.

Anovitz, L.M. and Cole, D.R., 2015. Characterization and analysis of porosity and pore structures. *Reviews in Mineralogy and geochemistry*, *80*(1), pp.61-164.

Arthur, M.A. and Cole, D.R., 2014. Unconventional hydrocarbon resources: prospects and problems. *Elements*, *10*(4), pp.257-264.

Awan, A.R., Teigland, R. and Kleppe, J., 2006, April. EOR survey in the North Sea. In SPE Improved Oil Recovery Conference? (pp. SPE-99546). SPE.

Bachu, S., 2008. CO2 storage in geological media: Role, means, status and barriers to deployment. *Progress in energy and combustion science*, *34*(2), pp.254-273.

Bai-Gang, S., Dong-Sheng, Z. and Fu-Shui, L., 2012. A new equation of state for hydrogen gas. *International journal of hydrogen energy*, *37*(1), pp.932-935.

Baker, R.W., 2023. *Membrane technology and applications*. John Wiley & Sons

Balcombe, P., Anderson, K., Speirs, J., Brandon, N. and Hawkes, A., 2017. The natural gas supply chain: the importance of methane and carbon dioxide emissions. *ACS Sustainable Chemistry & Engineering*, *5*(1), pp.3-20.

Basu, A., Akhtar, J., Rahman, M.H. and Islam, M.R., 2004. A review of separation of gases using membrane systems. *Petroleum science and technology*, *22*(9-10), pp.1343-1368.

Bear, J., 2013. Dynamics of fluids in porous media. Courier Corporation.

Berg, R.R. 2019. "Fundamentals of Reservoir Engineering." University of Oklahoma Press.

Berkowitz, B., 2002. Characterizing flow and transport in fractured geological media: A review. *Advances in water resources*, *25*(8-12), pp.861-884.

Bird, R.B., Stewart, W.E. and Lightfoot, E.N., 2002. Transport Phenomena 2nd edition.

Bitter, J.G., 2012. *Transport mechanisms in membrane separation processes*. Springer Science & Business Media.

Blunt, Martin. 2017. "Principles of Fluid Flow in Porous Media." Wiley-Blackwell.

Bocora, J., 2012. Global prospects for the development of unconventional gas. *Procedia-Social and Behavioral Sciences*, *65*, pp.436-442.

Buckley, S.E. and Leverett, M., 1942. Mechanism of fluid displacement in sands. *Transactions of the AIME*, *146*(01), pp.107-116.

Caineng, Z.O.U., Yunhong, D.I.N.G., Yongjun, L.U., Xiangui, L., Jianjun, C., Xin, W., Zhengming, Y.A.N.G., Bo, C.A.I., Zhi, Y.A.N.G., Chunming, H.E. and Zhen, W.A.N.G., 2017. Concept, technology and practice of "man-made reservoirs" development. *Petroleum Exploration and Development*, *44*(1), pp.146-158.

Chen, Z., & Zhao, H. 2020. "Reservoir Simulation: Mathematical Techniques in Oil Recovery." SIAM

Chevalier, J., et al. 2013. *Advanced Techniques in Core Sample Analysis*. Materials Science and Engineering.

Civan, F. (201. "Reservoir Formation Damage." 3rd Edition, Gulf Professional Publishing.

Craft, B. C., Hawkins, M., & Terry, R. E. 2014. *Applied Petroleum Reservoir Engineering* (3rd ed.). Pearson Education.

Cramer, M.S., 2012. Numerical estimates for the bulk viscosity of ideal gases. *Physics of fluids*, *24*(6).

Dake, L.P., 2001. The practice of reservoir engineering (revised edition). Elsevier.

Damen, K., Faaij, A. and Turkenburg, W., 2006. Health, safety and environmental risks of underground CO2 storage–overview of mechanisms and current knowledge. *Climatic Change*, *74*(1), pp.289-318.

Dantas, H.V., Barbosa, M.F., Nascimento, E.C., Moreira, P.N., Galvao, R.K. and Araujo, M.C., 2014. Screening analysis of natural gas with respect to methane content by near-infrared spectrometry. *Microchemical Journal*, *114*, pp.210-215.

Darcy, H., 1856. *Les fontaines publiques de la ville de Dijon: exposition et application des principes à suivre et des formules à employer dans les questions de distribution d'eau* (Vol. 1). Victor dalmont.

de Oliveira, S.B., Rocha, H.V. and Tassinari, C.C., 2022. 3D geochemical characterization of organic-rich shales of the Irati Formation, Paraná Sedimentary Basin: New perspective for CO2 geological storage in southeastern Brazil. *International Journal of Greenhouse Gas Control*, *114*, p.103563.

Dejam, M., et al. 2017. *Modeling Fluid Flow in Porous Media Under Various Conditions*. Transport in Porous Media.

Didi, C.N., Osinowo, O.O., Akpunonu, O.E. and Nwali, O.I., 2024. Petroleum system and hydrocarbon potential of the Kolmani Basin, Northeast Nigeria. *Journal of Sedimentary Environments*, pp.1-27.

Ding, W., et al. 2017. *Analysis of Mineralogical Compositions in Shale Reservoirs*. Geoscience Frontiers.

Dewals, B.J., Kantoush, S.A., Erpicum, S., Pirotton, M. and Schleiss, A.J., 2008. Experimental and numerical analysis of flow instabilities in rectangular shallow basins. *Environmental fluid mechanics*, *8*, pp.31-54.

Dullien, F.A., 2012. *Porous media: fluid transport and pore structure*. Academic press.

Dybbs, A. and Edwards, R.V., 1984. A new look at porous media fluid mechanics—Darcy to turbulent. *Fundamentals of transport phenomena in porous media*, pp.199-256.

Fetter, C.W., 2001. Applied Hydrogeology 4th edition. Prantice-Hall. *Inc. New Jersey, 621p*.

Fjaer, E., Holt, R.M., Horsrud, P., Raaen, A.M., Risnes, R. (2008). "Petroleum Related Rock Mechanics." Elsevier.

Gao, D. and Bi, Y., 2022. Technical advances in well type and drilling & completion for high-efficient development of coalbed methane in China. *Natural Gas Industry B*, *9*(6), pp.561-577.

Gao, L., Mastalerz, M. and Schimmelmann, A., 2020. The origin of coalbed methane. In *Coal Bed Methane* (pp. 3-34). Elsevier.

Gensterblum, Y., Ghanizadeh, A., Cuss, R.J., Amann-Hildenbrand, A., Krooss, B.M., Clarkson, C.R., Harrington, J.F. and Zoback, M.D., 2015. Gas transport and storage capacity in shale gas reservoirs–A review. Part A: Transport processes. *Journal of Unconventional Oil and Gas Resources*, *12*, pp.87-122.

Gensterblum, Y., Merkel, A., Busch, A., Krooss, B.M. and Littke, R., 2014. Gas saturation and CO2 enhancement potential of coalbed methane reservoirs as a function of depth. *Aapg Bulletin*, *98*(2), pp.395-420.

George Koperna, Matt Wallace, Teresa Reid Steve Melzer, Lon Whitma 2021. A Survey of U.S. CO2 Enhanced Oil Recovery Projects. [Available from] https://www.eoriwyoming.org/projects-resources/publications/data/299-a-survey-of-us-co2-enhanced-oil-recovery-projects (Access 04/03/2024)

Gholami, R., Raza, A. and Iglauer, S., 2021. Leakage risk assessment of a CO2 storage site: A review. *Earth-Science Reviews*, *223*, p.103849.

Goraya, N.S., Rajpoot, N. and Marriyappan Sivagnanam, B., 2019. Coal bed methane enhancement techniques: a review. *ChemistrySelect*, *4*(12), pp.3585-3601.

Green, D.W., and Willhite, G.P. 2018. "Enhanced Oil Recovery." SPE Textbook Series.

Griffiths, L., Tisa, A., & Lister, S. 2018. "Temperature-dependent fluid flow anomalies in deep geothermal reservoirs." Journal of Volcanology and Geothermal Research.

Guo, C., Xu, J., Wu, K., Wei, M. and Liu, S., 2015. Study on gas flow through nano pores of shale gas reservoirs. *Fuel*, *143*, pp.107-117.

Guo, H., Dong, J., Wang, Z., Liu, H., Ma, R., Kong, D., Wang, F., Xin, X., Li, Y. and She, H., 2018. EOR Survey in China-part 1. In SPE Improved Oil Recovery Conference? (p. D041S015R003). SPE.

Guo, X., Hu, D., Li, Y., Duan, J., Zhang, X., Fan, X., Duan, H. and Li, W., 2019. Theoretical progress and key technologies of onshore ultra-deep oil/gas exploration. *Engineering*, *5*(3), pp.458-470.

Hamza, A., Hussein, I.A., Al-Marri, M.J., Mahmoud, M., Shawabkeh, R. and Aparicio, S., 2021. CO2 enhanced gas recovery and sequestration in depleted gas reservoirs: A review. *Journal of Petroleum Science and Engineering*, *196*, p.107685.

Han, J., Kamber, M., & Pei, J. 2011. *Data Mining: Concepts and Techniques* (3rd ed.). Elsevier.

Han, S., Zhang, Y., Huang, J., Rui, Y. and Tang, Z., 2020. Elemental geochemical characterization of sedimentary conditions and organic matter enrichment for Lower Cambrian shale formations in Northern Guizhou, South China. *Minerals*, *10*(9), p.793.

He, L.I.U., Xu, J.I.N. and Bin, D.I.N.G., 2016. Application of nanotechnology in petroleum exploration and development. *Petroleum Exploration and development*, *43*(6), pp.1107-1115.

Heidari, Zoya. 2019. "Porosity and Permeability of Rocks Under Stress," SPE Journal.

Holstein, E. D., 2007. Temperature and Fluid Flow. In *Petroleum Engineering Handbook* (Vol. 5). Society of Petroleum Engineers.

Holcomb, D., & Olsson, W. A., 2017. Effects of temperature and pressure on permeability in rocks: Implications for geothermal energy. Geothermal Energy Science

Holditch, S.A., 2006. Tight gas sands. *Journal of petroleum Technology*, *58*(06), pp.86-93.

Hommel, J., Coltman, E. and Class, H., 2018. Porosity–permeability relations for evolving pore space: a review with a focus on (bio-) geochemically altered porous media. *Transport in Porous Media*, *124*(2), pp.589-629.

Hongjun, W.A.N.G., Feng, M.A., Xiaoguang, T.O.N.G., Zuodong, L., Zhang, X., Zhenzhen, W.U., Denghua, L.I., Bo, W.A.N.G., Yinfu, X.I.E. and Liuyan, Y.A.N.G., 2016. Assessment of global unconventional oil and gas resources. *Petroleum Exploration and Development*, *43*(6), pp.925-940

Huang, B., Tian, H., Wilkins, R.W.T., Xiao, X. and Li, L., 2013. Geochemical characteristics, palaeoenvironment and formation model of Eocene organic-rich shales in the Beibuwan Basin, South China Sea. *Marine and Petroleum Geology*, *48*, pp.77-89.

Jahns, H. O. 2001. Reservoir surveillance using time-lapse seismic data. *The Leading Edge, 20*(11), 1222-1229.

Jarrahian, A. and Heidaryan, E., 2014. A simple correlation to estimate natural gas viscosity. *Journal of Natural Gas Science and Engineering*, *20*, pp.50-57.

Jiang, F. and Tsuji, T., 2014. Changes in pore geometry and relative permeability caused by carbonate precipitation in porous media. *Physical Review E*, *90*(5), p.053306.

John, L., 2007. Fluid Flow Through Permeable Media. In Holstein, E.D., Ed., *Volume V–Reservoir Engineering and Petrophysics*. In Lake, LW, Ed., *Petroleum Engineering Handbook*, Pgs. 719-894. Society of Petroleum Engineers: Richardson, TX.

Johnson, L. 2018. "Designing EOR Projects: Integration of Geological and Engineering Principles." SPE Reservoir Evaluation & Engineering.

Jones, D., & Roberts, A. 2020. "Geological Assessments for Strategic Well Placement." Energy Exploration & Exploitation.

Joshi, S.D., 2003, May. Cost/benefits of horizontal wells. In *SPE Western Regional Meeting* (pp. SPE-83621). SPE.

Jones, M., Li, H., & Edwards, R. 2022. "Comparative Analysis of Nano-porous Materials and Field Data in Oil Recovery." Energy Sources, Part A: Recovery, Utilization, and Environmental Effects, 44(1), 10-22.

Kadoya, K., Matsunaga, N. and Nagashima, A., 1985. Viscosity and thermal conductivity of dry air in the gaseous phase. *Journal of physical and chemical reference data*, *14*(4), pp.947-970.

Kang, W.L., Zhou, B.B., Issakhov, M. and Gabdullin, M., 2022. Advances in enhanced oil recovery technologies for low permeability reservoirs. *Petroleum Science*, *19*(4), pp.1622-1640.

Kantzas, A., Bryan, J. and Taheri, S., 2012. Fundamentals of fluid flow in porous media. *Pore size distribution*.

Kanyo, J.E., Schafföner, S., Uwanyuze, R.S. and Leary, K.S., 2020. An overview of ceramic molds for investment casting of nickel superalloys. *Journal of the European Ceramic Society*, *40*(15), pp.4955-4973.

Karan, S., Samitsu, S., Peng, X., Kurashima, K. and Ichinose, I., 2012. Ultrafast viscous permeation of organic solvents through diamond-like carbon nanosheets. *Science*, *335*(6067), pp.444-447.

Kausik*, R., Craddock, P.R., Reeder, S.L., Kleinberg, R.L., Pomerantz, A.E., Shray, F., Lewis, R.E. and Rylander, E., 2015, July. Novel reservoir quality indices for tight oil. In *Unconventional Resources Technology Conference, San Antonio, Texas, 20-22 July 2015* (pp. 2649-2658). Society of Exploration Geophysicists, American Association of Petroleum Geologists, Society of Petroleum Engineers.

Khan, R. and Al-Nakhli, A.R., 2012, May. An overview of emerging technologies and innovations for tight gas reservoir development. In *SPE International Production and Operations Conference and Exhibition* (pp. SPE-155442). SPE.

Kittner, K. and Awiszus, B., 2010. Numerical and experimental investigations of the production processes of coextruded Al/Mg-compounds and the strength of the interface. *Key Engineering Materials*, *424*, pp.129-135.

Koornneef, J., Ramírez, A., Turkenburg, W. and Faaij, A., 2012. The environmental impact and risk assessment of CO2 capture, transport and storage–An evaluation of the knowledge base. *Progress in Energy and Combustion Science*, *38*(1), pp.62-86.

Kotsiantis, S. B., Zaharakis, I., & Pintelas, P. 2006. Machine learning: A review of classification and combining techniques. *Artificial Intelligence Review*, 26(3), 159-190.

Kuuskraa, V.A. and Haas, M.R., 1988, June. Natural gas from low permeability formations. In *SPE Unconventional Resources Conference/Gas Technology Symposium* (pp. SPE-17746). SPE.

Lake, L.W., and Fanchi, J.R. (2006). "Petroleum Engineering Handbook." Society of Petroleum Engineers

Lake, L.W. ed., 2007. Petroleum Engineering Handbook: Reservoir Engineering and Petrophysics (Vol. 5). Richardson, USA: Society of Petroleum Engineers.

Lake, L.W., 1989. Enhanced oil recovery.

Lee, J.R., Yoon, H.Y. and Park, J.Y., 2024. Transient full core analysis of PWR with multi-scale and multi-physics approach. *Nuclear Engineering and Technology*, *56*(3), pp.980-992.

Li, D. and Engler, T.W., 2001, May. Literature review on correlations of the non-Darcy coefficient. In *SPE permian basin oil and gas recovery conference* (pp. SPE-70015). SPE.

Li, D., and Horne, R.N. 2018. "Fundamentals of Enhanced Oil Recovery Methods for Unconventional Oil Reservoirs." Elsevier.

Li, J., & Horne, R. N. 2018. Temperature and Pressure Dependence of Permeability in Rocks: Experimental Observations. Journal of Petroleum Science and Engineering.

Li, K. and Horne, R.N., 2001b, January. Gas slippage in two-phase flow and the effect of temperature. In *SPE Western Regional Meeting*. Society of Petroleum Engineers

Li, M., & Horne, R.N. 2018. "Modern Enhanced Oil Recovery Methods." Wiley.

Li, S., Qin, Y., Tang, D., Shen, J., Wang, J. and Chen, S., 2023. A comprehensive review of deep coalbed methane and recent developments in China. *International Journal of Coal Geology*, p.104369.

Li, X., Yang, Z., Li, S., Huang, W., Zhan, J. and Lin, W., 2021. Reservoir characteristics and effective development technology in typical low-permeability to ultralow-permeability reservoirs of China National Petroleum Corporation. *Energy Exploration & Exploitation*, *39*(5), pp.1713-1726.

Li, W., Fang, H., Huang, X., Wang, T., Zhang, D., & Yuan, S., 2022. The hydraulic fracturing design technology and application of geological-engineering integration for tight gas in jinqiu gas field. Frontiers in Energy Research, 10.

Li, Y., Lu, L., Zhu, J., Yang, Z., Qu, J., Xue, H., … & Ouyang, J., 2022. Molecular Simulation of Ch4 Nanoscale Behavior and Enhanced Gas Recovery In Organic-rich Shale. Geofluids, (2022), 1-15.

Lin, F., et al. 2019. *Nanostructure Characterization of Reservoir Rocks Using SEM/EDXA*. Journal of Applied Geophysics.

Ling, K., McCain, W.D., Davani, E. and Falcone, G., 2009, December. Measurement of gas viscosity at high pressures and high temperatures. In *International Petroleum Technology Conference* (pp. IPTC-13528). IPTC.

Liu, G., Fan, Z., Lu, Y., Li, S., Feng, B., Xia, Y., & Zhao, Q., 2018. Experimental Determination of Gas Relative Permeability Considering Slippage Effect in a Tight Formation. Energies, 11(2), 467.

Liu, P. 2019. Chemical Reactor Design, Optimization, and Scaleup. McGraw-Hill Education

Liu, P., Wang, Z., Lu, K. and Zhang, Z., 2022. Effect of sandstone and mudstone thickness on artificial fracturing for hydrocarbon extraction from low-permeability reservoirs. *Natural Gas Industry B*, *9*(4), pp.411-425.

Liu, Z.X., Liang, Y., Wang, Q., Guo, Y.J., Gao, M., Wang, Z.B. and Liu, W.L., 2020. Status and progress of worldwide EOR field applications. Journal of Petroleum Science and Engineering, 193, p.107449.

Łukaszewicz, G. and Kalita, P., 2016. Navier–stokes equations. *Advances in Mechanics and Mathematics*, *34*.

Lumpkin, G.T. and Dess, G.G., 2001. Linking two dimensions of entrepreneurial orientation to firm performance: The moderating role of environment and industry life cycle. *Journal of business venturing*, *16*(5), pp.429-451.

Ma, T., Chen, P. and Zhao, J., 2016. Overview on vertical and directional drilling technologies for the exploration and exploitation of deep petroleum resources. *Geomechanics and Geophysics for Geo-Energy and Geo-Resources*, *2*, pp.365-395.

Marchetti, P. and Livingston, A.G., 2015. Predictive membrane transport models for Organic Solvent Nanofiltration: How complex do we need to be?. *Journal of Membrane Science*, *476*, pp.530-553.

Marriott, T., Gorman, J., & Regenauer-Lieb, K. 2020. "Thermal Stress Induced Permeability Loss in Granitic Rocks." Geomechanics and Geophysics for Geo-Energy and Geo-Resources.

McAllister, D., Warke, P. and McCabe, S., 2017. Stone temperature and moisture variability under temperate environmental conditions: Implications for sandstone weathering. *Geomorphology*, *280*, pp.137-152.

McCabe, W.L., Smith, J.C. and Harriott, P., 1993. *Unit operations of chemical engineering*. McGraw-hill

McPhee, C., Reed, J. and Zubizarreta, I., 2015. *Core analysis: a best practice guide*. Elsevier.

Melikoglu, M., 2014. Shale gas: Analysis of its role in the global energy market. *Renewable and Sustainable Energy Reviews*, *37*, pp.460-468.

Mills, C., Marshall, C., Kay, A. and MacDonald, M., 2013, October. Flow measurement of high viscosity fluids. In *Proceedings of the North Sea Flow Measurement Workshop*.

Mitchell, J., Chandrasekera, T.C., Holland, D.J., Gladden, L.F. and Fordham, E.J., 2013. Magnetic resonance imaging in laboratory petrophysical core analysis. *Physics Reports*, *526*(3), pp.165-225.

Mirzaei-Paiaman, A. and Ghanbarian, B., 2022. A new method for characterizing dynamic reservoir quality: Implications for quality maps in reservoir simulation and rock type classification. *Journal of Petroleum Science and Engineering*, *218*, p.111049.

Mo, D., Yu, J., Liu, N. and Lee, R., 2012, October. Study of the effect of different factors on nanoparticle-stablized CO2 foam for mobility control. In *SPE Annual Technical Conference and Exhibition?* (pp. SPE-159282). Spe.

Moore, T.A., 2012. Coalbed methane: A review. *International Journal of Coal Geology*, *101*, pp.36-81.

Muskat, M. (2020). "The Flow of Homogeneous Fluids Through Porous Media." Springer.

Naaktgeboren, C., Krueger, P.S. and Lage, J.L., 2012. Inlet and outlet pressure-drop effects on the determination of permeability and form coefficient of a porous medium.

Nabawy, B.S., Khalil, H.M., Fathy, M.S. and Ali, F., 2020. Impacts of microfacies type on reservoir quality and pore fabric anisotropy of the Nubia sandstone in the central Eastern Desert, Egypt. *Geological Journal*, *55*(6), pp.4507-4524.

Nelson, Philip H. 2009. "Pore-Throat Sizes in Sandstones, Tight Sandstones, and Shales." AAPG Bulletin.

Norton, D., & Knight, J. 2021. "Thermal effects on rock permeability: Natural and engineered manifestations." Geophysical Research Letters.

Otchere, D.A., Ganat, T.O.A., Gholami, R. and Ridha, S., 2021. Application of supervised machine learning paradigms in the prediction of petroleum reservoir properties: Comparative analysis of ANN and SVM models. *Journal of Petroleum Science and Engineering*, *200*, p.108182.

Palmer, G.E. and Wright, M.J., 2003. Comparison of methods to compute high-temperature gas viscosity. *Journal of Thermophysics and Heat Transfer*, *17*(2), pp.232-239.

Pandey, P. and Chauhan, R.S., 2001. Membranes for gas separation. *Progress in polymer science*, *26*(6), pp.853-893.

Patel, R. 2021. Advanced Chemical Process Design and Control. Springer.

Pruess, K., 1991. TOUGH2: A general-purpose numerical simulator for multiphase fluid and heat transfer. *LBL-29400. Lawrence Berkeley Laboratory, Berkeley, CA*.

Qinghai, Y., He, L., Jianwen, Y. and Gao, Y., 2013, October. Multi-Stage horizontal fracturing in casing for low permeability reservoirs. In *SPE Asia Pacific Oil and Gas Conference and Exhibition* (pp. SPE-166671). SPE.

Qun, L.E.I., Yun, X.U., Bo, C.A.I., Baoshan, G., Xin, W., Guoqiang, B.I., Hui, L.I., Shuai, L.I., Bin, D., Haifeng, F.U. and Zheng, T., 2022. Progress and prospects of horizontal well fracturing technology for shale oil and gas reservoirs. *Petroleum Exploration and Development*, *49*(1), pp.191-199.

Qun, L., Yun, X., Tingxue, J., Yunhong, D.I.N.G., Xiaoquan, W.A.N.G. and Haibing, L.U., 2009. " Fracture network" fracturing technique for improving post-fracturing performance of low and ultra-low permeability reservoirs. *Acta Petrolei Sinica*, *30*(2), p.237.

Rashid, M., Luo, M., Ashraf, U., Hussain, W., Ali, N., Rahman, N., Hussain, S., Aleksandrovich Martyushev, D., Vo Thanh, H. and Anees, A., 2022. Reservoir quality prediction of gas-bearing carbonate sediments in the Qadirpur field: Insights from advanced machine learning approaches of SOM and cluster analysis. *Minerals*, *13*(1), p.29.

Reagan, M.T., Moridis, G.J., Keen, N.D. and Johnson, J.N., 2015. Numerical simulation of the environmental impact of hydraulic fracturing of tight/shale gas reservoirs on near-surface groundwater: Background, base cases, shallow reservoirs, short-term gas, and water transport. *Water Resources Research*, *51*(4), pp.2543-2573.

Richardson, S.M., and Harker, J.H. 2017. "Chemical Engineering Volume 1: Fluid Flow, Heat Transfer and Mass Transfer." Butterworth-Heinemann.

Rosti, M.E., Pramanik, S., Brandt, L. and Mitra, D., 2020. The breakdown of Darcy's law in a soft porous material. *Soft Matter*, *16*(4), pp.939-944.

Salama, A., Amin, M.F.E., Kumar, K. and Sun, S., 2017. Flow and transport in tight and shale formations: A review. *Geofluids*, *2017*.

Sanjari, E., Lay, E.N. and Peymani, M., 2011. An accurate empirical correlation for predicting natural gas viscosity. *Journal of natural gas chemistry*, *20*(6), pp.654-658.

Sander, R., Pan, Z. and Connell, L.D., 2017. Laboratory measurement of low permeability unconventional gas reservoir rocks: A review of experimental methods. *Journal of Natural Gas Science and Engineering*, *37*, pp.248-279

Satter, A. and Iqbal, G.M., 2015. *Reservoir engineering: the fundamentals, simulation, and management of conventional and unconventional recoveries*. Gulf Professional Publishing.

Schaetzel, P., Vauclair, C., Nguyen, Q.T. and Bouzerar, R., 2004. A simplified solution–diffusion theory in pervaporation: the total solvent volume fraction model. *Journal of Membrane Science*, *244*(1-2), pp.117-127.

Selley, R. C. 2000. *Elements of Petroleum Geology* (2nd ed.). Academic Press.

Shafer, J., 2013. Recent advances in core analysis. *Petrophysics*, *54*(06), pp.554-579.

Sharma, S., Batshas, S., Joshi, S., Tewari, S., Shukla, S. and Agarwal, A., 2016, April. A Novel Approach to Compare Pressure Regimes for Compartment Identification in Low Mobility Environment. In *SPE Kingdom of Saudi Arabia Annual Technical Symposium and Exhibition* (pp. SPE-182775). SPE.

Shehu, Habiba, Gobina, Edward, Orakwe, Ifeyinwa, 2019. "Utilization of CO2 for syngas production by CH_4 partial oxidation using a catalytic membrane reactor.", International Journal of Hydrogen Energy.

Shen, P.F., Li, G., Li, X.S., Li, B. and Zhang, J.M., 2021. Application of fracturing technology to increase gas production in low-permeability hydrate reservoir: A numerical study. *Chinese Journal of Chemical Engineering*, *34*, pp.267-277.

Shiyi, Y.U.A.N. and Qiang, W.A.N.G., 2018. New progress and prospect of oilfields development technologies in China. *Petroleum Exploration and Development*, *45*(4), pp.698-711.

Singh, H., & Prasad, M. 2019. "Impact of Temperature on Fluid Flow through Porous Media in Hydrocarbon Reservoirs." Journal of Petroleum Science and Engineering.

Singh, A., & Chauhan, S. S. 2019. *Data Preprocessing Techniques for Data Mining*. Academic Press.

Slider, H.C., 1983. Worldwide practical petroleum reservoir engineering methods. PennWell Books. Tulsa, Oklahoma.

Smith, J.E. (2018). Modern Enhanced Oil Recovery: Principles and Practices. Elsevier.

Smith, J. & Johnson, B. (2017). "Enhancing Fluid Recovery in Petrophysical Models: Beyond Porosity." Journal of Reservoir Engineering, Vol. 34, No. 2, pp. 112-125.

Smith, J., et al. (2019). "Optimizing Reservoir Management for Enhanced Hydrocarbon Recovery." Journal of Petroleum Technology.

Smith, J., Khan, M. T., & Qadir, O. P. (2020). The impacts of thermal processes on permeability enhancement in oil reservoirs. Journal of Petroleum Exploration and Production Technology, 10(8), 3399-3411.
Smith, L. (2020). "Nano-porous Ceramic Cores for Experimental Modeling in Reservoir Engineering." Advanced Materials, 32(16), 1902761.

Soeder, D.J., 2018. The successful development of gas and oil resources from shales in North America. *Journal of Petroleum Science and Engineering*, *163*, pp.399-420.

Srinivasan, S., 2016. A generalized darcy–dupuit–forchheimer model with pressure-dependent drag coefficient for flow through porous media under large pressure gradients. *Transport in Porous Media*, *111*(3), pp.741-750.

Swartzendruber, D., 1962. Modification of Darcy's law for the flow of water in soils. *Soil Science*, *93*(1), pp.22-29.

Taylor, R., & Wang, F. 2021. "Economic Analysis of Enhanced Oil Recovery Techniques." Journal of Energy Resources Technology.

Terry, R.E., Rogers, J.B. and Craft, B.C., 2015. *Applied petroleum reservoir engineering*. Pearson Education.

Thompson, G., Davies, R., & Howell, S. 2019. "Revising Groundwater Contamination Models: The Role of Porosity in Hydrogeology." Environmental Geosciences, Vol. 22, No. 4, pp. 45-59

Tiab, D. and Donaldson, E.C., 2024. *Petrophysics: theory and practice of measuring reservoir rock and fluid transport properties*. Elsevier.

Tian, H., & Babadagli, T. 2022. Analysis of Temperature Effects on Permeability and Fluid Flow in Porous Media for Enhanced Oil Recovery Processes. Fuel.

Titze, T., Lauerer, A., Heinke, L., Chmelik, C., Zimmermann, N.E., Keil, F.J., Ruthven, D.M. and Kärger, J., 2015. Transport in nanoporous materials including MOFs: the applicability of Fick’s laws. *Angewandte Chemie International Edition*, *54*(48), pp.14580-14583.

Tran, N.H., and Nguyen, Q.P. 2019. "Impact of Temperature on Waterflooding Process in Low-Permeability Reservoirs," Journal of Petroleum Science and Engineering.

Vestavik, O.M., Syse, H., Hole, O. and Aleksandersen, J., 2010, October. New approach to improve the horizontal drilling reach. In *SPE Canada Unconventional Resources Conference?* (pp. SPE-137821). SPE.

WADA, S., NISHIYAMA, N. and NISHIDA, S.I., 1985. Modified Darcy's law for non-newtonian fluids. *Bulletin of JSME*, *28*(246), pp.3031-3037.

Wang, H., 2000. *Theory of linear poroelasticity with applications to geomechanics and hydrogeology* (Vol. 2). Princeton university press.

Wang, K., Li, Z., She, D., Xu, Q., Qiu, Y., Yu, J., Sun, J., Fan, X. and Yu, G., 2015. RMC–A Monte Carlo code for reactor core analysis. *Annals of Nuclear Energy*, *82*, pp.121-129.

Wang, L., Tian, Y., Yu, X., Wang, C., Yao, B., Wang, S., Winterfeld, P.H., Wang, X., Yang, Z., Wang, Y. and Cui, J., 2017. Advances in improved/enhanced oil recovery technologies for tight and shale reservoirs. *Fuel*, *210*, pp.425-445.

Wang, M., Janout, V. and Regen, S.L., 2013. Gas transport across hyperthin membranes. *Accounts of Chemical Research*, *46*(12), pp.2743-2754.

Wang, Y., Wang, Z., Zhang, Z., Yao, S., Zhang, H., Zheng, G., Luo, F., Feng, L., Liu, K. and Jiang, L., 2024. Recent techniques on analyses and characterizations of shale gas and oil reservoir. *Energy Reviews*, p.100067.

Wang, Z., Liu, S. and Qin, Y., 2021. Coal wettability in coalbed methane production: A critical review. *Fuel*, *303*, p.121277.

Waples, D.W., 2013. *Geochemistry in petroleum exploration*. Springer Science & Business Media.

Wenbin, C., Zhaomin, L., Xialin, Z., Bo, Z. and Qi, Z., 2009. Horizontal well fracturing technology for reservoirs with low permeability. *Petroleum Exploration and Development*, *36*(1), pp.80-85.

Wenrui, H.U., Yi, W.E.I. and Jingwei, B.A.O., 2018. Development of the theory and technology for low permeability reservoirs in China. *Petroleum Exploration and Development*, *45*(4), pp.685-697.

Westkämper, Engelbert. (2018) "Impact of Porosity on the Engineering Properties and Sustainability of Technical Systems," in Engineering Sustainability, Edited Volume, Springer.

White, D., & Zhao, L. 2021. "Statistical Approaches to Comparing Experimental and Field Data in Reservoir Studies." Journal of Statistical Analysis and Data Mining, 23(3), 142-156.

Williams, B.C. 2020. Reservoir Engineering in Modern Oilfields: Vertical, Deviated, Horizontal and Multilateral Well Systems. Wiley-Blackwell

Wilson, C.R., Spiegelman, M., van Keken, P.E. and Hacker, B.R., 2014. Fluid flow in subduction zones: The role of solid rheology and compaction pressure. *Earth and Planetary Science Letters*, *401*, pp.261-274.

Worden, R. H., & Utley, J. E. 2022. *Scanning Electron Microscopy and Energy Dispersive X-ray Analysis in Core Analysis*. Journal of Petroleum Technology.

Yakimchuk, I., Evseev, N., Korobkov, D., Varfolomeev, I., Dinariev, O., Khan, V., Koroteev, D., Orlov, D., Muravleva, E., Belozerov, B. and Krutko, V., 2019, October. Permeability and porosity study of achimov formation using digital core analysis. In *SPE Russian Petroleum Technology Conference?* (p. D033S025R007). SPE.

Xaba, B.M., Modise, S.J., Okoli, B.J., Monapathi, M.E. and Nelana, S., 2020. Characterization of selected polymeric membranes used in the separation and recovery of palladium-based catalyst systems. *Membranes*, *10*(8), p.166.

Yanda, M.D., 2014. Coalbed Methane: A Proposal for Mandated Production. *Appalachian Nat. Resources LJ*, *9*, p.51.

Yanjun, M.E.N.G., Dazhen, T.A.N.G., Hao, X.U., Yingjie, Q.U., Yong, L.I. and Zhang, W., 2014. Division of coalbed methane desorption stages and its significance. *Petroleum Exploration and Development*, *41*(5), pp.671-677.

Yu-shu, W. and Karsten P., 1996, Flow of Non-Newtonian fluid in porous media. In Corapcioglu, M.Y., 1996. *Advances in porous media* (p87-179). Elsevier Science B.V. Amsterdam.

Yuncong, G.A.O., Mifu, Z.H.A.O., Jianbo, W.A.N.G. and Chang, Z.O.N.G., 2014. Performance and gas breakthrough during CO2 immiscible flooding in ultra-low permeability reservoirs. *Petroleum Exploration and Development*, *41*(1), pp.88-95.

Zhou, D., Jia, L., Kamath, J., and Kovscek, A. 2021. "Effects of Temperature and Pressure on Oil Recovery," Energy & Fuels.

Zhou, D., & Thakur, P. "Effect of Temperature and Pressure on Permeability of Porous Media." Journal of Petroleum Science Engineering, 2020.

Zhou, J., Zhu, W., & Yu, H. 2020. Experimental study on the influence of temperature on permeability of sandstone and its mechanisms. Engineering Geology.

Zhou, X. and Kamal, M.S., 2019. Experimental study on the relationship between carbonate reservoir quality index and dynamic parameters of chemical solutions for oil recovery practice. *Energy & Fuels*, *33*(10), pp.9747-9758.

Zhou, X., Wang, Y., and Liu, H. 2021. "Viscosity and Its Effects on Permeability in Porous Media: An Experimental Approach with Microfluidics." Chemical Engineering Science.

Zhuang, H., Han, Y., Sun, H. and Liu, X., 2020. Dynamic well testing in petroleum exploration and development. Elsevier.

Zijl, W., 2004. A direct method for the identification of the permeability field based on flux assimilation by a discrete analog of Darcy's law. *Transport in porous media*, *56*(1), pp.87-112.

Zoback, M.D., 2010. *Reservoir geomechanics*. Cambridge university press.

Zou, C., Zhu, R., Liu, K., Su, L., Bai, B., Zhang, X., Yuan, X. and Wang, J., 2012. Tight gas sandstone reservoirs in China: characteristics and recognition criteria. *Journal of Petroleum Science and Engineering*, *88*, pp.82-91.

APPENDIX

APPENDIX A: Experimental Formula

Permeability formular.

$$k = \frac{Q\,\mu}{\pi h} \; \frac{In\,\frac{r_1}{r_2}}{(P_1^2 - P_2^2)}$$

Where:

Q is the volumetric flow rate in $cm^3.sec^{-1}$.

k is the permeability in mD.

μ is the fluid viscosity in cp.

h is the height of the core in cm.

r_1 and r_2 are the external and internal radii respectively.

P_1 and P_2 denote the pressures at the inlet and outlet respectively.

Mobility formular.

$$Mobility = \frac{k}{\mu} \tag{19}$$

Where:

k represents the permeability in millidarcies (mD), and

μ denotes the fluid viscosity in centipoise (cp).

Reservoir Index Quality Formular

$$Reservoir\ Quality\ Index = 0.0314\ x\ k\emptyset$$

Where:

k is the permeability in millidarcy (mD) and ∅ is the porosity in %

Flux Formular.

$$Flux = \frac{Q}{A}$$

Where:

Q is the volumetric flow rate in $cm^3.sec^{-1}$.

A is the cross-sectional area in cm^2

APPENDIX B: Experimental Database

1	s/n	Core Pore Size (nm)	Gas	Core height (cm)	External Radius (cm)	Internal Radius (cm)	Ln(r1/r2) (cm)	Core Volume (cm3)	Core Cross-Sectional Area (cm2)	Temperature (K)	Inlet Pressure (atm)	Outlet Pressure (atm)	Pressure Drop (atm)	P1^2 - P2^2 (atm)	Data Frequency	Flowrate (LPM))	Flowrate (cm3/sec)	Porosity (%)	Pore Size (nm)	Aspect Ratio	Aspect Quality Index	Viscosity (cp)	Flux (cm/s)	Permeability (mD)	Mobility (mD/cp)	Sample Quality Index (mD)
2	1	S15	CH4	34.7	0.505	0.355	0.3524406	20	111.3	293	1.382	0.987	0.395	0.935755	66	1.75	29.16725	0.306	15	1.00E+11	2.62E-12	0.011	0.2620597	0.0011091	0.1008231	0.00189036
3	2	S15	CH4	34.7	0.505	0.355	0.3524406	20	111.3	293	1.678	0.987	0.691	1.841515	84	2.54	42.33418	0.306	15	1.00E+11	3.80E-12	0.011	0.380361	0.000818	0.0743605	0.00162344
4	3	S15	CH4	34.7	0.505	0.355	0.3524406	20	111.3	293	1.974	0.987	0.987	2.922507	14	2.8	46.6676	0.306	15	1.00E+11	4.19E-12	0.011	0.4192956	0.0005682	0.051652	0.00135303
5	4	S15	CH4	34.7	0.505	0.355	0.3524406	20	111.3	293	2.27	0.987	1.283	4.178731	28	3.06	51.00102	0.306	15	1.00E+11	4.58E-12	0.011	0.4582302	0.0004343	0.0394785	0.00118289
6	5	S15	CH4	34.7	0.505	0.355	0.3524406	20	111.3	293	2.566	0.987	1.579	5.610187	57	3.27	54.50109	0.306	15	1.00E+11	4.90E-12	0.011	0.4896774	0.0003457	0.0314235	0.00105534
7	6	S15	CH4	34.7	0.505	0.355	0.3524406	20	111.3	293	2.862	0.987	1.875	7.216875	82	3.43	57.16781	0.306	15	1.00E+11	5.14E-12	0.011	0.5136371	0.0002819	0.025623	0.00095297
8	7	S15	CH4	34.7	0.505	0.355	0.3524406	20	111.3	293	3.158	0.987	2.171	8.998795	69	3.56	59.33452	0.306	15	1.00E+11	5.33E-12	0.011	0.5331044	0.0002346	0.021328	0.00086944
9	8	S15	CH4	34.7	0.505	0.355	0.3524406	20	111.3	293	3.454	0.987	2.467	10.955947	66	3.67	61.16789	0.306	15	1.00E+11	5.50E-12	0.011	0.5495767	0.0001987	0.0180593	0.00080005
10	9	S15	CH4	34.7	0.505	0.355	0.3524406	20	111.3	323	1.382	0.987	0.395	0.935755	32	1.74	29.00058	0.306	15	1.00E+11	2.61E-12	0.0119	0.2605623	0.0011929	0.100247	0.00196055
11	10	S15	CH4	34.7	0.505	0.355	0.3524406	20	111.3	323	1.678	0.987	0.691	1.841515	11	2.56	42.66752	0.306	15	1.00E+11	3.83E-12	0.0119	0.383356	0.0008919	0.0749461	0.00169518
12	11	S15	CH4	34.7	0.505	0.355	0.3524406	20	111.3	323	1.974	0.987	0.987	2.922507	14	2.8	46.6676	0.306	15	1.00E+11	4.19E-12	0.0119	0.4192956	0.0006147	0.0516519	0.0014073
13	12	S15	CH4	34.7	0.505	0.355	0.3524406	20	111.3	323	2.27	0.987	1.283	4.178731	72	3.07	51.16769	0.306	15	1.00E+11	4.60E-12	0.0119	0.4597277	0.0004713	0.0396076	0.00123234
14	13	S15	CH4	34.7	0.505	0.355	0.3524406	20	111.3	323	2.566	0.987	1.579	5.610187	80	3.28	54.66776	0.306	15	1.00E+11	4.91E-12	0.0119	0.4911748	0.0003751	0.0315196	0.00109934
15	14	S15	CH4	34.7	0.505	0.355	0.3524406	20	111.3	323	2.862	0.987	1.875	7.216875	70	E	57.50115	0.306	15	1.00E+11	5.17E-12	0.0119	0.5166321	0.0003067	0.0257724	0.00099408
16	15	S15	CH4	34.7	0.505	0.355	0.3524406	20	111.3	323	3.158	0.987	2.171	8.998795	21	3.59	59.83453	0.306	15	1.00E+11	5.38E-12	0.0119	0.5375969	0.0002559	0.0215077	0.00090811
17	16	S15	CH4	34.7	0.505	0.355	0.3524406	20	111.3	323	3.454	0.987	2.467	10.955947	49	3.71	61.83457	0.306	15	1.00E+11	5.56E-12	0.0119	0.5555667	0.0002172	0.0182561	0.00083666
18	17	S15	CH4	34.7	0.505	0.355	0.3524406	20	111.3	373	1.382	0.987	0.395	0.935755	18	1.73	28.83391	0.306	15	1.00E+11	2.59E-12	0.0135	0.2590648	0.0013456	0.0996709	0.00208219
19	18	S15	CH4	34.7	0.505	0.355	0.3524406	20	111.3	373	1.678	0.987	0.691	1.841515	39	2.54	42.33418	0.306	15	1.00E+11	3.80E-12	0.0135	0.380361	0.0010039	0.0743606	0.00179849
20	19	S15	CH4	34.7	0.505	0.355	0.3524406	20	111.3	373	1.974	0.987	0.987	2.922507	82	2.8	46.6676	0.306	15	1.00E+11	4.19E-12	0.0135	0.4192956	0.0006973	0.0516519	0.00149892
21	20	S15	CH4	34.7	0.505	0.355	0.3524406	20	111.3	373	2.27	0.987	1.283	4.178731	49	3.07	51.16769	0.306	15	1.00E+11	4.60E-12	0.0135	0.4597277	0.0005347	0.0396076	0.00131258
22	21	S15	CH4	34.7	0.505	0.355	0.3524406	20	111.3	373	2.566	0.987	1.579	5.610187	20	3.3	55.0011	0.306	15	1.00E+11	4.94E-12	0.0135	0.4941698	0.0004281	0.0317118	0.00117448
23	22	S15	CH4	34.7	0.505	0.355	0.3524406	20	111.3	373	2.862	0.987	1.875	7.216875	47	3.47	57.83449	0.306	15	1.00E+11	5.20E-12	0.0135	0.519627	0.0003499	0.0259218	0.00106186
24	23	S15	CH4	34.7	0.505	0.355	0.3524406	20	111.3	373	3.158	0.987	2.171	8.998795	76	3.63	60.50121	0.306	15	1.00E+11	5.44E-12	0.0135	0.5435868	0.0002936	0.0217473	0.00097261
25	24	S15	CH4	34.7	0.505	0.355	0.3524406	20	111.3	373	3.454	0.987	2.467	10.955947	69	3.76	62.66792	0.306	15	1.00E+11	5.63E-12	0.0135	0.5630541	0.0002498	0.0185021	0.00089711
26	25	S15	CH4	34.7	0.505	0.355	0.3524406	20	111.3	473	1.382	0.987	0.395	0.935755	33	1.68	28.00056	0.306	15	1.00E+11	2.52E-12	0.0163	0.2515774	0.0015777	0.0967902	0.00225465
27	26	S15	CH4	34.7	0.505	0.355	0.3524406	20	111.3	473	1.678	0.987	0.691	1.841515	37	2.48	41.33416	0.306	15	1.00E+11	3.71E-12	0.0163	0.3713761	0.0011834	0.072604	0.00195273
28	27	S15	CH4	34.7	0.505	0.355	0.3524406	20	111.3	473	1.974	0.987	0.987	2.922507	23	2.77	46.16759	0.306	15	1.00E+11	4.15E-12	0.0163	0.4148031	0.0008329	0.0510985	0.0016382
29	28	S15	CH4	34.7	0.505	0.355	0.3524406	20	111.3	473	2.27	0.987	1.283	4.178731	18	3.06	51.00102	0.306	15	1.00E+11	4.58E-12	0.0163	0.4582302	0.0006435	0.0394786	0.00143994
30	29	S15	CH4	34.7	0.505	0.355	0.3524406	20	111.3	473	2.566	0.987	1.579	5.610187	55	3.29	54.83443	0.306	15	1.00E+11	4.93E-12	0.0163	0.4926723	0.0005153	0.0316157	0.00128859
31	30	S15	CH4	34.7	0.505	0.355	0.3524406	20	111.3	473	2.862	0.987	1.875	7.216875	48	3.49	58.16783	0.306	15	1.00E+11	5.23E-12	0.0163	0.522622	0.000425	0.0260712	0.00117015
32	31	S15	CH4	34.7	0.505	0.355	0.3524406	20	111.3	473	3.158	0.987	2.171	8.998795	86	3.67	61.16789	0.306	15	1.00E+11	5.50E-12	0.0163	0.5495767	0.0003584	0.021987	0.0010746
33	32	S15	CH4	34.7	0.505	0.355	0.3524406	20	111.3	473	3.454	0.987	2.467	10.955947	56	3.85	64.16795	0.306	15	1.00E+11	5.77E-12	0.0163	0.5765314	0.0003088	0.018945	0.00099749
34	97	B15	CH4	61	1.3	0.98	0.282567	200	501.8	293	1.382	0.987	0.395	0.935755	43	2.4	40.0008	0.327	15	4.69E+10	1.70E-12	0.011	0.0797146	0.0006937	0.0630621	0.00144623
35	98	B15	CH4	61	1.3	0.98	0.282567	200	501.8	293	1.678	0.987	0.691	1.841515	79	2.82	47.00094	0.327	15	4.69E+10	2.00E-12	0.011	0.0936647	0.0004142	0.0376525	0.0011175
36	99	B15	CH4	61	1.3	0.98	0.282567	200	501.8	293	1.974	0.987	0.987	2.922507	53	3.17	52.83439	0.327	15	4.69E+10	2.25E-12	0.011	0.1052897	0.0002934	0.02667	0.00094051
37	100	B15	CH4	61	1.3	0.98	0.282567	200	501.8	293	2.27	0.987	1.283	4.178731	81	3.4	56.6678	0.327	15	4.69E+10	2.41E-12	0.011	0.1129291	0.0002201	0.0200057	0.00081457
38	101	B15	CH4	61	1.3	0.98	0.282567	200	501.8	293	2.566	0.987	1.579	5.610187	80	3.59	59.83453	0.327	15	4.69E+10	2.54E-12	0.011	0.1192398	0.0001731	0.0157339	0.00072239
39	102	B15	CH4	61	1.3	0.98	0.282567	200	501.8	293	2.862	0.987	1.875	7.216875	77	3.71	61.83457	0.327	15	4.69E+10	2.63E-12	0.011	0.1232255	0.000139	0.0126399	0.00064748
40	103	B15	CH4	61	1.3	0.98	0.282567	200	501.8	293	3.158	0.987	2.171	8.998795	38	3.83	63.83461	0.327	15	4.69E+10	2.71E-12	0.011	0.1272113	0.0001151	0.0104649	0.00058914
41	104	B15	CH4	61	1.3	0.98	0.282567	200	501.8	293	3.454	0.987	2.467	10.955947	76	3.92	65.33464	0.327	15	4.69E+10	2.78E-12	0.011	0.1302006	9.67717E-05	0.0087974	0.00054017
42	105	B15	CH4	61	1.3	0.98	0.282567	200	501.8	323	1.382	0.987	0.395	0.935755	35	2.42	40.33414	0.327	15	4.69E+10	1.71E-12	0.0119	0.0803789	0.0007567	0.0635876	0.00151048
43	106	B15	CH4	61	1.3	0.98	0.282567	200	501.8	323	1.678	0.987	0.691	1.841515	81	2.83	47.16761	0.327	15	4.69E+10	2.01E-12	0.0119	0.0939968	0.0004497	0.037786	0.00116438
44	107	B15	CH4	61	1.3	0.98	0.282567	200	501.8	323	1.974	0.987	0.987	2.922507	48	3.18	53.00106	0.327	15	4.69E+10	2.25E-12	0.0119	0.1056219	0.0003184	0.0267541	0.00097977
45	108	B15	CH4	61	1.3	0.98	0.282567	200	501.8	323	2.27	0.987	1.283	4.178731	26	3.38	56.33446	0.327	15	4.69E+10	2.39E-12	0.0119	0.1122648	0.0002367	0.019888	0.00084474
46	109	B15	CH4	61	1.3	0.98	0.282567	200	501.8	323	2.566	0.987	1.579	5.610187	71	3.57	59.50119	0.327	15	4.69E+10	2.53E-12	0.0119	0.1185755	0.0001862	0.0156462	0.00074926
47	110	B15	CH4	61	1.3	0.98	0.282567	200	501.8	323	2.862	0.987	1.875	7.216875	57	3.73	62.16791	0.327	15	4.69E+10	2.64E-12	0.0119	0.1238898	0.0001512	0.0127081	0.00067526
48	111	B15	CH4	61	1.3	0.98	0.282567	200	501.8	323	3.158	0.987	2.171	8.998795	27	3.84	64.00128	0.327	15	4.69E+10	2.72E-12	0.0119	0.1275434	0.0001249	0.0104922	0.00061357
49	112	B15	CH4	61	1.3	0.98	0.282567	200	501.8	323	3.454	0.987	2.467	10.955947	81	3.97	66.16799	0.327	15	4.69E+10	2.81E-12	0.0119	0.1318613	0.000106	0.0089097	0.00056541
50	113	B15	CH4	61	1.3	0.98	0.282567	200	501.8	373	1.382	0.987	0.395	0.935755	48	2.44	40.66748	0.327	15	4.69E+10	1.73E-12	0.0135	0.0810432	0.0008655	0.0641131	0.00161546
51	114	B15	CH4	61	1.3	0.98	0.282567	200	501.8	373	1.678	0.987	0.691	1.841515	42	2.88	48.00096	0.327	15	4.69E+10	2.04E-12	0.0135	0.0956576	0.0005191	0.0384536	0.0012511
52	115	B15	CH4	61	1.3	0.98	0.282567	200	501.8	373	1.974	0.987	0.987	2.922507	31	3.23	53.83441	0.327	15	4.69E+10	2.29E-12	0.0135	0.1072826	0.0003669	0.0271748	0.00105173
53	116	B15	CH4	61	1.3	0.98	0.282567	200	501.8	373	2.27	0.987	1.283	4.178731	70	3.47	57.83449	0.327	15	4.69E+10	2.46E-12	0.0135	0.1152541	0.0002756	0.0204176	0.00091164
54	117	B15	CH4	61	1.3	0.98	0.282567	200	501.8	373	2.566	0.987	1.579	5.610187	29	3.66	61.00122	0.327	15	4.69E+10	2.59E-12	0.0135	0.1215648	0.0002165	0.0160407	0.00080804
55	118	B15	CH4	61	1.3	0.98	0.282567	200	501.8	373	2.862	0.987	1.875	7.216875	47	3.82	63.66794	0.327	15	4.69E+10	2.71E-12	0.0135	0.1268791	0.0001757	0.0130147	0.00072785
56	119	B15	CH4	61	1.3	0.98	0.282567	200	501.8	373	3.158	0.987	2.171	8.998795	24	3.96	66.00132	0.327	15	4.69E+10	2.81E-12	0.0135	0.1315291	0.0001461	0.0108201	0.00066365
57	120	B15	CH4	61	1.3	0.98	0.282567	200	501.8	373	3.454	0.987	2.467	10.955947	81	4.09	68.16803	0.327	15	4.69E+10	2.90E-12	0.0135	0.135847	0.0001239	0.009179	0.00061125
58	121	B15	CH4	61	1.3	0.98	0.282567	200	501.8	473	1.382	0.987	0.395	0.935755	19	2.44	40.66748	0.327	15	4.69E+10	1.73E-12	0.0163	0.0810432	0.001045	0.0641131	0.0017751
59	122	B15	CH4	61	1.3	0.98	0.282567	200	501.8	473	1.678	0.987	0.691	1.841515	49	2.88	48.00096	0.327	15	4.69E+10	2.04E-12	0.0163	0.0956576	0.0006268	0.0384536	0.00137473
60	123	B15	CH4	61	1.3	0.98	0.282567	200	501.8	473	1.974	0.987	0.987	2.922507	26	3.28	54.66776	0.327	15	4.69E+10	2.32E-12	0.0163	0.1089433	0.0004498	0.0275955	0.00116458
61	124	B15	CH4	61	1.3	0.98	0.282567	200	501.8	473	2.27	0.987	1.283	4.178731	58	3.51	58.50117	0.327	15	4.69E+10	2.49E-12	0.0163	0.1165826	0.0003366	0.0206529	0.00100749
62	125	B15	CH4	61	1.3	0.98	0.282567	200	501.8	473	2.566	0.987	1.579	5.610187	50	3.7	61.6679	0.327	15	4.69E+10	2.62E-12	0.0163	0.1228934	0.0002643	0.016216	0.00089273
63	126	B15	CH4	61	1.3	0.98	0.282567	200	501.8	473	2.862	0.987	1.875	7.216875	46	3.87	64.50129	0.327	15	4.69E+10	2.74E-12	0.0163	0.1285398	0.0002149	0.013185	0.00080499
64	127	B15	CH4	61	1.3	0.98	0.282567	200	501.8	473	3.158	0.987	2.171	8.998795	51	4.04	67.33468	0.327	15	4.69E+10	2.86E-12	0.0163	0.1341863	0.0001799	0.0110387	0.00073656
65	128	B15	CH4	61	1.3	0.98	0.282567	200	501.8	473	3.454	0.987	2.467	10.955947	64	4.18	69.66806	0.327	15	4.69E+10	2.96E-12	0.0163	0.1388363	0.0001529	0.0093809	0.000679
66	193	S200	CH4	38.8	0.525	0.39	0.2972515	20	112.2	293	1.382	0.987	0.395	0.935755	42	1.96	32.66732	0.359	200	1.48E+12	1.97E-13	0.011	0.2911526	0.0009369	0.0851754	0.00160412
67	194	S200	CH4	38.8	0.525	0.39	0.2972515	20	112.2	293	1.678	0.987	0.691	1.841515	49	2.53	42.16751	0.359	200	1.48E+12	2.54E-13	0.011	0.3758245	0.0006146	0.0558683	0.00129916
68	195	S200	CH4	38.8	0.525	0.39	0.2972515	20	112.2	293	1.974	0.987	0.987	2.922507	25	2.83	47.16761	0.359	200	1.48E+12	2.84E-13	0.011	0.4203887	0.0004332	0.0393777	0.0010907
69	196	S200	CH4	38.8	0.525	0.39	0.2972515	20	112.2	293	2.27	0.987	1.283	4.178731	11	3.08	51.33436	0.359	200	1.48E+12	3.09E-13	0.011	0.4575255	0.0003297	0.0299727	0.00095157
70	197	S200	CH4	38.8	0.525	0.39	0.2972515	20	112.2	293	2.566	0.987	1.579	5.610187	47	3.26	54.33442	0.359	200	1.48E+12	3.27E-13	0.011	0.484264	0.0002599	0.0236298	0.00084491
71	198	S200	CH4	38.8	0.525	0.39	0.2972515	20	112.2	293	2.862	0.987	1.875	7.216875	48	3.41	56.83447	0.359	200	1.48E+12	3.42E-13	0.011	0.5065461	0.0002114	0.0192144	0.00076189
72	199	S200	CH4	38.8	0.525	0.39	0.2972515	20	112.2	293	3.158	0.987	2.171	8.998795	86	3.53	58.83451	0.359	200	1.48E+12	3.54E-13	0.011	0.5243717	0.0001755	0.0159518	0.0006942
73	200	S200	CH4	38.8	0.525	0.39	0.2972515	20	112.2	293	3.454	0.987	2.467	10.955947	37	3.63	60.50121	0.359	200	1.48E+12	3.64E-13	0.011	0.5392265	0.0001482	0.0134734	0.00063799
74	201	S200	CH4	38.8	0.525	0.39	0.2972515	20	112.2	323	1.382	0.987	0.395	0.935755	66	1.93	32.16731	0.359	200	1.48E+12	1.94E-13	0.0119	0.2866962	0.0009981	0.0838717	0.00165563
75	202	S200	CH4	38.8	0.525	0.39	0.2972515	20	112.2	323	1.678	0.987	0.691	1.841515	37	2.53	42.16751	0.359	200	1.48E+12	2.54E-13	0.0119	0.3758245	0.0006648	0.0558683	0.00135126
76	203	S200	CH4	38.8	0.525	0.39	0.2972515	20	112.2	323	1.974	0.987	0.987	2.922507	78	2.83	47.16761	0.359	200	1.48E+12	2.84E-13	0.0119	0.4203887	0.0004686	0.0393777	0.00113444
77	204	S200	CH4	38.8	0.525	0.39	0.2972515	20	112.2	323	2.27	0.987	1.283	4.178731	40	3.08	51.33436	0.359	200	1.48E+12	3.09E-13	0.0119	0.4575255	0.0003567	0.0299728	0.00098974
78	205	S200	CH4	38.8	0.525	0.39	0.2972515	20	112.2	323	2.566	0.987	1.579	5.610187	66	3.28	54.66776	0.359	200	1.48E+12	3.29E-13	0.0119	0.4872349	0.0002829	0.0237748	0.00088148
79	206	S200	CH4	38.8	0.525	0.39	0.2972515	20	112.2	323	2.862	0.987	1.875	7.216875	25	3.44	57.33448	0.359	200	1.48E+12	3.45E-13	0.0119	0.5110025	0.0002307	0.0193834	0.00079592
80	207	S200	CH4	38.8	0.525	0.39	0.2972515	20	112.2	323	3.158	0.987	2.171	8.998795	77	3.57	59.50119	0.359	200	1.48E+12	3.58E-13	0.0119	0.5303136	0.000192	0.0161326	0.00072612
81	208	S200	CH4	38.8	0.525	0.39	0.2972515	20	112.2	323	3.454	0.987	2.467	10.955947	57	3.68	61.33456	0.359	200	1.48E+12	3.69E-13	0.0119	0.5466538	0.0001625	0.013659	0.00066814
82	209	S200	CH4	38.8	0.525	0.39	0.2972515	20	112.2	373	1.382	0.987	0.395	0.935755	55	1.94	32.33398	0.359	200	1.48E+12	1.95E-13	0.0135	0.2881816	0.0011381	0.0843062	0.00176799
83	210	S200	CH4	38.8	0.525	0.39	0.2972515	20	112.2	373	1.678	0.987	0.691	1.841515	64	2.56	42.66752	0.359	200	1.48E+12	2.57E-13	0.0135	0.3802809	0.0007632	0.0565307	0.00144774
84	211	S200	CH4	38.8	0.525	0.39	0.2972515	20	112.2	373	1.974	0.987	0.987	2.922507	40	2.86	47.66762	0.359	200	1.48E+12	2.87E-13	0.0135	0.4248451	0.0005372	0.0397952	0.00121469
85	212	S200	CH4	38.8	0.525	0.39	0.2972515	20	112.2	373	2.27	0.987	1.283	4.178731	40	3.11	51.83437	0.359	200	1.48E+12	3.12E-13	0.0135	0.4619819	0.0004086	0.0302647	0.0010593
86	213	S200	CH4	38.8	0.525	0.39	0.2972515	20	112.2	373	2.566	0.987	1.579	5.610187	13	3.33	55.50111	0.359	200	1.48E+12	3.34E-13	0.0135	0.4946623	0.0003259	0.0241372	0.000946
87	214	S200	CH4	38.8	0.525	0.39	0.2972515	20	112.2	373	2.862	0.987	1.875	7.216875	70	3.49	58.16783	0.359	200	1.48E+12	3.50E-13	0.0135	0.5184299	0.0002655	0.0196651	0.00085388
88	215	S200	CH4	38.8	0.525	0.39	0.2972515	20	112.2	373	3.158	0.987	2.171	8.998795	13	3.64	60.66788	0.359	200	1.48E+12	3.65E-13	0.0135	0.5407119	0.0002221	0.0164489	0.00078094
89	216	S200	CH4	38.8	0.525	0.39	0.2972515	20	112.2	373	3.454	0.987	2.467	10.955947	43	3.77	62.83459	0.359	200	1.48E+12	3.78E-13	0.0135	0.5600231	0.0001889	0.013993	0.00072029
90	217	S200	CH4	38.8	0.525	0.39	0.2972515	20	112.2	473	1.382	0.987	0.395	0.935755	82	1.96	32.66732	0.359	200	1.48E+12	1.97E-13	0.0163	0.2911526	0.0013884	0.0851754	0.00195269
91	218	S200	CH4	38.8	0.525	0.39	0.2972515	20	112.2	473	1.678	0.987	0.691	1.841515	49	2.59	43.16753	0.359	200	1.48E+12	2.60E-13	0.0163	0.3847373	0.0009323	0.0571933	0.00160011
92	219	S200	CH4	38.8	0.525	0.39	0.2972515	20	112.2	473	1.974	0.987	0.987	2.922507	69	2.88	48.00096	0.359	200	1.48E+12	2.89E-13	0.0163	0.427816	0.0006532	0.0400735	0.00133938
93	220	S200	CH4	38.8	0.525	0.39	0.2972515	20	112.2	473	2.27	0.987	1.283	4.178731	13	3.16	52.66772	0.359	200	1.48E+12	3.17E-13	0.0163	0.4694093	0.0005012	0.0307512	0.0011733
94	221	S200	CH4	38.8	0.525	0.39	0.2972515	20	112.2	473	2.566	0.987	1.579	5.610187	13	3.38	56.33446	0.359	200	1.48E+12	3.39E-13	0.0163	0.5020897	0.0003993	0.0244996	0.00104726
95	222	S200	CH4	38.8	0.525	0.39	0.2972515	20	112.2	473	2.862	0.987	1.875	7.216875	25	3.58	59.66786	0.359	200	1.48E+12	3.59E-13	0.0163	0.5317991	0.0003288	0.0201722	0.00095028
96	223	S200	CH4	38.8	0.525	0.39	0.2972515	20	112.2	473	3.158	0.987	2.171	8.998795	90	3.75	62.50125	0.359	200	1.48E+12	3.76E-13	0.0163	0.5570521	0.0002762	0.016946	0.00087098
97	224	S200	CH4	38.8	0.525	0.39	0.2972515	20	112.2	473	3.454	0.987	2.467	10.955947	67	3.9	65.0013	0.359	200	1.48E+12	3.91E-13	0.0163	0.5793342	0.000236	0.0144755	0.000805

1	s/n	Core Pore Size (nm)	Gas	Core height (cm)	External Radius (cm)	Internal Radius (cm)	Ln(r1/r2) (cm)	Core Volume (cm3)	Core Cross-Sectional Area (cm2)	Temperature (K)	Inlet Pressure (atm)	Outlet Pressure (atm)	Pressure Drop (atm)	P1^2 - P2^2 (atm)	Data Frequency	Flowrate (LPM))	Flowrate (cm3/sec)	Porosity (%)	Pore Size (nm)	Aspect Ratio	Aspect Quality Index	Viscosity (cp)	Flux (cm/s)	Permeability (mD)	Mobility (mD/cp)	Sample Quality Index (mD)
146	401	B6000	CH4	32.8	1.29	1.035	0.2202408	140	267.8	373	1.382	0.987	0.395	0.935755	25	1.47	24.50049	0.29	6000	2.35E+13	3.89E-15	0.0135	0.091488	0.0007559	0.0559896	0.00160306
147	402	B6000	CH4	32.8	1.29	1.035	0.2202408	140	267.8	373	1.678	0.987	0.691	1.841515	84	1.97	32.83399	0.29	6000	2.35E+13	5.21E-15	0.0135	0.1226064	0.0005147	0.0381279	0.00132287
148	403	B6000	CH4	32.8	1.29	1.035	0.2202408	140	267.8	373	1.974	0.987	0.987	2.922507	76	2.11	35.16737	0.29	6000	2.35E+13	5.58E-15	0.0135	0.1313195	0.0003474	0.0257323	0.00108677
149	404	B6000	CH4	32.8	1.29	1.035	0.2202408	140	267.8	373	2.27	0.987	1.283	4.178731	89	2.26	37.66742	0.29	6000	2.35E+13	5.98E-15	0.0135	0.140655	0.0002602	0.0192759	0.0009406
150	405	B6000	CH4	32.8	1.29	1.035	0.2202408	140	267.8	373	2.566	0.987	1.579	5.610187	32	2.36	39.33412	0.29	6000	2.35E+13	6.24E-15	0.0135	0.1468787	0.0002024	0.0149929	0.00082955
151	406	B6000	CH4	32.8	1.29	1.035	0.2202408	140	267.8	373	2.862	0.987	1.875	7.216875	78	2.45	40.83415	0.29	6000	2.35E+13	6.48E-15	0.0135	0.15248	0.0001633	0.0120996	0.00074522
152	407	B6000	CH4	32.8	1.29	1.035	0.2202408	140	267.8	373	3.158	0.987	2.171	8.998795	56	2.53	42.16751	0.29	6000	2.35E+13	6.69E-15	0.0135	0.157459	0.0001353	0.0100204	0.00067817
153	408	B6000	CH4	32.8	1.29	1.035	0.2202408	140	267.8	373	3.454	0.987	2.467	10.955947	27	2.6	43.3342	0.29	6000	2.35E+13	6.88E-15	0.0135	0.1618155	0.0001142	0.0084581	0.00062307
154	409	B6000	CH4	32.8	1.29	1.035	0.2202408	140	267.8	473	1.382	0.987	0.395	0.935755	90	1.45	24.16715	0.29	6000	2.35E+13	3.84E-15	0.0163	0.0902433	0.0009002	0.0552278	0.00174946
155	410	B6000	CH4	32.8	1.29	1.035	0.2202408	140	267.8	473	1.678	0.987	0.691	1.841515	33	2	33.334	0.29	6000	2.35E+13	5.29E-15	0.0163	0.1244735	0.0009002	0.0552278	0.00174946
156	411	B6000	CH4	32.8	1.29	1.035	0.2202408	140	267.8	473	1.974	0.987	0.987	2.922507	10	2.13	35.50071	0.29	6000	2.35E+13	5.63E-15	0.0163	0.1325643	0.0004234	0.0259762	0.00119981
157	412	B6000	CH4	32.8	1.29	1.035	0.2202408	140	267.8	473	2.27	0.987	1.283	4.178731	38	2.28	38.00076	0.29	6000	2.35E+13	6.03E-15	0.0163	0.1418998	0.000317	0.0194465	0.00103811
158	413	B6000	CH4	32.8	1.29	1.035	0.2202408	140	267.8	473	2.566	0.987	1.579	5.610187	29	2.4	40.0008	0.29	6000	2.35E+13	6.35E-15	0.0163	0.1493682	0.0002485	0.0152471	0.00091922
159	414	B6000	CH4	32.8	1.29	1.035	0.2202408	140	267.8	473	2.862	0.987	1.875	7.216875	31	2.49	41.50083	0.29	6000	2.35E+13	6.59E-15	0.0163	0.1549695	0.0002004	0.0122971	0.00082552
160	415	B6000	CH4	32.8	1.29	1.035	0.2202408	140	267.8	473	3.158	0.987	2.171	8.998795	79	2.59	43.16753	0.29	6000	2.35E+13	6.85E-15	0.0163	0.1611932	0.0001672	0.0102581	0.00075398
161	416	B6000	CH4	32.8	1.29	1.035	0.2202408	140	267.8	473	3.454	0.987	2.467	10.955947	58	2.66	44.33422	0.29	6000	2.35E+13	7.04E-15	0.0163	0.1655497	0.000141	0.0086533	0.00069249
162	65	S15	CO2	34.7	0.505	0.355	0.3524406	20	111.3	293	1.382	0.987	0.395	0.935755	120	1.2	20.0004	0.306	15	1.00E+11	1.80E-12	0.0147	0.1796981	0.0010163	0.0691359	0.00180959
163	66	S15	CO2	34.7	0.505	0.355	0.3524406	20	111.3	293	1.678	0.987	0.691	1.841515	161	1.57	26.16719	0.306	15	1.00E+11	2.35E-12	0.0147	0.235105	0.0006757	0.0459631	0.00147548
164	67	S15	CO2	34.7	0.505	0.355	0.3524406	20	111.3	293	1.974	0.987	0.987	2.922507	142	1.8	30.0006	0.306	15	1.00E+11	2.70E-12	0.0147	0.2695472	0.0004881	0.0332048	0.00125409
165	68	S15	CO2	34.7	0.505	0.355	0.3524406	20	111.3	293	2.27	0.987	1.283	4.178731	148	1.98	33.00066	0.306	15	1.00E+11	2.97E-12	0.0147	0.2965019	0.0003755	0.025545	0.00109997
166	69	S15	CO2	34.7	0.505	0.355	0.3524406	20	111.3	293	2.566	0.987	1.579	5.610187	161	2.11	35.16737	0.306	15	1.00E+11	3.16E-12	0.0147	0.3159692	0.0002981	0.0202763	0.00097999
167	70	S15	CO2	34.7	0.505	0.355	0.3524406	20	111.3	293	2.862	0.987	1.875	7.216875	116	2.23	37.16741	0.306	15	1.00E+11	3.34E-12	0.0147	0.333939	0.0002449	0.0166586	0.00088827
168	71	S15	CO2	34.7	0.505	0.355	0.3524406	20	111.3	293	3.158	0.987	2.171	8.998795	145	2.31	38.50077	0.306	15	1.00E+11	3.46E-12	0.0147	0.3459189	0.0002034	0.0138393	0.00080962
169	72	S15	CO2	34.7	0.505	0.355	0.3524406	20	111.3	293	3.454	0.987	2.467	10.955947	181	2.38	39.66746	0.306	15	1.00E+11	3.56E-12	0.0147	0.3564013	0.0001722	0.0117115	0.00074479
170	73	S15	CO2	34.7	0.505	0.355	0.3524406	20	111.3	323	1.382	0.987	0.395	0.935755	133	1.2	20.0004	0.306	15	1.00E+11	1.80E-12	0.0161	0.1796981	0.0011131	0.0691358	0.0018938
171	74	S15	CO2	34.7	0.505	0.355	0.3524406	20	111.3	323	1.678	0.987	0.691	1.841515	181	1.58	26.33386	0.306	15	1.00E+11	2.37E-12	0.0161	0.2366025	0.0007447	0.0462558	0.00154905
172	75	S15	CO2	34.7	0.505	0.355	0.3524406	20	111.3	323	1.974	0.987	0.987	2.922507	181	1.82	30.33394	0.306	15	1.00E+11	2.73E-12	0.0161	0.2725421	0.0005405	0.0335738	0.00131972
173	76	S15	CO2	34.7	0.505	0.355	0.3524406	20	111.3	323	2.27	0.987	1.283	4.178731	182	2	33.334	0.306	15	1.00E+11	2.99E-12	0.0161	0.2994969	0.0004154	0.025803	0.00115696
174	77	S15	CO2	34.7	0.505	0.355	0.3524406	20	111.3	323	2.566	0.987	1.579	5.610187	143	2.13	35.50071	0.306	15	1.00E+11	3.19E-12	0.0161	0.3189642	0.0003295	0.0204685	0.00103045
175	78	S15	CO2	34.7	0.505	0.355	0.3524406	20	111.3	323	2.862	0.987	1.875	7.216875	178	2.23	37.16741	0.306	15	1.00E+11	3.34E-12	0.0161	0.333939	0.0002682	0.0166586	0.00092961
176	79	S15	CO2	34.7	0.505	0.355	0.3524406	20	111.3	323	3.158	0.987	2.171	8.998795	172	2.32	38.66744	0.306	15	1.00E+11	3.47E-12	0.0161	0.3474164	0.0002238	0.0138991	0.00084913
177	80	S15	CO2	34.7	0.505	0.355	0.3524406	20	111.3	323	3.454	0.987	2.467	10.955947	117	2.4	40.0008	0.306	15	1.00E+11	3.59E-12	0.0161	0.3593962	0.0001901	0.0118099	0.00078272
178	81	S15	CO2	34.7	0.505	0.355	0.3524406	20	111.3	373	1.382	0.987	0.395	0.935755	124	1.12	18.66704	0.306	15	1.00E+11	1.68E-12	0.0185	0.1677182	0.0011937	0.0645268	0.00196121
179	82	S15	CO2	34.7	0.505	0.355	0.3524406	20	111.3	373	1.678	0.987	0.691	1.841515	135	1.54	25.66718	0.306	15	1.00E+11	2.31E-12	0.0185	0.2306126	0.0008341	0.0450848	0.00163934
180	83	S15	CO2	34.7	0.505	0.355	0.3524406	20	111.3	373	1.974	0.987	0.987	2.922507	173	1.8	30.0006	0.306	15	1.00E+11	2.70E-12	0.0185	0.2695472	0.0006143	0.0332048	0.00140687
181	84	S15	CO2	34.7	0.505	0.355	0.3524406	20	111.3	373	2.27	0.987	1.283	4.178731	163	1.98	33.00066	0.306	15	1.00E+11	2.97E-12	0.0185	0.2965019	0.0004726	0.025545	0.00123398
182	85	S15	CO2	34.7	0.505	0.355	0.3524406	20	111.3	373	2.566	0.987	1.579	5.610187	187	2.12	35.33404	0.306	15	1.00E+11	3.17E-12	0.0185	0.3174667	0.0003769	0.0203724	0.00110199
183	86	S15	CO2	34.7	0.505	0.355	0.3524406	20	111.3	373	2.862	0.987	1.875	7.216875	147	2.23	37.16741	0.306	15	1.00E+11	3.34E-12	0.0185	0.333939	0.0003082	0.0166586	0.00099649
184	87	S15	CO2	34.7	0.505	0.355	0.3524406	20	111.3	373	3.158	0.987	2.171	8.998795	122	2.33	38.83411	0.306	15	1.00E+11	3.49E-12	0.0185	0.3489138	0.0002582	0.013959	0.00091218
185	88	S15	CO2	34.7	0.505	0.355	0.3524406	20	111.3	373	3.454	0.987	2.467	10.955947	148	2.41	40.16747	0.306	15	1.00E+11	3.61E-12	0.0185	0.3608937	0.0002194	0.0118591	0.00084078
186	89	S15	CO2	34.7	0.505	0.355	0.3524406	20	111.3	473	1.382	0.987	0.395	0.935755	190	1.23	20.50041	0.306	15	1.00E+11	1.84E-12	0.023	0.1841906	0.0016299	0.0708643	0.00229164
187	90	S15	CO2	34.7	0.505	0.355	0.3524406	20	111.3	473	1.678	0.987	0.691	1.841515	148	1.55	25.83385	0.306	15	1.00E+11	2.32E-12	0.023	0.2321101	0.0010437	0.0453775	0.00183381
188	91	S15	CO2	34.7	0.505	0.355	0.3524406	20	111.3	473	1.974	0.987	0.987	2.922507	167	1.81	30.16727	0.306	15	1.00E+11	2.71E-12	0.023	0.2710447	0.000768	0.0333893	0.00157303
189	92	S15	CO2	34.7	0.505	0.355	0.3524406	20	111.3	473	2.27	0.987	1.283	4.178731	141	2	33.334	0.306	15	1.00E+11	2.99E-12	0.023	0.2994969	0.0005935	0.025803	0.00138283
190	93	S15	CO2	34.7	0.505	0.355	0.3524406	20	111.3	473	2.566	0.987	1.579	5.610187	183	2.13	35.50071	0.306	15	1.00E+11	3.19E-12	0.023	0.3189642	0.0004708	0.0204685	0.00123162
191	94	S15	CO2	34.7	0.505	0.355	0.3524406	20	111.3	473	2.862	0.987	1.875	7.216875	163	2.25	37.50075	0.306	15	1.00E+11	3.37E-12	0.023	0.336934	0.0003866	0.016808	0.00111607
192	95	S15	CO2	34.7	0.505	0.355	0.3524406	20	111.3	473	3.158	0.987	2.171	8.998795	113	2.36	39.33412	0.306	15	1.00E+11	3.53E-12	0.023	0.3534063	0.0003252	0.0141388	0.00102362
193	96	S15	CO2	34.7	0.505	0.355	0.3524406	20	111.3	473	3.454	0.987	2.467	10.955947	168	2.46	41.00082	0.306	15	1.00E+11	3.68E-12	0.023	0.3683811	0.0002784	0.0121051	0.00094715

1	s/n	Core Pore Size (nm)	Gas	Core height (cm)	External Radius (cm)	Internal Radius (cm)	Ln(r1/r2) (cm)	Core Volume (cm3)	Core Cross-Sectional Area (cm2)	Temperature (K)	Inlet Pressure (atm)	Outlet Pressure (atm)	Pressure Drop (atm)	P1^2 - P2^2 (atm)	Data Frequency	Flowrate (LPM))	Flowrate (cm3/sec)	Porosity (%)	Pore Size (nm)	Aspect Ratio	Aspect Quality Index	Viscosity (cp)	Flux (cm/s)	Permeability (mD)	Mobility (mD/cp)	Sample Quality Index (mD)
98	289	S6000	CH4	32.8	0.52	0.384	0.3031863	20	107.1	293	1.382	0.987	0.395	0.935755	59	1.99	33.16733	0.355	6000	4.41E+13	7.02E-15	0.011	0.3096856	0.0011477	0.1043408	0.00178541
99	290	S6000	CH4	32.8	0.52	0.384	0.3031863	20	107.1	293	1.678	0.987	0.691	1.841515	76	2.55	42.50085	0.355	6000	4.41E+13	8.99E-15	0.011	0.3968333	0.0007473	0.0679405	0.00144071
100	291	S6000	CH4	32.8	0.52	0.384	0.3031863	20	107.1	293	1.974	0.987	0.987	2.922507	44	2.86	47.66762	0.355	6000	4.41E+13	1.01E-14	0.011	0.4450758	0.0005282	0.0480146	0.00121115
101	292	S6000	CH4	32.8	0.52	0.384	0.3031863	20	107.1	293	2.27	0.987	1.283	4.178731	79	3.11	51.83437	0.355	6000	4.41E+13	1.10E-14	0.011	0.483981	0.0004017	0.0365157	0.00105621
102	293	S6000	CH4	32.8	0.52	0.384	0.3031863	20	107.1	293	2.566	0.987	1.579	5.610187	22	3.3	55.0011	0.355	6000	4.41E+13	1.16E-14	0.011	0.513549	0.0003175	0.0288603	0.00093899
103	294	S6000	CH4	32.8	0.52	0.384	0.3031863	20	107.1	293	2.862	0.987	1.875	7.216875	68	3.44	57.33448	0.355	6000	4.41E+13	1.21E-14	0.011	0.5353359	0.0002573	0.0233869	0.00084528
104	295	S6000	CH4	32.8	0.52	0.384	0.3031863	20	107.1	293	3.158	0.987	2.171	8.998795	58	3.56	59.33452	0.355	6000	4.41E+13	1.26E-14	0.011	0.5540105	0.0002135	0.0194102	0.00077006
105	296	S6000	CH4	32.8	0.52	0.384	0.3031863	20	107.1	293	3.454	0.987	2.467	10.955947	52	3.66	61.00122	0.355	6000	4.41E+13	1.29E-14	0.011	0.5695725	0.0001803	0.0163906	0.00070764
106	297	S6000	CH4	32.8	0.52	0.384	0.3031863	20	107.1	323	1.382	0.987	0.395	0.935755	58	2	33.334	0.355	6000	4.41E+13	7.05E-15	0.0119	0.3112418	0.0012479	0.1048652	0.00186168
107	298	S6000	CH4	32.8	0.52	0.384	0.3031863	20	107.1	323	1.678	0.987	0.691	1.841515	71	2.57	42.83419	0.355	6000	4.41E+13	9.07E-15	0.0119	0.3999458	0.0008148	0.0684733	0.00150435
108	299	S6000	CH4	32.8	0.52	0.384	0.3031863	20	107.1	323	1.974	0.987	0.987	2.922507	60	2.88	48.00096	0.355	6000	4.41E+13	1.02E-14	0.0119	0.4481882	0.0005754	0.0483504	0.00126412
109	300	S6000	CH4	32.8	0.52	0.384	0.3031863	20	107.1	323	2.27	0.987	1.283	4.178731	78	3.13	52.16771	0.355	6000	4.41E+13	1.10E-14	0.0119	0.4870935	0.0004373	0.0367505	0.0011021
110	301	S6000	CH4	32.8	0.52	0.384	0.3031863	20	107.1	323	2.566	0.987	1.579	5.610187	74	3.33	55.50111	0.355	6000	4.41E+13	1.17E-14	0.0119	0.5182176	0.0003466	0.0291226	0.00098108
111	302	S6000	CH4	32.8	0.52	0.384	0.3031863	20	107.1	323	2.862	0.987	1.875	7.216875	35	3.49	58.16783	0.355	6000	4.41E+13	1.23E-14	0.0119	0.543117	0.0002823	0.0237268	0.00088554
112	303	S6000	CH4	32.8	0.52	0.384	0.3031863	20	107.1	323	3.158	0.987	2.171	8.998795	90	3.63	60.50121	0.355	6000	4.41E+13	1.28E-14	0.0119	0.5649039	0.0002355	0.0197918	0.00080878
113	304	S6000	CH4	32.8	0.52	0.384	0.3031863	20	107.1	323	3.454	0.987	2.467	10.955947	40	3.75	62.50125	0.355	6000	4.41E+13	1.32E-14	0.0119	0.5835784	0.0001998	0.0167936	0.00074501
114	305	S6000	CH4	32.8	0.52	0.384	0.3031863	20	107.1	373	1.382	0.987	0.395	0.935755	58	2.02	33.66734	0.355	6000	4.41E+13	7.13E-15	0.0135	0.3143542	0.0014298	0.1059139	0.00199278
115	306	S6000	CH4	32.8	0.52	0.384	0.3031863	20	107.1	373	1.678	0.987	0.691	1.841515	35	2.6	43.3342	0.355	6000	4.41E+13	9.17E-15	0.0135	0.4046144	0.0009352	0.0692726	0.00161162
116	307	S6000	CH4	32.8	0.52	0.384	0.3031863	20	107.1	373	1.974	0.987	0.987	2.922507	15	2.92	48.66764	0.355	6000	4.41E+13	1.03E-14	0.0135	0.4544131	0.0006618	0.049022	0.00135574
117	308	S6000	CH4	32.8	0.52	0.384	0.3031863	20	107.1	373	2.27	0.987	1.283	4.178731	24	3.17	52.83439	0.355	6000	4.41E+13	1.12E-14	0.0135	0.4933183	0.0005025	0.0372201	0.00118133
118	309	S6000	CH4	32.8	0.52	0.384	0.3031863	20	107.1	373	2.566	0.987	1.579	5.610187	23	3.38	56.33446	0.355	6000	4.41E+13	1.19E-14	0.0135	0.5259987	0.0003991	0.0295599	0.00105277
119	310	S6000	CH4	32.8	0.52	0.384	0.3031863	20	107.1	373	2.862	0.987	1.875	7.216875	11	3.56	59.33452	0.355	6000	4.41E+13	1.26E-14	0.0135	0.5540105	0.0003267	0.0242027	0.00095261
120	311	S6000	CH4	32.8	0.52	0.384	0.3031863	20	107.1	373	3.158	0.987	2.171	8.998795	43	3.7	61.6679	0.355	6000	4.41E+13	1.31E-14	0.0135	0.5757974	0.0002723	0.0201735	0.00086971
121	312	S6000	CH4	32.8	0.52	0.384	0.3031863	20	107.1	373	3.454	0.987	2.467	10.955947	18	3.83	63.83461	0.355	6000	4.41E+13	1.35E-14	0.0135	0.5960281	0.0002316	0.0171519	0.00080193
122	313	S6000	CH4	32.8	0.52	0.384	0.3031863	20	107.1	473	1.382	0.987	0.395	0.935755	88	2.04	34.00068	0.355	6000	4.41E+13	7.20E-15	0.0163	0.3174667	0.0017435	0.1069625	0.00220052
123	314	S6000	CH4	32.8	0.52	0.384	0.3031863	20	107.1	473	1.678	0.987	0.691	1.841515	70	2.66	44.33422	0.355	6000	4.41E+13	9.38E-15	0.0163	0.4139516	0.0011552	0.0708712	0.0017912
124	315	S6000	CH4	32.8	0.52	0.384	0.3031863	20	107.1	473	1.974	0.987	0.987	2.922507	32	2.96	49.33432	0.355	6000	4.41E+13	1.04E-14	0.0163	0.4606379	0.00081	0.0496935	0.00149989
125	316	S6000	CH4	32.8	0.52	0.384	0.3031863	20	107.1	473	2.27	0.987	1.283	4.178731	72	3.22	53.66774	0.355	6000	4.41E+13	1.14E-14	0.0163	0.5010993	0.0006163	0.0378072	0.00130827
126	317	S6000	CH4	32.8	0.52	0.384	0.3031863	20	107.1	473	2.566	0.987	1.579	5.610187	49	3.44	57.33448	0.355	6000	4.41E+13	1.21E-14	0.0163	0.5353359	0.0004904	0.0300846	0.00116703
127	318	S6000	CH4	32.8	0.52	0.384	0.3031863	20	107.1	473	2.862	0.987	1.875	7.216875	23	3.63	60.50121	0.355	6000	4.41E+13	1.28E-14	0.0163	0.5649039	0.0004023	0.0246787	0.00105699
128	319	S6000	CH4	32.8	0.52	0.384	0.3031863	20	107.1	473	3.158	0.987	2.171	8.998795	45	3.82	63.66794	0.355	6000	4.41E+13	1.35E-14	0.0163	0.5944719	0.0003395	0.0208277	0.00097102
129	320	S6000	CH4	32.8	0.52	0.384	0.3031863	20	107.1	473	3.454	0.987	2.467	10.955947	44	3.98	66.33466	0.355	6000	4.41E+13	1.40E-14	0.0163	0.6193712	0.0002905	0.0178236	0.00089827
130	385	B6000	CH4	32.8	1.29	1.035	0.2202408	140	267.8	293	1.382	0.987	0.395	0.935755	65	1.5	25.0005	0.29	6000	2.35E+13	3.97E-15	0.011	0.0933551	0.0006285	0.0571322	0.00146173
131	386	B6000	CH4	32.8	1.29	1.035	0.2202408	140	267.8	293	1.678	0.987	0.691	1.841515	35	1.95	32.50065	0.29	6000	2.35E+13	5.16E-15	0.011	0.1213617	0.0004151	0.0377408	0.00118804
132	387	B6000	CH4	32.8	1.29	1.035	0.2202408	140	267.8	293	1.974	0.987	0.987	2.922507	24	2.12	35.33404	0.29	6000	2.35E+13	5.61E-15	0.011	0.1319419	0.0002844	0.0258543	0.00098332
133	388	B6000	CH4	32.8	1.29	1.035	0.2202408	140	267.8	293	2.27	0.987	1.283	4.178731	48	2.26	37.66742	0.29	6000	2.35E+13	5.98E-15	0.011	0.140655	0.000212	0.0192759	0.00084905
134	389	B6000	CH4	32.8	1.29	1.035	0.2202408	140	267.8	293	2.566	0.987	1.579	5.610187	32	2.36	39.33412	0.29	6000	2.35E+13	6.24E-15	0.011	0.1468787	0.0001649	0.0149929	0.00074881
135	390	B6000	CH4	32.8	1.29	1.035	0.2202408	140	267.8	293	2.862	0.987	1.875	7.216875	66	2.39	39.83413	0.29	6000	2.35E+13	6.32E-15	0.011	0.1487458	0.0001298	0.0118032	0.0006644
136	391	B6000	CH4	32.8	1.29	1.035	0.2202408	140	267.8	293	3.158	0.987	2.171	8.998795	76	2.51	41.83417	0.29	6000	2.35E+13	6.64E-15	0.011	0.1562142	0.0001094	0.0099413	0.00060974
137	392	B6000	CH4	32.8	1.29	1.035	0.2202408	140	267.8	293	3.454	0.987	2.467	10.955947	54	2.56	42.66752	0.29	6000	2.35E+13	6.77E-15	0.011	0.1593261	9.16082E-05	0.008328	0.00055808
138	393	B6000	CH4	32.8	1.29	1.035	0.2202408	140	267.8	323	1.382	0.987	0.395	0.935755	64	1.5	25.0005	0.29	6000	2.35E+13	3.97E-15	0.0119	0.0933551	0.0006799	0.0571322	0.00152035
139	394	B6000	CH4	32.8	1.29	1.035	0.2202408	140	267.8	323	1.678	0.987	0.691	1.841515	76	1.97	32.83399	0.29	6000	2.35E+13	5.21E-15	0.0119	0.1226064	0.0004537	0.0381279	0.00124201
140	395	B6000	CH4	32.8	1.29	1.035	0.2202408	140	267.8	323	1.974	0.987	0.987	2.922507	12	2.13	35.50071	0.29	6000	2.35E+13	5.63E-15	0.0119	0.1325643	0.0003091	0.0259762	0.00102516
141	396	B6000	CH4	32.8	1.29	1.035	0.2202408	140	267.8	323	2.27	0.987	1.283	4.178731	49	2.27	37.83409	0.29	6000	2.35E+13	6.00E-15	0.0119	0.1412774	0.0002304	0.0193613	0.00088506
142	397	B6000	CH4	32.8	1.29	1.035	0.2202408	140	267.8	323	2.566	0.987	1.579	5.610187	49	2.36	39.33412	0.29	6000	2.35E+13	6.24E-15	0.0119	0.1468787	0.0001784	0.0149929	0.00077884
143	398	B6000	CH4	32.8	1.29	1.035	0.2202408	140	267.8	323	2.862	0.987	1.875	7.216875	78	2.46	41.00082	0.29	6000	2.35E+13	6.51E-15	0.0119	0.1531024	0.0001446	0.0121489	0.00070109
144	399	B6000	CH4	32.8	1.29	1.035	0.2202408	140	267.8	323	3.158	0.987	2.171	8.998795	86	2.53	42.16751	0.29	6000	2.35E+13	6.69E-15	0.0119	0.157459	0.0001192	0.0100205	0.00063672
145	400	B6000	CH4	32.8	1.29	1.035	0.2202408	140	267.8	323	3.454	0.987	2.467	10.955947	80	2.59	43.16753	0.29	6000	2.35E+13	6.85E-15	0.0119	0.1611932	0.0001003	0.0084256	0.00058386

1	s/n	Core Pore Size (nm)	Gas	Core height (cm)	External Radius (cm)	Internal Radius (cm)	Ln(r1/r2) (cm)	Core Volume (cm3)	Core Cross-Sectional Area (cm2)	Temperature (K)	Inlet Pressure (atm)	Outlet Pressure (atm)	Pressure Drop (atm)	P1^2 - P2^2 (atm)	Data Frequency	Flowrate (LPM))	Flowrate (cm3/sec)	Porosity (%)	Pore Size (nm)	Aspect Ratio	Aspect Quality Index	Viscosity (cp)	Flux (cm/s)	Permeability (mD)	Mobility (mD/cp)	Sample Quality Index (mD)
194	161	B15	CO2	61	1.3	0.98	0.282567	200	501.8	293	1.382	0.987	0.395	0.935755	167	1.49	24.83383	0.327	15	4.69E+10	1.06E-12	0.0147	0.0494895	0.0005755	0.039151	0.0013173
195	162	B15	CO2	61	1.3	0.98	0.282567	200	501.8	293	1.678	0.987	0.691	1.841515	186	1.81	30.16727	0.327	15	4.69E+10	1.28E-12	0.0147	0.0601181	0.0003553	0.024167	0.00103497
196	163	B15	CO2	61	1.3	0.98	0.282567	200	501.8	293	1.974	0.987	0.987	2.922507	148	2.04	34.00068	0.327	15	4.69E+10	1.45E-12	0.0147	0.0677574	0.0002523	0.0171631	0.00087219
197	164	B15	CO2	61	1.3	0.98	0.282567	200	501.8	293	2.27	0.987	1.283	4.178731	171	2.19	36.50073	0.327	15	4.69E+10	1.55E-12	0.0147	0.0727396	0.0001894	0.0128861	0.00075574
198	165	B15	CO2	61	1.3	0.98	0.282567	200	501.8	293	2.566	0.987	1.579	5.610187	175	2.31	38.50077	0.327	15	4.69E+10	1.64E-12	0.0147	0.0767253	0.0001488	0.010124	0.00066987
199	166	B15	CO2	61	1.3	0.98	0.282567	200	501.8	293	2.862	0.987	1.875	7.216875	182	2.4	40.0008	0.327	15	4.69E+10	1.70E-12	0.0147	0.0797146	0.0001202	0.0081767	0.00060201
200	167	B15	CO2	61	1.3	0.98	0.282567	200	501.8	293	3.158	0.987	2.171	8.998795	159	2.48	41.33416	0.327	15	4.69E+10	1.76E-12	0.0147	0.0823718	9.96102E-05	0.0067762	0.00054803
201	168	B15	CO2	61	1.3	0.98	0.282567	200	501.8	293	3.454	0.987	2.467	10.955947	143	2.54	42.33418	0.327	15	4.69E+10	1.80E-12	0.0147	0.0843646	8.37955E-05	0.0057004	0.00050265
202	169	B15	CO2	61	1.3	0.98	0.282567	200	501.8	323	1.382	0.987	0.395	0.935755	131	1.51	25.16717	0.327	15	4.69E+10	1.07E-12	0.0161	0.0501538	0.0006388	0.0396766	0.00138783
203	170	B15	CO2	61	1.3	0.98	0.282567	200	501.8	323	1.678	0.987	0.691	1.841515	170	1.83	30.50061	0.327	15	4.69E+10	1.30E-12	0.0161	0.0607824	0.0003934	0.024434	0.0010891
204	171	B15	CO2	61	1.3	0.98	0.282567	200	501.8	323	1.974	0.987	0.987	2.922507	133	2.05	34.16735	0.327	15	4.69E+10	1.45E-12	0.0161	0.0680896	0.0002777	0.0172471	0.00091501
205	172	B15	CO2	61	1.3	0.98	0.282567	200	501.8	323	2.27	0.987	1.283	4.178731	168	2.21	36.83407	0.327	15	4.69E+10	1.57E-12	0.0161	0.0734039	0.0002094	0.0130037	0.00079452
206	173	B15	CO2	61	1.3	0.98	0.282567	200	501.8	323	2.566	0.987	1.579	5.610187	163	2.33	38.83411	0.327	15	4.69E+10	1.65E-12	0.0161	0.0773896	0.0001644	0.0102117	0.00070407
207	174	B15	CO2	61	1.3	0.98	0.282567	200	501.8	323	2.862	0.987	1.875	7.216875	117	2.43	40.50081	0.327	15	4.69E+10	1.72E-12	0.0161	0.0807111	0.0001333	0.0082789	0.00063395
208	175	B15	CO2	61	1.3	0.98	0.282567	200	501.8	323	3.158	0.987	2.171	8.998795	185	2.5	41.6675	0.327	15	4.69E+10	1.77E-12	0.0161	0.0830361	0.00011	0.0068309	0.00057585
209	176	B15	CO2	61	1.3	0.98	0.282567	200	501.8	323	3.454	0.987	2.467	10.955947	118	2.56	42.66752	0.327	15	4.69E+10	1.81E-12	0.0161	0.0850289	9.24986E-05	0.0057453	0.00052811
210	177	B15	CO2	61	1.3	0.98	0.282567	200	501.8	373	1.382	0.987	0.395	0.935755	182	1.51	25.16717	0.327	15	4.69E+10	1.07E-12	0.0185	0.0501538	0.000734	0.0396766	0.00148768
211	178	B15	CO2	61	1.3	0.98	0.282567	200	501.8	373	1.678	0.987	0.691	1.841515	141	1.83	30.50061	0.327	15	4.69E+10	1.30E-12	0.0185	0.0607824	0.000452	0.0244341	0.00116745
212	179	B15	CO2	61	1.3	0.98	0.282567	200	501.8	373	1.974	0.987	0.987	2.922507	121	2.07	34.50069	0.327	15	4.69E+10	1.47E-12	0.0185	0.0687539	0.0003222	0.0174154	0.00098562
213	180	B15	CO2	61	1.3	0.98	0.282567	200	501.8	373	2.27	0.987	1.283	4.178731	143	2.22	37.00074	0.327	15	4.69E+10	1.57E-12	0.0185	0.073736	0.0002417	0.0130625	0.0008536
214	181	B15	CO2	61	1.3	0.98	0.282567	200	501.8	373	2.566	0.987	1.579	5.610187	166	2.35	39.16745	0.327	15	4.69E+10	1.67E-12	0.0185	0.0780539	0.0001905	0.0102994	0.00075796
215	182	B15	CO2	61	1.3	0.98	0.282567	200	501.8	373	2.862	0.987	1.875	7.216875	164	2.44	40.66748	0.327	15	4.69E+10	1.73E-12	0.0185	0.0810432	0.0001538	0.008313	0.00068096
216	183	B15	CO2	61	1.3	0.98	0.282567	200	501.8	373	3.158	0.987	2.171	8.998795	147	2.51	41.83417	0.327	15	4.69E+10	1.78E-12	0.0185	0.0833682	0.0001269	0.0068582	0.00061851
217	184	B15	CO2	61	1.3	0.98	0.282567	200	501.8	373	3.454	0.987	2.467	10.955947	126	2.58	43.00086	0.327	15	4.69E+10	1.83E-12	0.0185	0.0856932	0.0001071	0.0057902	0.00056831
218	185	B15	CO2	61	1.3	0.98	0.282567	200	501.8	473	1.382	0.987	0.395	0.935755	188	1.54	25.66718	0.327	15	4.69E+10	1.09E-12	0.023	0.0511502	0.0009307	0.0404649	0.00167517
219	186	B15	CO2	61	1.3	0.98	0.282567	200	501.8	473	1.678	0.987	0.691	1.841515	186	1.88	31.33396	0.327	15	4.69E+10	1.33E-12	0.023	0.0624431	0.0005773	0.0251017	0.00131938
220	187	B15	CO2	61	1.3	0.98	0.282567	200	501.8	473	1.974	0.987	0.987	2.922507	182	2.1	35.0007	0.327	15	4.69E+10	1.49E-12	0.023	0.0697503	0.0004064	0.0176678	0.00110691
221	188	B15	CO2	61	1.3	0.98	0.282567	200	501.8	473	2.27	0.987	1.283	4.178731	148	2.25	37.50075	0.327	15	4.69E+10	1.59E-12	0.023	0.0747325	0.0003045	0.0132391	0.00095818
222	189	B15	CO2	61	1.3	0.98	0.282567	200	501.8	473	2.566	0.987	1.579	5.610187	134	2.37	39.50079	0.327	15	4.69E+10	1.68E-12	0.023	0.0787182	0.0002389	0.010387	0.00084872
223	190	B15	CO2	61	1.3	0.98	0.282567	200	501.8	473	2.862	0.987	1.875	7.216875	163	2.49	41.50083	0.327	15	4.69E+10	1.76E-12	0.023	0.0827039	0.0001951	0.0084834	0.00076702
224	191	B15	CO2	61	1.3	0.98	0.282567	200	501.8	473	3.158	0.987	2.171	8.998795	111	2.55	42.50085	0.327	15	4.69E+10	1.81E-12	0.023	0.0846968	0.0001603	0.0069675	0.00069512
225	192	B15	CO2	61	1.3	0.98	0.282567	200	501.8	473	3.454	0.987	2.467	10.955947	176	2.63	43.83421	0.327	15	4.69E+10	1.86E-12	0.023	0.0873539	0.0001358	0.0059023	0.00063978
226	257	S200	CO2	38.8	0.525	0.39	0.2972515	20	112.2	293	1.382	0.987	0.395	0.935755	127	1.33	22.16711	0.359	200	1.48E+12	1.33E-13	0.0147	0.1975678	0.0008496	0.0577976	0.00152755
227	258	S200	CO2	38.8	0.525	0.39	0.2972515	20	112.2	293	1.678	0.987	0.691	1.841515	174	1.6	26.6672	0.359	200	1.48E+12	1.60E-13	0.0147	0.2376756	0.0005194	0.0353317	0.00119433
228	259	S200	CO2	38.8	0.525	0.39	0.2972515	20	112.2	293	1.974	0.987	0.987	2.922507	184	1.8	30.0006	0.359	200	1.48E+12	1.80E-13	0.0147	0.267385	0.0003682	0.0250459	0.00100556
229	260	S200	CO2	38.8	0.525	0.39	0.2972515	20	112.2	293	2.27	0.987	1.283	4.178731	136	1.97	32.83399	0.359	200	1.48E+12	1.98E-13	0.0147	0.2926381	0.0002818	0.0191709	0.00087976
230	261	S200	CO2	38.8	0.525	0.39	0.2972515	20	112.2	293	2.566	0.987	1.579	5.610187	182	2.08	34.66736	0.359	200	1.48E+12	2.09E-13	0.0147	0.3089783	0.0002216	0.0150767	0.00078018
231	262	S200	CO2	38.8	0.525	0.39	0.2972515	20	112.2	293	2.862	0.987	1.875	7.216875	156	2.19	36.50073	0.359	200	1.48E+12	2.20E-13	0.0147	0.3253184	0.0001814	0.01234	0.00070583
232	263	S200	CO2	38.8	0.525	0.39	0.2972515	20	112.2	293	3.158	0.987	2.171	8.998795	130	2.27	37.83409	0.359	200	1.48E+12	2.28E-13	0.0147	0.3372022	0.0001508	0.010258	0.00064353
233	264	S200	CO2	38.8	0.525	0.39	0.2972515	20	112.2	293	3.454	0.987	2.467	10.955947	121	2.34	39.00078	0.359	200	1.48E+12	2.35E-13	0.0147	0.3476005	0.0001277	0.0086853	0.00059215
234	265	S200	CO2	38.8	0.525	0.39	0.2972515	20	112.2	323	1.382	0.987	0.395	0.935755	111	1.31	21.83377	0.359	200	1.48E+12	1.31E-13	0.0161	0.1945969	0.0009165	0.0569284	0.00158657
235	266	S200	CO2	38.8	0.525	0.39	0.2972515	20	112.2	323	1.678	0.987	0.691	1.841515	120	1.61	26.83387	0.359	200	1.48E+12	1.61E-13	0.0161	0.2391611	0.0005724	0.0355525	0.00125381
236	267	S200	CO2	38.8	0.525	0.39	0.2972515	20	112.2	323	1.974	0.987	0.987	2.922507	180	1.83	30.50061	0.359	200	1.48E+12	1.83E-13	0.0161	0.2718414	0.00041	0.0254634	0.00106109
237	268	S200	CO2	38.8	0.525	0.39	0.2972515	20	112.2	323	2.27	0.987	1.283	4.178731	136	1.99	33.16733	0.359	200	1.48E+12	2.00E-13	0.0161	0.295609	0.0003118	0.0193655	0.00092536
238	269	S200	CO2	38.8	0.525	0.39	0.2972515	20	112.2	323	2.566	0.987	1.579	5.610187	119	2.12	35.33404	0.359	200	1.48E+12	2.13E-13	0.0161	0.3149201	0.0002474	0.0153666	0.0008243
239	270	S200	CO2	38.8	0.525	0.39	0.2972515	20	112.2	323	2.862	0.987	1.875	7.216875	144	2.23	37.16741	0.359	200	1.48E+12	2.24E-13	0.0161	0.3312603	0.0002023	0.0125654	0.00074539
240	271	S200	CO2	38.8	0.525	0.39	0.2972515	20	112.2	323	3.158	0.987	2.171	8.998795	110	2.31	38.50077	0.359	200	1.48E+12	2.32E-13	0.0161	0.3431441	0.0001681	0.0104388	0.00067939
241	272	S200	CO2	38.8	0.525	0.39	0.2972515	20	112.2	323	3.454	0.987	2.467	10.955947	129	2.38	39.66746	0.359	200	1.48E+12	2.39E-13	0.0161	0.3535424	0.0001422	0.0088338	0.00062498

1	s/n	Core Pore Size (nm)	Gas	Core height (cm)	External Radius (cm)	Internal Radius (cm)	Ln(r1/r2) (cm)	Core Volume (cm3)	Core Cross-Sectional Area (cm2)	Temperature (K)	Inlet Pressure (atm)	Outlet Pressure (atm)	Pressure Drop (atm)	P1^2 - P2^2 (atm)	Data Frequency	Flowrate (LPM))	Flowrate (cm3/sec)	Porosity (%)	Pore Size (nm)	Aspect Ratio	Aspect Quality Index	Viscosity (cp)	Flux (cm/s)	Permeability (mD)	Mobility (mD/cp)	Sample Quality Index (mD)
290	449	B6000	CO2	32.8	1.29	1.035	0.2202408	140	267.8	293	1.382	0.987	0.395	0.935755	166	1.05	17.50035	0.29	6000	2.35E+13	2.78E-15	0.0147	0.0653486	0.0005879	0.0399925	0.00141377
291	450	B6000	CO2	32.8	1.29	1.035	0.2202408	140	267.8	293	1.678	0.987	0.691	1.841515	176	1.25	20.83375	0.29	6000	2.35E+13	3.31E-15	0.0147	0.0777959	0.0003556	0.0241928	0.00109959
292	451	B6000	CO2	32.8	1.29	1.035	0.2202408	140	267.8	293	1.974	0.987	0.987	2.922507	166	1.35	22.50045	0.29	6000	2.35E+13	3.57E-15	0.0147	0.0840196	0.000242	0.0164638	0.0009071
293	452	B6000	CO2	32.8	1.29	1.035	0.2202408	140	267.8	293	2.27	0.987	1.283	4.178731	125	1.46	24.33382	0.29	6000	2.35E+13	3.86E-15	0.0147	0.0908656	0.0001831	0.0124526	0.00078889
294	453	B6000	CO2	32.8	1.29	1.035	0.2202408	140	267.8	293	2.566	0.987	1.579	5.610187	138	1.53	25.50051	0.29	6000	2.35E+13	4.05E-15	0.0147	0.0952222	0.0001429	0.00972	0.00069698
295	454	B6000	CO2	32.8	1.29	1.035	0.2202408	140	267.8	293	2.862	0.987	1.875	7.216875	187	1.55	25.83385	0.29	6000	2.35E+13	4.10E-15	0.0147	0.096467	0.0001125	0.0076548	0.00061852
296	455	B6000	CO2	32.8	1.29	1.035	0.2202408	140	267.8	293	3.158	0.987	2.171	8.998795	142	1.63	27.16721	0.29	6000	2.35E+13	4.31E-15	0.0147	0.1014459	9.49013E-05	0.0064559	0.00056802
297	456	B6000	CO2	32.8	1.29	1.035	0.2202408	140	267.8	293	3.454	0.987	2.467	10.955947	146	1.66	27.66722	0.29	6000	2.35E+13	4.39E-15	0.0147	0.103313	7.93829E-05	0.0054002	0.00051951
298	457	B6000	CO2	32.8	1.29	1.035	0.2202408	140	267.8	323	1.382	0.987	0.395	0.935755	154	1.06	17.66702	0.29	6000	2.35E+13	2.80E-15	0.0161	0.0659709	0.00065	0.0403734	0.00148659
299	458	B6000	CO2	32.8	1.29	1.035	0.2202408	140	267.8	323	1.678	0.987	0.691	1.841515	112	1.24	20.66708	0.29	6000	2.35E+13	3.28E-15	0.0161	0.0771736	0.0003864	0.0239993	0.00114615
300	459	B6000	CO2	32.8	1.29	1.035	0.2202408	140	267.8	323	1.974	0.987	0.987	2.922507	116	1.36	22.66712	0.29	6000	2.35E+13	3.60E-15	0.0161	0.084642	0.000267	0.0165858	0.00095282
301	460	B6000	CO2	32.8	1.29	1.035	0.2202408	140	267.8	323	2.27	0.987	1.283	4.178731	169	1.47	24.50049	0.29	6000	2.35E+13	3.89E-15	0.0161	0.091488	0.0002019	0.0125379	0.00082843
302	461	B6000	CO2	32.8	1.29	1.035	0.2202408	140	267.8	323	2.566	0.987	1.579	5.610187	160	1.54	25.66718	0.29	6000	2.35E+13	4.07E-15	0.0161	0.0958446	0.0001575	0.0097835	0.0007318
303	462	B6000	CO2	32.8	1.29	1.035	0.2202408	140	267.8	323	2.862	0.987	1.875	7.216875	143	1.59	26.50053	0.29	6000	2.35E+13	4.21E-15	0.0161	0.0989564	0.0001264	0.0078524	0.00065561
304	463	B6000	CO2	32.8	1.29	1.035	0.2202408	140	267.8	323	3.158	0.987	2.171	8.998795	152	1.64	27.33388	0.29	6000	2.35E+13	4.34E-15	0.0161	0.1020683	0.0001046	0.0064955	0.00059628
305	464	B6000	CO2	32.8	1.29	1.035	0.2202408	140	267.8	323	3.454	0.987	2.467	10.955947	189	1.68	28.00056	0.29	6000	2.35E+13	4.44E-15	0.0161	0.1045577	8.79907E-05	0.0054653	0.00054695
306	465	B6000	CO2	32.8	1.29	1.035	0.2202408	140	267.8	373	1.382	0.987	0.395	0.935755	146	1.02	17.00034	0.29	6000	2.35E+13	2.70E-15	0.0185	0.0634815	0.0007187	0.0388499	0.00156319
307	466	B6000	CO2	32.8	1.29	1.035	0.2202408	140	267.8	373	1.678	0.987	0.691	1.841515	123	1.23	20.50041	0.29	6000	2.35E+13	3.25E-15	0.0185	0.0765512	0.0004404	0.0238057	0.00122365
308	467	B6000	CO2	32.8	1.29	1.035	0.2202408	140	267.8	373	1.974	0.987	0.987	2.922507	179	1.35	22.50045	0.29	6000	2.35E+13	3.57E-15	0.0185	0.0840196	0.0003046	0.0164638	0.00101761
309	468	B6000	CO2	32.8	1.29	1.035	0.2202408	140	267.8	373	2.27	0.987	1.283	4.178731	116	1.44	24.00048	0.29	6000	2.35E+13	3.81E-15	0.0185	0.0896209	0.0002272	0.012282	0.00087892
310	469	B6000	CO2	32.8	1.29	1.035	0.2202408	140	267.8	373	2.566	0.987	1.579	5.610187	167	1.52	25.33384	0.29	6000	2.35E+13	4.02E-15	0.0185	0.0945999	0.0001786	0.0096565	0.00077934
311	470	B6000	CO2	32.8	1.29	1.035	0.2202408	140	267.8	373	2.862	0.987	1.875	7.216875	158	1.58	26.33386	0.29	6000	2.35E+13	4.18E-15	0.0185	0.0983341	0.0001444	0.007803	0.00070056
312	471	B6000	CO2	32.8	1.29	1.035	0.2202408	140	267.8	373	3.158	0.987	2.171	8.998795	186	1.62	27.00054	0.29	6000	2.35E+13	4.28E-15	0.0185	0.1008235	0.0001187	0.0064163	0.00063527
313	472	B6000	CO2	32.8	1.29	1.035	0.2202408	140	267.8	373	3.454	0.987	2.467	10.955947	186	1.66	27.66722	0.29	6000	2.35E+13	4.39E-15	0.0185	0.103313	9.99037E-05	0.0054002	0.0005828
314	473	B6000	CO2	32.8	1.29	1.035	0.2202408	140	267.8	473	1.382	0.987	0.395	0.935755	143	1.03	17.16701	0.29	6000	2.35E+13	2.72E-15	0.023	0.0641038	0.0009023	0.0392308	0.00175149
315	474	B6000	CO2	32.8	1.29	1.035	0.2202408	140	267.8	473	1.678	0.987	0.691	1.841515	182	1.23	20.50041	0.29	6000	2.35E+13	3.25E-15	0.023	0.0765512	0.0005475	0.0238057	0.00136438
316	475	B6000	CO2	32.8	1.29	1.035	0.2202408	140	267.8	473	1.974	0.987	0.987	2.922507	132	1.37	22.83379	0.29	6000	2.35E+13	3.62E-15	0.023	0.0852643	0.0003843	0.0167077	0.00114302
317	476	B6000	CO2	32.8	1.29	1.035	0.2202408	140	267.8	473	2.27	0.987	1.283	4.178731	155	1.46	24.33382	0.29	6000	2.35E+13	3.86E-15	0.023	0.0908656	0.0002864	0.0124526	0.00098679
318	477	B6000	CO2	32.8	1.29	1.035	0.2202408	140	267.8	473	2.566	0.987	1.579	5.610187	149	1.54	25.66718	0.29	6000	2.35E+13	4.07E-15	0.023	0.0958446	0.000225	0.0097835	0.00087467
319	478	B6000	CO2	32.8	1.29	1.035	0.2202408	140	267.8	473	2.862	0.987	1.875	7.216875	163	1.6	26.6672	0.29	6000	2.35E+13	4.23E-15	0.023	0.0995788	0.0001817	0.0079017	0.00078606
320	479	B6000	CO2	32.8	1.29	1.035	0.2202408	140	267.8	473	3.158	0.987	2.171	8.998795	127	1.65	27.50055	0.29	6000	2.35E+13	4.36E-15	0.023	0.1026906	0.0001503	0.0065351	0.00071486
321	480	B6000	CO2	32.8	1.29	1.035	0.2202408	140	267.8	473	3.454	0.987	2.467	10.955947	179	1.69	28.16723	0.29	6000	2.35E+13	4.47E-15	0.023	0.1051801	0.0001264	0.0054978	0.00065567

1	s/n	Core Pore Size (nm)	Gas	Core height (cm)	External Radius (cm)	Internal Radius (cm)	Ln(r1/r2) (cm)	Core Volume (cm3)	Core Cross-Sectional Area (cm2)	Temperature (K)	Inlet Pressure (atm)	Outlet Pressure (atm)	Pressure Drop (atm)	P1^2 - P2^2 (atm)	Data Frequency	Flowrate (LPM))	Flowrate (cm3/sec)	Porosity (%)	Pore Size (nm)	Aspect Ratio	Aspect Quality Index	Viscosity (cp)	Flux (cm/s)	Permeability (mD)	Mobility (mD/cp)	Sample Quality Index (mD)
242	273	S200	CO2	38.8	0.525	0.39	0.2972515	20	112.2	373	1.382	0.987	0.395	0.935755	134	1.32	22.00044	0.359	200	1.48E+12	1.32E-13	0.0185	0.1960824	0.0010612	0.057363	0.0017072
243	274	S200	CO2	38.8	0.525	0.39	0.2972515	20	112.2	373	1.678	0.987	0.691	1.841515	128	1.62	27.00054	0.359	200	1.48E+12	1.62E-13	0.0185	0.2406465	0.0006618	0.0357734	0.00134818
244	275	S200	CO2	38.8	0.525	0.39	0.2972515	20	112.2	373	1.974	0.987	0.987	2.922507	161	1.84	30.66728	0.359	200	1.48E+12	1.84E-13	0.0185	0.2733269	0.0004736	0.0256025	0.00114054
245	276	S200	CO2	38.8	0.525	0.39	0.2972515	20	112.2	373	2.27	0.987	1.283	4.178731	121	2	33.334	0.359	200	1.48E+12	2.01E-13	0.0185	0.2970945	0.0003601	0.0194628	0.00099442
246	277	S200	CO2	38.8	0.525	0.39	0.2972515	20	112.2	373	2.566	0.987	1.579	5.610187	130	2.12	35.33404	0.359	200	1.48E+12	2.13E-13	0.0185	0.3149201	0.0002843	0.0153666	0.0008836
247	278	S200	CO2	38.8	0.525	0.39	0.2972515	20	112.2	373	2.862	0.987	1.875	7.216875	140	2.22	37.00074	0.359	200	1.48E+12	2.23E-13	0.0185	0.3297749	0.0002314	0.012509	0.00079722
248	279	S200	CO2	38.8	0.525	0.39	0.2972515	20	112.2	373	3.158	0.987	2.171	8.998795	114	2.31	38.50077	0.359	200	1.48E+12	2.32E-13	0.0185	0.3431441	0.0001931	0.0104388	0.00072827
249	280	S200	CO2	38.8	0.525	0.39	0.2972515	20	112.2	373	3.454	0.987	2.467	10.955947	151	2.39	39.83413	0.359	200	1.48E+12	2.40E-13	0.0185	0.3550279	0.0001641	0.0088709	0.00067136
250	281	S200	CO2	38.8	0.525	0.39	0.2972515	20	112.2	473	1.382	0.987	0.395	0.935755	142	1.31	21.83377	0.359	200	1.48E+12	1.31E-13	0.023	0.1945969	0.0013094	0.0569284	0.00189632
251	282	S200	CO2	38.8	0.525	0.39	0.2972515	20	112.2	473	1.678	0.987	0.691	1.841515	181	1.62	27.00054	0.359	200	1.48E+12	1.62E-13	0.023	0.2406465	0.0008228	0.0357734	0.00150323
252	283	S200	CO2	38.8	0.525	0.39	0.2972515	20	112.2	473	1.974	0.987	0.987	2.922507	119	1.84	30.66728	0.359	200	1.48E+12	1.84E-13	0.023	0.2733269	0.0005889	0.0256025	0.00127171
253	284	S200	CO2	38.8	0.525	0.39	0.2972515	20	112.2	473	2.27	0.987	1.283	4.178731	153	2.01	33.50067	0.359	200	1.48E+12	2.02E-13	0.023	0.2985799	0.0004499	0.0195601	0.00111156
254	285	S200	CO2	38.8	0.525	0.39	0.2972515	20	112.2	473	2.566	0.987	1.579	5.610187	140	2.13	35.50071	0.359	200	1.48E+12	2.14E-13	0.023	0.3164056	0.0003551	0.0154391	0.00098755
255	286	S200	CO2	38.8	0.525	0.39	0.2972515	20	112.2	473	2.862	0.987	1.875	7.216875	113	2.25	37.50075	0.359	200	1.48E+12	2.26E-13	0.023	0.3342313	0.0002916	0.0126781	0.0008949
256	287	S200	CO2	38.8	0.525	0.39	0.2972515	20	112.2	473	3.158	0.987	2.171	8.998795	155	2.35	39.16745	0.359	200	1.48E+12	2.36E-13	0.023	0.349086	0.0002442	0.0106195	0.00081903
257	288	S200	CO2	38.8	0.525	0.39	0.2972515	20	112.2	473	3.454	0.987	2.467	10.955947	122	2.43	40.50081	0.359	200	1.48E+12	2.44E-13	0.023	0.3609698	0.0002074	0.0090194	0.00075481
258	353	S6000	CO2	32.8	0.52	0.384	0.3031863	20	107.1	293	1.382	0.987	0.395	0.935755	123	1.36	22.66712	0.355	6000	4.41E+13	4.80E-15	0.0147	0.2116444	0.0010482	0.0713083	0.00170626
259	354	S6000	CO2	32.8	0.52	0.384	0.3031863	20	107.1	293	1.678	0.987	0.691	1.841515	156	1.63	27.16721	0.355	6000	4.41E+13	5.75E-15	0.0147	0.2536621	0.0006384	0.0434286	0.00133156
260	355	S6000	CO2	32.8	0.52	0.384	0.3031863	20	107.1	293	1.974	0.987	0.987	2.922507	146	1.83	30.50061	0.355	6000	4.41E+13	6.46E-15	0.0147	0.2847863	0.0004516	0.0307227	0.00111996
261	356	S6000	CO2	32.8	0.52	0.384	0.3031863	20	107.1	293	2.27	0.987	1.283	4.178731	111	2.01	33.50067	0.355	6000	4.41E+13	7.09E-15	0.0147	0.312798	0.0003469	0.0236001	0.00098159
262	357	S6000	CO2	32.8	0.52	0.384	0.3031863	20	107.1	293	2.566	0.987	1.579	5.610187	165	2.13	35.50071	0.355	6000	4.41E+13	7.51E-15	0.0147	0.3314725	0.0002738	0.018628	0.00087208
263	358	S6000	CO2	32.8	0.52	0.384	0.3031863	20	107.1	293	2.862	0.987	1.875	7.216875	144	2.23	37.16741	0.355	6000	4.41E+13	7.87E-15	0.0147	0.3470346	0.0002229	0.0151607	0.00078674
264	359	S6000	CO2	32.8	0.52	0.384	0.3031863	20	107.1	293	3.158	0.987	2.171	8.998795	154	2.3	38.3341	0.355	6000	4.41E+13	8.11E-15	0.0147	0.3579281	0.0001843	0.0125403	0.00071553
265	360	S6000	CO2	32.8	0.52	0.384	0.3031863	20	107.1	293	3.454	0.987	2.467	10.955947	161	2.37	39.50079	0.355	6000	4.41E+13	8.36E-15	0.0147	0.3688216	0.000156	0.0106136	0.00065827
266	361	S6000	CO2	32.8	0.52	0.384	0.3031863	20	107.1	323	1.382	0.987	0.395	0.935755	141	1.38	23.00046	0.355	6000	4.41E+13	4.87E-15	0.0161	0.2147569	0.0011649	0.072357	0.00179874
267	362	S6000	CO2	32.8	0.52	0.384	0.3031863	20	107.1	323	1.678	0.987	0.691	1.841515	171	1.66	27.66722	0.355	6000	4.41E+13	5.86E-15	0.0161	0.2583307	0.0007121	0.0442279	0.0014063
268	363	S6000	CO2	32.8	0.52	0.384	0.3031863	20	107.1	323	1.974	0.987	0.987	2.922507	161	1.87	31.16729	0.355	6000	4.41E+13	6.60E-15	0.0161	0.2910111	0.0005054	0.0313942	0.00118482
269	364	S6000	CO2	32.8	0.52	0.384	0.3031863	20	107.1	323	2.27	0.987	1.283	4.178731	164	2.03	33.83401	0.355	6000	4.41E+13	7.16E-15	0.0161	0.3159105	0.0003837	0.023835	0.00103237
270	365	S6000	CO2	32.8	0.52	0.384	0.3031863	20	107.1	323	2.566	0.987	1.579	5.610187	126	2.15	35.83405	0.355	6000	4.41E+13	7.58E-15	0.0161	0.334585	0.0003027	0.0188029	0.00091694
271	366	S6000	CO2	32.8	0.52	0.384	0.3031863	20	107.1	323	2.862	0.987	1.875	7.216875	130	2.24	37.33408	0.355	6000	4.41E+13	7.90E-15	0.0161	0.3485909	0.0002452	0.0152287	0.0008252
272	367	S6000	CO2	32.8	0.52	0.384	0.3031863	20	107.1	323	3.158	0.987	2.171	8.998795	111	2.34	39.00078	0.355	6000	4.41E+13	8.25E-15	0.0161	0.3641529	0.0002054	0.0127584	0.00075531
273	368	S6000	CO2	32.8	0.52	0.384	0.3031863	20	107.1	323	3.454	0.987	2.467	10.955947	123	2.4	40.0008	0.355	6000	4.41E+13	8.47E-15	0.0161	0.3734902	0.000173	0.010748	0.00069325
274	369	S6000	CO2	32.8	0.52	0.384	0.3031863	20	107.1	373	1.382	0.987	0.395	0.935755	127	1.38	23.00046	0.355	6000	4.41E+13	4.87E-15	0.0185	0.2147569	0.0013386	0.072357	0.00192815
275	370	S6000	CO2	32.8	0.52	0.384	0.3031863	20	107.1	373	1.678	0.987	0.691	1.841515	121	1.66	27.66722	0.355	6000	4.41E+13	5.86E-15	0.0185	0.2583307	0.0008182	0.0442279	0.00150747
276	371	S6000	CO2	32.8	0.52	0.384	0.3031863	20	107.1	373	1.974	0.987	0.987	2.922507	111	1.89	31.50063	0.355	6000	4.41E+13	6.67E-15	0.0185	0.2941235	0.000587	0.0317299	0.00127684
277	372	S6000	CO2	32.8	0.52	0.384	0.3031863	20	107.1	373	2.27	0.987	1.283	4.178731	124	2.04	34.00068	0.355	6000	4.41E+13	7.20E-15	0.0185	0.3174667	0.0004431	0.0239524	0.00110937
278	373	S6000	CO2	32.8	0.52	0.384	0.3031863	20	107.1	373	2.566	0.987	1.579	5.610187	115	2.17	36.16739	0.355	6000	4.41E+13	7.65E-15	0.0185	0.3376974	0.0003511	0.0189778	0.00098747
279	374	S6000	CO2	32.8	0.52	0.384	0.3031863	20	107.1	373	2.862	0.987	1.875	7.216875	143	2.27	37.83409	0.355	6000	4.41E+13	8.01E-15	0.0185	0.3532595	0.0002855	0.0154326	0.00089047
280	375	S6000	CO2	32.8	0.52	0.384	0.3031863	20	107.1	373	3.158	0.987	2.171	8.998795	134	2.36	39.33412	0.355	6000	4.41E+13	8.32E-15	0.0185	0.3672654	0.000238	0.0128674	0.00081311
281	376	S6000	CO2	32.8	0.52	0.384	0.3031863	20	107.1	373	3.454	0.987	2.467	10.955947	182	2.43	40.50081	0.355	6000	4.41E+13	8.57E-15	0.0185	0.3781588	0.0002013	0.0108823	0.00074776
282	377	S6000	CO2	32.8	0.52	0.384	0.3031863	20	107.1	473	1.382	0.987	0.395	0.935755	190	1.38	23.00046	0.355	6000	4.41E+13	4.87E-15	0.023	0.2147569	0.0016642	0.072357	0.00214991
283	378	S6000	CO2	32.8	0.52	0.384	0.3031863	20	107.1	473	1.678	0.987	0.691	1.841515	152	1.67	27.83389	0.355	6000	4.41E+13	5.89E-15	0.023	0.2598869	0.0010234	0.0444943	0.0016859
284	379	S6000	CO2	32.8	0.52	0.384	0.3031863	20	107.1	473	1.974	0.987	0.987	2.922507	131	1.9	31.6673	0.355	6000	4.41E+13	6.70E-15	0.023	0.2956797	0.0007337	0.0318979	0.00142745
285	380	S6000	CO2	32.8	0.52	0.384	0.3031863	20	107.1	473	2.27	0.987	1.283	4.178731	147	2.06	34.33402	0.355	6000	4.41E+13	7.27E-15	0.023	0.3205791	0.0005563	0.0241872	0.001243
286	381	S6000	CO2	32.8	0.52	0.384	0.3031863	20	107.1	473	2.566	0.987	1.579	5.610187	127	2.2	36.6674	0.355	6000	4.41E+13	7.76E-15	0.023	0.342366	0.0004425	0.0192402	0.00110862
287	382	S6000	CO2	32.8	0.52	0.384	0.3031863	20	107.1	473	2.862	0.987	1.875	7.216875	121	2.33	38.83411	0.355	6000	4.41E+13	8.22E-15	0.023	0.3625967	0.0003643	0.0158406	0.00100592
288	383	S6000	CO2	32.8	0.52	0.384	0.3031863	20	107.1	473	3.158	0.987	2.171	8.998795	146	2.41	40.16747	0.355	6000	4.41E+13	8.50E-15	0.023	0.3750464	0.0003022	0.01314	0.00091617
289	384	S6000	CO2	32.8	0.52	0.384	0.3031863	20	107.1	473	3.454	0.987	2.467	10.955947	188	2.5	41.6675	0.355	6000	4.41E+13	8.82E-15	0.023	0.3890523	0.0002575	0.0111957	0.00084568

APPENDIX C: Field Database

1			Formation	Depth, ft	Temperature, K		Area, acres	Radial Thickness, ft	Porosity, %	Viscosity, cp	Permeability, mD	Mobility, mD/cp	Darcy Velocity, ft/s		
2	Column9	Column11	Formation	Depth, ft2	Temperature, K	Frequency	Area, acres	Radia Thickness	AVG Porosity %2	Avg Oil, Viscosity cp2	AVG Permeability, md2	Intrinsic Mobility (Perm/viscosity(mD/u))	Flux (ft/s)	Flux (cm/s)	Reservoir Quality Index (mD)
3	CHINA	CH4	s	11273.52	366	61	6175	2.00E+06	7.8	1.75	110	63.03			0.117917616
4	NORTH SE/	CH4	SS	1500	329	56			13	1	500	500	33497.72286	1021011	0.194734533
5	NORTH SE/	CH4	SS	2600	373	27			16.4	0.5	2500	5000			0.387683867
6	NORTH SE/	CH4	SS	800	301	20			18	1.4	15	10.71			0.028664147
7	NORTH SE/	CH4	SS	610	310	61			21.7	3.2	22	6.72			0.031616306
8	NORTH SE/	CH4	SS	2300	363	70			24	0.65	1950	3000			0.283035775
9	CHINA	CH4	s		373	64			15.1	8.5	68	8.01			0.066633961
10	CHINA	CH4	s			20				10200					
11	CHINA	CH4	s	11483.5	373	13			21.3	1000	346	0.35			0.126554588
12	CHINA	CH4	s	11483.5	373	84			21.3	1000	346	0.35			0.126554588
13	CHINA	CH4	s	11483.5	389	38			21.3	1000	346	0.35			0.126554588
14	CHINA	CH4	s	7867.84	349	54			16.8	2.58	63	24.42			0.060805839
15	NORTH SE/	CH4	SS	3900	413	57			14	0.16	300	1875	125982.6895	3839952	0.145353756
16	NORTH SE/	CH4	SS	3200	381	21			17	0.5	400	795.63	54410.70914	1658438	0.152212373
17	NORTH SE/	CH4	SS	3110	386	84			17.5	0.3	1003	3341.67	223227.5305	6803975	0.237717465
18	NORTH SE/	CH4	SS	2575	372	81			21	0.29	750	2586.21	174788.4012	5327550	0.187650892
19	US	CH4	S	7000	350	26	20000	3.00E+06	22	4	40	10	750.6981539	22881	0.042339751
20	NORTH SE/	CH4	SS	2744	376	44			25	0.25	2000	8000	557013.4943	16977771	0.280850138
21	NORTH SE/	CH4	LS	3030	404	25			30	0.17	50	294.12	20233.91863	616730	0.040537226
22	BRAZIL	CH4		2650	321	30	10	8.00E+04		20	35	1.75	127.2279442	3878	#DIV/0!
23	CANADA	CH4	Dolo.	4040	361	90	221	4.00E+05	4.25	0.55	160	292.5	19885.50761	606110	0.192661605
24	CANADA	CH4	Dolo.	6200	357	33	490	5.00E+05	6	0.3	40	133.33	8958.769028	273063	0.081074451
25	CANADA	CH4	Dolo.	6000	355	17	1920	1.00E+06	6	0.25	1000	4000	256784.7724	7826800	0.405372257
26	CANADA	CH4	Dolo.	4160	360	15	102	2.00E+05	7.3	0.59	180	305.08	20863.84348	635930	0.155920949
27	CANADA	CH4	LS	6330	364	42	240	4.00E+05	8	0.4	50	125	8207.419275	250162	0.0785
28	CANADA	CH4	Dolo.	6000	360	21	2500	1.00E+06	8	0.83	300	361.45	24572.378	748966	0.192284945
29	CANADA	CH4	Dolo.	9541		26	328	4.00E+05	8	0.33	900	2727.27	179890.9819	5483077	0.333047294
30	CANADA	CH4	LS	8300	380	72	19440	3.00E+06	8.5	0.4	54	135	9018.169562	274874	0.07914383
31	CANADA	CH4	Dolo., LS	5500	361	67	320	4.00E+05	8.5	0.46	2550	5543.48	374655.1382	11419489	0.543863954
32	CANADA	CH4	Dolo.	4330	360	59	222	4.00E+05	8.6	0.69	320	463.77	31160.93575	949785	0.191538204
33	CANADA	CH4	Dolo., LS	5500	357	56	800	7.00E+05	8.6	0.47	2550	5425.53	366683.7523	11176521	0.540692708
34	CANADA	CH4	Dolo.	9333	365	17	192	3.00E+05	9	0.14	540	3857.14	257512.7048	7848987	0.243223354
35	CANADA	CH4	LS	6400	364	22	478	5.00E+05	9.1	0.39	50	128.21	8466.105843	258047	0.073602735
36	CANADA	CH4	Dolo.	9421	364	57	301	4.00E+05	9.8	0.42	1970	4690.48	312785.7257	9533709	0.445194431
37	CANADA	CH4	Dolo.	9531	366	41	420	5.00E+05	10.3	0.36	2400	6666.67	434264.8073	13236391	0.479310184
38	CANADA	CH4	Dolo.	9415	366	83	625	6.00E+05	10.5	0.42	1060	2523.81	168691.4383	5141715	0.315491695
39	CANADA	CH4	Dolo.	6500	348	87	2725	1.00E+06	10.5	0.54	1375	2546.3	173106.3357	5276281	0.359324101
40	NORTH SE/	CH4	SS			13			11	0.3	130	433.33	29990.35368	914106	0.107945609

			Formation	Depth, ft	Temperature, K		Area, acres	Radial Thickness, ft	Porosity, %	Viscosity, cp	Permeability, mD	Mobility, mD/cp	Darcy Velocity, ft/s		
1	CANADA	CH4	Dolo.	9332	361	85	346	5.00E+05	11.8	0.32	3100	9687.5	638257.0693	19454075	0.508943405
2	CANADA	CH4	Dolo.	9469	365	31	126	3.00E+05	12.7	0.37	2020	5459.46	359283.4621	10950960	0.396007556
3	CANADA	CH4	LS	9150	383	38	2847	1.00E+06	13	0.3	136	453.33	30283.23606	923033	0.101561107
4	VENEZUELA	CH4	S	13750	416	50	12000	3.00E+06	13	0.3	505	1683.33	121996.319	3718448	0.195705784
5	VENEZUELA	CH4	S	13750	416	10	9500	2.00E+06	15	0.3	505	1683.33	120107.8311	3660887	0.18219217
6	VENEZUELA	CH4	S	13650	416	59	36769	5.00E+06	15	0.5	600	1200	87795.93648	2676020	0.198591037
7	US	CH4	S	7000	344	38	40000	5.00E+06	19	0.45	20	44.44	2986.256343	91021	0.03221572
8	US	CH4	S	8800	386	51	4000	2.00E+06	19	1	130	130	9511.226452	289902	0.082134293
9	NORTH SE/	CH4	SS	2770	386	73			19	0.41	500	1218.78	82857.30065	2525491	0.161078601
0	US	CH4	S	6700	339	65	10000	2.00E+06	20	2	50	25	1852.60718	56467	0.049647759
1	US	CH4	S	6600	344	56	9000	2.00E+06	20	2	100	50	3646.587551	111148	0.070212534
2	NORTH SE/	CH4	SS	2804	370	32			20.5	1.1	111	100.91	6860.161167	209098	0.073065811
3	US	CH4	S	5200	334	67	2400	1.00E+06	21	0.6	20	33.33	2279.568084	69481	0.030643262
4	US	CH4	S	8800	372	41	55000	6.00E+06	22	0.9	400	444.44	32311.85885	984865	0.13389005
5	US	CH4	S	8800	356	51	6240	2.00E+06	23	0.9	200	222.22	16155.92943	492433	0.092593548
6	US	CH4	S	6000	344	81	70000	7.00E+06	24	2	275	137.5	10189.33949	310571	0.106289502
7	NORTH SE/	CH4	SS	2080	361	10			25	0.56	101	179.46	12346.30357	376315	0.063113219
8	US	CH4	S	4900	311	49	5000	2.00E+06	25	73.5	150	2.04	155.7401901	4747	0.076913978
9	US	CH4	S	4500	302	80	11000	3.00E+06	25	73.5	150	2.04	156.2575993	4763	0.076913978
0	US	CH4	S	11000	347	47	20	1.00E+05	26	1	1000	1000	67983.57913	2072139	0.194734533
1	US	CH4	S	10000	355	48	204	4.00E+05	26	0.5	1250	2500	169958.9478	5180349	0.217719827
2	NORTH SE/	CH4		2360	365	13			28	0.31	2300	7419.35	495622.222		0.284586668
3	NORTH SE/	CH4	SS	1740	347	15			31	1.12	265	236.61		0	0.091806142
4	NORTH SE/	CH4	LS	2900	404	80			32.5	0.17	50	294.12	20233.91863	616730	0.038946907
5	NORTH SE/	CH4	SS	2900	372	27				0.46	550	1193.81	80683.13159	2459222	
6	NORTH SE/	CH4	SS	2300	356	70				0.41	1100	2682.93	185681.3642		
7		CH4				29									
8															
9		CH4	Dolo.	6500	348	49	2725	1.00E+06	10.5	0.54	1375	2546.3	173106.3357		
0	US	CO2	LS/Dolo.	5600	312	101	190	3.00E+05	3	0.8	50	62.5	4151.014648	126523	0.128189963
1	US	CO2	LS	6700	330	141	49900	5.00E+06	4	1	19	19	1284.112121	39140	0.068434713
2	US	CO2	LS/Dolo.	5600	312	166	75	2.00E+05	5	0.8	50	62.5	4151.014648	126523	0.099295519
3	US	CO2	LS/Dolo.	5500	311	103	85	2.00E+05	5	0.8	50	62.5	4127.226598	125798	0.099295519
4	US	CO2	LS/Dolo.	5500	311	179	70	2.00E+05	5	0.8	50	62.5	4175.078501	127256	0.099295519
5	US	CO2	Dolo.	7850	330	126	1700	1.00E+06	7	1.9	2	1.05	76.04828683	2318	0.016784006
6	US	CO2	Dolo.	5800	316	93	4437	2.00E+06	7	3	4	1.33	95.13491569	2900	0.023736169

1			Formation	Depth, ft	Temperature, K		Area, acres	Radial Thickness, ft	Porosity, %	Viscosity, cp	Permeability, mD	Mobility, mD/cp	Darcy Velocity, ft/s		
77	US	CO2	S	7000		138	120	3.00E+05	7		10				
78	US	CO2	Dolo.	8200	322	170	4720	2.00E+06	7	1.1	15	13.64	943.7523884		0.045964893
79	US	CO2	Dolo.	4500	314	93	1923	1.00E+06	8.6	1	2	2	140.0998986	4270	0.015142425
80	US	CO2	Dolo.	4900	314	157	1561	1.00E+06	9	2	4	2	140.9567787	4296	0.020933333
81	US	CO2	Dolo.	4700	313	173	3600	1.00E+06	9	2	4	2	140.9567787	4296	0.020933333
82	US	CO2	Dolo.	4300	309	172	8500	2.00E+06	9	6	20	3.33	239.3191415	7294	0.046808356
83	US	CO2	S	5000	354	118	1345	9.00E+05	9.9	1	32	32	2214.672271	67503	0.056453002
84	US	CO2	Dolo.	5100	314	145	8500	2.00E+06	10	2	2	0.75	52.85879203	1611	0.014042507
85	US	CO2	Dolo.	4900	314	112	6412	2.00E+06	10	1.8	2	1.11	78.79122504	2402	0.014042507
86	US	CO2	Dolo.	4950	314	126	1048	8.00E+05	10	2	2	1	70.47838937	2148	0.014042507
87	US	CO2	Dolo.	5400	311	132	1143	8.00E+05	10	3	3	1	71.35118676	2175	0.017198488
88	US	CO2	Dolo.	5000	315	93	8559	2.00E+06	10	2	3	1.5	105.7175841	3222	0.017198488
89	US	CO2	Dolo.	4000	303	144	1020	8.00E+05	10	2	4	2	139.2533736	4244	0.019859104
90	US	CO2	Dolo.	5000	315	180	177	3.00E+05	10	1.6	4	2.5	177.2802563	5404	0.019859104
91	US	CO2	Dolo.	5000	315	122	1240	9.00E+05	10	1.6	4	2.5	177.2802563	5404	0.019859104
92	US	CO2	Dolo.	5500	313	109	340	5.00E+05	10	1	4	4	281.9135575	8593	0.019859104
93	US	CO2	Dolo./LS	4950	314	149	1600	1.00E+06	10	1.8	4	2.22	157.5824501	4803	0.019859104
94	US	CO2	Dolo.	5700	314	94	113	3.00E+05	10	1	5	5	352.3919469	10741	0.022203153
95	US	CO2	Dolo./LS	5100	316	108	7800	2.00E+06	10	1.3	5	3.85	267.7949492	8162	0.022203153
96	US	CO2	Dolo./LS	4950	314	98	246	4.00E+05	10	1.8	5	2.78	196.9780626	6004	0.022203153
97	US	CO2	S/LS-Dolo.	6400	350	134	810	7.00E+05	10	1	5	5	346.0425424	10547	0.022203153
98	US	CO2	Dolo.	11100	384	107	980	8.00E+05	10	0.64	10	15.63			0.0314
99	US	CO2	S	9000	366	158	25	1.00E+05	10	2	16	8	570.8094941		0.039718207
00	US	CO2	S	6000	346	132	1400	9.00E+05	10	1	20	20	1384.17017	42190	0.044406306
01	US	CO2	LS	6600	325	100	1400	9.00E+05	10	0.4	70	175	11556.23448	352234	0.083076591
02	US	CO2	Dolo.	4200	306	126	465	5.00E+05	10	1.5					0
03	US	CO2	S/LS-Dolo.	5400	356	113	790	7.00E+05	10.3	1	4	4	276.8340339		0.019567756
04	CHINA	CO2	s	6955.72	381	154	583	6.00E+05	10.4	3.6	1	0.29			0.009736727
05	US	CO2	LS/Dolo.	6700	332	183	700	7.00E+05	10.4	0.4	170	425			0.126951384
06	US	CO2	Dolo.	5500	313	107	1120	8.00E+05	10.5	1	4	4	281.9135575		0.019380501
07	US	CO2	Dolo.	4900	310	167	1160	8.00E+05	11	2.3	4	1.74	121.0898901	3691	0.018934912
08	US	CO2	Dolo.	5040	314	96	1235	9.00E+05	11	1.5	4	2.67	185.6711648	5659	0.018934912
09	US	CO2	Dolo.	4950	314	124	5500	2.00E+06	11	1	6	6	420.2996959	12811	0.023190437
10	US	CO2	Dolo.	5250	314	190	1780	1.00E+06	11	1.2	8	6.67	464.1779119	14148	0.02677801
11	CHINA	CO2	s	7874.4	372	159	568	6.00E+05	11.1	1.85	4	1.93			0.018849427
12	US	CO2	Dolo.	6500	318	121	160	3.00E+05	11.5	1	4	4	268.7630708		0.01851871
13	US	CO2	Dolo.	4200	314	171	330	4.00E+05	11.6	3.06	32	10.45	723.2598625	22045	0.052152561
14	US	CO2	Dolo.	4500	311	139	4900	2.00E+06	11.7	1	11	11	747.8193704	22794	0.030446197
15	US	CO2	Dolo.	4500	311	161	4900	2.00E+06	11.7	1	11	11	747.8193704	22794	0.030446197

1			Formation	Depth, ft	Temperature, K		Area, acres	Radial Thickness, ft	Porosity, %	Viscosity, cp	Permeability, mD	Mobility, mD/cp	Darcy Velocity, ft/s		
116	US	CO2	Dolo.	4900	315	105	1179	8.00E+05	12	1.4	2	1.43	99.4666954	3032	0.012818996
117	US	CO2	Dolo./LS	4950	314	179	5700	2.00E+06	12	1.8	5	2.78	196.9780626	6004	0.020268613
118	US	CO2	Dolo.	5200	314	99	27848	4.00E+06	12	1.2	8	6.67	466.9996621	14234	0.025637993
119	US	CO2	S	6000	344	93	18000	3.00E+06	12	2	10	5	346.0425424	10547	0.028664147
120	US	CO2	LS	5700	327	101	1200	9.00E+05	12	1.5	19	12.87	854.5555488	26047	0.0395108
121	US	CO2	Dolo.	4550	311	140	1084	8.00E+05	12	1	22	22	1495.638741	45587	0.042515801
122	CANADA	CO2	LS	8200	370	188	80	2.00E+05	12	0.65	50	76.92	5123.706831	156171	0.064094982
123	US	CO2	Dolo.	5300	313	185	15699	3.00E+06	12	1	62	62	4290.927526	130787	0.071373151
124	US	CO2	Dolo.	5500	313	123	480	5.00E+05	12	1	62	62			0.071373151
125	US	CO2	Dolo.	5500	313	153	2320	1.00E+06	12	1	62	62	4290.927526		0.071373151
126	US	CO2	Dolo.	5500	313	169	500	5.00E+05	12	1	63	63	4360.136034	132897	0.071946438
127	US	CO2	S	11600	394	125	200	3.00E+05	12	0.24	200	848.06	56325.1805	1716792	0.128189963
128	US	CO2	Dolo.	8500	325	92	2550	1.00E+06	12.4	0.96	28	29.1	1932.938732	58916	0.047184333
129	US	CO2	Dolo.	4900	316	145	569	6.00E+05	12.5	1	6	6	422.8703362	12889	0.021754558
130	CHINA	CO2	s	8038.45	370	92	232	4.00E+05	13	2.08	5	2.16			0.019473453
131	US	CO2	Dolo.	5100	316	98	640	6.00E+05	13	1	6	6	420.2996959		0.021332099
132	US	CO2	LS	6800	327	116	2684	1.00E+06	13	0.7	6	8.57	575.9208661	17554	0.021332099
133	US	CO2	S	9400	337	143	3400	1.00E+06	13	1	44	44	2991.277482	91174	0.057767598
134	CANADA	CO2	S	4900	329	101	6625	2.00E+06	13	1.14	500	438.6	29129.92735	887880	0.194734533
135	US	CO2	Dolo./Tri- politic chert	8000	323	122	6183	2.00E+06	13.5	1.27	9	7.1			0.025637993
136	CHINA	CO2	s	9678.95	399	97	178	3.00E+05	13.9	1.59	4	2.37			0.016844272
137	US	CO2	Dolo.	4800	312	150	2870	1.00E+06	14	2.3	5	2.17	153.2138899		0.018765089
138	US	CO2	LS	5600	325	178	13440	3.00E+06	14	1	5	5	334.0062801	10181	0.018765089
139	US	CO2	S	9400	339	162	700	7.00E+05	14	1	50	50	3399.178956	103607	0.059340422
140	US	CO2	Dolo.	4789	313	131	5338	2.00E+06	14.1	3.77	4	1.06			0.016724382
141	CHINA	CO2	s	5715.5	341	115			14.5	6.4	1	0.22			0.008246044
142	CANADA	CO2	LS/Dolo.	4655	333	163	17280	3.00E+06	15	3	10	3.33	240.819575		0.025637993
143	US	CO2	Dolo.	4200	312	180	3100	1.00E+06	15	0.9	15	16.67	1153.475141	35158	0.0314
144	US	CO2	S	7260	340	179	2320	1.00E+06	15	2	63	31.5	2135.184264	65080	0.064350851
145	US	CO2	S	7300	340	101	2500	1.00E+06	15.2	2	63	31.5	2141.482743	65272	0.063926088
146	CHINA	CO2	s	8038.45	370	169			16	2.08	5	2.16			0.017553134
147	CANADA	CO2	S	5300	326	123	80	2.00E+05	16	1	20	20	1336.02512		0.035106267
148	US	CO2	SS	6200	336	183	7000	2.00E+06	16	1	35	35	2351.67687	71679	0.046441226
149	US	CO2	SS	2600	301	92	16300	3.00E+06	16	1.6	37	23.13	1590.891853	48490	0.047749686
150	US	CO2	SS	6200	336	148	11000	3.00E+06	16	1	50	50	3359.538386	102399	0.055507882
151	US	CO2	SS	6200	336	92	21000	4.00E+06	16	1	50	50	3359.538386	102399	0.055507882
152	US	CO2	S	6200	319	117	1100	8.00E+05	16	3	70	23.33	1664.861025	50745	0.065677812
153	CANADA	CO2	Dolo., LS	4600	338	148	30483	4.00E+06	16.3	3	8	2.5	178.3779669	5437	0.021997881
154	US	CO2	SS	1750	314	109	570	6.00E+05	17	0.6	25	41.67	2816.035353	85833	0.038078093
155	US	CO2	SS	1600	310	149	600	6.00E+05	17	0.6	30	50	3460.425424	105474	0.041712461
156	US	CO2	S	1150	310	99	5	5.00E+04	17	0.6	30	50	3460.425424	105474	0.041712461
157	US	CO2	S	1150	310	129	5	5.00E+04	17	0.6	30	50	3460.425424	105474	0.041712461

1			Formation	Depth, ft	Temperature, K		Area, acres	Radial Thickness, ft	Porosity, %	Viscosity, cp	Permeability, mD	Mobility, mD/cp	Darcy Velocity, ft/s		
58	US	CO2	S	11500	382	140	1800	1.00E+06	17	0.21	171	807.39	52712.64621	1606681	0.099587136
59	US	CO2	Dolo.	1400	301	134	26000	4.00E+06	17	6	175	29.17	2081.076281	63431	0.100745165
60	US	CO2	S	11950	385	136	2600	1.00E+06	17	0.24	273	1118.26	73844.69565	2250786	0.125830671
61	US	CO2	Tripol.	5400	313	172	1326	9.00E+05	18	0.4	2	5	332.0811718	10122	0.010466667
62	US	CO2	SS	2200	317	169	1325	9.00E+05	18	0.6	30	50	3379.242423	102999	0.040537226
63	US	CO2	S	11550	391	189	280	4.00E+05	18	0.38	40	104.95	7135.063431	217477	0.046808356
64	TURKEY	CO2	LS	4265	327	158	12890	3.00E+06	18	592	58	0.1	7.812898233	238	0.056364725
65	US	CO2	S	1900	314	103	6000	2.00E+06	18	0.6	75	125	8548.380313		0.064094982
66	US	CO2	S	6500	334	150	2010	1.00E+06	18.1	2	48	24	1575.824501	48031	0.051134143
67	US	CO2	S	4900	314	188	4392	2.00E+06	19.5	2	32	16	1100.725174	33550	0.040224192
68	US	CO2	LS	6300	325	172	12000	3.00E+06	20	1	12	12	811.0181815	24720	0.024322335
69	US	CO2	S	10100	373	126	3500	1.00E+06	20	0.41	30	73.54	4941.12553	150606	0.038456989
70	US	CO2	S	8060	354	142	1325	9.00E+05	20	2	50	25	1689.621212	51500	0.049647759
71	US	CO2	S	5400	314	157	98	2.00E+05	20	45	271	6.02	461.0988137	14054	0.115584419
72	US	CO2	Tripol.	5200	313	126	2090	1.00E+06	21	0.6	4	6.67	440.2375038	13418	0.013704084
73	US	CO2	S	8060	354	137	577	6.00E+05	21	2	50	25	1689.621212	51500	0.048451252
74	US	CO2	S	8060	354	151	829	7.00E+05	21	2	109	54.5	3683.374241	112269	0.071537416
75	US	CO2	Tripol.	5300	314	92	809	7.00E+05	21.9	1	3	3	199.2487031	6073	0.011621661
76	US	CO2	Tripol.	5500	311	153	2084	1.00E+06	22	1	4	4	268.7630708	8192	0.013389005
77	US	CO2	Tripol.	5300	313	134	1155	8.00E+05	22	0.4	5	12.5	820.7419275	25016	0.014969363
78	US	CO2	Tripol.	7500	324	163	1280	9.00E+05	22	0.5	5	10	671.9076771	20480	0.014969363
79	US	CO2	S	4500	309	91	7100	2.00E+06	22	1.1	24	21.82	1457.481949	44424	0.03279623
80	US	CO2	S	2680	301	114	1953	1.00E+06	23	1	30	30			0.035861327
81	US	CO2	S	11000	394	180	4100	2.00E+06	23	0.26	90	344.08			0.062113641
82	US	CO2	S	10750	394	188	6200	2.00E+06	23	0.29	90	309.43	20791.16635	633715	0.062113641
83	US	CO2	S	10300	400	175	7754	2.00E+06	23	0.3	100	334.21	22587.61285	688470	0.065473526
84	US	CO2	S	5000	346	145	10104	2.00E+06	23	1.39	500	359.94	25061.19037	763865	0.146403255
85	US	CO2	S	10400	390	122	840	7.00E+05	23.4	0.35	65	187.5	12672.06853	386245	0.052333333
86	CHINA	CO2	s	6857.29	349	184	141	3.00E+05	23.4	2.43	854	351.44	#DIV/0!	#DIV/0!	0.189692716
87	US	CO2	Tripol.	5500	314	98	400	5.00E+05	23.7	0.51	5	8.82	586.0255973		0.014422498
88	US	CO2	S	4500	315	127	2800	1.00E+06	24	1.2	700	583.33	39892.44146	1215922	0.169579382
89	US	CO2	S	10300	394	95	10800	3.00E+06	25.5	0.29	60	206.29	13860.77757	422477	0.048165401
90	US	CO2	S	10550	393	104	880	7.00E+05	26	0.3	75	253.65	17042.74549	519463	0.053330248
91	US	CO2	S	10550	393	188	8240	2.00E+06	26	0.3	75	253.65	17042.74549	519463	0.053330248
92	US	CO2	S	10900	394	123	12600	3.00E+06	26	0.29	90	309.43	20791.16635	633715	0.05842036
93	US	CO2	S	8500	365	129	180	3.00E+05	27	120.57	107	0.89	71.76379092	2187	0.062508583
94	US	CO2	S	5050	340	128	2100	1.00E+06	27	10.54	250	23.71	1779.840485	54250	0.095547157
95	US	CO2	S	4800	340	125	2500	1.00E+06	28	10.54	300	28.45	2135.808582	65099	0.102780626
96	US	CO2	S	8500	361	108	3900	2.00E+06	28	0.57	2000	3511.79	237343.537	7234231	0.265378436
97	US	CO2	S	4700	340	176	2000	1.00E+06	29	8.71	300	34.44	2568.714163	78294	0.100993001
98	US	CO2	S	3500	330	188	14010	3.00E+06	29.5	0.77	2000	2597.4			0.258543508

1			Formation	Depth, ft	Temperature, K		Area, acres	Radial Thickness, ft	Porosity, %	Viscosity, cp	Permeability, mD	Mobility, mD/cp	Darcy Velocity, ft/s		
199	TRINIDAD P	CO2	S	2400	322	156	175	3.00E+05	30	5	36	7.2	516.9293456		0.034396977
200	TRINIDAD P	CO2	S	2600	322	141	29	1.00E+05	30	32	150	4.69	363.7378997	11087	0.070212534
201	US	CO2	S	5700	347	150	4420	2.00E+06	30	1.24	1000	806.45	57187.17947	1743065	0.181287985
202	TRINIDAD P	CO2	S	4200	327	136	184	3.00E+05	31	6	300	50	3681.53887	112213	0.09768085
203	TRINIDAD P	CO2	S	3000	322	109	58	2.00E+05	32	16	175	10.94	837.4430714	25525	0.073430026
204	CHINA	CO2	s			166	445	5.00E+05			4				
205	BRAZIL	CO2	0	7400	380	128	1250	9.00E+05		1	15	15	1007.861516		
206	US	CO2	LS/Dolo.	5450	312	109	60	2.00E+05		0.8	50	62.5	4127.226598	125798	
207	US	CO2	LS/Dolo.	5450	312	139	285	4.00E+05		0.8	50	62.5			
208	BRAZIL	CO2	0	5900	353	175	1235	9.00E+05		3	100	33.33			
209	BRAZIL	CO2	0	3773	338	134	2000	1.00E+06		3	175	58.33			
210	BRAZIL	CO2	0	3940	333	96	740	7.00E+05		3	250	83.33			
211	BRAZIL	CO2	0	3600	333	95	740	7.00E+05		5	300	60			
212	BRAZIL	CO2	0	1970	318	144	2000	1.00E+06		8	400	50			
213															

APPENDIX C: Python Codes

```
# Firstly, import dependencies

import pandas as pd
import matplotlib.pyplot as plt
import seaborn as sns
from sklearn.model_selection import train_test_split
from sklearn.linear_model import LinearRegression
from sklearn.linear_model import Lasso
from sklearn import metrics
from scipy import stats
from scipy.interpolate import *

# Loading the data from csv file to pandas dataframe
data = pd.read_csv('/Users/brandan/Downloads/NEW DATA.csv')

# Checking the number of rows and columns
data.head()

# Statistical description of the data
data.describe()

# Constructing a heatmap to understand the correlation
correlation = data.corr()
plt.figure(figsize = (10,10))
sns.heatmap(correlation, cbar=True, square=True, fmt='.2f', annot=True,
annot_kws={'size': 8}, cmap='RdYlGn')
plt.title('Correlation Heatmap for the Experimental Data')

# Plotting Permeability vs Pressure at different Temperatures
plt.figure()
sns.lineplot(x = data['Pressure_(atm)'], y = data['Permeability_(mD)'], hue =
data['Temperature_(K)'], palette = 'bright')
plt.plot(data['Pressure_(atm)'], slope * data['Pressure_(atm)'] + intercept,
color='none', label='Linear fit')
plt.xlabel('Pressure (atm)', fontsize = 10)
plt.ylabel('Permeability (mD)', fontsize = 10)
plt.title('Permeability response to pressure at different temperatures')
stats.linregress(x = data['Pressure_(atm)'], y = data['Permeability_(mD)'])
slope, intercept, rvalue, pvalue, stderr = stats.linregress(x =
data['Pressure_(atm)'], y = data['Permeability_(mD)'])
plt.annotate('             y = %.2ex+%.2e\n            R$^2$ =
%.2f'%(slope,intercept, rvalue**2), xy=(0.17,0.7), xycoords='figure fraction')

# Plotting Mobility vs Pressure at different Temperatures
plt.figure()
sns.lineplot(x = data['Pressure_(atm)'], y = data['Mobility_(mD/cp)'], hue =
data['Temperature_(K)'], palette = 'bright')
plt.plot(data['Pressure_(atm)'], slope * data['Pressure_(atm)'] + intercept,
color='none', label='Linear fit')
plt.xlabel('Pressure (atm)')
plt.ylabel('Mobility (mD/cp)')
```

```
plt.title('Mobility response to pressure at different temperatures')
stats.linregress(x = data['Pressure_(atm)'], y = data['Mobility_(mD/cp)'])
slope, intercept, rvalue, pvalue, stderr = stats.linregress(x =
data['Pressure_(atm)'], y = data['Mobility_(mD/cp)'])
plt.annotate('            y = %.2ex+%.2e\n            R$^2$ =
%.2f'%(slope,intercept, rvalue**2), xy=(0.17,0.7), xycoords='figure fraction')

# Plotting Darcy Flux vs Pressure at different Temperatures
plt.figure()
sns.lineplot(x = data['Pressure_(atm)'], y = data['Flux_(cm3/cm2*sec)'], hue =
data['Temperature_(K)'], palette = 'bright')
plt.plot(data['Pressure_(atm)'], slope * data['Pressure_(atm)'] + intercept,
color='none', label='Linear fit')
plt.xlabel('Pressure (atm)')
plt.ylabel('Darcy flux (cm3/cm2sec)')
plt.title('Darcy flux response to pressure at different temperatures')
stats.linregress(x = data['Pressure_(atm)'], y = data['Flux_(cm3/cm2*sec)'])
slope, intercept, rvalue, pvalue, stderr = stats.linregress(x =
data['Pressure_(atm)'], y = data['Flux_(cm3/cm2*sec)'])
plt.annotate('y = %.2ex+%.2e\nR$^2$ = %.1f'%(slope,intercept, rvalue**2),
xy=(0.17,0.7),     xycoords='figure fraction')

# Plotting Quality Index vs Pressure at different Temperatures
plt.figure()
sns.lineplot(x = data['Pressure_(atm)'], y = data['Quality _Index_(µm)'], hue =
data['Temperature_(K)'], palette = 'bright')
plt.plot(data['Pressure_(atm)'], slope * data['Pressure_(atm)'] + intercept,
color='none', label='Linear fit')
plt.xlabel('Pressure (atm)')
plt.ylabel('Quality index (µm)')
plt.title('Quality index response to pressure at different temperatures')
stats.linregress(x = data['Pressure_(atm)'], y = data['Quality _Index_(µm)'])
slope, intercept, rvalue, pvalue, stderr = stats.linregress(x =
data['Pressure_(atm)'], y = data['Quality _Index_(µm)'])
plt.annotate('            y = %.2ex+%.2e\n            R$^2$ =
%.1f'%(slope,intercept, rvalue**2), xy=(0.17,0.7),     xycoords='figure fraction'

# Plotting Permeability vs Viscosity for the different Gases
plt.figure()
sns.lineplot(x = data['Viscosity_(cp)'], y = data['Permeability_(mD)'], hue =
data['Gas '])
plt.plot(data['Viscosity_(cp)'], slope * data['Viscosity_(cp)'] + intercept,
color='none', label='Linear fit')
plt.xlabel('Viscosity (cp)')
plt.ylabel('Permeability (mD)')
plt.title('Permeability response to viscosity for the different gases')
stats.linregress(x = data['Viscosity_(cp)'], y = data['Permeability_(mD)'])
slope, intercept, rvalue, pvalue, stderr = stats.linregress(x =
data['Viscosity_(cp)'], y = data['Permeability_(mD)'])
plt.annotate('            y = %.2ex+%.2e\n            R$^2$ =
%.2f'%(slope,intercept, rvalue**2), xy=(0.17,0.7), xycoords='figure fraction')
```

```
# Plotting Mobility vs Viscosity for the different Gases
plt.figure()
sns.lineplot(x = data['Viscosity_(cp)'], y = data['Mobility_(mD/cp)'], hue =
data['Gas '])
plt.plot(data['Viscosity_(cp)'], slope * data['Viscosity_(cp)'] + intercept,
color='none', label='Linear fit')
plt.xlabel('Viscosity (cp)')
plt.ylabel('Mobility (mD/cp)')
plt.title('Mobility response to viscosity for the different gases')
stats.linregress(x = data['Viscosity_(cp)'], y = data['Mobility_(mD/cp)'])
slope, intercept, rvalue, pvalue, stderr = stats.linregress(x =
data['Viscosity_(cp)'], y = data['Mobility_(mD/cp)'])
plt.annotate('            y = %.2ex+%.2e\n             R$^2$ =
%.2f'%(slope,intercept, rvalue**2), xy=(0.17,0.7), xycoords='figure fraction')

# Plotting Darcy Flux vs Viscosity for the different Gases
plt.figure()
sns.lineplot(x = data['Viscosity_(cp)'], y = data['Flux_(cm3/cm2*sec)'], hue =
data['Gas '])
plt.plot(data['Viscosity_(cp)'], slope * data['Viscosity_(cp)'] + intercept,
color='none', label='Linear fit')
plt.xlabel('Viscosity (cp)')
plt.ylabel('Darcy flux (cm3/cm2sec)')
plt.title('Darcy flux response to viscosity for different gas')
stats.linregress(x = data['Viscosity_(cp)'], y = data['Flux_(cm3/cm2*sec)'])
slope, intercept, rvalue, pvalue, stderr = stats.linregress(x =
data['Viscosity_(cp)'], y = data['Flux_(cm3/cm2*sec)'])
plt.annotate('            y = %.2ex+%.2e\n             R$^2$ =
%.3f'%(slope,intercept, rvalue**2), xy=(0.17,0.7), xycoords='figure fraction')

# Plotting Reservoir Quality Index vs Viscosity for the different Gases
plt.figure()
sns.lineplot(x = data['Viscosity_(cp)'], y = data['Quality _Index_(µm)'], hue =
data['Gas '])
plt.plot(data['Viscosity_(cp)'], slope * data['Viscosity_(cp)'] + intercept,
color='none', label='Linear fit')
plt.xlabel('Viscosity (cp)')
plt.ylabel('Quality index (µm)')
plt.title('Quality index response to viscosity for different gases')
stats.linregress(x = data['Viscosity_(cp)'], y = data['Quality _Index_(µm)'])
slope, intercept, rvalue, pvalue, stderr = stats.linregress(x =
data['Viscosity_(cp)'], y = data['Quality _Index_(µm)'])
plt.annotate('y = %.2ex+%.2e\nR$^2$ = %.2f'%(slope,intercept, rvalue**2),
xy=(0.17,0.7), xycoords='figure fraction')
```